Structural geology, Stratigraphy, and Gold Deposits of the New Britannia Mining District of the Paleoproterozoic Snow Lake arc assemblage (Snow Lake, Manitoba, Canada)

by

Kate Elizabeth Louise Rubingh

A thesis submitted in partial fulfillment
of the requirements for the degree of
Doctor of Philosophy (PhD)
in Mineral Deposits and Precambrian Geology

The Faculty of Graduate Studies
Laurentian University
Sudbury, Ontario, Canada

© Kate Elizabeth Louise Rubingh, 2019

THESIS DEFENCE COMMITTEE/COMITÉ DE SOUTENANCE DE THÈSE
Laurentian Université/Université Laurentienne
Faculty of Graduate Studies/Faculté des études supérieures

Title of Thesis Titre de la thèse	Structural Geology, Stratigraphy, and Gold Deposits of the New Britannia Mining District in the Paleoproterozoic Snow Lake Arc Assemblage (Snow Lake, Manitoba, Canada)
Name of Candidate Nom du candidat	Rubingh, Kate
Degree Diplôme	Doctor of Philosophy
Department/Program Département/Programme	Mineral Deposits and Precambrian Geology
Date of Defence February 21, 2019 Date de la soutenance	

APPROVED/APPROUVÉ

Thesis Examiners/Examinateurs de thèse:

Dr. Bruno Lafrance
(Co-Supervisor/Co-directeur de thèse)

Dr. Harold Gibson
(Co-Supervisor/Co-directeur de thèse)

Dr. Doug Tinkham
(Committee member/Membre du comité)

Dr. Simon Gagné
(Committee member/Membre du comité)

Dr. Kevin Ansdell
(External Examiner/Examinateur externe)

Dr. Eugene Ben-Awuah
(Internal Examiner/Examinateur interne)

Approved for the Faculty of Graduate Studies
Approuvé pour la Faculté des études supérieures
Dr. David Lesbarrères
Monsieur David Lesbarrères
Dean, Faculty of Graduate Studies
Doyen, Faculté des études supérieures

ACCESSIBILITY CLAUSE AND PERMISSION TO USE

I, **Kate Rubingh**, hereby grant to Laurentian University and/or its agents the non-exclusive license to archive and make accessible my thesis, dissertation, or project report in whole or in part in all forms of media, now or for the duration of my copyright ownership. I retain all other ownership rights to the copyright of the thesis, dissertation or project report. I also reserve the right to use in future works (such as articles or books) all or part of this thesis, dissertation, or project report. I further agree that permission for copying of this thesis in any manner, in whole or in part, for scholarly purposes may be granted by the professor or professors who supervised my thesis work or, in their absence, by the Head of the Department in which my thesis work was done. It is understood that any copying or publication or use of this thesis or parts thereof for financial gain shall not be allowed without my written permission. It is also understood that this copy is being made available in this form by the authority of the copyright owner solely for the purpose of private study and research and may not be copied or reproduced except as permitted by the copyright laws without written authority from the copyright owner.

Abstract

Orogenic gold deposits in the Snow Lake area in the southeastern Trans Hudson Orogen, Manitoba, include the New Britannia deposit which, with a past production of a 1.4M oz Au (43 699 kg), is the largest Proterozoic gold deposit in Manitoba and Saskatchewan. The deposits are hosted by the ca. 1.89 Ga Paleoproterozoic Snow Lake arc (SLA) assemblage of the Flin Flon Glennie Complex (FFGC). The FFGC is bound by a sedimentary basin to the north, namely the Kisseynew Domain. It represents an oceanic protocontinent within an ancestral ocean, the Manikewan Ocean, which occupied the region between three Archean cratons (Hearne, Sask, Superior).

The deposits occur within a sequence of explosive, submarine, bimodal volcanic rocks emplaced during an early episode of rifting and subsidence of the SLA. Deformation of these rocks began with their imbrication along brittle thrust faults during a D1 event. It continued during a ca. 1.84-1.82 Ga D2 event with thrusting of the Kisseynew basin and FFGC above the colliding Sask craton. The D2 event produced a penetrative regional foliation axial planar to map-scale isoclinal folds (NorAcme Anticline), sheath-like gneiss domes along the Kisseynew-FFGC boundary, and regional southwest-directed ductile thrust faults, such as the McLeod Road Thrust. Final collision of the FFGC and Sask craton with the Superior craton during a ca. 1.83-1.80 Ga D3 event reactivated the ductile thrust faults, folded the gneiss domes, and enabled the development of an orogen-parallel regional stretching lineation during lateral flow parallel to the cold Superior craton.

The New Britannia deposit and nearby gold deposits were emplaced in the hinge of the Nor-Acme Anticline early during the D2 event, were folded during tightening of the fold, stretched parallel to the regional stretching lineation, and transposed along a late crosscutting shear zone, the Howe

Sound fault, which formed as a transfer fault during thrusting. The deposits formed at amphibolite facies conditions during a prograde metamorphic event that culminated during the collision of the FFGC and Sask craton with the Superior craton during the D3 event. Thus, the deposits are atypical compare to most other Proterozoic and Archean orogenic gold deposits which typically form at greenschist facies conditions.

Keywords

Snow Lake arc assemblage, Flin Flon Glennie Complex, explosive submarine felsic volcanism, rifting, orogen-parallel stretching lineation, amphibolite facies orogenic gold deposits, thrusting, LA-ICP-MS mapping of arsenopyrite

Co-Authorship Statement

This thesis consists of three manuscripts, which were prepared for publication in peer-reviewed scientific journals; one of which is published. The Appendix contains two "Report of Activity Papers", and one preliminary published map published by the Manitoba Geological Survey. Additionally, a field trip guide is included, which was presented to Hudbay Minerals Inc. Chapters two to four and the papers in the appendices were co-authored by the candidate and several collaborators, who provided constructive suggestions and edits. The candidate is the first author on all manuscripts. Chapter 2, 3 and 4 of this dissertation are co-authored with Drs. Bruno Lafrance and Harold Gibson.

The candidate completed the field work and analytical work under the main guidance and supervision of Drs. Bruno Lafrance and Harold Gibson. Field work included mapping of outcrops, core-logging, and sample collection. Drill core was provided by Alexis Minerals Corporation and QMX Gold Corporation, and samples were chosen specifically by the candidate for further analytical work. Analytical work involved petrography, SEM analyses, data processing and subsequent interpretation. The geochemical, analyses discussed in Chapters 2 and 4 were completed by: i) the Activation Laboratories Ltd. in Ancaster, Ontario, ii) the Geoscience Laboratories of the Ministry of Northern Developments and Mines in Sudbury, Ontario, iii) ALS Limited, Sudbury, Ontario. The isotope analysis was conducted at the Pacific Centre for Isotopic and Geochemical Research (PCIGR), at the Department of Earth, Ocean and Atmospheric Sciences, University of British Columbia, Vancouver, British Columbia. Laser ablation – inductively coupled plasma – mass spectrometry (LA-ICP-MS) analytical work and data reduction was performed at the Geochemical Fingerprinting Laboratory of Laurentian University in Sudbury by Dr. Joseph A. Petrus.

Dr. Bruno Lafrance and Dr. Harold Gibson contributed to this study by providing scientific guidance on various subjects discussed in Chapters 2 to 4 and the Appendices. Dr. Bruno Lafrance and Dr. Harold Gibson assisted with the improvement of the manuscripts presented in Chapters 2 and 3. Dr. Bruno Lafrance assisted with the improvement of Chapter 4 and Dr. Shawna White reviewed and edited Chapters 1 and 5.

Acknowledgments

I would like to thank first and foremost my supervisors, Drs. Bruno Lafrance and Harold Gibson, for their guidance, expertise and support throughout this research project. I would also like to thank my committee members Dr. Doug Tinkham, and Simon Gagné who provided support as needed.

The research project received funding from several sources which made this research possible and I am grateful to the following organizations: - QMX Gold Corporation, Natural Sciences and Engineering Research Council of Canada, the Society of Economic Geologists, and the Goodman School of Mines.

My field work was made possible by the in-kind support from the Manitoba Geological Survey, and I would like to express my appreciation to all my field assistants, for the hard work over the years. In addition, I sincerely appreciate Simon Gagné and Dr. Alan Bailes, whose knowledge in the field area and discussions on my research were greatly appreciated.

I would like to thank all the technical laboratory staff at Laurentian University: Willard Desjardins for making thin sections, Dr. Joe Petrus for work on the LA-ICP-MS, and Dr. William Zhe for work on the SEM.

Last I thank my late father Bernard, my cat Portia, and my mother Berenice Rubingh who have supported me relentlessly to the end, with encouragement and support.

Table of Contents

List of Tables

List of Figures

List of Appendices

Chapter 1 - Introduction to the Thesis

1.1. Research problem

The New Britannia Mine is located in the McLeod Road - Birch Lake (MB) thrust panel in the eastern part of the Flin Flon-Glennie complex (FFGC) of the southeastern Trans Hudson Orogen in Manitoba. This region, an important base metal producer, hosts several significant volcanogenic massive sulphide (VMS) and gold deposits. The New Britannia Mine is the most significant past gold-producer in the Trans Hudson Orogen of Manitoba and Saskatchewan, producing 1, 404 950 oz. (43 694 kg) gold from 1949 to 2005. The mine has been renamed 'Snow Lake mine' by QMX Minerals Corporation in 2012; however, for consistency with earlier publications, this thesis will continue to use the name 'New Britannia Mine'.

Several geologic investigations were conducted to interpret the stratigraphy and geochemistry of the Snow Lake arc assemblage and its associated VMS mineralization (Bailes and Galley, 1996, 1999, 2007; Bailes and Schledewitz, 1998), the structural history of the FFGC (Connors et al., 1996; Lucas et al., 1996; Syme et al., 1995; Zwanzig, 1999; Zwanzig and Bailes, 2010), the structural geology and metamorphic history of the Snow Lake area (Connors et al., 2002; David et al., 1996; Froese and Moore, 1980; Gagné, 2009; Kraus, 1998; Kraus and Menard, 1997; Kraus and Williams, 1999, 2001; Stewart et al., 2018), and the emplacement of gold mineralization at the New Britannia Mine and surrounding occurrences (Harrison, 1949; Hogg, 1957; Russel, 1957; Galley et al., 1988; Bailes and Schledewitz, 1998; Fieldhouse, 1999; Fulton, 1999; Gale, 1997, 2002; Beaumont-Smith and Lavigne, 2008). These studies have advanced our

understanding of the geology of the Snow Lake area and have provided an excellent knowledge base for a more comprehensive investigation of the structural and stratigraphic framework of the MB panel and controls on gold mineralization at the New Britannia Mine. Several research problems remained which are addressed in this thesis. The stratigraphy of the MB panel was previously undefined, and the definition of a stratigraphy for the panel led to the recognition of early brittle thrust faults repeating stratigraphy. These early structures explained the formation of later ductile thrust faults, regional cleavages and sheath-like gneiss domes, and resulted in a new structural framework to interpret the formation of the New Britannia deposit for which no comprehensive study had previously been done.

1.2. Objectives of the Thesis

The main objective of this thesis is to determine the controls on gold mineralization in the New Britannia mining district through a comprehensive study of its stratigraphy, structural geology and gold occurrences. The research provides a new interpretation for the formation of gold deposits in the New Britannia Mine area.

More specifically, the main thesis objectives are to:

1) Characterize the rock units exposed in the MB panel using field mapping, and whole rock and trace element geochemistry to define a volcanic stratigraphy for the MB panel,
2) Propose a new interpretation for the development of structures in the MB panel and more widely in the eastern FFGD,
3) Determine the relative timing of gold mineralization relative to metamorphic and deformation events,
4) Present an interpretation for the formation of orogenic gold deposits in the New Britannia

Mine area and compare their formation to that of other deposits in the southeastern Trans Hudson Orogen.

1.3. Methodology

1.3.1. Field Work

Detailed field mapping was done over four field seasons (2011, 2012, 2013, 2014). Field mapping during the first two field seasons was conducted at 1:1000 to 1:500 scales along three transect lines across the MB thrust panel. Two of the three transect lines were along electrical power lines where the rocks are better exposed. Volcanic facies and textural information were recorded as well as structural measurements. Representative samples of stratigraphic units, established by field mapping, were collected along each of the transect lines, examined under the microscope, and submitted for whole rock geochemical and isotopic analysis to further define the key volcanic stratigraphic units within the MB panel.

Eight drill holes from Alexis Minerals Corporation 2011 and 2012 drilling program were selected for detailed characterization of the main mineralized zones on the mine property. Six drill holes intersected the Toots, Dick/Hogg, Ruttan and Mine East ore bodies at the New Britannia Mine. Two drill holes crossed the Boundary and No. 3 Zones. Graphic logs showing lithofacies, alteration, mineralization and structures along mineralized and non-mineralized intervals, were completed for each drill hole. Samples were collected for further petrographical and geochemical characterization of both mineralized and non-mineralized intervals.

Detailed structural mapping was done in 2013 and 2014 at 1:50 scale on: 1) the few available

stripped outcrop exposures of the mineralized zones, and 2) key locations where structural overprinting relationships, repetition of stratigraphic units along fault contacts, and kinematic indicators, are well exposed. Structural samples were collected for further microstructural characterization, and grab samples and channel samples were taken across the exposed mineralized zones for assay, trace and major element geochemical analyses, and further petrographical characterization of the sulphide and alteration mineralogy. This provided the data for a new structural interpretation of the MB thrust panel and eastern FFGD presented in the thesis.

1.3.2. Petrography and Mineral Chemistry

Detailed petrography was done on 150 polished and normal thin sections under a transmitted and reflected light optical microscope. All thin sections were prepared by Willard Desjardins at Laurentian University. Petrography was done to: 1) characterize the mineralogy and textures of volcanic units of the MB panel, 2) describe microstructures and shear sense indicators, (3) determine alteration and sulphide mineralogy at each mineralized zones.

The scanning electron microscope (SEM) at the Central Analytical Facilities of Laurentian University was used to identify the sulphide minerals present in each mineralized zones and analyze the mineral chemistry of silicate and carbonate minerals from non-mineralized to mineralized zones. The minerals analyses are semi-quantitative and were done under the supervision of Dr. William Zhe using an Oxford energy-dispersive spectrometer mounted on a JEOL JSM-6400 scanning electron microscope.

1.3.3. Whole-rock Geochemistry

A total of 203 samples were submitted from 2011 to 2018 for major elements, trace elements, S and CO_2 whole-rock geochemistry to: (1) characterize the composition of volcanic stratigraphic units and assist in the interpretation of their petrogenesis, (2) determine trace metal associations with gold mineralization, and (3) calculate alteration mass gains and losses during mineralization. Of these 203 samples, 121 were submitted to Geoscience Laboratories, Ministry of Northern Development and Mines, Sudbury, Ontario (2011, 2012 and 2018) for geochemical analyses of major and trace elements. Mineralized samples were further analyzed by fire assay for their gold composition. 62 were sent to Activation Laboratories Ltd (Act Labs), Ancaster, Ontario (2013) for geochemical analyses of major and trace elements and another 12 samples were sent for fire assay to Act Labs. The remaining 17 samples were submitted to ALS Limited, Sudbury, Ontario in 2014 for both fire assay and whole rock major and trace element analyses.

1.3.4. Laser ablation – inductively coupled plasma – mass spectrometry (LA ICP-MS)

LA-ICP-MS was used to characterize the trace element composition of arsenopyrite grains collected across the No.3 zone, Boundary zone, and the New Britannia ore zones. These analyses were done to document the siting of gold and association with other metals. A combination of 16 laser maps and 20 line scans was performed across a total of 36 arsenopyrite grains. The analyses were performed at the Chemical Fingerprinting Laboratory at Laurentian University, using the Thermo X Series II ICP-MS under the direction of Dr. Joe Petrus.

1.3.5. Isotope Geochemistry

Lead and Neodymium isotopic geochemistry was performed on nine samples that best represent the mafic and felsic coherent flow and primary mafic volcaniclastic lithofacies of the McLeod

Road Birch Lake sequence. Analyses were conducted at the Pacific Centre for Isotopic and Geochemical Research (PCIGR) of the Department of Earth, Ocean and Atmospheric Sciences, University of British Columbia, Vancouver, British Columbia. Neodymium isotopes were analyzed using a Nu1700 and a Nu Plasma Multicollector-Inductively Coupled Plasma Mass Spectrometer (MC–ICP–MS). Lead isotopes were measured using a MC–ICP–MS. The isotopic data was used to interpret the petrogenesis of these rocks, the degree of crustal contamination and, in conjunction with their trace element composition, their tectonic setting at the time of deposition.

1.4. Organization of the Thesis

This thesis is presented in manuscript style and is written as three papers ready for publication in peer-reviewed journals. Because the three papers are meant to be read independently, there is overlap in the background information presented in each paper. The thesis consists of five chapters. Chapter 1 is an introductory chapter addressing the research problem, thesis objectives and methodology. Chapters 2, 3 and 4 are manuscripts written for publication in peer-reviewed journals. Chapter 2 has been published in the Canadian Journal of Earth Sciences. The subsequent chapters 3 and 4 will be submitted to Precambrian Research and Economic Geology, respectively. More specifically:

Chapter 1 introduces the research problem, prior work performed in the area, the goals of the thesis, and the methodology used in these investigations.

Chapter 2 is a manuscript published in the Canadian Journal of Earth Sciences as *Rubingh, K.E.,*

Gibson, H.L., Lafrance, B., 2017. Evidence for voluminous, bimodal pyroclastic volcanism, during rifting of a Paleoproterozoic Arc at Snow Lake, Manitoba. Canadian Journal of Earth Sciences 54, 654–676. The manuscript proposes a new stratigraphy for the McLeod Road - Birch Lake Thrust Panel (MB panel) based on detailed volcanological field mapping, whole rock and trace element lithogeochemistry, and isotope geochemistry. It correlates stratigraphic units of the MB panel to those of the Snow Lake arc assemblage and proposes that extensive, submarine, pyroclastic flow deposits were emplaced during an explosive volcanic event that accompanied rifting of the Snow Lake arc.

Chapter 3 is written as a manuscript to be submitted to Precambrian Research. The title is "*Early brittle faulting, lateral crustal flow and the development of an orogen-parallel stretching lineation in the Trans-Hudson Orogen, Canada*". The chapter focuses on the structural geology of the MB panel and addresses the regional structural development of the FFGC. The importance of previously unrecognized, stratigraphy-repeating, brittle thrust faults is discussed, as well as the role played by lateral crustal flow in the formation of an orogen-parellel regional stretching lineation during continental collision. The manuscript is co-authored by B. Lafrance and H.L. Gibson.

Chapter 4 is prepared as a manuscript for submission to Economic Geology. The title is "*The amphibolite facies Paleoproterozoic Snow Lake gold deposits: Formation and modification of orogenic gold deposits during early thrusting in the Paleoproterozoic Trans Hudson Orogen, Manitoba*". This manuscript describes the formation of the Snow Lake gold deposits during regional folding and thrusting early during the Trans-Hudson Orogen and their modification

during shearing along a transfer fault that formed during the same tectonic event. The manuscript is co-authored by B. Lafrance and H.L. Gibson.

Chapter 5 summarizes and integrates the main conclusions presented in chapters 2, 3 and 4.

1.5. References

Bailes, A.H. and Galley, A.G. 1996: Setting of Paleoproterozoic volcanic-hosted massive base metal sulphide deposits, Snow Lake, Manitoba; in EXTECH I: A Multidisciplinary Approach to Massive Sulphide Research in the Rusty Lake– Snow Lake Greenstone Belts, Manitoba, G.F. Bonham Carter, A.G. Galley and G.E.M. Hall (ed.), Geological Survey of Canada, Bulletin 426, p. 105–138.

Bailes, A.H. and Galley, A.G. 1999. Evolution of the Paleoproterozoic Snow Lake arc assemblage and geodynamic setting for associated volcanic-hosted massive sulphide deposits, Flin Flon Belt, Manitoba, Canada; Canadian Journal of Earth Sciences, v. 36, p. 1789–1805.

Bailes, A.H. and Galley, A.G. 2007. Geology of the Chisel– Anderson lakes area, Snow Lake, Manitoba (NTS areas 63K16SW and west half of 63K13SE); Manitoba Science, Technology, Energy and Mines, Manitoba Geological Survey, Geoscientific Map MAP2007-1, scale 1:20 000, 1 map plus notes.

Bailes, A.H. and Schledewitz, D.C.P. 1998. Geology and geochemistry of the Paleoproterozoic volcanic rocks between the McLeod Road and Birch Lake faults, Snow Lake area, Flin Flon belt (parts of NTS 63K/16 and 63J/13); in Report of Activities 1998, Manitoba Energy and Mines,

Geological Services, p. 4–13.

Beaumont-Smith, C.J. and Lavigne, J. 2008. Structural geology and gold metallogenesis of the New Britannia Mine area, Snow Lake, Manitoba (NTS 63K16); in Report of Activities 2008, Manitoba Science, Technology, Energy and Mines, Manitoba Geological Survey, p. 7–17.

Connors, K.A., Ansdell, K.M. and Lucas, S.B. 1996. Coeval sedimentation, magmatism, and fold-thrust development in the Trans-Hudson Orogen: propagation of deformation into an active continental arc setting, Wekusko Lake area, Manitoba; Canadian Journal of Earth Sciences, v. 36, p. 275–291.

Connors, K.A., Ansdell, K.M., and Lucas, S.B. 2002. Development of a transverse to orogen parallel extension lineation in a complex collisional setting, Trans-Hudson Orogen, Manitoba, Canada. Journal of Structural Geology, **24**: 89–106.

David, J., Bailes, A.H. and Machado, N. 1996. Evolution of the Snow Lake portion of the Paleoproterozoic Flin Flon and Kisseynew belts, Trans-Hudson Orogen, Manitoba Canada. Precambrian Research, **80**: 107–124.

Fieldhouse, I. 1999. Geological setting of gold mineralization in the vicinity of the New Britannia mine, Snow Lake, Manitoba; M.Sc. thesis, University of Manitoba, Winnipeg, Manitoba, 136 p.

Froese, E. and Moore, J.M. 1980. Metamorphism in the Snow Lake area, Manitoba; Geological Survey of Canada, Paper 78-27, 16 p.

Fulton, P.J. 1999. Distribution of gold mineralization at the New Britannia mine in Snow Lake, Manitoba: implications for exploration and processing; M.Sc. thesis, University of Manitoba, Winnipeg, Manitoba, 207 p.

Gagné, S. 2009. Geological investigation of the McLeod Road Birch Lake allochthon east of Snow Lake, Manitoba (part of NTS 63J13); in Report of Activities 2009, Manitoba Innovation, Energy and Mines, Manitoba Geological Survey, p. 58–68.

Gale, G.H. 1997. Geological settings and genesis of gold mineralization in the Snow Lake area (NTS 63K/16); in Report of Activities 1997, Manitoba Energy and Mines, Geological Services, p. 73–78.

Gale, G.H. 2002. Geology of the New Britannia Mine, Snow Lake (NTS 63K16), Manitoba; in Report of Activities 2002, Manitoba Industry, Trade and Mines, Manitoba Geological Survey, p. 83–86.

Galley, A.G., Bailes, A.H., Syme, E.C., Bleeker, W., Macek, J.J. and Gordon, T.M. 1991.Geology and mineral deposits of the Flin Flon and Thompson belts, Manitoba (Field Trip 10); Geological Survey of Canada, Open File 2165, 8th IAGOD Symposium Field Trip Guidebook, 137 p.

Galley, A.G., Franklin, J.M. and Ames, D.E. 1988.Geological setting of gold mineralization, Snow Lake, Manitoba; Geological Survey of Canada, Open File 1700, scale 1:50 000.

Galley, A.G., Ziehlke, D.V., Franklin, J.M., Ames, D.E. and Gordon, T.M. 1986. Gold mineralization in the Snow Lake–Wekusko Lake region, Manitoba; in Gold in the Western Shield, A.L. Clark (ed.), Canadian Institute of Mining and Metallurgy, Special Volume 38, p. 379–398.

Harrison, J.M. 1949. Geology and Mineral Deposits of FileTramping Lakes area, Manitoba; Geological Survey of Canada Memoir 250, 92 p. Hogg, N. 1957: Nor-Acme mine; in Structural Geology of Canadian Ore Deposits, Volume II; Canadian Institute of Mining and Metallurgy, 6th Commonwealth Mining and Metallurgical Congress, p. 262–275.

Hogg, N. 1957. Nor-Acme Mine. Structural Geology of Canadian Ore deposits. Canadian Institute of Mining and Metallurgy. Sixth Commonwealth Mining and Metallurgical Congress, Vol. 2, pp.262-275.

Kraus, J. 1998. Structural and metamorphic studies in the Snow Lake area, Trans-Hudson Orogen, Manitoba, central Canada; Ph.D. thesis, University of New Brunswick, Fredericton, New Brunswick, 229 p.

Kraus, J., Menard, T., 1997. A thermal gradient at constant pressure: implications for low- to

medium-pressure metamorphism in a compressional tectonic setting, Flin Flon and Kisseynew domains, Trans-Hudson Orogen, central Canada. The Canadian Mineralogist 35, 1117–1136.

Kraus, J. and Williams, P.F. 1999. Structural development of the Snow Lake allochthon and its role in the evolution of the southeastern Trans-Hudson Orogen in Manitoba, central Canada; Canadian Journal of Earth Sciences, v. 36, p. 1881–1899.

Kraus, J. and Williams, P.F. 2001. A new spin on 'non-rotating' porphyroblasts: implications of cleavage refraction and reference frames. Journal of Structural Geology. v. 23, p. 963–971.

Lucas, S.B., Stern, R.A., Syme, E.C., Reilly, B.A. and Thomas, D.J. 1996. Intraoceanic tectonics and the development of continental crust: 1.92–1.84 Ga evolution of the Flin Flon Belt, Canada; Geological Society of America Bulletin, v. 108, p. 602–629.

Russell, G.A. 1957. Structural studies of the Snow Lake–Herb Lake area. Manitoba Mines and Natural Resources, Mines Branch, Publication 55-3.

Schledewitz, D.C.P. 1997. Squall Lake Project: geology and gold mineralization north of Snow Lake (NTS 63K/16NE); in Report of Activities 1997, Manitoba Energy and Mines, Geological Services, p. 79–83.

Schledewitz, D.C.P. 1998. Squall Lake Project: geology and mineralization in the area of Snow Lake and Squall Lake (NTS 63K/16NE); in Report of Activities 1998, Manitoba Energy and

Mines, Geological Services, p. 14–18.

Stewart, M., Lafrance, B., Gibson, H.L., 2018. Early thrusting and folding in the Snow Lake camp, Manitoba: Tectonic implications and their effects on volcanogenic massive sulphide deposits. Canadian Journal of Earth Sciences 55, 935–957.

Syme, E.C, Bailes, A.H. and Lucas, S.B. 1995. Geology of the Reed Lake area (parts of NTS 63K/9 and 10); in Report of Activities 1997, Manitoba Energy and Mines, Geological Services, Report of Field Activities, p. 42–60.

Syme, E.C., Bailes, A.H. and Lucas, S.B. 1996. Tectonic assembly of the Paleoproterozoic Flin Flon belt and setting of VMS deposits; Geological Association of Canada– Mineralogical Association of Canada, Joint Annual Meeting, Winnipeg, Manitoba, May 27–29, 1996, Field Trip Guidebook B1, 131 p.

Zwanzig, H.V. 1999. Structure and stratigraphy of the south flank of the Kisseynew Domain in the Trans-Hudson Orogen, Manitoba: implications for 1.845–1.77 Ga collision tectonics; in NATMAP Shield Margin Project, Volume 2, Canadian Journal of Earth Sciences, v. 36, p. 1859–1880.

Zwanzig, H.V., Bailes, A.H., 2010. Geology and geochemical evolution of the northern Flin Flon and southern Kisseynew domains, Kississing – File lakes area, Manitoba (parts of NTS 63K, N). Manitoba Innovation, Energy and Mines, Manitoba Geological Survey, Geoscientific Report

GR2010-1, pp. 1–135.

Chapter 2 - Evidence for voluminous, bimodal pyroclastic volcanism, during rifting of a Paleoproterozoic Arc at Snow Lake, Manitoba

2.1. Abstract

The thrust bounded McLeod Road - Birch Lake sequence (MB sequence) occurs within the Paleoproterozoic Snow Lake arc assemblage (SLA) of the Flin Flon Belt. Stratigraphic correlation of volcanic strata of the MB sequence with strata of the thrust bounded Chisel sequence, indicates that distinctive, submarine, eruption-fed, pyroclastic flow deposits are more extensive and voluminous than previously recognized (>10 km^3). These voluminous felsic pyroclastic deposits define a distinct magmatic and explosive volcanic event during bimodal volcanism that accompanied rifting of the Snow Lake arc. The felsic pyroclastic deposits define the remnants of a basin, or of nested basins, that formed during arc rifting and subsidence, and their eruption immediately preceded formation of the Chisel sequence volcanogenic massive sulphide (VMS) deposits. Although the Chisel sequence ore interval is recognized in the MB sequence, the lack of VMS-related alteration indicates that VMS hydrothermal activity was restricted to the Chisel portion of the basin. However, the MB sequence is host to the younger Snow Lake gold mine, a 1.4M oz. (43,699kg) gold producer. The overlying MORB-like Birch Lake Basalts, if conformable with the MB sequence, may represent a progression from a rifted-arc to a back-arc setting, however if thrust fault bounded they may represent the initial phases of arc-rifting, prior to the voluminous felsic pyroclastic eruptions. Correlation and integrity of stratigraphy between the thrust bounded MB and the SLA sequences indicates that the bounding

thrust faults, which developed during accretionary processes, have less regional significance than previously interpreted.

2.2. Key words

Snow Lake Arc assemblage, Flin Flon belt, Explosive submarine felsic volcanism, Rifting

VMS deposits

2.3. Introduction

The Snow Lake area is located within the eastern portion of the Flin Flon belt of northern Manitoba (Fig. 2-1), which lies in the southeastern portion of the Reindeer Zone of the Trans Hudson Orogen. The Paleoproterozoic Flin Flon belt is renowned for its base metal endowment and contains 29 volcanogenic massive sulphide (VMS) deposits (Bailes et al. 2013). The VMS deposits at Snow Lake occur in volcanic rocks of the SLA, which is host to 8 past -producing and 2 producing base metal mines (Fig. 2-2) (Stern et al. 1995a; Lucas et al. 1996; Bailes and Galley 1999). The SLA assemblage is divisible into three submarine volcanic sequences, which are interpreted to define an evolution from a primitive arc (Anderson sequence) to a mature arc (Chisel sequence) to an evolved arc-rift environment (Snow Creek sequence; Bailes and Galley 1996; Bailes 1997; Bailes and Schledewitz 1998) (Fig. 2-2).

Strata within a thrust bounded panel, which lies to the north of the SLA is herein named the McLeod Road – Birch Lake (MB) sequence (Fig. 2-2). It was interpreted as a homoclinal, north-facing sequence of mafic and felsic volcanic and volcaniclastic rocks, with no identified internal stratigraphy (Bailes and Schledewitz 1998; Bailes and Galley 1999), bound to the south by the

McLeod Road Thrust, and to the north by the Birch Lake fault (Fig. 2-3). The MB sequence has no known VMS deposits, but is host to four structurally controlled gold deposits located along stratigraphic contacts at the intersection of a fault and fold hinge in the hanging wall of the McLeod Road Thrust (Fig. 2-3). The largest gold deposit, the Nor-Acme, of the New Britannia Mine (renamed the Snow Lake Mine by QMX Gold Corporation in 2012), produced 1,404,950 oz. gold (43,699 kg) between 1949–1958 and 1995–2005 (Beaumont Smith and Lavigne 2008) (Fig. 2-3).

The structural geology of the MB sequence, regional structural history of the Snow Lake area and geochemistry of the SLA volcanic rocks, have been studied by numerous researchers (Harrison 1949, Hogg 1957; Russell 1957; Froese and Moore 1980; Bailes 1980; Bailes and Galley 1996, 1999; Bailes and Schledewitz 1998; Kraus 1998; Kraus and Williams 1999; Ansdell 2005; Connors 1996; and Zwanzig 1999; Beaumont-Smith and Gagné 2008). The setting and geological controls on gold mineralization at the Nor-Acme and associated deposits have been described by Hogg (1957), Galley et al. (1986, 1988, 1991); Fieldhouse (1999), Fulton (1999), Gale (2002), Beaumont-Smith and Lavigne (2008), and Gagné (2009).

A stratigraphy for the MB sequence has not been defined; however, Bailes and Schledewitz (1998), based on geochemical and lithological data, interpreted the MB sequence to be correlative with the Upper Chisel, and Snow Creek sequences of the SLA. They interpreted the MB sequence to comprise discontinuous lenses of mafic and felsic lavas, and volcaniclastic rocks, that lacked an internal stratigraphy, and the potential for VMS deposits was not discussed.

In this paper we: 1) present a new informal stratigraphy for the MB sequence, and provide evidence for previously unreported, voluminous submarine felsic and mafic explosive volcanism, and arguments for concomitant synvolcanic subsidence; 2) present a new lithostratigraphic correlation with strata of the Lower and Upper Chisel and Snow Creek sequences of the SLA and discuss implications for voluminous explosive eruptions that may link the thrust-bounded Chisel and MB sequences; and 3) discuss structural implications of the proposed correlation on accretionary processes.

2.4. Regional Geology

The Flin Flon Belt, which is in the internides of the Paleoproterozoic Trans Hudson Orogen represents a broad collision zone that formed during the closure of the Manikewan Ocean and ultimate formation of Laurentia (Hoffman 1988; Lucas et al. 1996). The Flin Flon Belt is bounded to the north by the Kisseynew Domain, and south by a Phanerozoic cover sequence. The Pikwitonei Granulite belt and the Superior Craton lie to the east and to the west lies the Rottenstone Domain, Wollaston fold belt and the Hearne Craton. The depositional setting of the Flin Flon Belt has been interpreted as a submarine environment, based on the remnants of ocean floor and island arc assemblages (ca.1.9 Ga) that differ in geochemistry, metamorphic grade and structural history (Lucas et al. 1996; Syme et al.1996). From east to west these are: - the SLA, the Amisk Collage, and the Hanson Lake Block (Lucas et al. 1996; Connors et al. 2002; Ansdell 2005). The younger metasedimentary rocks of the Kisseynew domain (ca. 1.86 – 1.84 Ga) are interleaved with the volcanic assemblages which were intruded by synvolcanic intrusions (ca. 1.89 – 1.88 Ga). The volcanic assemblages and the younger metasedimentary rocks were

intruded by later felsic plutons at ca 1.84 - 1.83 (Lucas et al. 1994; Stern et al. 1995a; Bailes and Galley 1996; David et al. 1996; Lucas et al. 1996; Connors 1996; Connors et al. 1999, 2002) (Fig. 1).

The Flin Flon Belt is interpreted to have formed in four stages: 1) formation of submarine arc and ocean floor assemblages at ca. 1.92 – 1.88 Ga, 2) intra-oceanic accretion at ca. 1.88–1.87 Ga, 3) ca. 1.87 – 1.84 Ga formation of submarine and subaerial inter - arc basins and successor arc plutons with deposition of the metasedimentary rocks of the Kisseynew domain, including the ca. 1.855 – 1.84 Ga Burntwood turbidites (Bailes 1980; Zwanzig 1990; David et al. 1996) and the ca. 1.845 – 1.835 Ga alluvial - fluvial sandstones of the Missi Group, (Ansdell and Connors 1995; Connors et al. 2002), and 4) terminal collision in the Trans Hudson Orogen at ca. 1.84–1.81 Ga (Lewry and Collerson 1990; Stern et al. 1995a; Lucas et al. 1996, Ansdell 2005). VMS deposits are interpreted to have formed during rifting of arc assemblages during stages 1 and 2 (Galley et al. 2007; Pehrsson et al. 2016) and gold deposits are interpreted to be pre (Fieldhouse 1999) – syn (Beaumont – Smith and Lavigne 2008) or post Stage 4 (Galley et al. 1988; 1991).

In the Amisk Collage, older crust is preserved as thrust-imbricated slices interleaved with juvenile arc and back-arc crust (David et al. 1996; Lucas et al. 1996, Syme et al. 1999). In the SLA there is a higher proportion of Archean crustal slices compared to the Amisk Collage, as demonstrated by εNd values that range from -0.4 to +2.4 for mafic volcanic rocks (Stern et al. 1992), and a U-Pb age of 2.65 to 2.82 Ga for inherited zircons in a 1.892 Ga rhyolitic breccia (David et al. 1996; Syme et al. 1999).

Juvenile, submarine arc assemblages (ca. 1.9 Ga) of the SLA are intruded by the Richards Lake and Sneath Lake synvolcanic intrusions 1.89 – 1.88 Ga) (David et al. 1996), and younger felsic plutons at ca 1.84 - 1.83 Ga (Connors 1996; David et al. 1996). The SLA is dominated by 1.84–1.81 Ga fold-thrust–style tectonics, and is interpreted to have been thrust over the Amisk Collage along the Morton Lake fault (Syme et al. 1995; Connors 1996, David et al. 1996; Ansdell et al. 1999; Zwanzig 1999; Bailes and Galley 1999). Late during this event at ca. 1.82 – 1.81 Ga (Froese and Moore 1980; David et al. 1996), the SLA underwent - amphibolite facies conditions with temperatures and pressures in the range 500 – 700 °C and 4-6 kbar, respectively (Zaleski et al. 1991; Menard and Gordon 1995; Kraus and Menard 1997).

2.5. Terminology

The term volcaniclastic is a descriptive term that refers to rocks composed primarily of volcanic components including lithic and vitric fragments and crystals and may encompass primary autoclastic, pyroclastic, and sedimentary deposits as originally defined by Fisher (1961). In interpreting volcaniclastic rocks, the term “primary” refers to a deposit that formed directly from an explosive eruption or is an in situ deposit produced through fragmentation (i.e. quench fragmentation - hyaloclastite) (Fisher, 1961; Gibson et al. 1999).

Syneruptive, as defined by McPhie and Allen (2003) includes deposits where primary clasts were transported and deposited following initial fragmentation (pyroclastic or autoclastic) and deposition; essentially primary deposits that were resedimented. However, it is often difficult to differentiate primary volcaniclastic deposits from syneruptive deposits, especially in ancient volcanic successions where the rocks have undergone significant

alteration, metamorphism and deformation (Cas et al. 1990; Cas and Wright 1991; Kano et al.1996; Gibson et al. 1999; Kano 2003; McPhie and Allen 2003; Allen and McPhie 2000, 2009; White 2000; White et al. 2003; Jutzeler et al. 2014). Recognizing these difficulties, the granulometric terminology proposed by Fisher (1961), based on the size and percentage of fragments and crystals, is used herein in a non-genetic sense to classify volcaniclastic deposits as proposed by Gibson et al. (1999), Busby et al. (2003) and White and Houghton (2006). In this terminology tuff represents a particle size of <2mm, lapilli 2-64mm, and blocks and bombs >64mm.

The term "unit" is used herein as an informal, mappable stratigraphic unit comprised of one or more depositional units that share distinct internal structures, textures or compositions that distinguishes them from bounding units. Lithofacies is an informal stratigraphic unit that has characteristic lithologic features (i.e. rock type).

2.6. Stratigraphy and Lithofacies of the McLeod Road – Birch Lake sequence

The MB sequence (Rubingh 2011, Rubingh et al. 2012a, b) which has been metamorphosed to amphibolite facies, contains 5 distinct lithostratigraphic units (Figs. 2-3, 2-4), with typical features of the units illustrated in (Figs. 2-5a – e). It is intruded by four mafic and two felsic intrusions, which are not described herein. The units are repeated by two bedding-parallel thrust faults, which subdivide the MB sequence into 3 structural panels (Rubingh et al. 2012a, b, Rubingh et al. 2013). The location of the lower thrust fault (Fig. 2-3) is inferred by the juxtaposition of unit 1 above younger unit 3. The upper thrust fault, called the Bounter Fault (Fig. 2-3) is associated with gold occurrences (Hogg 1957). It repeats units 1, 2 and 3. The

latter is locally marked by a single, aphyric felsic sill.

2.6.1. Unit 1: Heterolithic felsic volcaniclastic lithofacies

Lithology and Distribution

Unit 1 is repeated in all structural panels (Fig. 2-3) its maximum thickness is 450 m and its strike length is continuous for 3.5 km. The unit weathers to an orange/grey colour and is pale pink to pale yellow on fresh surface. It consists of heterolithic, plagioclase-porphyritic and lesser quartz-porphyritic felsic volcaniclastic rocks with distinctive, dark wispy fragments (Fig. 2-5a). The 4 volcaniclastic lithofacies are grouped as a single unit because they share the distinctive dark wispy fragments (Fig. 2-5a). The 4 volcaniclastic lithofacies are further subdivided into 13 depositional units based on bedforms and components (i.e. fragments, tuff, crystals), as described below, and as shown in Figure 2-4.

Lithofacies 1.1: Heterolithic volcaniclastic lithofacies with dominantly dark wispy fragments

Lithofacies 1.1 ranges from 110 to 410 meters in thickness along a strike length of 3.5 kilometers (Fig. 2-3). Round epidotized alteration patches are a common feature throughout this lithofacies. Its lower contact is sharp and in contact with a felsic intrusion. It comprises 6 depositional units (1a-1f) (Fig. 2-4), which have thicknesses of 25 to 45 meters.

Depositional units are defined by normal grading of mafic lithic and dark wispy fragments, and by an increase in fine tuff (ash sized component), which occurs towards the top of some beds

(1c and 1d, Fig. 2-4). The components, in variable amounts, comprising each of the depositional units are; i) tuff (< 2mm), ii) intact and broken plagioclase crystals (1 to 2 mm), iii) dark wispy fragments, iv) mafic lithic fragments, and v) plagioclase-porphyritic felsic fragments.

In the massive, block-rich base of depositional units, matrix tuff constitutes from 25 to 45% and it increases to greater than 60% in the upper portion of the depositional units, with units 1c and 1d (Fig. 2-4) having upper portions composed only of tuff over 2 meter intervals. The crystal content ranges from 5–12% feldspar and averages 8%. Dark wispy fragments (Fig. 2-5a) range in abundance from 10 – 45%, and consist entirely of biotite. The wispy fragments are markedly elongate (up to 15 cm min size), have length to width ratios of 15 to 1, and have irregular curved margins; in some only a relict ghost wispy dark outline remains. The wispy fragments are reversely graded in the upper, finer-grained portion of depositional units 1a, 1b, and 1d (Fig. 2-4).

Mafic lithic fragments consist of biotite and hornblende. They vary in size from 5 cm to 30 cm and in abundance from 0 - 20%. They do not show the same degree of elongation common to the dark wispy fragments, and have a blocky, angular appearance (Fig. 2-5a). Plagioclase-porphyritic felsic fragments in depositional unit 1f (Fig. 2-4) range in size from 3 to 7cm, are typically densely packed and framework supported (Fig. 2-4). The fragments are ellipsoid in shape, but do not exhibit the same degree of elongation as the dark wispy fragments.

Lithofacies 1.2: Heterolithic volcaniclastic lithofacies with dominantly quartz and feldspar

– porphyritic rhyolite breccias

Lithofacies 1.2 comprises 3 depositional units (h-j) (Fig. 2-4), ranges in thickness from 20 to 150 meters, and is continuous along strike for 3.0 kilometers. This lithofacies is dominated by a monomictic, coarse, framework supported, angular to subangular monolithic quartz and feldspar-porphyritic rhyolite breccia that is crudely bedded; the matrix tuff component ranges from 20 - 40 % in abundance. Fragments range from 20 – 60 cm in size and contain 8–15% quartz and 8–15% plagioclase feldspar crystals that are up to 10mm in size (Fig. 2-5b). Some beds contain dark wispy fragments, as described for lithofacies 1.1; however, the abundance of the dark wispy fragments is less than 15% and they are not observed in the densely packed fragment supported beds. The lower contact of this lithofacies was not observed.

Lithofacies 1.3: Heterolithic volcaniclastic lithofacies

Lithofacies 1.3 is 25 m thick, and comprises two depositional units (1k-l; Fig.2-4). Depositional unit 1k is massive, contains plagioclase- and quartz-porphyritic felsic fragments (25 – 40%), and plagioclase crystals (5-8%). Depositional unit 1l (Fig. 2-4), has plagioclase- and quartz-porphyritic fragments (50-60%), is framework supported, and contains plagioclase crystals (5-8%). The matrix tuff comprises up to 45% of both depositional units. The lower contact of lithofacies 1.3 is sharp and defined by a 30 cm thick bed of fine (<1/16mm) tuff.

Lithofacies 1.4: Monolithic quartz and feldspar-porphyritic volcaniclastic lithofacies

Lithofacies 1.4 is a single depositional unit that is framework supported, and contains 60-65%

subangular quartz- and feldspar-porphyritic fragments in a fine tuff matrix (25%) containing plagioclase and quartz crystals (10-15 %). The lower contact of lithofacies 1.4 is not exposed.

2.6.2. Unit 2: Felsic lavas and volcaniclastic lithofacies

Lithology and Distribution

This unit is repeated in 2 structural panels within the MB sequence (Fig. 2-3). It is continuous along strike for 3.7 kilometers and changes in thickness from 80 to 110 m. It comprises two, lithofacies: a lesser felsic volcaniclastic lithofacies (lithofacies 2.1), which defines depositional unit 2a and a plagioclase-porphyritic (1–5%) coherent felsic lithofacies (lithofacies 2.2), which defines 3 depositional units (2b – 2d) (Fig. 2-4). The unit weathers to a dark orange to grey color and is salmon pink to orange on fresh surfaces. The felsic groundmass contains 50-60 % quartz, 15 % feldspar, 3-5 % garnet, 5-8% biotite, 3-8% white mica.

Lithofacies 2.1: Felsic volcaniclastic lithofacies

The felsic lapillistone to lapilli tuffs contain quartz and feldspar-porphyritic felsic fragments that are similar to unit 1, lithofacies 1.4 and range in size from 2 to 5 cm. The lithofacies is crudely bedded, beds are matrix supported, and the matrix contains 10% feldspar crystals. The lower contacts with lithofacies 1.4 are not observed. At one locality, densely packed, jigsaw fit angular fragments and a fine, well bedded tuff (10cm thick), occur near the contact.

Lithofacies 2.2: Plagioclase-porphyritic rhyolitic lava

The coherent lithofacies contains lobe-like forms of massive rhyolite defined by a massive interior and margins that display a lobe-parallel "flow foliation" outlined by the alignment of biotite. The flow foliation imparts a banded appearance with bands 0.5-1.5 cm wide. The lobe margins grade into a breccia containing fragments identical to coherent rhyolite. The gradation is marked by in situ or jigsaw fit fragments that grade inwards into a massive coherent lobe and outwards into clast rotated breccia in contact with the lobes (Fig. 2-5c).

2.6.3. Unit 3: Mafic volcanic and volcaniclastic lithofacies

Lithology and distribution

Unit 3 is continuous along strike for 3.5 kilometers (Fig. 2-3) and ranges in thickness from 40 to 250 meters. It weathers to a dark green to grey green / black colour and is green/ grey on fresh surface. The dominant lithofacies include well-bedded, heterolithic, lapilli tuff, lapillistone to tuff breccia and lesser plagioclase-porphyritic pillowed lavas. Fragments are lapilli and block size, and fragment types include aphyric to plagioclase-porphyritic mafic, aphyric to plagioclase-porphyritic felsic, scoriaceous mafic, and plagioclase- and pyroxene-porphyritic mafic fragments. The matrix contains 50 –55% hornblende, 35 –40% plagioclase feldspar, 10 – 15% quartz, 5 – 8 % chlorite, 3 – 5% biotite, and 1% white mica. The unit is subdivided into seven lithofacies, which are, in turn divisible into 17 depositional units defined by changes in lithofacies (Fig. 2-4).

Lithofacies 3.1: Mafic tuff lithofacies

Lithofacies 3.1 comprises depositional unit 3a (Fig. 2-4), ranges in thickness from 0 – 30 meters, and extends along strike for 1 kilometer. It consists of mafic tuff to lapilli tuff containing plagioclase and up to 5% hornblende crystals, the latter are all after pyroxene (1 – 3mm in size). The lower contact with unit 2 is not observed.

Lithofacies 3.2: Heterolithic volcaniclastic lithofacies with scoriaceous fragments

Lithofacies 2 comprises 4 depositional units (3b – e; Fig. 2-4), ranges in thickness from 5–80 m, has a 3 kilometers strike length, and consists of well bedded, heterolithic lapillistone and tuff breccia, with lesser scoriaceous mafic fragments. It is intruded by basaltic sills. The rocks are framework- to matrix- supported, contain subangular to subrounded fragments of rhyolite (aphyric to feldspar-porphyritic) and subrounded mafic scoriaceous fragments (0.5 – 25 cm in size) in a finer, mafic tuff matrix containing <5% plagioclase crystals. Fragment elongation is approximately 6:1. Lapillistone beds are massive and moderately well bedded, 8 to 50 cm in thickness, as defined by changes in clast size and a decrease in the proportion of fragments to matrix towards the top of beds. Normal grading is common and indicates a consistent younging direction to the north. The lower contact with lithofacies 3.1 mafic tuffs is sharp.

Lithofacies 3.3: Plagioclase-porphyritic pillowed lithofacies

Lithofacies 3.3 is characterized by plagioclase-porphyritic pillow lava of depositional units 3f and 3k (Fig. 2-4). The pillow lavas range in thickness from 3–56 m over a strike length of 3 kilometers, and consist of densely packed pillows (Fig. 2-5d) with narrow thin aphanitic selvages. The pillows contain plagioclase (10%) and amphibole after pyroxene (10%) phenocrysts, and up to 25 % amygdules, which range in size from 0.3 to 1.5 cm and are located

in the center and top of the pillows. The lower contact was not observed.

Lithofacies 3.4: Well-bedded, crystal-rich mafic volcaniclastic lithofacies

Lithofacies 3.4 consists of mafic, plagioclase and amphibole after pyroxene crystal-rich (35 – 50 %; 1-3mm), well-bedded, crystal and crystal lapilli tuff and comprises depositional units 3g-i (Fig. 2-4). It ranges in thickness from 5 to 24 meters over a strike length of 3 kilometers. Beds are 0.3 to 1.5 meters thick. Normal grading is common, and thin beds of fine felsic tuff separate individual crystal-rich lapilli tuff beds; cross bedding within crystal rich beds was observed. The lower contact is not exposed.

Lithofacies 3.5: Monolithic scoriaceous bomb lithofacies

Lithofacies 3.5 is a framework- to matrix-supported, monolithic, scoriaceous breccia that comprises depositional unit 3j (Fig. 2-4). It has a strike length of 1 kilometer and a thickness of 4 to 10 meters. The breccia is monolithic and contains mafic, scoriaceous bombs (5% abundance) and scoriaceous clasts (40-45% abundance) within an amphibole after pyroxene – feldspar crystal rich (35 –40%) tuff matrix. The scoriaceous bombs (Figs. 2-6 a, b) are elliptical in shape and some display asymmetric tails. They contain 10-15% quartz and feldspar-filled amygdules, of which the coarser amygdules are distributed towards the center of the bombs and finer amygdules are localized towards the rims. The bombs which have intact chilled margins, indicate depression into the underlying beds, and the beds are locally reverse graded. Beds of tuff, 15 cm thick, with sharp contacts occur intermittently throughout this lithofacies. The lower contact is sharp and defined by a tuff bed, which is 15 cm thick.

Lithofacies 3.6: Dominantly felsic heterolithic volcaniclastic lithofacies

Lithofacies 3.6 is continuous along strike for 3 kilometers, ranges in thickness from 6–27 meters, and comprises depositional units 3l – n (Fig. 2-4). The lapillistone and tuff breccia are framework to matrix supported, and contain subangular to subrounded fragments of plagioclase-porphyritic rhyolite, mafic scoria and rare basaltic fragments in a pyroxene –feldspar crystal-rich (35– 45 %) matrix. Rhyolite fragments (2 - 40 cm) dominate and some subangular fragments exhibit jigsaw fit fractures. The rhyolite fragments contain 5% quartz-filled amygdules and 10% plagioclase phenocrysts. Mafic fragments (aphyric basalt and mafic scoria) comprise 3–5% of the fragment population; the fragments have a strong lineation, which is more pronounced than the foliation in the rock. Round epidote alteration patches up to 5 cm in diameter occur locally throughout the unit. Mafic bombs up to 30cm in size constitute 5% of the breccia. These mafic bombs are similar to those observed and illustrated in the Threehouse basalts of the SLA, as subsequently described and compared to Unit 3 of the MB sequence. The bed thickness ranges from 0.5 to 2 meters, where grading of beds is defined by variations in clast size; and the beds are normally graded. The lower contact is sharp.

Lithofacies 3.7: Dominantly mafic heterolithic volcaniclastic lithofacies

Lithofacies 3.7 has a strike length of 3 kilometers, ranges in thickness from 8 to 25 meters, and comprises depositional units 3o – q (Fig. 2-4). It consists of lapillistone with subrounded fragments of; i) fine-grained basalt, ii) plagioclase-porphyritic basalt, iii) aphyric basalt, iv) scoriaceous basalt, v) plagioclase-porphyritic rhyolite, and vi) aphyric rhyolite; 15% of the fragments (2-10 cm in size) are felsic. The fragments occur within a pyroxene –feldspar crystal rich (35 – 40%) tuff matrix. Graded beds, defined by variations in fragment size, range in

thickness from 1 to 2 meters. The lower contact is gradational, as defined by a decrease in the percentage of felsic rhyolite fragments and an increase in the percentage of mafic fragments.

2.6.4. Unit 4: Felsic lava lithofacies

Lithology and distribution

Unit 4 is a massive, aphyric, aphanitic coherent rhyolite (Figs. 2-4, 2-5e). The rhyolite ranges from 110 to 155 meters in thickness over a 4 kilometers strike length (Fig. 2-3). It weathers a dark grey to orange, and is salmon pink to light grey/white on fresh surfaces. The groundmass contains 60-70 % quartz, 5-10% feldspar, 10 % garnet, 5-8% biotite and 3-8% white mica. This rhyolite has a well-developed, spaced disjunctive cleavage defined by biotite, and a mineral stretching lineation defined by quartz, feldspar and garnet (Fig. 2-5e). A characteristic feature of the rhyolite is well-developed lobes that have a banded appearance along their margins reflecting different biotite content (Fig. 2-5f). The lobes are mantled by breccia containing fragments that are identical to coherent rhyolite. The rhyolite displays columnar jointing and contains rare quartz-filled amygdules (2 to 5 mm). The lower contact of the coherent rhyolite unit with mafic volcaniclastic rocks of unit 3, lithofacies 3.7, is sharp and highly strained.

2.6.5. Unit 5: Mafic volcaniclastic and lava lithofacies

Lithology and distribution

Unit 5 comprises mafic volcaniclastic and lava lithofacies, which comprise depositional units 5a and 5b, respectively (Fig. 2-4). It ranges from 45 to 90 meters in thickness over a 4 kilometer strike length). Unit 5 weathers to a dark black / brown to dark green and dark green on fresh

surfaces. The groundmass comprises 55-60% hornblende, 20-25% feldspar, 5-7% biotite, 5% quartz, 5% chlorite, and 3 - 5% white mica.

Lithofacies 5.1: Mafic volcaniclastic lithofacies

The distinguishing characteristic of this unit are coarse relict pyroxene crystals, replaced by amphibole, ranging in size from 0.5 to 1 cm (Fig. 2-5g). The unit consist of lapillistone and tuff breccia, which are distinct from mafic volcaniclastic rocks of unit 1 by their crystal-rich matrix of pyroxene and plagioclase and monolithic fragments of similar mineralogy and composition. The lower contact with the underlying coherent rhyolitic lavas (unit 5) is sharp and highly strained.

Lithofacies 5.2: Mafic lava Lithofacies

Pyroxene-plagioclase–porphyritic mafic lava (Fig. 2-5h) conformably overlies the crystal-rich, mafic pyroxene-plagioclase volcaniclastic lithofacies. The pillowed and massive lavas contain large (5 -10mm) pyroxene phenocrysts, replaced by amphibole. The pillows have thin selvages.

2.7. Geochemistry of the McLeod Road Birch Lake sequence

Samples collected are representative of all the stratigraphic units established during mapping. Forty-nine representative samples were selected for petrography, from which a subset of samples were submitted for geochemical and isotope analysis. Samples selected for geochemical analysis were carefully chosen to be i) free from significant alteration and ii) as homogeneous as possible. Samples submitted did not contain cracks, veins or voids. Where volcaniclastic rocks contained felsic and mafic clasts, areas within the units dominated by one of the clasts types were sampled.

Analytical techniques

Sample preparation was completed at the Ontario Geoscience Laboratories (Geoscience Laboratory), Sudbury, Ontario. The samples were crushed using mild steel, and pulverized using an agate ball mill, to reduce contamination by Cr, Fe and Al, although minor Si may be added to the sample. A closed beaker multi acid digest method, was used to achieve total dissolution. Major elements were determined by wavelength dispersive X ray fluorescence (XRF) spectrometry, on fused disks, with a borate flux, at the Geoscience Laboratory, and one sample batch was analyzed at Activation Laboratories. Analysis of minor and trace elements for all samples was performed using Inductively Coupled Plasma-Mass Spectrometry (ICP-MS) at the Geoscience Laboratory. The analytical procedures and quality assurance and quality control (QA/QC) used at the Geoscience Laboratory, are discussed in Burnham (2008).

Quality assurance and quality control

Accuracy was measured using international standards SY-4, BHVO-2, GSD-11, AGV-2 and NCS DC73304 (GBW 07106) at the Geoscience and Activation Laboratories, respectively. The majority of major, and trace elements analyzed from either laboratory are accurate to +/- 10%. The exceptions are Li, Rb, Ta, Nb, which are accurate within the range of >10% - <20%, and MgO, P_2O_5, and Sb which are accurate within the range of 20% to 23%. Na_2O is accurate to <48%.

Precision was measured by comparing duplicate analysis of a submitted sample that was powdered and then the powder re analyzed. The relative precision is better than 10%, for all

major and minor elements, except for Sn, Mo, Cd, and V, which are precise within the range of 10 % to 20%, BaO, Bi and P_2O_5, which are precise within the range 20% to 48% and Cr_2O_3 which has a precision of <84%. LOI has a precision of <5%, however one analysis has a precision of 37.2%.

Isotope geochemistry

Neodymium isotopic geochemistry was completed at the Pacific Centre for Isotopic and Geochemical Research (PCIGR), Department of Earth, Ocean and Atmospheric Sciences, the University of British Columbia, Vancouver, B.C. Samples were analyzed using a Nu1700 and a Nu Plasma MC-ICP-MS according to procedures outlined in Weiss et al. (2006). The reference materials G-3, JB-3, and Kil93, yielded $^{143}Nd/^{144}Nd$ ratios of 0.512244 (± 0.000006), 0.513069 (± 0.000006), and 0.512977(± 0.000006) respectively at 2 sigma deviation. The precision and the accuracy of Nd isotopic analyses were established relative to the JNdi-1 standard (Tanaka et al. 2000), and the Rennes standard, which have true values of $^{143}Nd/^{144}Nd$ = 0.512116 and an average value of $^{143}Nd/^{144}Nd$ of 0.512117 (n=15) +/- 0.000011 and $^{143}Nd/^{144}Nd$ 0.512051 (n=15) +/- 0.000020 (2SD). Neodymium isotopic compositions are normalized to $^{146}Nd/^{144}Nd$ = 0.7219, and initial epsilon (ε) Nd values are reported relative to a chondritic uniform reservoir (CHUR) with present-day values of $^{147}Sm/^{144}Nd$ = 0.1967 (Jacobsen and Wasserburg 1980) and $^{143}Nd/^{144}Nd$ = 0.512638 (Goldstein et al. 1984). Initial $^{143}Nd/^{144}Nd$ ratios and εNd values were calculated at 1890 Ma, which is the assumed age of all reported samples in the Snow Lake area (Stern et al. 1992).

Lead isotopic geochemistry was also performed at the PCIGR. Pb isotopes were measured

using a multiple collector inductively-coupled plasma mass spectrometer (MC-ICP-MS). Each isotope ratio of Pb (208, 207, 206 and 204) is measured with Tl (205 and 203), to monitor and correct for instrumental mass bias, following the procedures outlined in Weiss et al. (2006). Sample precision was achieved using the SRM981 standard (Todt et al. 1996), which has accepted Pb isotopic ratios of $^{206}Pb/^{204}Pb$ = 16.9356, $^{207}Pb/^{204}Pb$ = 15.4891, and $^{208}Pb/^{204}Pb$ = 36.7005. Analyses at the PCIGR measured Pb isotopic ratios relative to the standard. Average ratios for SRM981 are $^{206}Pb/^{204}Pb$ = 16.9430 = +/- 0.0007, $^{207}Pb/^{204}Pb$ = 15.4999 +/- 0.0007, and $^{208}Pb/^{204}Pb$ =36.7260 +/- 0.0018 (all corrected to 2 standard deviations).

2.8. Results

The geochemical data were normalized to 100% volatile free, and several geochemical filters were applied to select a least altered subset. Alteration was identified by loss on ignition values greater than 4.5wt. %, depletion in Na_2O values to less than 1 wt. %, Al_2O_3 / Na_2O ratios greater than 10 (Spitz and Darling 1978), the Chlorite Carbonate Pyrite Index, <15 or >85% (Large et al. 2001) and a Hashimoto index <20 or >65% (Ishikawa et al. 1976). Rare earth element (REE) mobility was evaluated using Ce, where Ce/Ce* (Ce sample / Ce interpolated) values that deviate from 1 are anomalous, and those within the range 0.9-1.1 are acceptable (Polat and Hoffman, 2003). Of the 39 samples analyzed, 14 did not meet the geochemical screens for alteration, and 5 were removed as they contained mixed clast types, leaving 20 samples for geochemical evaluation. On some of the geochemical plots, altered samples are included where only a few least altered representatives are available; these are displayed by light grey symbols. The trace element geochemistry for units 1 to 5 are:

contained in Tables 2-1 and 2-2, displayed in Figures 2-7, 2-8 and 2-9 and are described below. Their $\varepsilon Nd_{(1.9Ga)}$ and Pb isotopic data are contained in Table 2-3.

Unit 1: Heterolithic felsic volcaniclastic lithofacies

Unit 1 plots as rhyodacite – dacite on a Winchester and Floyd (1977)'s diagram; all samples have similar ratios of Zr /TiO_2 (Fig. 7a), but differ in their Nb/Y ratio. The four volcaniclastic lithofacies are divided into those containing black wispy fragments and those that do not (Figs. 2-8a and 2-9a). The trace element profiles for the wispy fragment lithofacies define a consistent trend on primitive mantle (Fig. 2-8a) and chondrite normalized plots (Fig. 2-9a) whereas profiles for the volcaniclastic lithofacies, without wispy fragments, show more variability. For example, one sample is relatively enriched in LREE, whereas another sample has a flatter REE profile (Fig. 2-9a); this variability may reflect differences in fragment types and or matrix.

The wispy fragment volcaniclastic lithofacies provides a consistent geochemical dataset that is used for comparison with other units. Wispy fragment volcaniclastic lithofacies are enriched in LREE and their profile is identical to that of the Powderhouse Dacite unit (Fig. 2-9a) with Nb/La mn = 0.40– 0.58 (mn, primitive mantle normalized) and negative Nb (Nb/Th mn = 0.21 –0.29) and Ti anomalies (Table 2-2; Fig. 2-8a). Chondrite normalized geochemical plots (Fig. 2-9a) display a slight negative Eu anomaly and flat consistent HREE patterns, which are similar to felsic units 2 and 4 (Figs. 2-9b and 2-9c). However, the wispy fragment volcaniclastic lithofacies have a steeper negative La /Yb (LREE) trend than other coherent rhyolitic lavas of the MB sequence (La /Yb ch =2.66 – 3.44; Table 2-2; Fig.

2-9a).

Unit 2: Felsic lavas and volcaniclastic lithofacies

Felsic volcanic and volcaniclastic rocks of unit 2 plot as rhyodacite – dacite on Fig. 2-7a. The felsic lavas of unit 2 have consistent trace element profiles compared to the volcaniclastics lithofacies (Fig. 2-8b, 2-9b). Felsic lavas and volcaniclastic lithofacies show a decrease in the LREE abundance, relative to unit 1, with slight negative Eu anomalies and flat HREE patterns (Fig. 2-9b). The Zr/Y and Nb/Y values are similar to those of unit 4 (Fig.2-8c), and are lower than those of unit 1. On a primitive mantle normalized plot, the felsic lavas display negative Nb (Nb/Th mn = 0.28 – 0.30; Nb/La mn = 0.27 – 0.45; Nb/Th mn = 0.28 – 0.30) and negative Ti anomalies (Table 2-2; Fig. 2-8b). On a chondrite normalized diagram, the felsic lavas display a moderately steep LREE trend; (La /Yb ch = 2.69– 3.11; Table 2-2; Fig. 2-9b).

Unit 4: Felsic lava lithofacies

Felsic lavas plot in a tight cluster within the rhyodacite/dacite field of Figure 2-7a and exhibit consistent trace element profiles (Fig. 2-8c, 2-9c). On primitive mantle normalized plots, felsic lavas display negative Nb (Nb/Th mn = 0.29 – 0.30; Nb/La mn = 0.35 – 0.36: Nb/Th mn = 0.29 – 0.30) and negative Ti anomalies (Table 2-2; Fig. 2-8c). On chondrite normalized plots (Fig. 2-9c) the felsic lavas are most similar to felsic lavas of unit 2 (Fig. 2-9b) as they display a slight negative Eu anomaly, and a flat HREE pattern, which are comparable to felsic units 1 and 2. On the chondrite normalized plot, the felsic lavas display a moderate slope of the LREE (La /Yb ch = 2.42 – 2.73; Table 2-2; Fig. 2-9c), which is

consistent with that displayed for units 2 and 1.

Mafic lavas and volcaniclastic lithofacies (units 3 and 5)

Altered mafic lavas and least altered and altered volcaniclastic lithofacies of unit 3 plot in the subalkaline basalt field of Fig. 2-7a, but exhibit a wide range of Zr/TiO_2 and Nb/Y ratios. The two least altered volcaniclastic samples plot as andesite/basalts. Altered and least altered mafic lavas of Unit 5 fall within the subalkaline basalt field of Fig. 2-7a; they have similar Zr/TiO_2 but different Nb/Y ratios. Basaltic lavas for unit 3 and 5 plot in the low Ti/ Island Arc Tholeiite and Boninite field on Shervais (1982)'s diagram (Fig. 2-7b).

Basaltic volcaniclastic rocks of unit 3 display a negative Nb anomaly (Nb/Th mn = 0.42– 0.43; Nb/La mn = 0.43 – 0.47) on primitive mantle normalized plots; and all samples display negative Ti anomalies (Table 2-2; Fig. 2-8d). Chondrite normalized patterns show a variable LREE enrichment (La /Yb ch = 2.43 – 2.62; Table 2-2: Fig. 2-9d). A basaltic lava from unit 5 displays a similar profile to unit 3 mafic volcaniclastic lithofacies, with negative Nb, Zr, and Ti anomalies on primitive mantle normalized plots (Table 2-2; Fig.2-8e). However, Chondrite normalized patterns for the unit 5 basaltic lavas have a flat profile, compared to the slight LREE enrichment (La /Yb ch = 1.38; Table 2-2: Fig. 2-9e) of unit 3 volcaniclastic rocks.

2.9. Discussion

Felsic, mafic and heterolithic volcaniclastic lithofacies comprise more than 60% of the 1.0 kilometers thick MB sequence. Rhyolitic lavas and basalt lithofacies and their associated breccias comprise less than 40% of the sequence. We will first address the origin and

mechanism of emplacement for lithofacies that define depositional units of the MB sequence, followed by a discussion of their geochemistry, a reconstruction of volcanic events, and will end with a comparison to strata that comprise the VMS-hosting Chisel Sequence. A primitive to more evolved marine arc setting for the SLA and MB has been proposed (Stern et al. 1995a, 1995b; Bailes and Galley 1996, 1999; David et al. 1996; Lucas et al. 1996; Bailes and Schledewitz 1998; Syme et al. 1996, 1999). Evidence that the MB sequence was emplaced into a subaqueous environment include: pillows in mafic lava, hyaloclastite, mass flow deposits, and planar cross bedding. None of these features have water depth implications, and cross bedding may indicate in situ reworking by bottom currents and is not evidence for shallow water. The 1 kilometer thickness of the MB sequence requires a water depth in excess of 1.2 kilometers to account for the lack of storm wave base bed forms (>200m) (Cas and Wright, 1991; Kano et al. 1996; Hudak et al. 2003; Kessel and Busby 2003; Cas et al. 2003; Busby 2005; Allen and McPhie 2009); however, water depth could have been much shallower if subsidence accompanied emplacement of the units.

Felsic Volcaniclastic Lithofacies

The most voluminous and widespread felsic volcaniclastic lithofacies is represented by the wispy fragment depositional units 1a to 1f, and 1i of unit 1 (Fig. 2-4). These are characterized by their dark wispy fragments and crystal-rich nature, and they are interpreted to be a product of explosive submarine eruptions. Interpreting a pyroclastic origin for deposits in ancient successions is difficult at best, as alteration, deformation and metamorphism can destroy or modify the delicate textures (e.g. Y-shaped shards, pumice), which are required to unequivocally identify explosive fragmentation and, along with other criteria, primary deposits.

This is particularly true for volcaniclastic deposits of the MB sequence, which have been deformed and metamorphosed to amphibolite facies, where arguments in support of an explosive origin must be based on larger textures and structures that can "survive" deformation and metamorphism, and are consistent with documented primary submarine volcaniclastic rocks.

Explosive fragmentation results in the formation of i) ash, ii) pumice/scoria, iii) lithic (rock) fragments, and iv) the liberation of crystals; the occurrence, and relative proportion of each is dependent, in part, on the explosivity of the eruption, magma composition, crystal content, and magmatic versus hydrovolcanic explosive fragmentation processes (Fiske, 1963). Felsic volcaniclastic lithofacies of unit 1 preserve components consistent with explosive fragmentation, these include lithic, crystal, and wispy fragments.

The distinctive, dark wispy fragments, which characterize the felsic volcaniclastic lithofacies display a pronounced elongation – flattening, which defines a bedding parallel foliation. The flattening is, in part, a product of deformation. However, the differential flattening of wispy fragments, as compared to adjacent lithic or scoriaceous fragments indicates that their flattening was, in part, pre-deformation. This is consistent with a pre-deformational phyllosilicate mineralogy, which would preferentially develop in glassy and vitric juvenile fragments, making them more susceptible to synvolcanic alteration, hydration, and flattening during submarine burial and compaction (e.g. Allen and Cas 1990; Gifkins and Allen 2001; McPhie and Allen 2003; Gifkins et al. 2005; Bull and McPhie 2007). The wispy nature of the fragments, and their characteristic delicate tails are consistent with altered and deformed

pumice (Gifkins and Allen 2001; Kessel and Busby 2003; Gifkins et al. 2005; Bull and McPhie 2007).

Crystals, principally feldspar and less commonly quartz occur within the dark wispy fragments (10 %), but are more concentrated within the tuff matrix where they comprise from 15 to 30 % of depositional units. The occurrence of feldspar and quartz crystals, in both wispy fragments and tuff matrix is consistent with a common magma source for both, and their greater concentration within the matrix, is consistent with crystal liberation during explosive fragmentation and concentration during transport and deposition.

Tuff comprises 30-70% of the Unit 1 volcaniclastic lithofacies and consists of a fine, <2mm in size, compositionally and mineralogically homogeneous assemblage of quartz and feldspar crystals with <1% mafic minerals and <30% feldspar, +/- quartz. Tuff is interpreted to represent original volcanic ash which, along with contained crystals, were produced by explosive fragmentation. Collectively, the association of wispy – pumice – fragments, lithic fragments, crystals, and matrix tuff is typical of pyroclastic deposits (Fiske and Matsuda 1964; Fisher and Schminke 1984; Kano et al. 1996; Gibson, et al. 1999). The compositional uniformity of Unit 1 felsic volcaniclastic rocks (Figs. 8a and 9a) indicates a single magmatic source, consistent with a primary pyroclastic origin for the deposits.

The internal organization of components and bedforms within the unit 1 depositional units mirrors those that were first described by Fiske (1963), Fiske and Matsuda (1964), Bond (1973), Yamada (1973), Niem (1977), Morton and Nebel (1984) and later by others (e.g., Kano 1996;

Gibson et al. 1999) for primary pyroclastic deposits produced by submarine, eruption-fed and water-supported pyroclastic flows (Figs. 2-10a and b, respectively). Both are characterized by a massive lithic –and crystal- rich base, which grades upwards into finer crystal and wispy –pumice- fragments, and ultimately into a predominantly finer ash-sized uppermost section that may display plane parallel beds. The flattened shape of the wispy fragments is consistent with hot deposition and welding, but can equally be attributed to an earlier primary compaction and subsequent tectonic deformation. Evidence of welding would have been destroyed by metamorphism and deformation.

The 13 depositional units of Unit 1 are interpreted to represent the successive emplacement of eruption-fed, submarine pyroclastic flows. The term submarine pyroclastic flow is used herein as the subaqueous equivalent of subaerial pyroclastic flows, where the former refers to water (gas) supported eruption-fed density currents, regardless of emplacement temperature (Fiske and Matsuda 1964; Kano 1996; Gibson et al. 1999, Hudak et al. 2003, Busby et al. 2003; White and Houghton 2006), and the latter refers to hot, gas supported eruption-fed density currents (Cas and Wright 1987; Stix 1991; McPhie et al. 1993).

Unit 1 represents a significant pyroclastic event(s). The deposits have a thickness of up to 400 meters, are continuous for 3.5 kilometers along strike, and have an estimated volume of approximately 5 cubic kilometers based on an estimated depth extent that is half of the strike extent (1.75 kilometers) and structural repetition within two fault panels. This volume is smaller than some subaqueous pyroclastic flows deposits. For example, the volume of pyroclastic flow deposits associated with subaerial calderas ranges from 10's – 1000's of cubic

kilometers, and the volume of submarine pyroclastic flow deposits associated with the collapse of the Archean Sturgeon Lake Caldera Complex, is estimated to range from 7 to 24 cubic kilometers (Hudak et al. 2003). The Mount Read pyroclastic deposits are more than 800 meters thick and extend 14 kilometers strike length (McPhie and Allen 2003). The large volumes associated with pyroclastic flow deposits are often interpreted to be the product of caldera forming eruptions (Scott et al. 2003; Wright et al. 2003). The estimated 5 km^3 volume for unit 1 pyroclastic flows suggests that synvolcanic subsidence was likely, but of unknown depth, size or shape.

Explosive, subaqueous magmatic pyroclastic eruptions are interpreted to be restricted to water depths less than 2000 meters due to the limiting effects of hydrostatic pressure on the critical pressure of water (Kokelaar 1986; Cas 1991; Gibson et al. 1999). This is supported by documented deeper water felsic pyroclastic fragmentation at around 1000 meters on the modern seafloor such as the Healy caldera, southern Kermadec arc, New Zealand (Wright and Gamble 1999; and Wright et al. 2003) and the Brothers caldera located to the northeast (Embley et al. 2012). There is evidence for pumice at depths > 2100 meters in extensional rift settings, such as the Woodlark and Manus Basins, of Papua New Guinea (Binns 2003). Studies of ancient deposits such as those of the Archean Sturgeon Lake Caldera by Hudak et al. (2003) and of the Bald Mountain caldera in northern Maine (Kessel and Busby 2003) indicate that pyroclastic eruptions can occur in deeper water settings (> 1.5 kilometers). Therefore, the wispy fragment depositional units of unit 1 (Fig. 2-4), suggest a maximum vent water depth of 2 km and a minimum water depth that was below storm wave base (>200 meters).

Monolithic tuff breccias of lithofacies 2, 3 and 4 of unit 1 (Fig. 2-4) have a higher crystal content and contain only sparse dark wispy fragments. They are not interpreted as resedimented, due to their lack of internal structure and thick monomictic clast supported beds; they are interpreted as primary dome collapse breccia deposits.

The higher crystal content of lithofacies 2, relative to lithofacies 1, is perhaps a result of derivation from a different magma (McPhie and Allen 2003). The sparse wispy fragments may indicate: i) that dome collapse occurred during pyroclastic eruptions, ii) that the wispy fragments were incorporated during transport from underlying pyroclastic flow, or iii) they were derived from pumiceous parts of a dome.

Mafic Volcaniclastic Lithofacies

Features that indicate a primary pyroclastic fragmentation for units 3 and 5 include i) mafic scoriaceous and fluidal bombs (e.g. depositional unit 3j, Figure 2-4, Figure 2-6a and b) characterized by amygdule-rich interiors, thin non-amgydaloidal crusts and equant bomb-like, to fluidal shapes, all typical of submarine fire fountain pyroclasts, which can form at water depths of >3000 meters (Gill et al. 1990; Cas et al. 2003), and ii) mafic bombs (depositional units 3l - n, Figure 2-4) that indent underlying beds, indicating pyroclastic fragmentation and ballistic emplacement in a shallower water environment (White et al. 2000).

Mafic volcaniclastic lithofacies of the MB sequence are divided into 2 types: 1) monomictic and 2) heterolithic. Monomictic volcaniclastic lithofacies, are interpreted as primary or syneruptive pyroclastic deposits, owing to their homogeneity (one provenance) and the bedded to massive

depositional units (e.g. depositional units 3a, and 3g-j, Figure 2-4). Heterolithic volcaniclastic deposits that contain mafic and felsic components indicate a dual provenance, which suggests re-sedimentation of unconsolidated deposits during active volcanism, consistent with syneruptive deposits (depositional units 3b – e and 3l – 3q, Figure 2-4).

Felsic and Mafic Lava Lithofacies

Felsic lava lithofacies of units 2 and 4 (Fig. 2-4) are interpreted as subaqueous rhyolitic lavas or domes. The difference between the coherent rhyolites is in their plagioclase crystal content. Characteristic features observed in the rhyolitic lavas include columnar joints and hyaloclastite, which occur at the margins of the lavas and indicate slow, steady cooling and quenching by seawater, respectively. Lobes, defined by amygdules and flow banding are typical features. Breccias at the margins of the lava lobes (Fig. 2-5c) which are of the same composition as the felsic lavas, and which transition into massive rhyolitic lavas through an in-situ breccia, are interpreted to be autobreccias. The rhyolitic lavas or domes are interpreted to have been erupted from intrabasinal vents.

The dominantly feldspar-porphyritic, pillowed basaltic lavas of depositional units 3f, 3k, (Fig. 2-4) indicate a submarine environment, and are evidence for intrabasinal effusive vents, which deposited pillowed basaltic lavas in-between heterolithic mass flow deposition. Pyroxene-porphyritic pillowed lavas of unit 5 (Fig. 2-5h) were emplaced following mass flow deposition. The overlying Birch Lake basalts consist of massive to pillowed aphyric lavas. The pillowed lavas have thin selvages, minimal hyaloclastite and quartz-rimmed gas cavities up to 12 cm in diameter, whereas the more massive lavas have a gabbroic textured interior (Bailes and

Schledewitz 1998).

The mafic and heterolithic volcaniclastic and rhyolitic and basaltic lava lithofacies were deposited in a below storm wave base, intrabasinal setting. There is no evidence of shallow water features, within or in the bounding lithofacies. The association of voluminous pyroclastic lithofacies (Unit1), rhyolitic lavas and domes, and basaltic lavas, and the compositional similarity of the felsic and mafic volcaniclastic rocks to their associated rhyolitic and basaltic lava lithofacies is consistent with a proximal volcanic environment and their derivation from submarine pyroclastic and effusive eruptions.

Tectonic Setting

Coherent felsic lavas and volcaniclastic lithofacies of Units 1 to 3 are all rhyodacite to dacite in composition (Fig. 2-7 a). Their ratios of La/Yb_{ch} (2.66-6.12) and Zr/Y (3.89-7.25), Yb (1.54 – 3.64 ppm) and Y (14.06-31.46) contents, flat HREE patterns, negative Eu anomalies, and weak LREE enrichment are typical of FIII-IV felsic volcanic rocks, as defined by Hart et al. (2004; Figs. 2-8 and 2-9; Tables 2-1 and 2-2); their depletion in high-field strength elements and the REE are consistent with FIV felsic volcanic rocks. Hart et al. (2004), interpreted FIII-IV felsic volcanic rocks to be a product of partial melting of hydrated mafic volcanic rocks at a shallow crustal level in a high-heat flow, rift environment. The negative Nb anomalies of the felsic volcanic rocks are consistent with rifting of a suprasubduction zone arc setting.

The mafic volcanic and volcaniclastic lithofacies (Fig. 2-7 a) have a tholeiitic affinity, and an island arc geochemical signature (Fig. 2-7 b). The mafic lavas and volcaniclastic lithofacies of

units 3 and 5 have higher contents of Th relative to Nb (Fig. 2-8 d-e), negative Nb and Zr anomalies, and low overall HREE contents on primitive-normalized plots (Fig.2-8 d-e), features that are consistent with subduction-related magmas formed within an oceanic arc setting (Gill 1981; Pearce 1983). The Birch Lake basalts (Fig. 2-8f) have a MORB-like geochemical signature, with no depletion of Nb relative to Th (Bailes and Schledewitz 1998).

Initial εNd values for coherent and primary mafic volcaniclastic lithofacies range from +2.0 to +3.8 (Table 2-3) which implies juvenile magmas within minimal contamination or contamination by a crust of similar age (Stern et al. 1992; Bailes and Galley 1999). The low εNd value of +0.7 obtained for the felsic sill within unit 1 (depositional unit, 1g, Fig. 2-4) may indicate contamination from an Archean crust with strongly negative εNd values, as suggested for the Stroud Breccia of the SLA by Stern (1992). The Pb reference isochron (Fig. 2-11a) for the basaltic lavas and volcaniclastic rocks lies between upper crust and model N-MORB isochrons (data from Kramers and Tolstikhin 1997), consistent with an end-member depleted mantle source and contamination by slab-derived fluids (and/or melts) or through sediment subduction (Stern et al. 1992). Recent work by Babechuk and Kamber (2011) and Kamber (2015) suggested alternatively that the depleted mantle curve of Kramers and Tolstikhin (1997) (Fig. 2-11a) may not be suitable for comparison with Paleoproterozoic rocks. The higher ^{207}Pb/^{204}Pb and ^{206}Pb/^{204}Pb values observed for the Flin Flon Arc assemblage and ocean floor rocks, may be an actual feature of the average depleted mantle in the Paleoproterozoic, arising from re-fertilisation of the depleted mantle after mixing with less depleted (lower) mantle (Babechuk and Kamber 2011).

The data plotted on a Th/Yb vs. Nb/Yb diagram together with other basaltic lavas and volcaniclastic rocks (Fig. 2-11 b) define a linear array that falls within the volcanic arc field and suggests crustal input via subduction processes or contamination by crust of similar age, to account for initial positive ƐNd values.

The geochemical signature, and Nd and Pb isotope data for the MB mafic volcanic rocks are consistent with a submarine, volcanic arc setting, as proposed for the SLA by Stern (1992); Bailes and Schledewitz (1998); Bailes and Galley, (1999). However, the bimodal nature of the volcanic rocks and associated subvolcanic intrusions (Bailes and Galley 1999), the FIII-IV geochemistry of the felsic volcanic rocks (Hart et al. 2004), and the presence of VMS deposits have been interpreted to indicate a rifted arc environment for the SLA by Bailes and Galley (1999), Galley et al. (2007), Bailes et al (2016) and Pehrsson et al. (2016).

The Birch Lake Basalts, which are inferred to lie structurally and stratigraphically above unit 5 of the MB sequence have a distinctive MORB signature indicating a change, or progression to, a back-arc tectonic setting.

Inferred Volcanic and Subsidence Events of the MB sequence

Thick successions of volcaniclastic rocks accumulate in topographic basins (Cas and Wright 1987). The MB sequence is interpreted to have been emplaced in a submarine basin that was undergoing subsidence during concomitant rifting and volcanism. The restricted strike length of depositional units 1f – 1m and 3k, as illustrated in Figure 2-12, may result from subsidence; however, these depositional units are dome collapse breccias and flows respectively, and may

have had a limited strike length. The limited extent of units such as the thinly bedded tuffs of unit 3a (Fig. 2-12), which would be expected to have had a more extensive distribution, may indicate lateral restriction due to subsidence. Thus, although the evidence for localized synvolcanic faulting and subsidence within a larger basin is not unequivocal, the large volume of Unit 1 deposits (5 cubic kilometers), their interpreted rapid emplacement by eruption-fed submarine pyroclastic flows, and location within a rifted arc tectonic environment are consistent with large scale subsidence, which is most clearly evident by the basin they occupy.

The change to MORB-like basaltic lavas of the Birch Lake Sequence marks the onset of back-arc type volcanism, which may represent a progression from the rifted arc environment interpreted for the MB sequence. However, the abrupt contact between the MB and Birch Lake sequences is not exposed and, although interpreted to be conformable (Bailes and Schledewitz 1998), it could be structural.

Stratigraphic Correlation with the SLA and Implications

The thrust bound MB and SLA sequences are separated by intervening clastic metasedimentary rocks of the Burntwood group, and collectively they constitute a west verging thrust fault panel (Fig. 2-2). The stratigraphy established for the MB sequence (Fig. 2-4 a) allows, for the first time, a lithostratigraphic correlation with volcanic units of the Lower and Upper Chisel sequence of the SLA (Figs. 2-2; 2-4 a, b). Bailes and Schledewitz (1998) proposed a correlation between the MB sequence and SLA based on the geochemical attributes of the units.

Stratigraphic correlation between strata of the MB and SLA is based on lithologic and, compositional similarities and mirrored cyclicity in explosive and effusive events as follows: 1) Voluminous felsic pyroclastic volcanism: Unit 1 with the Powderhouse Dacite, 2) Effusive felsic volcanism: Unit 2 and Unit 4 with the Chisel / Photo rhyolite, 3) Mafic pyroclastic volcanism: Unit 3 with the Threehouse and 4) Voluminous MORB-like effusive volcanism: Birch Lake Basalt with the Snow Creek Basalts, as illustrated in Fig. 2-4.

Unit 1 of the MB sequence and the Powderhouse Dacite of the SLA, share consistent physical characteristics such as the tuff-rich nature, crystal type and content, and occurrence of distinctive dark wispy "pumice" fragments and mafic lithic fragments; Fig. 2-13 a - d). On chondrite normalized plots the REE profile (Fig. 2-9a) of the Powderhouse Dacite is similar to that of Unit 1; both have negative Nb and Ti anomalies and a distinct slightly steeper LREE trend (Fig. 2-9a), compared to felsic units 2 and 4 (Fig. 2-9 b, c).

Unit 2 and 4 rhyolitic lavas are flow banded and have lobes and associated breccias (Fig. 2-5c), which are similar to those described for the Photo Lake / Ghost / Chisel and un-subdivided rhyolite of the SLA (Bailes 1996; Bailes and Schledewitz 1998). Their primitive mantle and chondrite normalized trace element profiles are also similar (Figs. 2-8b, 2-9b), with both characterized by negative Nb, Ti (Fig. 8b) and weak negative Eu anomalies and similar LREE enrichment (Fig. 2-9b) (Bailes and Galley 1996; Bailes 1997; Bailes and Galley 1999). However, rhyolites of the MB sequence do not have a negative Zr anomaly (Fig. 2-8b) and have a higher REE abundance. There is no comparable unit in the Chisel sequence to unit 4; however, it may be correlative with the undivided felsic lavas of the

Chisel sequence, which lie at the same interpreted stratigraphic position (Fig. 2-4).

Mafic volcaniclastic rocks of unit 3 and the Threehouse unit of the Chisel sequence (Fig. 2-4) are plagioclase and pyroxene crystal-rich (Fig. 2-13e, f), well bedded, and contain scoriaceous and amoeboid fragments and associated bomb sags (Fig. 2-13g, h). Their REE profiles on primitive mantle and chondrite normalized plots (Fig. 2-9d) are similar and both display negative Nb and Ti anomalies, although unit 3 has a minimal Zr anomaly and higher REE abundances. Unit 5 porphyritic basalts are similar to Threehouse basalts, in that they both display negative Nb, Zr, and Ti, anomalies, on mantle normalized plots (Fig. 2-8e; Bailes and Schledewitz 1998), implying an arc influence, and therefore unit 5 is considered to be analogous to the Chisel sequence.

The Birch Lake basalts are identical to basalts of the Snow Creek sequence of the SLA in their morphology and in their distinct MORB-like signature expressed as a relatively flat profile on primitive mantle normalized plots without negative Nb or Ti anomalies (Fig. 2-8f). Their position at the stratigraphic top of the MB and SLA sequences may indicate a change or progression to a back-arc basin or ocean floor geodynamic setting. However, the lower contacts of the Birch Lake and Snow Creek basalts are not exposed and may be structural. If so, the Birch Lake and Snow Creek Basalts are fault bounded and may have been thrust over the MB and SLA sequences.

The litho- and chemo-stratigraphic correlation between the MB and SLA sequences has implications for the interpretations presented herein. First, the pyroclastic deposits of Unit 1

and the Powderhouse Dacite, when combined, define the remnants of an originally much larger and more extensive pyroclastic deposit. Using the same methodology used to estimate a volume for Unit 1 pyroclastic deposits, the Powderhouse Dacite (units J16 and J11 of Bailes and Galley 2007) with a total strike length of 11.9 km and a total average thickness of 2.31 km, has an estimated volume of 6.2 km^3, and when combined with Unit 1, a total estimated volume of >10 km^3.

Second, this unique magmatic and pyroclastic event, characterized by voluminous pyroclastic deposits, occurred immediately prior to VMS formation in the Chisel Sequence. The proposed stratigraphic correlation places the Chisel VMS hosting ore interval (Engelbert, et al. 2014) within the MB sequence (Figs. 2-4 and 2-12). However, no significant VMS-related hydrothermal alteration or VMS mineralization has been found in the MB sequence, at least in surface exposures.

Third, the entire MB sequence is subaqueous, and is interpreted to have been erupted and deposited within a deeper water (below storm wave base) basin or subsidence structure within a larger rift environment. However, an interpreted shallower water, to intertidal environment for parts of the uppermost unit of the Upper Chisel sequence (the Threehouse; Bailes and Galley (1996) suggests that variable water depths occurred with a single common basin, or between nested basins within a larger rifted-arc setting. The VMS hydrothermal system was apparently confined to the Chisel basin.

Thrust faults identified within the Snow Lake area and Flin Flon Belt are of three orders of

magnitude: 1) thrusts which duplicate stratigraphy of the MB sequence, 2) thrusts which have juxtaposed the volcanic rocks and younger metasedimentary rocks of the Burntwood and Missi groups, McLeod Road Thrust, Birch Lake Fault, Snow Lake Fault (Fig. 2-2), and 2-3) regional scale faults, such as the Morton Lake Fault Zone (Fig. 3) (Syme et al. 1995; Lucas et al. 1996; Bailes and Schledewitz 1998), which separates the Snow Lake area from the central Flin Flon Belt and which bound different geodynamic environments and juxtapose different exotic terranes.

The correlation of stratigraphy and the reconstruction of a common volcanic edifice between thrust panels separated by the Snow Lake and McLeod Road Thrust Faults indicates that these thrust faults do not have regional-scale dislocation as the integrity of the volcanic stratigraphy is still in place. However, the Snow Lake Fault had been interpreted to have regional offset as it is interpreted to extend across the Flin Flon Belt as the Loonhead Lake Ductile fault (David et al. 1996; Connors 1996; Kraus and Williams 1998; Kraus and Williams 1999; Zwanzig 1999).

2.10. Conclusions

1. Voluminous felsic pyroclastic volcanism represents a unique magmatic and volcanic event during MB sequence volcanism, which may have been accompanied by localized subsidence within a larger submarine, rifted-arc setting. Felsic, mafic and heterolithic volcaniclastic, rhyolitic and basaltic lava lithofacies were deposited in a below storm wave base setting, as there is no evidence of shallow water features.

2. The compositional similarity of the bimodal felsic and mafic volcaniclastic rocks with equivalent lava lithofacies, is consistent with a proximal intrabasinal volcanic rift environment and derivation from submarine pyroclastic and effusive eruptions.

3. The MORB-like Birch Lake Basalts, if conformable with the MB sequence, may represent a progression from a rifted-arc to a back-arc setting. However, if the Birch Lake Basalts are thrust bounded, they may have been thrust over the MB sequence, in which case they could represent the initial phases of arc-rifting prior to voluminous pyroclastic eruption associated with Unit 1.

4. A new informal stratigraphy for the MB sequence and a stratigraphic correlation with strata of the Chisel sequence, indicates that Unit 1 pyroclastic deposits are more extensive, and of larger volume then previously recognized.

5. The hydrothermal environment of the MB sequence is different from the Chisel sequence. Stratigraphic correlation between the two sequences recognized the VMS interval in the MB sequence; however, it lacks the hydrothermal alteration assemblages that are typical of the Chisel Sequence VMS deposits.

6. During accretion some faults are major and juxtaposed different exotic terranes, whereas others resulted in duplexed stratigraphy and the interleaving of younger metasedimentary rocks with older volcanic rocks. In particular, correlation of individual volcanic complexes of the Chisel versus the MB sequence across structures such as the McLeod Road Thrust and

Snow Lake Fault, implies that movement on these faults was not as significant as previously interpreted.

2.11. Acknowledgments

Funding for the project was provided through a Collaborative Research and Development (CRD) grant, with the Natural Sciences and Engineering Research Council of Canada (NSERC), and QMX Gold Corporation. Additional funding for radiogenic isotope analysis, was provided by a Society of Economic Geologists Canada Research Foundation Grant (SEGCF). The Manitoba Geological Survey kindly provided full logistical field support, and field assistants: S. Kushner, C. Hanasyk, E. Reimer and E. Tetlock, whose enthusiastic assistance was invaluable in completion of the field work. The authors would like to thank S. Gagné for his support and advice and A. Bailes for their useful discussions both in and out of the field. We would also like to thank the QMX Gold Corporation geologist, D. Rigg, who supplied additional field support when required and provided useful discussions during the project.

2.12. References

Allen, R., 1988. False pyroclastic textures in altered silicic lavas, with implications for volcanic-associated mineralization. Economic Geology **83**: 1424–1446.

Allen, R., and Cas, R., 1990. The Rosebery controversy: distinguishing prospective ignimbrite-like units from true subaerial ignimbrites in the Rosebery–Hercules Zn–Cu–Pb massive sulphide district, Tasmania. 10th Australian Geological Convention. Geological Society of Australia

Abstracts, **25**: 31–32.

Allen, S.R., and McPhie, J., 2000. Water-settling and resedimentation of submarine rhyolitic pumice at Yali, eastern Aegean, Greece. Journal of Volcanology and Geothermal Research, **95**: 285–307. doi: 10.1016/S0377- 0273(99)00127-4.

Allen, S. R., and McPhie J. 2009. Products of Neptunian eruptions. Geology, **37**: 639–642.

Ansdell, K.M. 2005. Tectonic evolution of the Manitoba–Saskatchewan segment of the Paleoproterozoic Trans-Hudson Orogen, Canada. Canadian Journal of Earth Sciences, **42**: 741–759. doi:10.1139/e05-035.

Ansdell, K.M., and Connors, K.A. 1995. Geochemistry of mafic volcanic rocks, east Wekusko Lake, Manitoba. *In* Trans-Hudson Orogen Transect, Report of 5th Transect Meeting, 1995, Regina, Sask. *Edited by* Z. Hajnal and J. Lewry. Lithoprobe Report **48**: 198–205.

Ansdell, K.M., Connors, K.A., Stern, R., and Lucas, S.B. 1999. Coeval sedimentation, magmatism, and fold-thrust belt development in the Trans-Hudson Orogen: geochronological evidence from the Wekusko Lake area, Manitoba, Canada. Canadian Journal of Earth Sciences, **36**: 293–312.

Babechuk, M.G., Kamber, B.S, 2011. An estimate of 1.9 Ga mantle depletion usingthe high-field-strength elements and Nd–Pb isotopes of ocean floor basalts, FlinFlon Belt, Canada.

Precambrian Res. 189, 114–139.Bailes, A.H. 1980. Origin of Early Proterozoic volcaniclastic turbidites, south margin of the Kisseynew sedimentary gneiss belt. Precambrian Research, **12**: 197–225.

Bailes, A. H. 1997. Geochemistry of Paleoproterozoic volcanic rocks in the Photo Lake area, Flin Flon Belt (parts of NTS 63 K/16). *In* Manitoba Energy and Mines, Mineral Resources Division, Report of Activities, 1997, pp. 61-62.

Bailes, A. H., and Galley, A. G. 1996. Setting of Paleoproterozoic volcanic-hosted massive base metal sulphide deposits, Snow Lake, Manitoba. *In* EXTECH I: a multidisciplinary approach to massive sulphide research in the Rusty Lake– Snow Lake greenstone belts, Manitoba. *Edited by* G. F. Bonham- Carter, A. G. Galley and G. E. M. Hall. Geological Survey of Canada, Bulletin 426, pp. 105–138.

Bailes, A.H., and Galley, A.G. 1999. Evolution of the Paleoproterozoic Snow Lake arc assemblage and geodynamic setting for associated volcanic-hosted massive sulphide deposits, Flin Flon Belt, Manitoba Canada. Canadian Journal of Earth Sciences, **36**:1789–1805.

Bailes, A.H., and Galley, A.G. 2007. Geology of the Chisel–Anderson lakes area, Snow Lake, Manitoba (NTS areas 63K16SW and west half of 63K13SE); Manitoba Science, Technology, Energy and Mines, Manitoba Geological Survey, Geoscientific Map MAP2007-1, scale1:20000, map plus notes.

Bailes, A.H., and Schledewitz, D.C.P. 1998. Geology and geochemistry of the Paleoproterozoic volcanic rocks between the McLeod Road and Birch Lake faults, Snow Lake area, Flin Flon belt (parts of NTS 63K/16 and 63J/13). In Manitoba Energy and Mines, Geological services, Report of Activities, 1998, pp. 4 -13.

Bailes, A., Rubingh, K., Gagné, S., Taylor, C., Galley, A., Bernaeur, S. and Simms, D. 2013. Volcanological and Structural Setting of Paleoproterozoic VMS and Gold deposits at Snow Lake, Manitoba; Geological Association of Canada–Mineralogical Association of Canada Joint Annual Meeting, Field Trip Guidebook FT-A2. Manitoba Innovation, Energy and Mines, Manitoba Geological Survey, Open File Report OF2013-3, pp. 1 - 73.

Bailes, A.H., Galley, A.G., Paradis, S., and Taylor, B.E., 2016. Variations in Large Synvolcanic Alteration zones at Snow Lake, Manitoba, Canada, with Proximity to Associated Volcanogenic Massive Sulphide Deposits. Economic Geology, **111**: 933 – 962.

Beaumont-Smith, C. J., and Gagné, S. 2008. Structural geology of the Snow Lake–Squall Lake area, Manitoba (parts of NTS 63K16, 63J13); Manitoba Science, Technology, Energy and Mines, Manitoba Geological Survey, Preliminary Map PMAP2008-1, scale 1:20 000.

Beaumont-Smith, C.J., and Lavigne, J. 2008. Structural geology and gold metallogenesis of the New Britannia Mine area, Snow Lake, Manitoba (NTS 63K16). In Report of Activities 2008, Manitoba Science, Technology, Energy and Mines, Manitoba Geological Survey, pp. 7–17.

Binns, R. A. 2003. Deep marine pumice from the Woodlark and Manus basins, Papua New Guinea. *In* Explosive subaqueous volcanism. *Edited by* J.D. White, J.L. Smellie and D.A. Clague: American Geophysical Union, Geophysical Monograph Series. Vol. **140**, pp. 329-343.

Bond, G.C., 1973. A late Paleozoic volcanic arc in the eastern Alaska Range, Alaska. Journal of Geology, **81**: 557 – 575.

Bull, K.F., and McPhie, J. 2007. Fiamme textures in volcanic successions: Flaming issues of definition and interpretation. Journal of Volcanology and Geothermal Research **164**: 205 – 216.

Burnham, O.M. 2008. Trace element analysis of geological samples by inductively coupled plasma mass spectrometry (ICP-MS) at the Geoscience Laboratories: Revised capabilities due to method improvements. *In* Summary of field work and other activities. Ontario Geological Survey, Open File Report 6226. pp. 38-1 – 38-10.

Busby, C.J. 2005. Possible distinguishing characteristics of very deepwater explosive and effusive silicic volcanism. Geology, **33**: 845–848. doi: 10.1130/G21216.1.

Busby, C. J., Kessel, L., Schulz, K. J., Foose, M. P., and Slack, J. F. 2003. Volcanic setting of the Ordovician Bald Mountain massive sulphide deposit, northern Maine. Massive Sulphide Deposits of the Bathurst Mining Camp, New Brunswick, and Northern Maine.

Economic Geology Monograph, **11**: 210-244.

Cas, R. A. F. 1992. Submarine volcanism; eruption styles, products, and relevance to understanding the host-rock successions to volcanic-hosted massive sulphide deposits. Economic Geology, **87**: 511-541.

Cas, R.A.F., and Wright, J.V.1987. Volcanic Successions: Modern and Ancient. A geological approach to processes, products and successions. Chapman and Hall. Allen and Unwin

Cas, R.A.F., and Wright, J.V. 1991. Subaqueous pyroclastic flows and ignimbrites: an assessment. Bulletin of Volcanology, **53**: 357-380.

Cas, R.A.F., Allen, R.F., Bull, S.W., Clifford, B.A., and Wright, J.V. 1990. Subaqueous, rhyolitic dome-top tuff cones: A model based on the Devonian Bunga Beds, southeastern Australia and a modern analogue. Bulletin of Volcanology, **52**: 159–174. doi:10.1007/BF00334802.

Cas, R.A.F., Yamagishi, H.M., Moore, L., and Scutter, C. 2003. Miocene submarine fire fountain deposits, Ryugazaki Headland, Oshoro Penninsula, Hokkaido, Japan: Implications for submarine fire fountain dynamics and fragmentation processes. *In* Explosive subaqueous volcanism. *Edited by* J.D. White, J.L. Smellie and D.A. Clague: American Geophysical Union, Geophysical Monograph Series. Vol. **140**, pp. 299-316.

Connors, K.A., 1996. Unravelling the boundary between turbidites of the Kisseynew belt and volcano-plutonic rocks of the Flin Flon belt, Trans-Hudson Orogen, Canada; Canadian Journal of Earth Sciences, **33**: 811–829.

Connors, K.A., Ansdell, K.M., and Lucas, S.B. 1999. Coeval sedimentation, magmatism, and fold-thrust development in the Trans- Hudson Orogen: propagation of deformation into an active continental arc setting, Wekusko Lake area, Manitoba. Canadian Journal of Earth Sciences, **36**: 275–291.

Connors, K.A., Ansdell, K.M., and Lucas, S.B. 2002. Development of a transverse to orogen parallel extension lineation in a complex collisional setting, Trans-Hudson Orogen, Manitoba, Canada. Journal of Structural Geology, **24**: 89–106.

David, J., Bailes, A.H. and Machado, N. 1996. Evolution of the Snow Lake portion of the Paleoproterozoic Flin Flon and Kisseynew belts, Trans-Hudson Orogen, Manitoba Canada. Precambrian Research, **80**: 107–124.

Embley, R. W., de Ronde, C. E. J., Merle, S. G., Davy, B., and Tontini, F. C. (2012). Detailed morphology and structure of an active submarine arc caldera: Brothers volcano, Kermadec arc. Economic Geology, **107**: 1557-1570.

Engelbert, M.S., Friesen, V., Gibson, H.L., and Lafrance, B.2014. Volcanic reconstruction of the

productive VMS ore interval in the Paleoproterozoic Chisel sequence, Snow Lake, Manitoba. Geological Association of Canada – Mineralogical Association of Canada (GAC-MAC) Annual Meeting.

Fieldhouse, I. 1999. Geological setting of gold mineralization in the vicinity of the New Britannia mine, Snow Lake, Manitoba; M.Sc. thesis, University of Manitoba, Winnipeg, Manitoba.

Fisher, R.V., 1961. Proposed classification of volcaniclastic sediments and rocks. Geological Society of America Bulletin, **72**: 1409-1414.

Fisher, R.V., and Schmincke, H.-U. 1984. Pyroclastic Rocks; Springer-Verlag Berlin, Heidelberg, New York and Tokyo.

Fiske, R. S. 1963. Subaqueous pyroclastic flows in the Ohanapecosh Formation, Washington. Geological Society of America Bulletin, **74**: 391- 406.

Fiske, R.S., and Matsuda, T. 1964. Submarine equivalents of ash flows in the Tokiwa formation, Japan. American Journal of Science, **262**: 76-106.

Fiske, R.S., Naka, J., Iizasa, K., Yuasa, M., Klaus, A. 2001. Submarine silicic caldera at the front of the Izu-Bonin arc, Japan: Voluminous seafloor eruptions of rhyolite pumice. Geological Society of America Bulletin, **113**: 813-824.

Friesen, V., Engelbert, M., DeWolfe, M., and Gibson, H.L., 2015. Volcanic reconstruction of the Powderhouse Dacite in the Paleoproterozoic VMS hosting Chisel Sequence, Snow Lake, Manitoba. In, Program with Abstracts, GAC/MAC/AGU Joint-Annual Meeting, Montreal.

Froese, E. and Moore, J.M. 1980. Metamorphism in the Snow Lake area, Manitoba; Geological Survey of Canada, pp. 78-27.

Fulton, P.J. 1999. Distribution of gold mineralization at the New Britannia mine in Snow Lake, Manitoba: implications for exploration and processing; M.Sc. thesis, University of Manitoba, Winnipeg, Manitoba.

Gagné, S. 2009. Geological investigation of the McLeod Road- Birch Lake allochthon east of Snow Lake, Manitoba (part of NTS 63J13). *In* Report of Activities 2009, Manitoba Innovation, Energy and Mines, pp. 58–68.

Gale, G.H. 2002. Geology of the New Britannia Mine, Snow Lake (NTS 63K16), Manitoba. *In* Report of Activities 2002, Manitoba Industry, Trade and Mines, pp. 83–86.

Galley, A.G., Ziehlke, D.V., Franklin, J.M., Ames, D.E. and Gordon, T.M. 1986. Gold mineralization in the Snow Lake-Wekusko Lake region, Manitoba. In Gold in the Western Shield. *Edited by* L.A. Clark, The Canadian Institute of Mining and Metallurgy Special Volume **38**, pp. 379-398.

Galley, A.G., Ames, D.E. and Franklin, J.M. 1988. Geological setting of gold mineralization, Snow Lake, Manitoba; Geological Survey of Canada, Open File 1700, annotated 1:5000 map.

Galley, A.G., Bailes, A.H., Syme, E.C., Bleeker, W., Macek, J.J. and Gordon, T.M. 1991. Geology and mineral deposits of the Flin Flon and Thompson belts, Manitoba (Field Trip 10); Geological Survey of Canada, Open File 2165, 8th IAGOD Symposium Field Trip Guidebook.

Galley, A.G., Syme, E.C., and Bailes, A.H., 2007, Metallogeny of the Paleoproterozoic Flin Flon Belt, Manitoba and Saskatchewan. *In* Mineral Deposits of Canada: A Synthesis of Major Deposit Types, District Metallogeny, the Evolution of Geological Provinces, and Exploration Methods. *Edited by* G.D. Goodfellow. Geological Association of Canada. Mineral Deposits Division, Special Publication No. 5, pp. 509-531.

Gibson, H.L., Morton, R.L., and Hudak, G.J. 1999. Submarine volcanic processes, deposits and environments favorable for the location of volcanic-hosted massive sulphide deposits. *In*, Volcanic-Associated Massive Sulphide Deposits: Processes and Examples in Modern and Ancient Settings. *Edited by* C.T. Barrie and M. D. Hannington. Reviews in Economic Geology, **8**, pp. 13-51.

Gifkins, C., Allen, R., 2001. Textural and chemical characteristics of diagenetic and hydrothermal alteration in glassy volcanic rocks; examples from the Mount Read Volcanics.

Economic Geology, **9**: 973–1002.

Gifkins, C., Allen, R., McPhie, J. 2005. Apparent welding textures in altered pumice-rich rocks. Journal of Volcanology and Geothermal Research, **142:** 29–47.

Gill, J.B., 1981. Orogenic Andesites and Plate Tectonics. Springer-Verlag, Berlin, Heidelberg, and New York.

Gill, J., Torssander, P., Lapierre, H., Taylor, R., Kaiho, K., Koyama, M., and Fujioka, K. 1990. Explosive deep water basalt in the Sumisu backarc rift. *Science*, **248**:1214-1217.

Goldstein, R.L., O'nions, R.K., and Hamilton, P.J. 1984. A Sm–Nd isotopic study of atmospheric dusts and particulates from major river systems. Earth and Planetary Science Letters, **70**: 221– 236. doi:10.1016/0012-821X(84)90007-4.

Harrison, J.M. 1949**.** Geology and mineral deposits of File - Tramping Lakes area, Manitoba. Geological Survey of Canada, Memoir 250, pp.92

Hart, T.R., Gibson, H.L., and Lesher, C.M., 2004. Trace Element Geochemistry and Petrogenesis of Felsic Volcanic Rocks associated with Volcanogenic Massive Cu-Zn-Pb Sulphide Deposits. Economic Geology, **99**: 1003 – 1013.

Hoffman, P. F. 1988. United Plates of America, the birth of a craton-Early Proterozoic

assembly and growth of Laurentia. Annual Review of Earth and Planetary Sciences, **16**: 543-603.

Hogg, N. 1957. Nor-Acme Mine. Structural Geology of Canadian Ore deposits. Canadian Institute of Mining and Metallurgy. Sixth Commonwealth Mining and Metallurgical Congress, Vol. 2, pp.262-275.

Hudak, G.J., Morton, R.L., Franklin, J.M., Peterson, D.M. 2003. Morphology, Distribution, and Estimated Eruption Volumes for Intracaldera Tuffs Associated With Volcanic-Hosted Massive Sulphide Deposits in the Archean Sturgeon Lake Caldera Complex, Northwestern Ontario. *In* Explosive subaqueous volcanism. *Edited by* J.D. White, J.L. Smellie and D.A. Clague. American Geophysical Union, Geophysical Monograph Series. Vol. **140**, pp. 345-359.

Ishikawa, Y., Sawaguchi, T., Iwaya, S., and Horiuchi, M., 1976, Delineation of prospecting targets for Kuroko deposits based on modes of volcanism of underlying dacite and alteration halos (in Japanese with English abs.). Mining Geology, **26**: 105–117

Jacobsen, H.B., and, Wasserburg, G.J. 1980. Sm–Nd isotopic evolution of chondrites. Earth and Planetary Science Letters, **50**: 139–155.

Jutzeler M, McPhie J, Allen SR. 2014. Submarine eruption-fed and resedimented pumice-rich facies: the Dogashima Formation (Izu Peninsula, Japan). Bulletin of Volcanology **76**: 867. doi 10.1007/s00445-014-0867-x

Kamber, B.S. 2015. The evolving nature of terrestrial crust from the Hadean, through the Archaean, into the Proterozoic. Precambrian Research, **258**: 48-52.

Kano, K. 1996. A Miocene coarse volcaniclastic mass-flow deposit in the Shimane Peninsula, SW Japan: product of a deep submarine eruption? Bull Volcanology **58**:131–143. doi:10.1007/s004450050131

Kano, K. 2003. Subaqueous pumice eruptions and their products. *In* Explosive subaqueous volcanism. *Edited by* J.D. White, J.L. Smellie and D.A. Clague. American Geophysical Union, Geophysical Monograph Series. Vol. **140**, pp. 213-230.

Kano, K., Yamamoto, T., and Ono, K. 1996. Subaqueous eruption and emplacement of the Shinjima Pumice, Shinjima (Moeshima) Island, Kagoshima Bay, SW Japan. Journal of Volcanology and Geothermal Research, **71**: 187– 206, doi: 10.1016/0377- 273(95)00077-1.

Kessel, L.G., Busby, C.J. 2003. Analysis of VHMS-Hosting Ignimbrites Erupted at Bathyal Water Depths (Ordovician Bald Mountain Sequence, Northern Maine). *In* Explosive subaqueous volcanism. *Edited by* J.D. White, J.L. Smellie and D.A. Clague. American Geophysical Union, Geophysical Monograph Series. Vol. **140**, pp. 361-378.

Kokelaar, P. 1986. Magma-water interactions in subaqueous and emergent basaltic. Bulletin of Volcanology, **48**: 275-289.

Kramers, J. D., and I. N. Tolstikhin. 1997. Two terrestrial lead isotope paradoxes, forward transport modelling, core formation and the history of the continental crust. Chemical Geology, **139**: 75-110.

Kraus, J. 1998. Structural and metamorphic studies in the Snow Lake area, Trans-Hudson Orogen, Manitoba, central Canada; Ph.D. thesis, University of New Brunswick, Fredericton, New Brunswick.

Kraus, J. and Menard, T. 1997. A thermal gradient at constant pressure: implications for low- to medium-pressure metamorphism in a compressional tectonic setting, Flin Flon and Kisseynew domains, Trans-Hudson Orogen, central Canada. The Canadian Mineralogist, **35:** 1117–1136.

Kraus, J. and Williams, P.F. 1999. Structural development of the Snow Lake allochthon and its role in the evolution of the southeastern Trans-Hudson Orogen in Manitoba, central Canada. Canadian Journal of Earth Sciences. **36**: 1881–1899.

Large, R.R., Gemmell, J.B., Paulick, H., and Huston, D., 2001. The alteration box plot: A simple approach to understanding the relationship between alteration mineralogy and lithogeochemistry associated with VHMS deposits, Economic Geology **96**: 957–972.

Lewry, J.F. and Collerson, K.D. 1990. The Trans-Hudson Orogen: extent, subdivisions and problems. *In* The Early Proterozoic Trans-Hudson Orogen of North America. *Edited by* J. F.

Lewry and M.R. Stauffer. Geological Association of Canada, Special Paper 37, pp. 1-14.

Lucas, S.B., Stern, R.A., Syme, E.C., Reilly, B.A. and Thomas, D.J. 1996. Intraoceanic tectonics and the development of continental crust: 1.92–1.84 Ga evolution of the Flin Flon Belt, Canada. Geological Society of America Bulletin, **108**: 602–629.

McPhie, J., Allen, R.L. 2003. Submarine, Silicic, Syn-Eruptive Pyroclastic Units in the Mount Read Volcanics, Western Tasmania: Influence of Vent Setting and Proximity on Lithofacies Characteristics. *In* Explosive subaqueous volcanism. *Edited by* J.D. White, J.L. Smellie and D.A. Clague. American Geophysical Union, Geophysical Monograph Series. Vol. **140**, pp. 245-258.

Morton, R.L., and Nebel, M., 1984, Hydrothermal alteration of felsic volcanic rocks at the Helen siderite deposit, Wawa, Ontario. Economic Geology, **79**: 1319 – 1333.

Niem, A. R., 1977. Mississipian pyroclastic flow and ash – fall deposits in the deep-marine Ouachita flysch basin, Oklahoma and Arkansas. Geological Society of America Bulletin, **88**: 49 – 61.

Pearce, J.A. 1983: Role of the subcontinental lithosphere in magma genesis at active continental margins. *In* Andesite. *Edited by* R.S. Thorpe. J. Wiley and Sons, Chichester, pp. 525-547.

Pearce, J.A. 2008. Geochemical fingerprinting of oceanic basalts with applications to ophiolite classification and the search for Archean oceanic crust. Lithos, **100**: 14–48. doi:10.1016/j.

lithos.2007.06.016.

Pehrsson, S., Gibson, H.L., and Gilmore, K., 2016. A special issue on volcanogenic massive sulphide deposits of the Trans-Hudson Orogen. Economic Geology, **111**: 803-816.

Polat, A., and Hoffman, A.W. 2003. Alteration and geochemical patterns in the 3.7-3.8 Ga Isua greenstone belt, West Greenland. Precambrian Research, **126**:197–218.

Rubingh, K.E 2011. Stratigraphy of the McLeod Road–Birch Lake thrust panel, Snow Lake, west-central Manitoba (parts of NTS 63K16 and 63J13). *In* Report of Activities, 2011 Manitoba Innovation, Energy and Mines, 2011, pp. 68–78.

Rubingh, K.E., Lafrance, B., Gibson, H.L. and Gagné, S. 2012a. Preliminary lithostratigraphic map of the McLeod Road– Birch Lake thrust panel, Snow Lake, west-central Manitoba (parts of NTS 63K16, 63J13). *In* Report of Activities 2012a, Manitoba Innovation, Energy and Mines, Preliminary Map PMAP2012-7, 1:5000 scale.

Rubingh, K.E., Lafrance, B. and Gibson, H.L. 2012b. Lithostratigraphy and structural geology of the McLeod Road–Birch Lake thrust panel, Snow Lake, west-central Manitoba (parts of NTS 63K16, 63J13). *In* Report of Activities 2012b, Manitoba Innovation, Energy and Mines, pp. 104–114.

Rubingh, K.E., Lafrance, B. and Gibson, H.L. 2013. Structural analysis of the McLeod Road-

Birch Lake thrust panel, Snow Lake, west-central Manitoba (parts of NTS 63K16, 63J13). *In* Report of Activities 2013, Manitoba Innovation, Energy and Mines, pp. 106–113.

Russell, G.A. 1957. Structural studies of the Snow Lake–Herb Lake area. Manitoba Mines and Natural Resources, Mines Branch, Publication 55-3.

Scott, C.R., Richard, D., Fowler, A.D. 2003. An Archean Submarine Pyroclastic Flow Due to Submarine Dome Collapse: The Hurd Deposit, Harker Township, Ontario, Canada. *In* Explosive subaqueous volcanism. *Edited by* J.D. White, J.L. Smellie and D.A. Clague: American Geophysical Union, Geophysical Monograph Series. Vol. **140**, pp. 317-327.

Shervais, J.W. 1982. Ti–V plots and the petrogenesis of modern and ophiolitic lavas. Earth and Planetary Science Letters, **59**:101–118.

Stern, R.A., Syme, E.C., Bailes, A.H., Galley, A.G., Thomas, D.J. and Lucas, S.B. 1992. Nd isotopic stratigraphy of Early Proterozoic Amisk Group metavolcanic rocks from the Flin Flon Belt, Manitoba and Saskatchewan. *In* Radiogenic age and isotopic studies. Geological Survey of Canada, Report 5, Paper 92-2, pp. 73–84.

Stern, R.A., Syme, E.C., Bailes, A.H. and Lucas, S.B.1995a. Paleoproterozoic (1.86-1.90 Ga) arc volcanism in the Flin Flon belt, Trans-Hudson Orogen, Canada. Contributions to Mineralogy and Petrology, **119**: 117-141.

Stern, R.A., Syme, E.C. and Lucas, S.B. 1995b. Geochemistry of 1.9 Ga MORB- and OIB-like basalts from the Amisk collage, Flin Flon belt, Canada: Evidence for an intra-oceanic origin. Geochimica et Cosmochimica Acta, **59**: 3131-3154.

Stix, J., 1991, Subaqueous intermediate to silicic-composition explosive volcanism: a review. Earth Science Review, **31**: 21-35.

Sun, S.S., and McDonough, W.F. 1989. Chemical and isotopic systematics of oceanic basalts: implications for mantle composition and processes. In Magmatism in the ocean basins, *Edited by* A.D. Saunders and M.J. Norry. Geological Society Special Publications **42**: 313–345.

Syme, E.C, Bailes, A.H. and Lucas, S.B. 1995. Geology of the Reed Lake area (parts of NTS 63K/9 and 10). In Report of Activities, 1997, Manitoba Energy and Mines, Geological Services, pp. 42–60.

Syme, E.C., Bailes, A.H. and Lucas, S.B. 1996. Tectonic assembly of the Paleoproterozoic Flin Flon belt and setting of VMS deposits. Geological Association of Canada–Mineralogical Association of Canada, Joint Annual Meeting, Field Trip Guidebook B1, 130 p.

Syme, E.C., Lucas, S.B., Bailes, A.H., and Stern, R.A. 1999. Contrasting arc and MORB-like assemblages in the Paleoproterozoic Flin Flon Belt, Manitoba, and the role of intra-arc extension in localizing volcanic-hosted massive sulphide deposits. Canadian Journal of Earth Sciences, **36**: 1767–1788. doi:10.1139/cjes- 36-11-1767.

Tanaka, T., Togashi, S., Kamioka, H., Amakawa, H., Kagami, H., Hamamoto, Ti., Yuhara, M., Orihashi, Y., Yondea, S., Shimizu, H., Kunimaru, T., Takahashi, K., Yanagi, T., Nakano, T., Fujimaki, H., Shinjo, R., Ashahara, Y., Tanimizu, M., and Dragusanu, C. 2000. JNdi-1: A neodymium isotopic reference in consistency with La Jolla neodymium. Chemical Geology, **168**: 279-281.

Todt, W., Cliff, R.A., Hanser, A., and Hofmann, A.W. 1996. Evaluation of 202Pb-205Pb double spike for high-precision lead isotope analysis. Earth Process: Reading the Isotopic Code. Geophysical Monograph, **95**: 429–437.

Weis, D., Kieffer, B., Maerschalk, C., Barling, J., de Jong, J., Williams, G.A., et al. 2006. High-precision isotopic characterization of USGS reference materials by TIMS and MC–ICP–MS. Geochemistry Geophysics Geosystems, **7**(8): Q08006. doi:10.1029/2006GC001283.

White, J.D.L. 2000. Subaqueous eruption-fed density currents and their deposits. Precambrian Research, **101**: 87-109.

White, J.D.L., Houghton, B.F. 2006. Primary volcaniclastic rocks, Geological Society of America. Geology, **34**: 677 – 680.

White, J.D.L., Smellie, J.L., and Clague, D.A. 2003. Introduction: A deductive outline and topical overview of subaqueous explosive volcanism. *In* Explosive subaqueous volcanism.

Edited by J.D. White, J.L. Smellie and D.A. Clague: American Geophysical Union, Geophysical Monograph Series. Vol. **140**, pp. 1- 23.

Winchester, J.A. and Floyd, P.A. 1977. Geochemical Discrimination of Different Magma Series and Their Differentiation Products Using Immobile Elements. Chemical Geology, **20**: 325-343.

Wright, I.C., and Gamble, J.A. 1999. Southern Kermadec submarine caldera arc volcanoes (SW Pacific): Caldera formation by effusive and pyroclastic eruption. Marine Geology, **161**: 207-227.

Wright, I.C., Gamble, J.A., and Shane, P.A. 2003. Submarine, silicic volcanism of the Healy caldera, southern Kermadec arc (SW Pacific): I. Volcanology and eruption mechanisms. Bulletin of Volcanology, **65**: 15–29.

Yamada, E., 1973. Subaqueous pumice flow deposits in the Onikobe Caldera, Miyagi Prefecture, Japan: Journal of the Geological Society of Japan, **79**: 585 - 597.

Zwanzig, H.V. 1999. Structure and stratigraphy of the south flank of the Kisseynew Domain in the Trans-Hudson Orogen, Manitoba: implications for 1.845–1.77 Ga collision tectonics; *in* NATMAP Shield Margin Project, Volume 2. Canadian Journal of Earth Sciences, **36**: 1859 – 1880.

Table 2 - 1: Ranges in composition for stratigraphic units 1 to 5 for the McLeod Road Birch Lake sequence

	Unit 1 wispy fragments	Unit 1 QFP breccia	Coherent lavas unit 2	Volcaniclastic rocks Unit 2	Volcaniclastic rocks unit 3	Coherent lavas unit 4	Volcaniclastic rocks unit 4	Volcanic lavas unit 5
Major oxides (wt.%)								
SiO_2	71.54 - 74.52	75.36 - 80.53	74.76 - 79.86	72.85 - 74.54	54.30 - 55.11	77.78 - 77.92	74.48 - 76.06	47.81
TiO_2	0.23 - 0.28	0.21 - 0.28	0.18 - 0.25	0.25 - 0.26	0.48 - 0.49	0.20 - 0.22	0.23 - 0.24	0.46
Al_2O_3	11.90 - 13.10	9.97 - 12.57	10.47 - 12.14	12.40 - 14.20	14.98 - 15.66	9.85 - 9.96	10.94 - 11.39	14.27
Fe_2O_3	3.91 - 4.84	2.72 - 4.09	3.14 - 3.84	2.16 - 5.70	11.47 - 12.99	3.86 - 4.82	5.29 - 5.62	13.18
MnO	0.06 - 0.10	0.04 - 0.06	0.04 - 0.08	0.04 - 0.09	0.18 - 0.19	0.09 - 0.10	0.08 - 0.12	0.23
MgO	0.65 - 1.11	0.58 - 0.72	0.29 - 0.63	0.49 - 1.10	4.34 - 4.76	0.49 - 0.66	0.65 - 0.78	9.75
CaO	2.08 - 2.61	1.00 - 1.77	1.45 - 3.33	1.46 - 4.11	8.42 - 9.33	1.77 - 3.74	0.64 - 1.44	9.35
Na_2O	3.48 - 4.22	2.03 - 4.04	2.57 - 4.54	2.39 - 4.32	2.73 - 3.41	1.35 - 2.12	2.56 - 4.39	3.59
K_2O	1.57 - 3.35	2.10 - 3.46	1.44 - 1.75	1.98 - 2.06	0.42 - 0.47	1.95 - 2.03	2.19 - 2.40	0.51
P_2O_5	0.06 - 0.07	0.05 - 0.07	0.04 - 0.07	0.05 - 0.08	0.07 - 0.08	0.03 - 0.03	0.03 - 0.04	0.08
LOI	0.25 - 1.00	0.50 - 1.95	0.47 - 1.32	0.55 - 0.60	0.37 - 1.31	1.88 - 4.02	0.63 - 1.27	3.68
Trace elements (ppm)								
Li	7.80 - 12.40	11.60 - 17.60	7.90 - 13.80	13.60 - 17.30	9.00 - 12.50	15.90 - 26.60	9.80 - 21.20	27.70
Be	0.71 - 0.77	0.65 - 0.97	0.73 - 0.85	0.76 - 0.87	0.47 - 0.51	0.65 - 0.85	0.75 - 1.03	0.35
Bi	0.15 - 0.15	0.15 - 0.15	0.15 - 0.15	0.15 - 0.15	0.15 - 0.15	0.15 - 0.15	0.15 - 0.15	0.15
Cr	32.00 - 47.00	24.00 - 72.00	23.00 - 37.00	28.00 - 41.00	63.00 - 99.00	34.00 - 37.00	25.00 - 31.00	214.00
Ni	1.60 - 5.10	1.60 - 14.50	1.60 - 3.60	3.10 - 3.90	17.40 - 18.40	1.60 - 1.80	1.60 - 1.60	44.40
Sc	11.80 - 16.70	8.10 - 11.70	11.60 - 19.90	11.90 - 16.00	40.50 - 46.80	11.10 - 12.70	14.30 - 15.20	50.90
Ti	1258.00 - 1551.00	1180.00 - 1463.00	1018.00 - 1464.00	1427.00 - 1528.00	2487.00 - 2604.00	1045.00 - 1096.00	1274.00 - 1322.00	2274.00
V	24.10 - 45.20	20.00 - 36.10	3.30 - 23.80	15.60 - 22.00	264.60 - 310.60	1.30 - 1.60	1.10 - 2.40	307.60
Cu	13.60 - 55.50	8.30 - 46.20	12.80 - 38.60	7.30 - 19.20	88.10 - 129.70	15.50 - 21.90	54.60 - 64.80	104.50
Co	6.07 - 10.00	5.59 - 6.58	3.35 - 7.77	5.06 - 6.75	32.87 - 36.89	1.34 - 1.57	1.55 - 2.16	50.16
Pb	3.20 - 14.50	5.90 - 10.80	3.20 - 6.80	3.10 - 3.80	2.50 - 3.80	2.70 - 3.40	2.60 - 3.70	1.10
Zn	53.00 - 98.00	32.00 - 59.00	55.00 - 142.00	39.00 - 58.00	92.00 - 93.00	70.00 - 72.00	101.00 - 199.00	76.00

Table 2 – 1. Ranges in composition for stratigraphic units 1 to 5 for the McLeod Road Birch Lake sequence (continued)

	Unit 1 wispy fragments	Unit 1 QFP breccia	Coherent lavas unit 2	Volcaniclastic rocks Unit 2	Volcaniclastic rocks unit 3	Coherent lavas unit 4	Volcaniclastic rocks unit 4	Volcanic lavas unit 5
Trace elements (ppm)								
Ga	9.33 - 11.27	9.76 - 11.38	9.26 - 12.35	11.87 - 12.34	14.48 - 14.80	9.09 - 10.40	11.18 - 12.66	11.68
Rb	22.67 - 45.88	37.07 - 51.65	18.57 - 30.30	28.23 - 28.77	1.37 - 1.85	23.45 - 30.34	19.83 - 31.71	5.50
Mo	1.50 - 1.79	0.99 - 1.76	1.06 - 3.18	1.18 - 8.47	0.40 - 0.82	1.51 - 2.47	1.71 - 2.27	0.14
Cd	0.03 - 0.13	0.04 - 0.06	0.05 - 0.23	0.03 - 0.07	0.09 - 0.12	0.09 - 0.10	0.08 - 0.64	0.08
In	0.03 - 0.04	0.02 - 0.03	0.04 - 0.07	0.03 - 0.05	0.05 - 0.05	0.06 - 0.07	0.06 - 0.10	0.04
Sn	1.03 - 1.33	0.77 - 1.31	0.79 - 1.31	0.60 - 1.09	0.59 - 0.65	0.96 - 1.14	1.15 - 1.50	0.26
Sb	0.15 - 1.03	0.18 - 0.39	0.11 - 0.41	0.12 - 0.43	0.25 - 0.30	0.19 - 0.38	0.18 - 1.12	0.22
Cs	0.21 - 0.37	0.48 - 0.85	0.21 - 1.02	0.20 - 0.48	0.01 - 0.03	0.42 - 0.73	0.56 - 0.64	0.56
Ba	582.30 - 1088.50	627.60 - 966.80	505.90 - 1104.00	342.00 - 823.50	98.00 - 109.80	159.60 - 445.20	423.10 - 866.10	492.80
Sr	115.20 - 129.90	89.60 - 230.20	58.90 - 185.50	104.70 - 144.30	180.60 - 224.10	45.00 - 54.10	53.80 - 57.60	94.80
Nb	5.95 - 6.51	4.68 - 6.23	3.10 - 6.39	2.56 - 5.39	2.90 - 3.04	4.71 - 4.87	5.64 - 5.88	0.69
Hf	3.26 - 3.50	2.72 - 3.62	2.55 - 3.52	2.35 - 2.85	1.29 - 1.49	2.70 - 2.72	3.11 - 3.26	0.49
Zr	119.00 - 128.00	102.00 - 133.00	91.00 - 128.00	85.00 - 102.00	46 - 54	96.00 - 97.00	111.00 - 114.00	16.00
Y	19.07 - 28.10	14.06 - 23.44	23.42 - 31.46	14.00 - 33.43	14.54 - 16.13	30.08 - 34.20	36.21 - 36.32	10.42
Th	2.45 - 2.68	2.61 - 6.83	1.33 - 2.58	0.95 - 2.27	0.80 - 0.86	1.91 - 1.93	2.16 - 2.29	0.31
U	0.85 - 1.13	0.95 - 1.64	0.53 - 0.98	0.56 - 0.88	0.34 - 0.34	0.86 - 0.91	1.09 - 1.17	0.19
La	9.96 - 15.56	11.15 - 23.51	10.89 - 13.64	6.62 - 16.95	5.91 - 6.85	12.62 - 13.49	14.68 - 14.80	2.34
Ce	24.60 - 32.64	21.31 - 47.59	24.18 - 29.33	14.85 - 34.24	13.34 - 13.78	28.03 - 28.97	32.53 - 32.94	5.55
Pr	2.69 - 4.08	3.09 - 5.29	3.20 - 3.73	2.03 - 4.75	1.81 - 1.99	3.69 - 3.81	4.30 - 4.32	0.79
Nd	10.67 - 16.69	12.95 - 19.21	13.67 - 15.96	8.49 - 20.25	7.86 - 8.47	16.11 - 16.50	18.54 - 18.78	3.82
Sm	2.50 - 3.86	2.84 - 3.47	3.21 - 4.25	2.05 - 4.82	1.99 - 2.11	4.21 - 4.25	4.77 - 4.88	1.20

Table 2 – 1. Ranges in composition for stratigraphic units 1 to 5 for the McLeod Road Birch Lake sequence (continued)

	Unit 1 wispy fragments	Unit 1 QFP breccia	Coherent lavas unit 2	Volcaniclastic rocks Unit 2	Volcaniclastic rocks unit 3	Coherent lavas unit 4	Volcaniclastic rocks unit 4	Volcanic lavas unit 5
Trace elements (ppm)								
Eu	0.54 - 0.81	0.56 - 0.90	0.66 - 1.34	0.54 - 1.16	0.64 - 0.65	1.04 - 1.04	1.17 - 1.23	0.51
Gd	2.45 - 3.97	2.76 - 3.60	3.58 - 4.81	2.17 - 5.28	2.22 - 2.43	4.80 - 5.05	5.28 - 5.32	1.52
Tb	0.45 - 0.68	0.41 - 0.61	0.58 - 0.85	0.36 - 0.87	0.38 - 0.41	0.83 - 0.85	0.90 - 0.91	0.27
Dy	3.09 - 4.60	2.51 - 3.97	3.91 - 5.65	2.32 - 5.70	2.59 - 2.85	5.58 - 5.65	6.20 - 6.22	1.82
Ho	0.70 - 1.02	0.51 - 0.86	0.83 - 1.22	0.49 - 1.22	0.56 - 0.62	1.15 - 1.26	1.36 - 1.37	0.40
Er	2.35 - 3.13	1.55 - 2.66	2.59 - 3.64	1.51 - 3.59	1.75 - 1.87	3.41 - 3.91	4.23 - 4.26	1.23
Tm	0.38 - 0.48	0.23 - 0.41	0.38 - 0.54	0.23 - 0.51	0.26 - 0.28	0.51 - 0.60	0.65 - 0.65	0.19
Yb	2.68 - 3.25	1.54 - 2.76	2.51 - 3.64	1.55 - 3.33	1.74 - 1.87	3.31 - 4.00	4.40 - 4.41	1.22
Lu	0.42 - 0.50	0.23 - 0.43	0.39 - 0.56	0.25 - 0.52	0.27 - 0.29	0.49 - 0.62	0.68 - 0.69	0.19
Ta	0.35 - 0.38	0.32 - 0.35	0.18 - 0.30	0.15 - 0.31	0.15 - 0.17	0.26 - 0.27	0.31 - 0.33	0.03
W	0.23 - 0.97	0.22 - 1.69	0.17 - 0.60	0.18 - 0.33	0.09 - 0.15	0.47 - 0.57	0.59 - 0.64	0.09
Tl	0.10 - 0.20	0.15 - 0.30	0.06 - 0.11	0.12 - 0.31	0.01 - 0.01	0.09 - 0.11	0.12 - 0.12	0.03

Note: LOI, loss on ignition.

Table 2 - 2. Average values for key element ratios for the units of the McLeod Road Birch Lake sequence.

	Unit 1 wispy fragments	Unit 1 QFP breccia	Coherent lavas unit 2	Volcaniclastic rocks unit 2	Volcaniclastic rocks unit 3	Coherent lavas unit 4	Volcaniclastic rocks unit 4	Coherent lavas unit 5
Al_2O_3 / Na_2O	3.11 - 3.42	3.11 - 4.90	2.67 - 4.07	3.28 - 5.19	4.59 - 5.49	4.70 - 7.27	2.60 - 4.27	3.97
Al_2O_3 / TiO_2	46.54 - 51.35	44.47 - 47.16	48.08 - 57.52	48.97 - 54.30	31.08 - 31.78	45.52 - 48.30	46.96 - 47.17	31.23
Ti/V	34.31 - 52.20	40.53 - 59.00	61.51 - 308.48	69.45 - 91.47	8.38 - 9.40	685.00 - 803.85	550.83 - 1158.18	7.39
Zr/Y	4.56 - 6.24	5.67 - 7.25	3.89 - 4.07	3.05 - 6.07	3.16 - 3.35	2.84 - 3.19	3.07 - 3.14	1.54
Zr/Ti	0.083 - 0.095	0.091 - 0.086	0.087 - 0.089	0.060 - 0.067	0.021 - 0.018	0.089 - 0.092	0.086 - 0.087	0.01
Nb/Y	0.23 - 0.31	0.27 - 0.33	0.13 - 0.20	0.16 - 0.18	0.19 - 0.20	0.14 - 0.16	0.16 - 0.16	0.07
Ti/Sc	92.87 - 106.61	125.04 - 145.68	73.57 - 87.76	95.50 - 119.92	55.64 - 61.41	86.30 - 94.14	86.97 - 89.09	44.68
Nb/La(mn)	0.40 - 0.58	0.26 - 0.40	0.27 - 0.45	0.31 - 0.37	0.43 - 0.47	0.35 - 0.36	0.37 - 0.38	0.28
Nb/Th (mn)	0.29 - 0.21	0.28 - 0.21	0.28 - 0.30	0.28 - 0.32	0.43 - 0.42	0.29 - 0.30	0.31 - 0.31	0.27
La/Sm (ch)	2.53 - 2.57	2.53 - 4.37	2.07 - 2.19	2.08 - 2.27	1.92 - 2.10	1.93 - 2.05	1.96 - 1.99	1.26
La/Yb (ch)	2.66 - 3.44	5.19 - 6.12	2.69 - 3.11	3.06 - 3.65	2.43 - 2.62	2.42 - 2.73	2.39 - 2.41	1.38
Sm/Yb(ch)	1.03 - 1.32	1.40 - 2.05	1.30 - 1.42	1.30 - 1.47	1.27 - 1.25	1.18 - 1.41	1.20 - 1.23	1.09

Note: (mn), primitive mantle normalized ratios calculated from Sun and McDonough(1989); (ch), chondrite-normalized ratios using values of Sun and McDonough (1989).

Table 2 - 3. Calculated ƐNd values and Pb Isotopic data for the mafic and felsic units 1- 5 of the McLeod Road Birch Lake sequence

MB sequence Unit	Sample number	Measured ppm Nd	Measured ppm Sm	Measured 143Nd/144Nd	Calculated Epsilon Nd (εNdT)	$^{208}Pb/^{204}Pb$	$^{207}Pb/^{204}Pb$	$^{206}Pb/^{204}Pb$
Unit 5 pillow lava	KR11 - 093	3.64	0.951	0.5124	3.8	35.775	15.445	17.482
Unit 4 aphyric rhyolitic lava	KR11 – 090	16.11	4.249	0.5123	3.1	37.126	15.626	19.446
Unit 3 pillow lava	KR11 – 073	2.89	0.855	0.5126	3.2	35.555	15.406	17.500
Unit 3 pillow lava	KR11 – 012	2.54	0.864	0.5129	2.0	35.741	15.544	18.738
Unit 2 plagioclase - porphyritic rhyolitic lava	12KR075A02	15.20	3.451	0.5121	3.4	36.339	15.436	17.478
Unit 2 plagioclase - porphyritic rhyolitic lava	KR11 – 032	15.84	3.781	0.5121	2.8	36.781	15.701	19.963
Unit 1 amygdaloidal rhyolite sill	KR11 – 028	6.37	1.638	0.5122	0.7	36.108	15.454	17.658
Unit 1 massive dacite	KR11 – 067	16.69	3.860	0.5121	2.6	36.431	15.489	18.080
Unit 1 massive dacite	KR11 - 081	15.65	3.675	0.5121	2.7	37.399	15.758	20.408

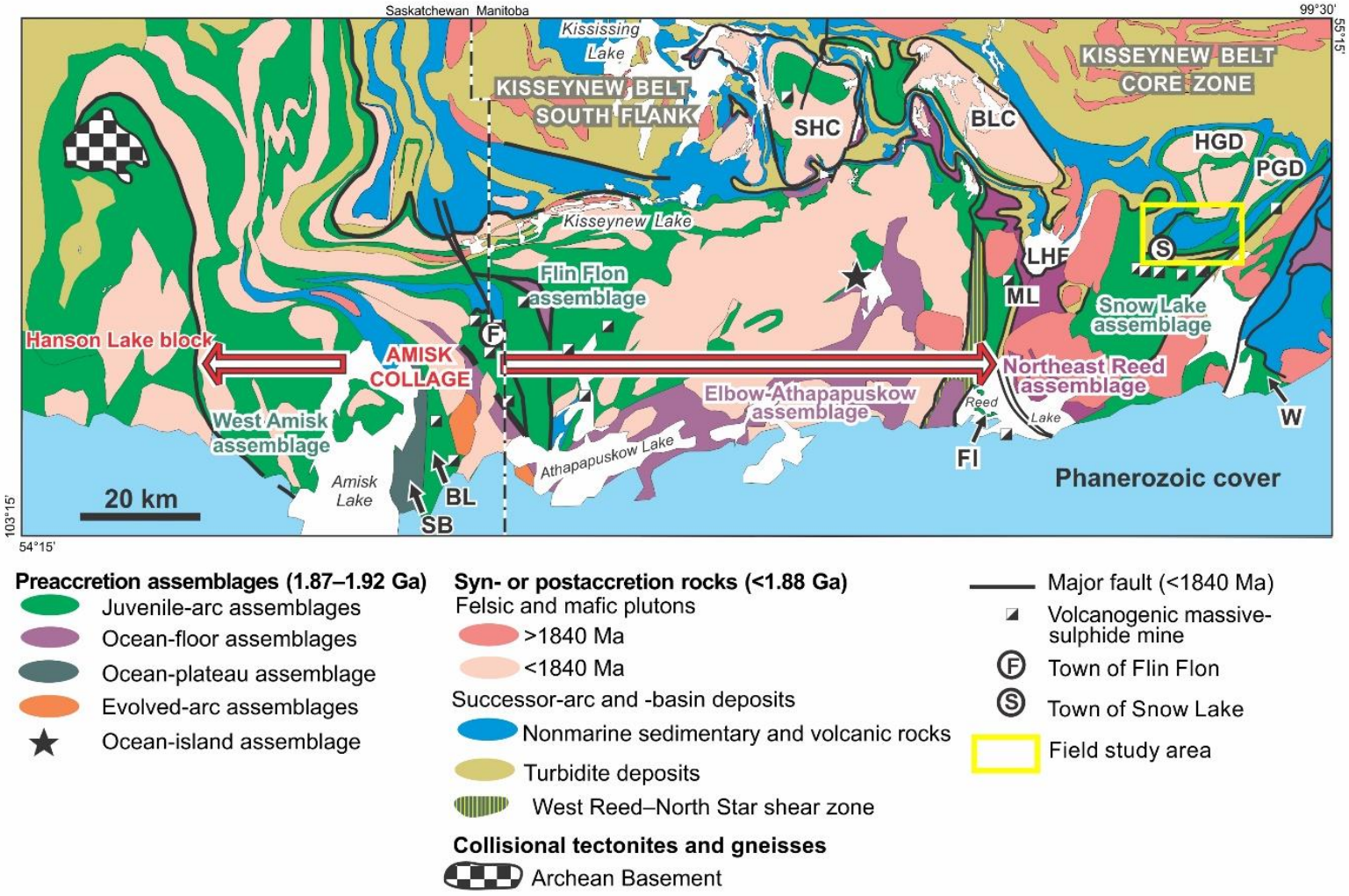

Figure 2 - 1. Geology of the Snow Lake arc assemblage and the McLeod Road-Birch Lake sequence, showing the location of the Snow Lake gold mine and volcanogenic massive sulphide (VMS) deposits. Modified after Bailes and Galley (2007).

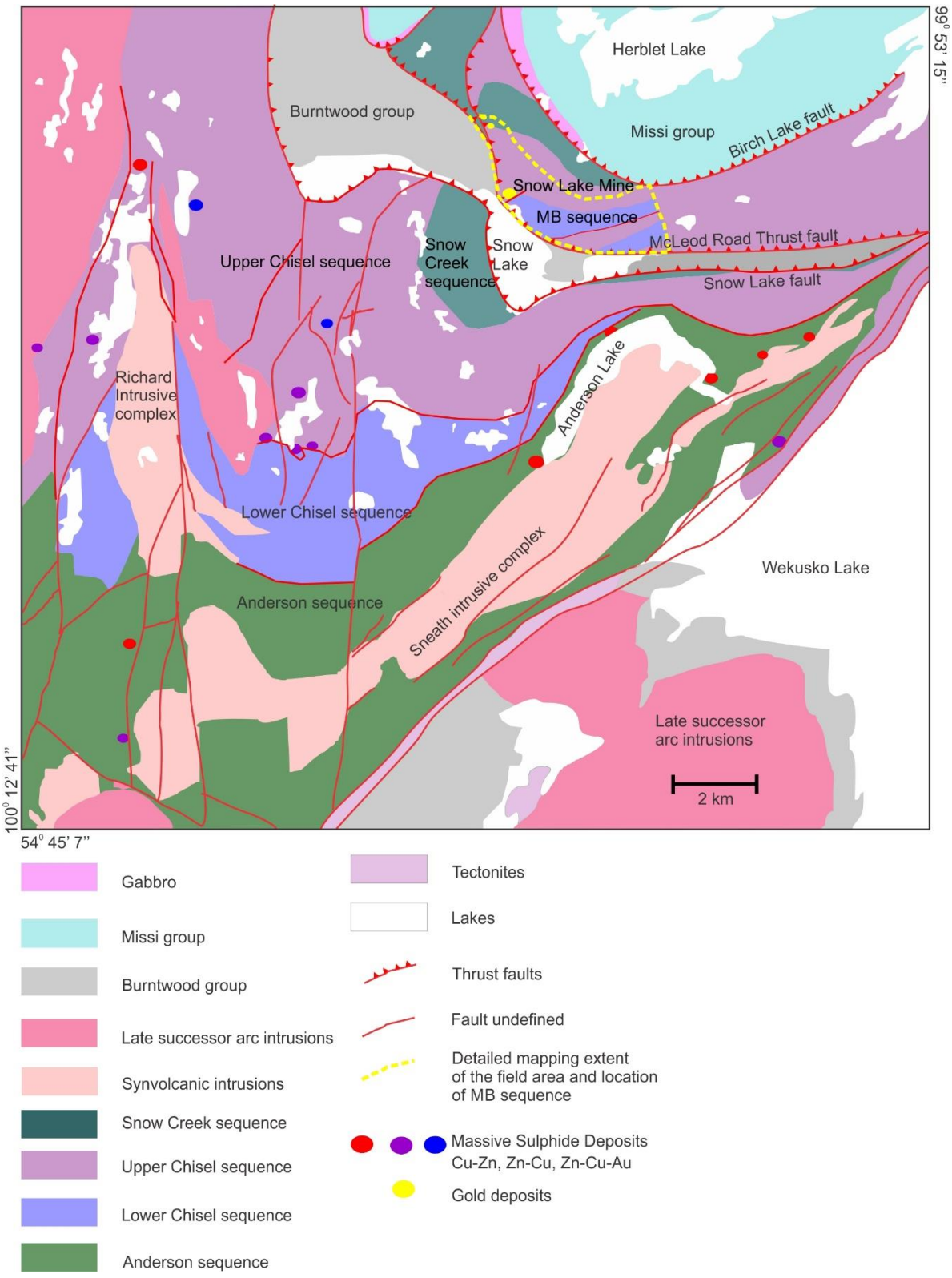

Figure 2 - 2. Geology of the Snow Lake arc assemblage and the McLeod Road-Birch Lake sequence, showing the location of the Snow Lake gold mine and volcanogenic massive sulphide (VMS) deposits. Modified after Bailes and Galley (2007).

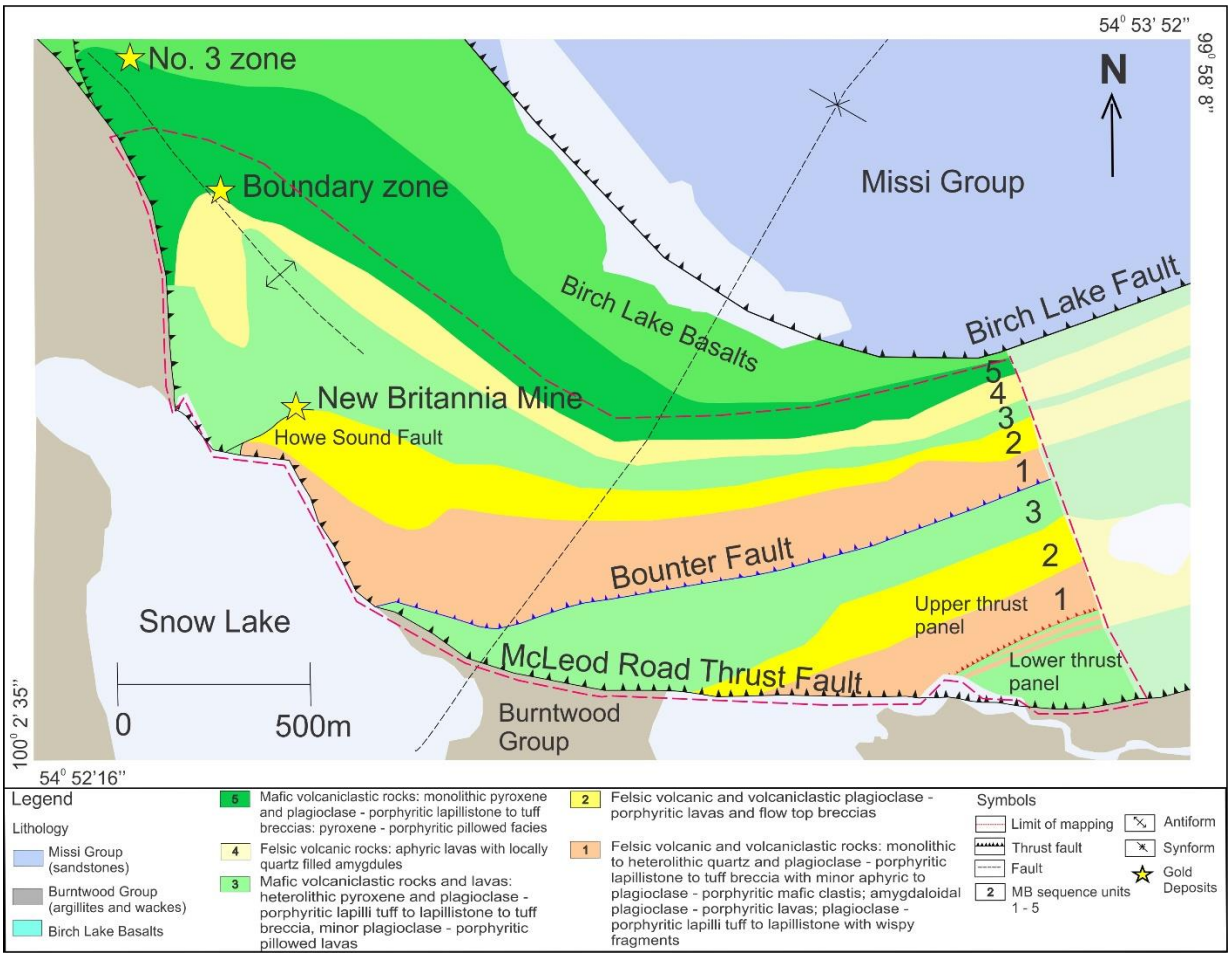

Figure 2 - 3. Geology of the McLeod Road - Birch Lake thrust panel, showing the locations of gold deposits (1:7000 scale; modified after Rubingh et al. 2012).

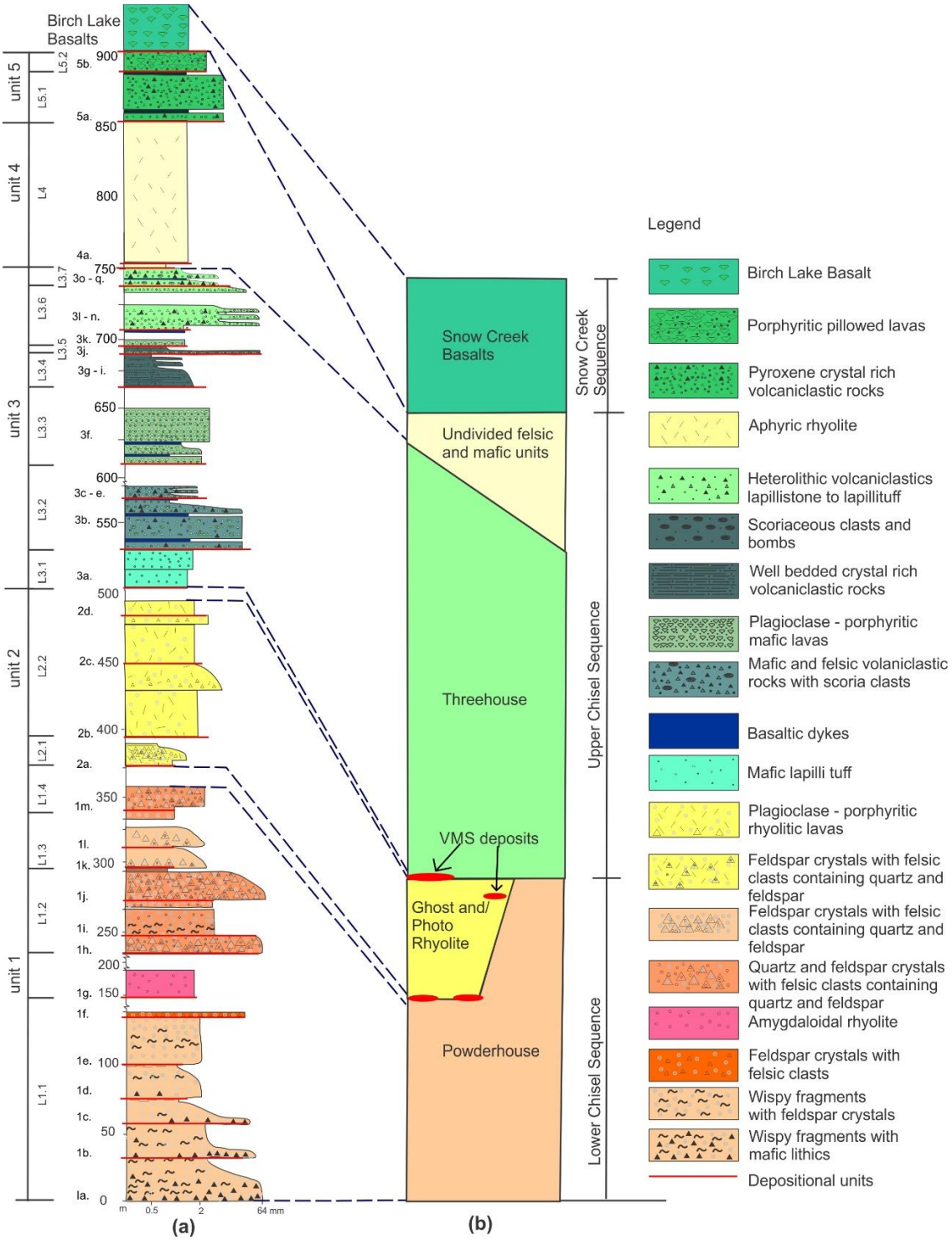

Figure 2 - 4. Idealized stratigraphic column illustrating lithostratigraphic units of the McLeod Road - Birch Lake sequence. The five lithostratigraphic units are denoted with their depositional units, which are outlined by red solid lines. Individual lithofacies for each unit are denoted by (L). The vertical scale is in meters. There are breaks in the scale bar at 135, 168, 205 and 576 meters. The Chisel sequence stratigraphic column lies to the right and proposed correlations with the MB sequence are denoted by black dashed lines. Location of VMS deposits are shown in red (modified after Bailes and Galley 2007).

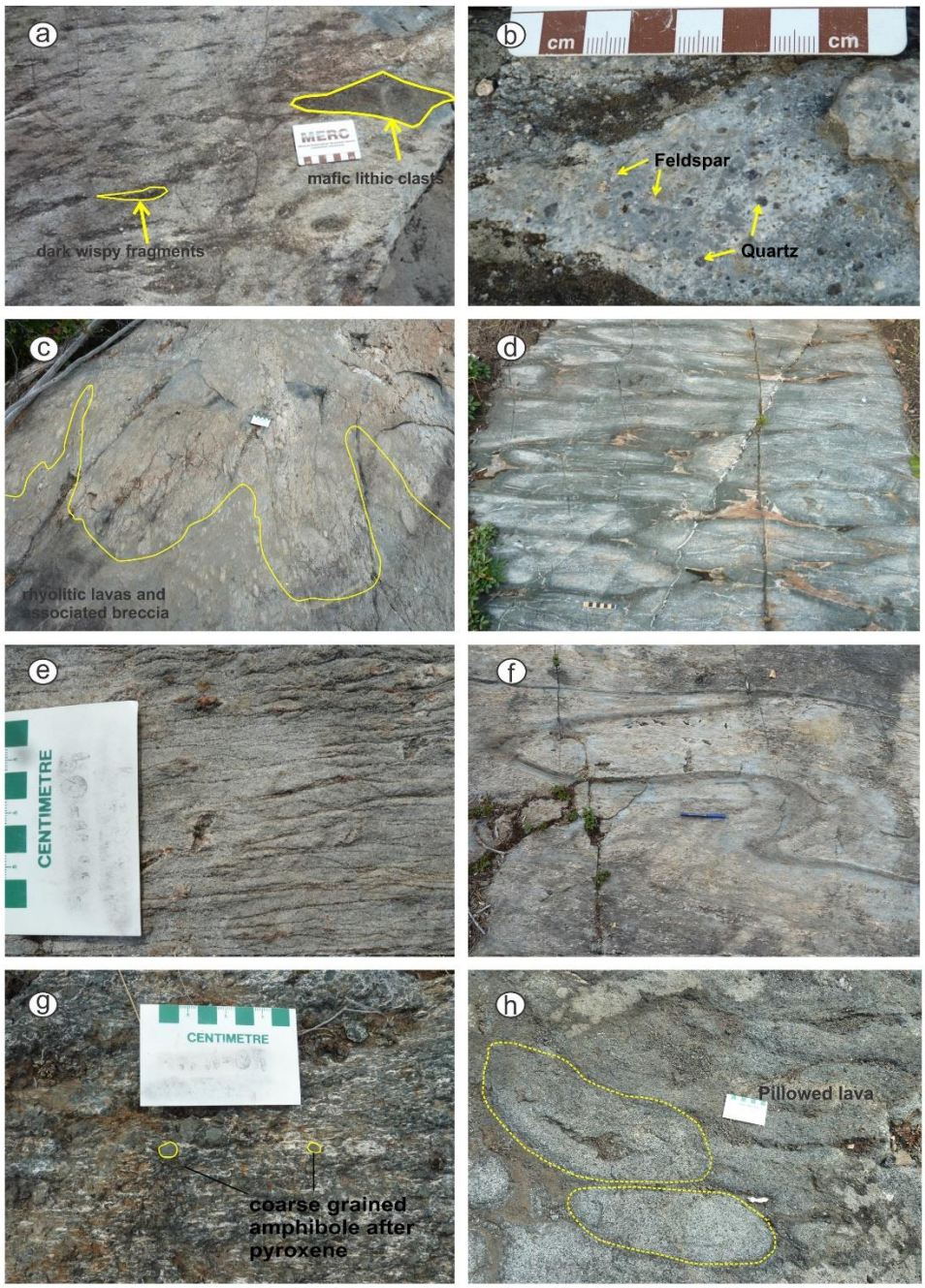

Figure 2 - 5. Typical features for lithostratigraphic units of the McLeod Road - Birch Lake sequence. (a) Unit 1, depositional units 1 (a-e): Felsic lapilli tuff with dark wispy fragments (wf) and mafic lithic fragments (ml), outlined in yellow. (b) Unit 1, depositional units 1 (k-l): crystal rich (quartz and feldspar crystals are labelled), with no dark wispy fragments. (c) Unit 2: Rhyolitic lava and associated breccias. Note the lobate shape of the rhyolitic lava highlighted in yellow. (d) Unit 3: Plagioclase-porphyritic pillowed basalt. (e) Unit 4: Aphyric, rhyolitic lava with a well-developed spaced cleavage defined by biotite and recrystallized quartz, feldspar and garnet. (f) Unit 4: Aphyric rhyolitic lava lobes with margins defined by biotite. (g) Unit 5: Coarse pyroxene and plagioclase-porphyritic volcaniclastic rocks. (h) Unit 5: Pillowed lava of the coarse pyroxene and plagioclase-porphyritic lithofacies. (a-h) Scale is denoted by a pen or 8.5 cm white scale card.

Figure 2 - 6. Characteristic features of scoriaceous bombs of the MB sequence (a) Scoriaceous bomb showing asymmetrical shape with a distinct tail, highlighted in yellow, which indents into the underlying beds. The interior of the bomb is quartz amygdaloidal (10-15%) and is mantled by an intact chilled margin. (b) Equant elliptical bomb displaying an intact chilled margin. There are smaller amygdules around the margin of the bomb and larger ones predominantly in the center. (a-b) Scale is denoted by an 8.5cm white scale card.

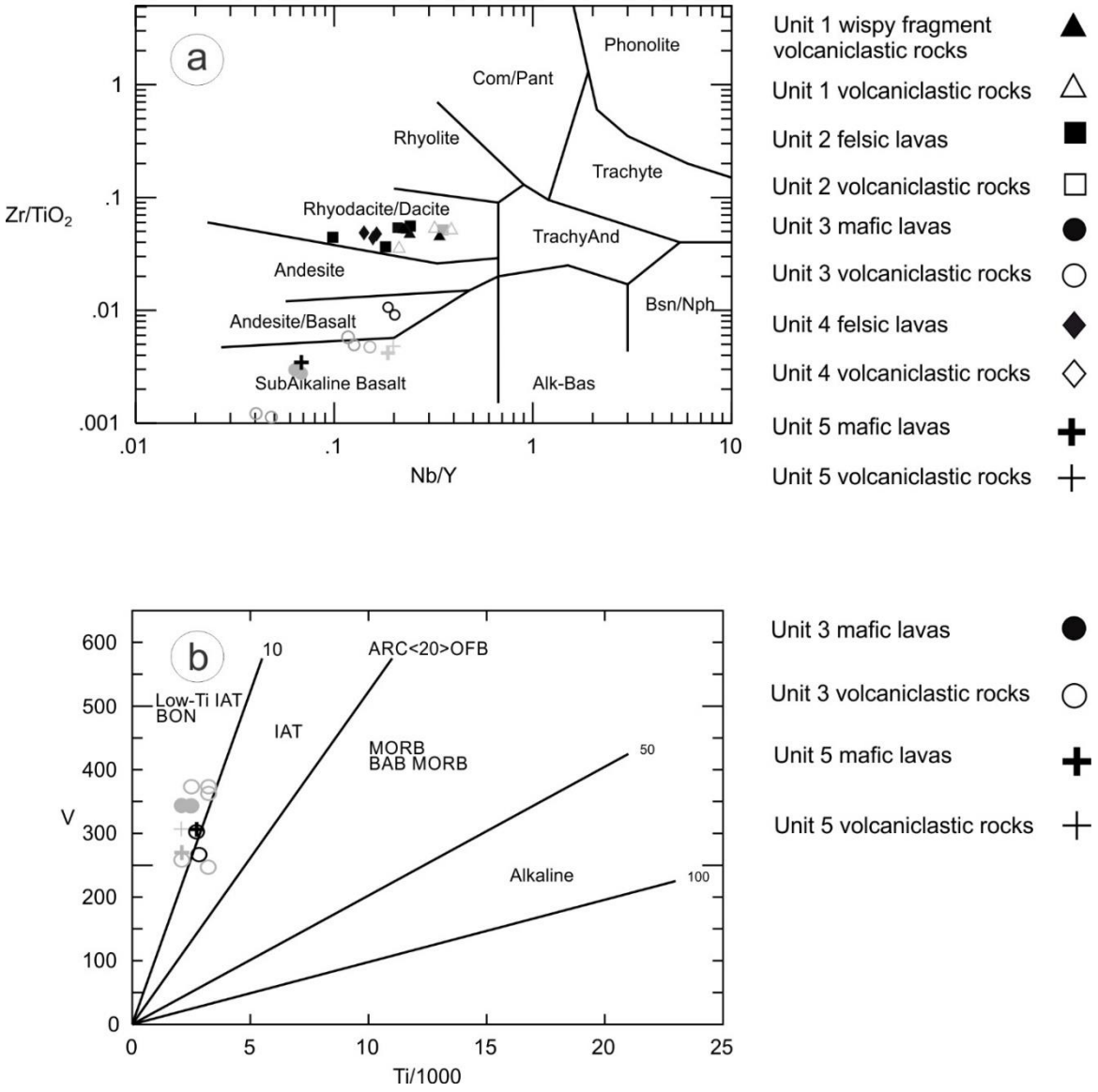

Figure 2 - 7. (a) Discrimination diagram to classify the felsic units 1, 2 and 4 and mafic units, 3 and 5 (from Winchester and Floyd 1977). (b) V vs Ti tectonomagmatic discrimination diagram for mafic units 3 and 5 (from Shervais 1982). Altered samples, where shown, are denoted in pale grey on all diagrams.

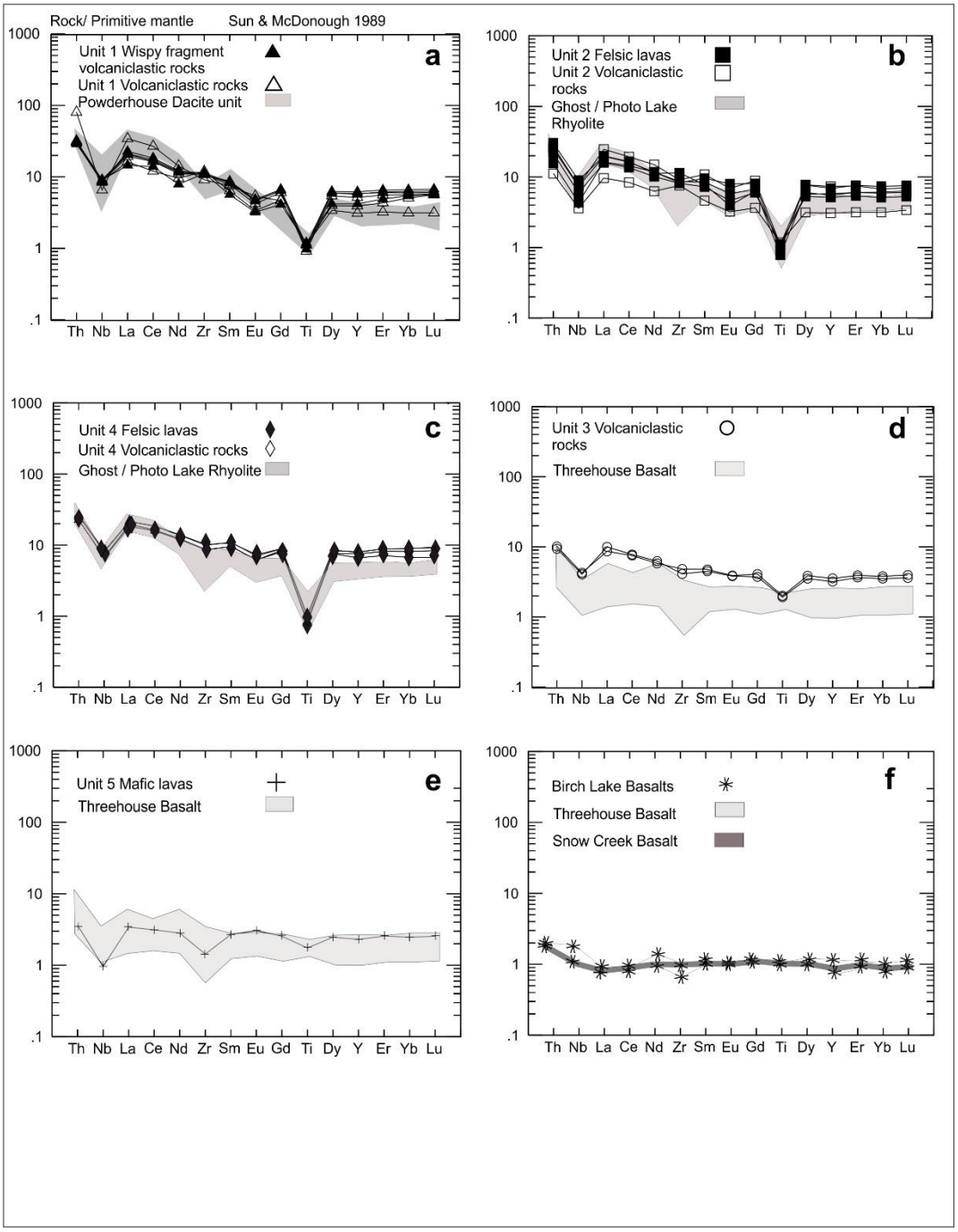

Figure 2 - 8. Primitive mantle-normalized trace element plots (normalized to values from Sun and McDonough 1989) for all units of the MB sequence. (a) Unit 1 is subdivided to show wispy fragment volcaniclastic rocks and volcaniclastic rocks. (b) Unit 2 felsic lava and volcaniclastic lithofacies. (c) Unit 4 felsic lava and volcaniclastic lithofacies. (d) Unit 3 volcaniclastic lithofacies. (e) Unit 5 mafic lava lithofacies. (f) Birch Lake Basalts. Data for mafic and felsic units of the Snow Lake Arc assemblage, are from Bailes and Schledewitz (1998) and the Powderhouse dacite analysis are from Bailes, A. (written comm. 2014) North Chisel Dacite unit, which is now included within the Powderhouse of Friesen et al. (2015) and are included for comparison where applicable.

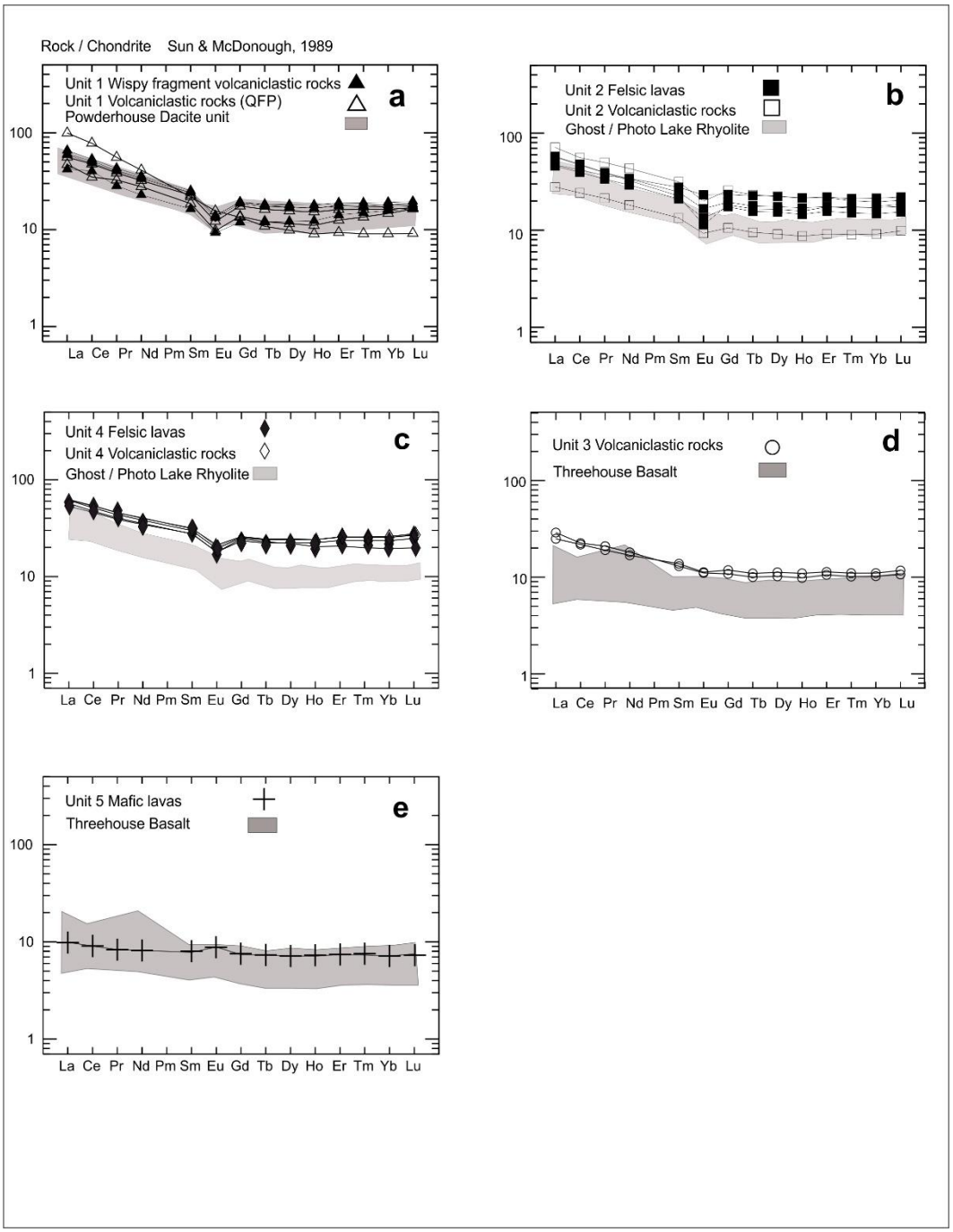

Figure 2 - 9. Chondrite normalized trace element plots (normalized to chondrite values from Sun and McDonough 1989) for the MB sequence. (a) Unit 1 is subdivided to differentiate wispy fragment volcaniclastic rocks and volcaniclastic rocks. (b) Unit 2 felsic lava and volcaniclastic lithofacies. (c) Unit 4 felsic lava and volcaniclastic lithofacies. (d) Unit 3 volcaniclastic lithofacies. (e) Unit 5 mafic lava lithofacies. Data for mafic and felsic units of the Snow Lake Arc assemblage, are from Bailes and Schledewitz (1998) and the Powderhouse dacite analysis are from Bailes' (written comm. 2014) North Chisel Dacite unit, which is now included within the Powderhouse of Friesen et al. (2015) and are included for comparison where applicable.

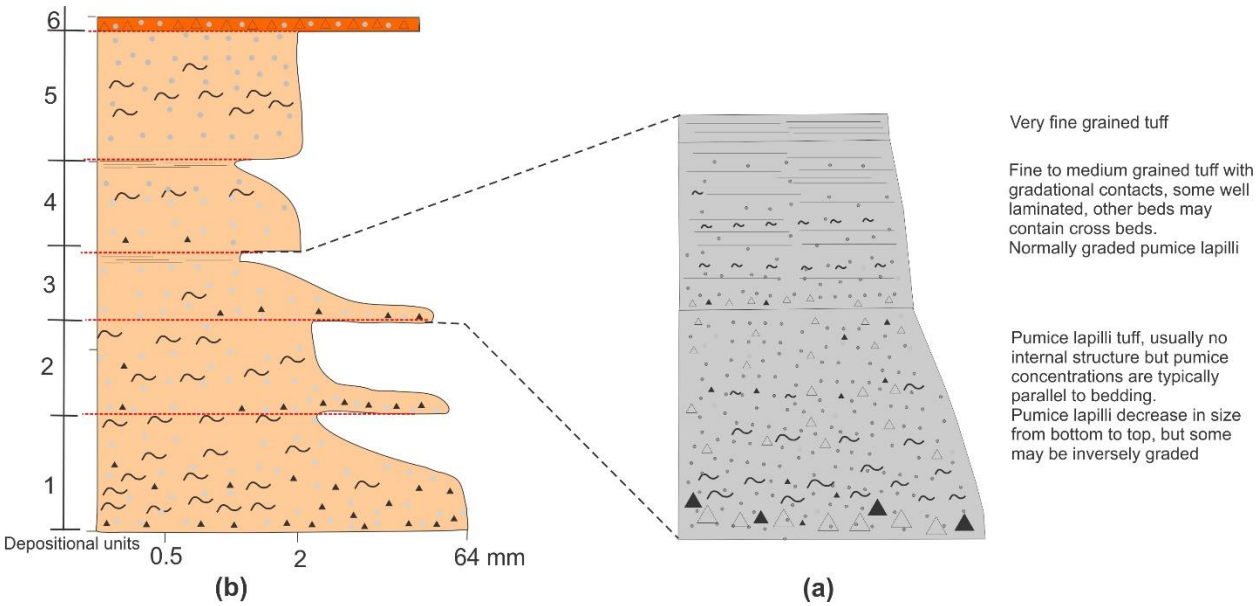

Figure 2 - 10. (a) Submarine pyroclastic flow depositional unit modified after Fiske (1963), Fiske and Matsuda (1964), Bond (1973), Yamada (1973), Niem (1977) and Morton and Nebel (1984). (b) The 6 depositional units (1a – f) from unit 1 illustrated in Fig.2-4a.

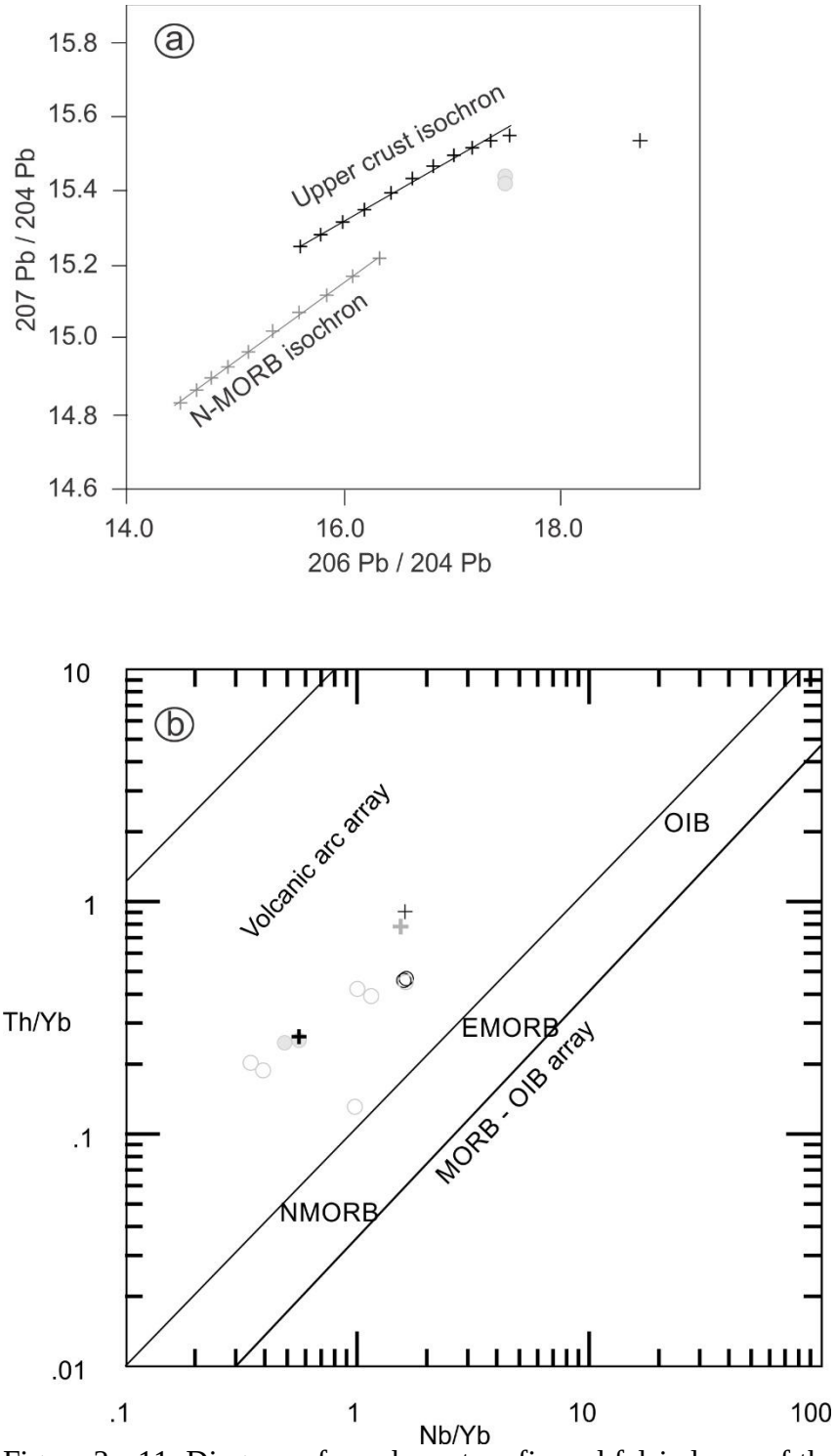

Figure 2 - 11. Diagrams for coherent mafic and felsic lavas of the MB sequence that illustrate crustal input: (a) Common Pb diagram (utilising data from Kramers and Tolstikhin (1997), to plot N-MORB and upper crust isochrones). (b) Th/Yb vs Nb/Yb diagram from Pearce (2008) N-MORB, E (enriched)-MORB, and OIB (ocean-island basalt)

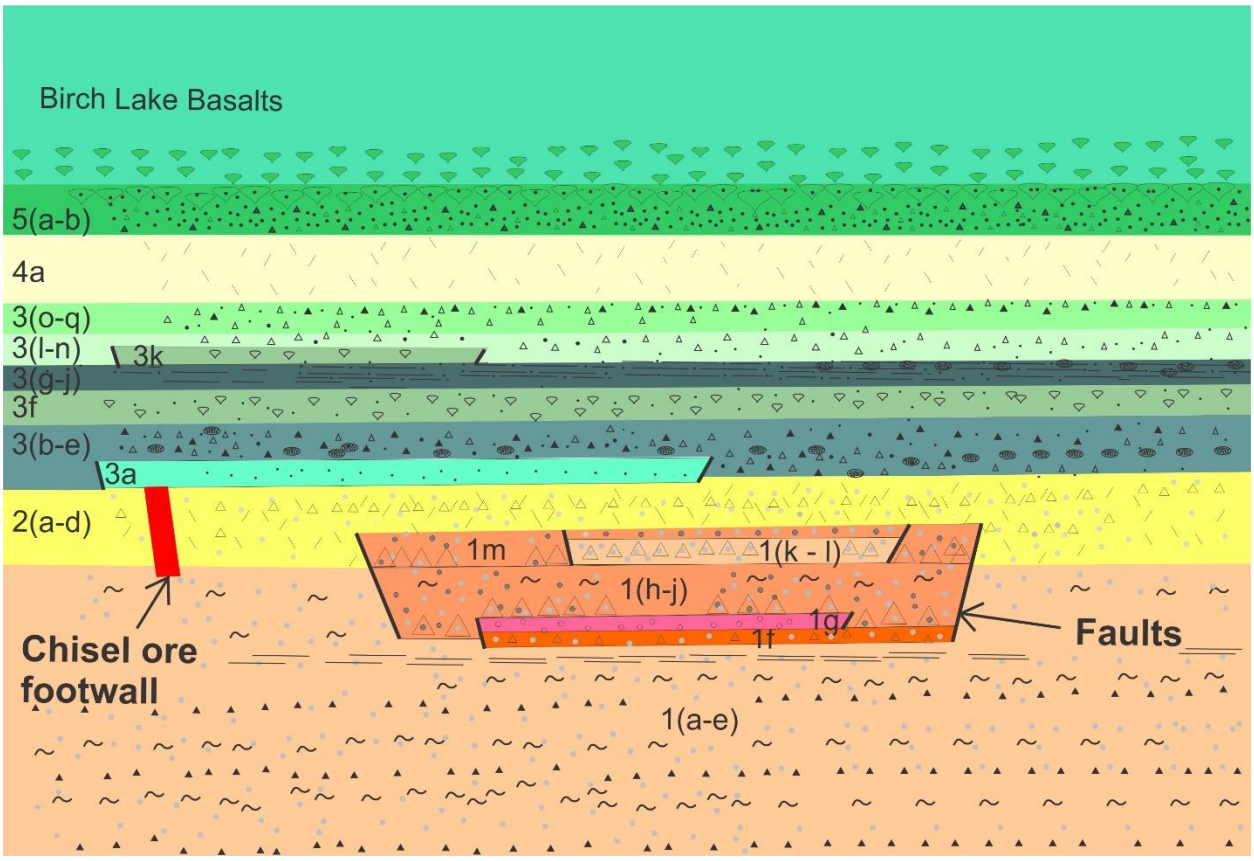

Figure 2 - 12. Schematic cross section to illustrate the sequence of eruptive events for the McLeod Road – Birch Lake sequence and the volcanic environment. Labels for the depositional units correspond to units illustrated in the stratigraphic section in Fig. 4.

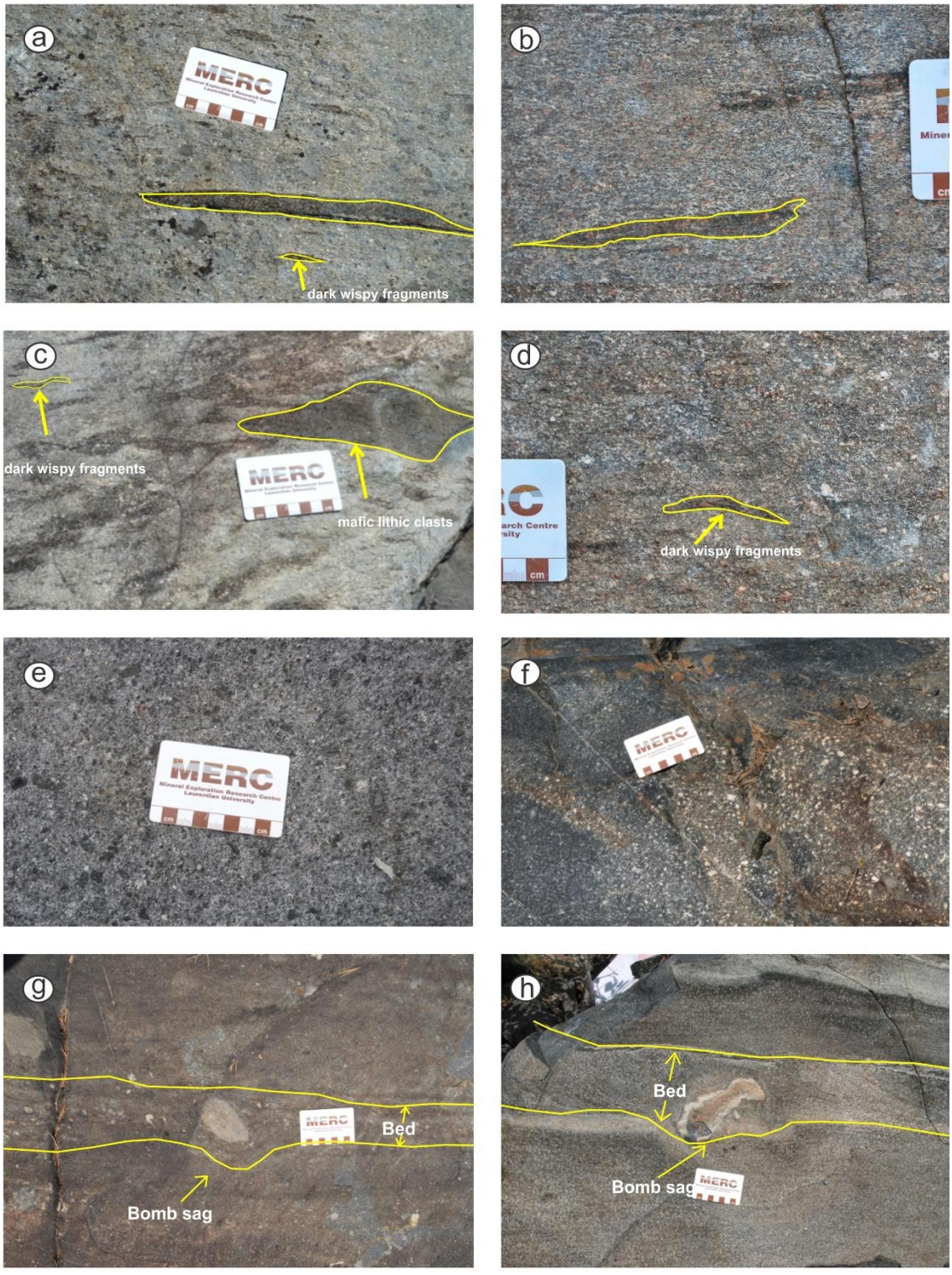

Figure 2 - 13. Comparison of features for units in the Chisel sequence and McLeod Road - Birch Lake (MB) sequences. (a) Unit 1 pyroclastic flow deposits of the MB sequence with dark wispy fragments highlighted in yellow. (b) Powderhouse Dacite (Lalor shaft location)

showing flattened dark wispy fragments highlighted in yellow. (c) Unit 1 pyroclastic flow deposits of the MB sequence, with mafic lithic fragments and dark wispy fragments both highlighted in yellow. (d) Powderhouse Dacite (Lalor shaft location) showing a high percentage of flattened dark wispy fragments. One clast highlighted in yellow. (e) Unit 3: Crystal rich mafic volcaniclastic rocks of the MB sequence. (f) Threehouse mafic volcaniclastic rocks of the Chisel sequence. (g) Unit 3: Well bedded, mafic MB sequence volcaniclastic rocks with bomb sags and draping over the top of the bomb. (h) Chisel sequence Threehouse mafic volcaniclastic rocks with bomb sags. (a-h) Scale is denoted by a white 8.5cm scale card.

Chapter 3 – Early brittle faulting, lateral crustal flow and the development of an orogen-parallel stretching lineation in the Trans-Hudson Orogen, Canada

3.1. Abstract

During orogenic collisional events, a regional stretching lineation generally forms perpendicular to the orogenic front and parallel to the tectonic transport direction. The formation of orogen-parallel stretching lineations is more complex and may involve oblique collision and strain partitioning, orogen-parallel extension, or lateral ductile flow/extrusion. During the Proterozoic Trans-Hudson Orogen in Manitoba (Canada), an orogen-parallel stretching lineation formed during two overlapping and roughly orthogonal collisional events. During the first collisional event at ca.1.84 – 1.82 Ga, a NE-trending regional stretching lineation formed perpendicular to the contact zone between a volcanic oceanic protocontinent (ca. 1.88 – 1.87 Ga Flin Flon-Glennie Complex) and a metasedimentary basin (ca.1.855 - 1.84 Ga Kisseynew Domain) as these two Trans-Hudson juvenile terranes were thrusted towards the SW above a NE-migrating and colliding Archean microcraton (Sask craton). Previously unrecognized, early brittle thrust faults repeated volcanic stratigraphy and interleaved these rocks with turbiditic rocks of the Kisseynew basin. They established the boundary conditions that enabled non-coaxial ductile flow and the formation of several generations of isoclinal folds, sheath-like gneiss domes, and a regional NE-trending stretching lineation within thrust-repeated panels of volcanic and metasedimentary rocks and also along the major ductile thrust faults bounding those panels. During this progressive deformation event, the isoclinal folds were folded into sheath-like gneiss domes and their fold hinges and stretching lineation were rotated into the direction of tectonic

transport. During the second collisional event at ca. 1.83 – 1.80 Ga, the stacked Flin Flon – Glennie Complex and Kisseynew Domain collided with the WNW-converging Superior craton as SW-directed thrusting over the Sask craton continued. This collisional event reactivated the ductile thrust faults as sinistral and dextral shear zones and refolded the sheath-like gneiss domes and thrust faults around NE-striking folds. This event forced the Kisseynew and Flin Flon-Glennie Complex to flow laterally parallel to the cold Archean Superior craton, enhancing the development of the NE-trending regional stretching lineation as an orogen-parallel stretching lineation parallel to the Superior orogenic front.

3.2. Introduction

Orogenic belts form at convergent continental margins due to sustained subduction, or collision with a second continent or an arc (Moores and Twiss, 1995). During collision, a regional stretching lineation may form parallel to the tectonic transport direction during ductile flow perpendicular to the orogenic front (Kvale, 1953; Bryant and Reed, 1969; Escher and Watterson, 1974; Burg et al., 1987; Norman et al., 1995; Kraus and Williams, 1999; Indares et al., 2000). Regional stretching lineations can also form during later gravitational collapse of the collision-thickened crust as extension and thinning of the crust act to reduce the gravitational potential energy and re-equilibrate the crust (Dewey, 1988; Rey et al., 2001). This may result in the formation of stretching lineations with plunges and trends varying from steep to shallow and from perpendicular to parallel, respectively, to the orogenic front.

Strain partitioning and overprinting by younger orogenic events may also result in the formation of regional stretching lineations with varying trends and plunges. Examples include: i) the

folding of a pre-existing lineation during younger orogenic events (Goscombe and Trouw, 1999), e.g. the Hualapai Mountains, Arizona (Duebendorfer, 2003) and North Cascades, Washington (Miller et al., 2006); ii) the formation of multiple stretching lineations during successive orogenic events, e.g. the western and central Alps (Choukroune et al., 1986; Ring et al., 1988); the French Massif Central, southern Variscan belt (Matte, 2007); the Malpica-Tui complex, NW Iberia (Fernández-Diez and Catalán, 2012); and the central Betic Cordillera, Spain (Rossetti et al., 2005; Williams and Platt, 2017); and iii) the vertical and lateral partitioning of the strain during collision, e.g. the Variscan belt (Brun and Bern, 1982; Ellis and Watkinson, 1987); the Caledonides in NE Greenland (Holdsworth and Strachan, 1991); the Caledonides in Norway (Northrup and Burchfiel, 1996); the Wekusko Lake area in the Flin Flon – Snow Lake Belt in the Trans Hudson Orogen (Connors et al., 2002); the Pan-African Damara belt in Namibia (Kisters et al., 2004); the Borborema Province in NE Brazil (Neves et al., 2005); the Malpica-Tui complex in NW Iberia (Fernández and Catalán, 2012; Fernández and Pereira, 2016).

How orogen-perpendicular stretching lineations form during collision is easily understood (Kvale, 1953; Bryant and Reed, 1969; Escher and Watterson, 1974; Burg et al., 1987; Norman et al., 1995; Kraus and Williams, 1999; Indares et al., 2000), but how orogen-parallel stretching lineations form requires more complex deformation paths. Several explanations have been proposed, including: (1) oblique continental collision with partitioning of the oblique component of convergence along orogen-parallel strike-slip faults (Holdsworth and Strachan, 1991; Ring et al., 1988; Fernández and Catalán, 2012); (2) lateral ductile flow of hot weak crusts against strong rigid cratons (Kisters et al., 2004; Gapais et al. 2005; Cagnard et al. 2006; Duclaux et al. 2007; Chardon et al. 2011); and (3) orogen-parallel extension during ongoing continental collision and

gravitational collapse (Seyferth and Henk, 2004). Orogen-parallel extension may be accommodated by slip along normal faults oriented perpendicular to the orogenic front and by slip along conjugate strike-slip faults oriented roughly parallel to the orogenic front, leading to the lateral escape of large crustal blocks away from the orogenic front, e.g. the European Variscides (Burg et al., 1994; Matte, 2007; Fernández and Catalán, 2012); the eastern Alps (Ratschbacher et al., 1991; Frisch et al., 1998, 2000; Scharf et al., 2013); the Grenville (Indares et al., 2000); the Himalayas (Coleman, 1996; Murphy and Copeland, 2005; Jessup et al., 2008; Jessup and Cottle, 2010; Styron et al 2011; Nagy et al., 2015); the Superior Boundary Zone in the Trans Hudson Orogen (Kuiper et al., 2011); the Canadian Cordillera (Staples et al., 2016).

The main goal of this study is to explain the formation of the orogen-parallel stretching lineation in the metavolcanic Flin Flon – Glennie Complex (FFGC) (Lucas et al., 1997) of the Paleoproterozoic Trans Hudson Orogen in Manitoba, Canada. Deformation of the FFGC occurred during collision with two Archean cratons: the Superior and Sask cratons. As the development of the regional stretching lineation is the sum of the total strain history of the FFGC, we: (1) first explain how early brittle thrust faults controlled later ductile flow during continental collision; (2) then discuss the development of the stretching lineation, sheath-like gneiss domes and ductile thrust faults during collision of the FFGC with the Archean Sask craton; and (3) explain how these structures were reactivated and folded during continued development of the regional stretching lineation during lateral crustal flow of the accreted FFGC and Sask craton against the Archean Superior Craton.

3.3. Regional Geology

The Trans Hudson Orogen in Manitoba and Saskatchewan consists of an internal zone, called the Reindeer Zone, in fault contact with three Archean cratons (Fig. 3.1; Hoffman, 1988; Lewry and Collerson, 1990; Corrigan et al., 2005). The Reindeer Zone (Fig. 3.1) is bound to the west by the Hearne craton, to the east by the Superior craton, and is underlain by the Sask microcraton (Ansdell et al., 1995). Of these three cratons, the Sask microcraton is the smallest and is composed of ca. 3117 Ma to ca. 2450 Ma gneisses and intrusions that are exposed in only three tectonic windows through the structurally overlying Reindeer Zone (Chiarenzelli et al., 1998; Ashton et al., 1999; Bickford et al., 2005; Rayner et al., 2005b). The latter consists of structurally juxtaposed juvenile volcanic belts, a continental batholith, and large metasedimentary belts (Lucas et al., 1993; Ansdell et al., 1995; Ansdell, 2005; Hajnal et al., 1996, 2005; White et al., 2005). The juvenile volcanic belts are represented by the La Ronge Domain and the FFGC, which is itself represented by several amalgamated volcanic terranes including, from west to east, the Glennie Domain, the Hanson Lake Block, the Amisk collage, and the Snow Lake Arc (SLA) assemblage (Figs. 3.1, 3.2; Lucas et al. 1996). These terranes formed at ca. 1.92-1.88 Ga, as ocean floor, oceanic volcanic arcs and ocean plateaux rocks were forming within an intervening ancestral ocean, called the Manikewan Ocean (Stauffer, 1984), which separated the three Archean cratons. The La Ronge Domain formed as an oceanic volcanic arc that was accreted to the eastern margin of the Hearne craton before ca. 1.865 Ga (Bickford et al., 1990; Ansdell et al., 1995; Corrigan et al., 2005, 2009) at roughly the same time as intraoceanic accretion at ca. 1.88-1.87 Ga created an oceanic microcontinent, the Amisk Collage (Lucas et al., 1996), which stood within the Manikewan Ocean between the accreted La Ronge arc to the west and the SLA to the east. The SLA (Fig. 3.2) is of similar age as the other terranes but it differs by

its geochemistry and by the presence of old 2.82-2.65 Ga xenocrystic zircons (David et al., 1996), indicating an involvement of older continental material during construction of the SLA as a pericratonic arc outboard of the Superior craton (Stern et al., 1992; David et al., 1996; Lucas et al., 1996; Corrrigan et al., 2009).

Bordering the FFGC to the north is a large oceanic basin, represented by the Kisseynew Domain, which opened after the docking of the FFGC to the accreted La Ronge arc and the emplacement of the ca. 1.865 Ga – 1.85 Ga continental arc Wathaman batholith along the eastern margin of the Hearne craton (Fumerton et al., 1984; Bickford et al., 1990). Turbiditic sandstone of the Burntwood Group was deposited within this basin between ca. 1.855 Ga and 1.84 Ga (Ansdell et al., 1995; David et al., 1996; Machado et al., 1999; Corrigan et al., 2009). It overlaps in age with the ca. 1.845 Ga to 1.835 Ga Missi Group (Ansdell et al., 1995; Lucas et al., 1996), which consists of fluvial to shallow marine conglomerate and sandstone that were deposited in restricted sedimentary basins unconformably overlying the FFGC (Ansdell et al., 1995; Lucas et al., 1996; Machado et al., 1999; Corrigan et al., 2009). The Missi Group represents the youngest supracrustal sequence in the Trans-Hudson Orogen and its deposition marks the onset of widespread tectonism across the orogen during terminal collision of the three Archean cratons.

Terminal collision of the FFGC with the Sask craton began at ca. 1.84 Ga to ca. 1.83 Ga with SW-directed thrusting of the Kisseynew basin and FFGC over the NE-migrating Sask craton (Ansdell et al., 1995; Ashton et al., 1999, 2005; Connors et al., 1999; Kraus and Williams, 1999; Norman and Williams, 1999; Corrigan et al., 2005, 2007, 2009). During this thrusting event, metasedimentary units of the Burntwood and Missi groups were interleaved with volcanic units

of the FFGC along the southern margin of the Kisseynew Domain and northern margin of the FFGC. At ca. 1.83 Ga, collision with the Superior craton (Bleeker, 1990) folded these rocks and thrust faults (Kraus and Williams, 1999), and culminated with peak regional metamorphism that varies in age from ca. 1.82 to 1.79 Ga across the orogen (Ansdell and Norman, 1995; Ansdell, 2005; Corrigan et al., 2005, 2007, 2009). Ongoing convergence of the Superior craton between ca. 1.80 Ga and 1.77 Ga led to post-collisional northwest - southeast shortening, orogen-parallel extension along dextral strike slip faults (Ashton et al., 2005; Nemeth et al., 2005; Schneider et al., 2007), and lateral escape of crustal blocks along the eastern margin of the FFGC (Hajnal et al., 1996) and Superior boundary zone (Kuiper et al., 2011).

3.3.1. Snow Lake area

The SLA assemblage consists of submarine volcanic rocks deposited in primitive arc (Anderson sequence), to mature arc (Chisel sequence), to evolved arc rift settings (Snow Creek sequence) (Bailes and Galley, 1999). The assemblage is intruded by early juvenile arc plutons, including the 1889 +8/-6 Ma Richard Lake pluton (Bailes et al., 1991) and the 1886 +17/-9 Ma Sneath Lake pluton (David et al., 1996), and later successor arc plutons (1.84 – 1.83 Ga) (Bailes and Galley 1996; Bailes 1997; Bailes and Schledewitz 1998; Bailes and Galley, 1999; Syme et al., 1999). It is bound to the west by the Morton Lake fault (Fig. 3.2), an inferred thrust fault that juxtaposed the SLA against the Amisk Collage (Syme et al., 1995), and to the north by the Snow Lake Fault, which juxtaposed the SLA against a sliver of Burntwood turbidites (Figs. 3.3, 3.4). From south to north, the latter is in fault contact (McLeod Road Thrust, MRT) with structurally overlying metavolcanic rocks of the McLeod Road - Birch Lake (MB) sequence, which are in turn in fault contact (Birch Lake Fault) with structurally overlying Missi conglomerates and

sandstones (Figs. 3.3, 3.4).

The MB sequence consists of five distinct lithostratigraphic units (Fig. 3.4) intruded by mafic and felsic intrusions and stratigraphically overlain by pillowed flows of the Birch Lake Basalts (Rubingh et al., 2017). Units 1 and 2, and units 3 and 4 correlate with the Lower and Upper Chisel sequence of the SLA assemblage, respectively, and the Birch Lake Basalts correlates with the Snow Creek sequence of the SLA assemblage (Rubingh et al., 2017). The main physical characteristics of these units are summarised in Table 1.

The Snow Lake, MRT and Birch Lake faults trend roughly east-west parallel to the contact zone between the FFGC and the Kisseynew Domain. The contact zone corresponds to a 30° to 50° north-dipping reflector on Lithoprobe seismic profiles (Lucas et al., 1994) and is characterized by several gneiss dome structures, including the Herblet Lake and the Pulver Lake gneiss domes (Bailes, 1975). A sample from the tonalitic and granodioritic core of the Herblet Lake gneiss dome yielded a zircon $^{207}Pb/^{206}Pb$ age of 1889 ±5 Ma (Percival et al., 2005), which is similar to that of the syn-volcanic Richard Lake Pluton and Sneath Lake pluton. Metamorphic isograds are parallel to the contact zone with metamorphic grade increasing to the north from upper amphibolite along the contact zone to granulite facies in the center of the Kisseynew domain and decreasing to the south to lower amphibolite to greenschist facies in the SLA assemblage (Kraus and Menard, 1997; Zwanzig and Bailes, 2010; Growdon et al., 2006; 2008; Growdon, 2010). Peak metamorphic temperatures and pressures of 500 -700 ° C and 4-6 kbar (Zaleski et al., 1991; Menard and Gordon, 1997; Kraus and Menard, 1997) were attained at 1.812 +/- 7 Ma to 1803 +/- 2 Ma in the FFGC (David et al., 1996) during terminal collision of the FFGC with the Superior

craton.

3.4. Structural Geology

Six generations of structures (G1 to G6) have been identified in metavolcanic and metasedimentary rocks of the Snow Lake area. They are assigned to three deformation events (D1 – D3) and correlated with structures described in previous studies in Table 2.

3.4.1. D1 deformation event: Early thrusting within the MB sequence

G1 structures

Over a distance of 5 km east of the Town of Snow Lake, the MB sequence forms a homoclinal panel consistently younging to the north. Repetitions of volcanic units 1, 2 and 3 suggest the presence of thrust faults (Rubingh et al., 2017), namely the Bounter Fault (Hogg, 1957) and Lower Fault, which are parallel to volcanic strata. Although they are difficult to recognize in outcrop and drill core due to overprinting deformation and metamorphic events, the Bounter Fault is exposed within the town limits of Snow Lake as a 10 cm wide structure along the contact between a sliver of north-younging Burntwood turbidites and older, structurally overlying and north-younging, pillowed volcanic rocks (Fig. 3.5a). The fault is defined by a contact-parallel compositional layering expressed by coarse green amphiboles (Fig. 3.5 b, c) and is overprinted by two regional cleavages (Fig. 3.5 b, d). Beds in the Burntwood turbidites are oblique to the fault contact and are rich in garnet porphyroblasts. Burntwood turbidites in the immediate footwall of the MRT are also rich in garnet porphyroblasts and define a distinctive marker unit named the Corley Lake member, which can be traced over several kilometres along the fault (Bailes, 1980). The lower contact of the sliver of Burntwood turbidites (Fig. 3.5a) is not exposed

on surface and could represent either an unconformity, a faulted unconformity, or a fault. Because the Bounter Fault terminates along strike to the west against the MRT and is overprinted by the two regional cleavages, it is interpreted as an early structure that predates the formation of regional ductile structures.

3.4.2. D2 deformation event: Sask craton collision

D2 is a progressive deformation event expressed by the formation of a regional stretching lineation, three generations of isoclinal folds, a regional cleavage and ductile thrust faults.

G2 structures

Second generation G2 structures consist of outcrop- and map-scale F2 folds with an associated axial planar regional S2 cleavage (Figs. 3.3, 3.6). The latter is well expressed at the Bounter Fault outcrop (Fig. 3.5a, b) where it overprints the fault (Fig. 3.5 c, d). Elsewhere across the volcanic MB sequence, the S2 cleavage is generally parallel to lithological units (Fig. 3.4) and is defined by biotite, muscovite and amphibole, and by the flattening of volcanic clasts, pillows and fragments. Garnet porphyroblasts overgrow the S2 cleavage which is also deflected around the porphyroblasts suggesting that they grew during the development of the cleavage. The S2 cleavage is parallel to the axial plane of the map-scale, isoclinal, F2 Nor-Acme Anticline (Fig. 3.4) and it refracts as it passes from competent to less competent beds near the hinge of the anticline (Fig. 3.7), suggesting that the cleavage is syn-folding. On map scale (Fig. 3.4), the axial planar cleavage is anticlockwise and clockwise to lithological contacts and bedding on the west and east limbs of the fold, respectively, which is consistent with cleavage formation during folding. As the metamorphic grade increases from middle amphibolite facies at the Nor Acme

anticline to upper amphibolite facies at the FFGC-Kisseynew contact, the S2 cleavage becomes strongly differentiated and evolves into a gneissic banding defined by alternating quartz-feldspar and biotite-amphibole layers.

Excellent examples of isoclinal F2 folds with a S2 biotite cleavage are present in the fault-bounded sliver of Burntwood turbidites, south of the MB sequence (Fig. 3.8a). The folds are on the scale of a few meters only within an otherwise homoclinal sequence which tops to the north. Younging directions are based on inverse metamorphic grading resulting from the growth of garnet and staurolite porphyroblasts in the upper pelitic horizons of the beds. The porphyroblasts overgrow the S2 foliation which is preserved as internal inclusion trails within the porphyroblasts (Kraus and Williams, 1999).

A penetrative regional lineation lies along the S2 cleavage and bedding. It is expressed as a biotite and amphibole mineral stretching lineation and as a form stretching lineation (Fig. 3.9) defined by elongate clasts and fragments in volcanic rocks and by elongate pebbles in conglomerates of the Missi Group. On stereonet plots (Figs. 3.10a, b), the fold axis of the Nor Acme anticline and other F2 folds plunge ~50° to the northeast parallel to the lineation (Harrison, 1949).

G3 structures

Third generation G3 structures are represented by the McLeod Lake F3 synform, east of the Nor Acme anticline, and by isoclinal F3 folds within the Herblet Lake and Pulver Lake gneiss domes (Fig. 3.6). The folds overprint the S2 cleavage and lack their own axial plane cleavage. The

McLeod Lake synform is defined by tightly folded gabbroic sills emplaced in cross-bedded sandstone of the Missi Group (Fig. 3.3). It plunges moderately (~30°) to the northeast, roughly parallel to the regional stretching lineation (Fig. 3.10c).

G4 structures

Fourth generation G4 structures are represented by the Herblet Lake and Pulver Lake gneiss domes (Fig. 3.6). The two gneiss domes have inner cores of tonalitic and granodiorite gneiss with concentric S2 foliations and outer shells of S2-foliated and F2- and F3-folded metavolcanic and metasedimentary rocks. The domes are doubly-plunging F4 folds with moderate to steep plunges of 60°-70° to the north-northeast and moderate plunges of 40°-60° to the southeast. Interleaved Missi sandstone and metavolcanic rocks between the domes are tightly folded by F4 folds, including the Whitefish Bay synform which flanks the Pulver Lake gneiss dome to the east (Figs. 3.3, 3.6). Poles to the folded S2 foliation in the Whitefish Bay and Herblet Lake area using measurements by Froese and Moore (1980) and Gagné and Beaumont-Smith (2010) have great circle distributions on stereonet plots. The pole to the great circles represents the axis of the folds (Figs. 3.10 d, e), which is parallel to the regional stretching lineation expressed by strongly elongate pebbles in the hinge of the Whitefish Bay synform (Fig. 3.9).

Ductile shear zones

The Snow Lake, MRT, Cleaver Lake and Birch Lake faults constitute a series of related shear zones that diverge, merge and truncate each other. The Snow Lake Fault is poorly exposed and will not be further discussed. All faults including the MRT (Fig. 3.10f), have a pronounced foliation and a mineral stretching lineation, plunging 21° to 43° to the NE within strongly

sheared rocks that underwent intense carbonate, biotite and chlorite alteration. Shear sense indicators observed along the faults formed during later D3 reactivation of the faults and are described later.

The MRT (Fig. 3.4) is one of the most prominent thrust faults in the FFGC. It is exposed over a strike length of approximately 10 km eastward from Snow Lake and 40 km westward from Snow Lake, where it merges with the Loonhead Lake Fault at File Lake. At Snow Lake, it is located at the contact between Burntwood Group turbidites and strongly sheared volcanic rocks of the MB sequence. It is curviplanar with an average strike of 295° (Beaumont-Smith and Gagné, 2008), and an average dip of 40 - 50° to the NE based on drill hole data (Alexis Minerals 2012 data). The Cleaver Lake Fault occurs along the sheared east limb of the F3 McLeod Lake synform (Fig. 3.3), where it juxtaposes mafic pillowed flows of the Birch Lake Basalt against a gabbro sill emplaced in Missi sandstone. The fault terminates to the southwest against the MRT and it merges to the northeast with the upper bounding Birch Lake Fault, which form the contact between the Birch Lake basalts to the south and the Missi Group to the north (Fig. 3.6).

3.4.3. D3 deformational event: Superior craton collision

G5 structures

Fifth generation G5 structures include a regional, NNW- to N-striking, S5 cleavage and outcrop-scale F5 folds. The S5 cleavage is best exposed in Burntwood Group turbidites south of the MRT, where it is expressed as a differentiated biotite-rich cleavage that wraps around garnet and staurolite porphyroblasts. The porphyroblasts are surrounded by strain shadows filled with quartz and feldspar and they have internal inclusion trails representing the S2 cleavage (Kraus and

Menard, 1997; Kraus and Williams, 1999). Excellent overprinting relationships between the S2 and S5 cleavages are observed in outcrop in the Town of Snow Lake, where a F2 fold and its axial planar S2 cleavage are crenulated by the overprinting S5 cleavage (Fig. 3.8b).

From this outcrop, the S5 cleavage can be traced in a northerly direction across the sliver of Burntwood Group turbidites to its bounding MRT and Bounter faults. Immediately south of the Bounter Fault (Location c in Figure 3.5b), the S5 cleavage refracts in anticlockwise manner due to sinistral shear as it passes from competent to less competent beds with a bedding-parallel S2 cleavage. It also refracts across the Bounter Fault, where it is axial planar to open, S-shaped folds. It overprints the coarse amphibole compositional layering along the fault and, although it is the most prominent foliation in the Burntwood Group turbidites, it disappears within 2 metres in the MB sequence where it is superseded by the strong S2 cleavage defined by flattened pillows. Similar structural relationships are observed along the MRT on an outcrop located along a major electrical power line, northwest of the Nor-Acme Anticline hinge closure (Figs. 3.10f). South of the fault in the Burntwood Group turbidites, the S5 cleavage is expressed as a strong biotite differentiated cleavage that refracts in sinistral manner as it passes from competent to less competent beds (Fig. 3.11a). It can be traced to the north into the MRT fault, where it is axial planar to S-shaped folds overprinting the shear zone foliation (Fig. 3.11b). The asymmetry of the folds and the presence of sinistral shear bands overprinting the shear zone foliation suggest that the MRT fault was reactivated as a sinistral fault during the formation of the S5 cleavage (Fig. 3.11 c, d). The S5 cleavage and the axes of the folds are parallel to the stretching lineation along the MRT, which is itself parallel to the regional stretching lineation (Fig. 3.10f).

Similar structural overprinting relationships are present along the Cleaver Lake Fault (Fig. 3.12). The fault has a shear zone foliation defined by alternating carbonate-rich layers and lenses of deformed and altered gabbro (Fig. 3.12a). The shear zone foliation is overprinted by the S5 cleavage, which is oriented anticlockwise to the shear zone foliation on horizontal surface and is deflected in normal (east-side-down) fashion on the vertical surface (Fig. 3.12b). The cleavage refracts from the gabbro lenses, where it is oriented at ~45° to the lenses, to the carbonate-rich layers, where it is oriented near parallel to the layers (Fig. 3.12c). This suggests that shear was localized along the weak carbonate-rich layers during dextral-east-side-down reactivation of the Cleaver Lake Fault (Fig. 3.12a, b, c). This is corroborated by the dextral offset of the MRT along the Cleaver Lake Fault on a first vertical derivative aeromagnetic map of the area done by Golder Associates Limited (Fig. 3.13). The orientation of the S5 cleavage, which indicates E to ENE bulk shortening, is consistent with both dextral reactivation of the NE-striking Cleaver Lake Fault and sinistral reactivation of the NW-striking MRT during formation of the cleavage.

G6 structures

G6 structures are represented by NE-trending F6 folds and a spaced S6 cleavage, which overprints the S5 cleavage along the Bounter Fault (Fig. 3.5b). Map-scale F6 folds include the late Threehouse synform (Fig. 3.3; Bailes, 1975; Froese and Moore, 1980; Kraus and Williams, 1999; Beaumont-Smith and Gagné, 2008) and an unnamed F6 fold which refolded the sheath-like gneiss domes into their present map configuration and orientation (Fig. 3.14a). Sections across the gneiss domes are drawn roughly perpendicular and parallel to the axial plane of the overprinting unnamed F6 fold (Figs. 3.14b, c). Together with the 3D diagram shown in Figure 3.15, they illustrate the geometry of the refolded gneiss domes and their relationships to major

thrust faults and refolded older folds.

3.5. Discussion

Early D1 and late D2 thrusting

Over a distance of 20 km to 30 km across a structural-stratigraphic transition zone between the FFGC and Kisseynew Domain, metavolcanic rocks of the FFGC and metasedimentary rocks of the Burntwood and Missi groups are thrust-imbricated across major ductile thrust faults or shear zones (Fig. 3.16a) (Zwanzig, 1990, 1999; Ansdell and Norman, 1995; Ansdell et al., 1995; Norman et al., 1995; Connors, 1996; Lucas et al. 1996; Bailes and Galley, 1999; Kraus and Williams, 1999). Shear sense indicators suggest transport to the southwest parallel to the regional stretching lineation (Norman et al., 1995; Connors, 1996; Kraus and Williams, 1999; Connors et al., 2002). Thrusting began at ca. 1.84 Ga during deposition of molassic Missi basins and coeval calc-alkaline magmatism, and continued until ca. 1.82 Ga prior to peak thermal metamorphism (Ansdell, 2005; Corrigan et al., 2009). A conglomerate at the base of the Missi group in Flin Flon overlies a regolith (Holland et al., 1989; Babechuk and Kamber 2013), thus it is likely that the entire package of volcanic rocks was uplifted and weathered prior to deposition of the Missi group. Older volcanic-Missi contacts are faulted in the Snow Lake area, so primary contact relationships are not observed, but the uplift of the volcanic rocks likely occurred early during this brittle thrusting event.

In the Snow Lake area, major thrust faults are represented by D2 ductile shear zones, such as the MRT and the Birch Lake Fault, which interleaved metavolcanic rocks of the MB sequence between metasedimentary rocks of the Burntwood and Missi groups. Internal repetitions of

stratigraphic units within the MB sequence require the presence of internal thrust faults (Rubingh et al., 2017). This cannot be reconciled with the apparent absence on outcrop and drill core of high strain zones or shear zones along contacts between repeated units. In the absence of ductile shear fabrics, thrust repetition by early, pre-metamorphic, brittle faults followed by healing of these faults during regional metamorphism is the most plausible explanation. Recrystallization and the growth of metamorphic minerals would have healed the faults masking their original brittle expression.

Brittle faults typically have a core zone of cataclasites and ultracataclasites surrounded by damaged zones of fractured rocks that extend for less than 1 metre to several meters in the adjacent country rocks (Sibson, 1977; Chester and Logan, 1986; Caine et al., 1996). The core zone may be strongly foliated or it may have a massive, very-fine-grained matrix surrounding comminuted fragments. The passage of fluids during faulting can alter the rocks in both the core and damage zone, changing their composition. If the faults were later metamorphosed, the foliation in the core zone would be overgrown by metamorphic minerals and the damage zone would differ in metamorphic mineralogy relative to unaltered rocks away from the fault. These features are present along the Bounter Fault, which structurally juxtaposes metavolcanic rocks above younger Burntwood Group turbidites. The fault is overprinted by two regional cleavages suggesting that it is an early structure. It is characterized by a strong compositional layering defined by coarse green amphiboles, representing the metamorphosed cataclastic foliation in the core zone, and is bounded by garnet-rich Burntwood Group turbidites, representing the hydrothermally altered damage zone. A similar garnet-rich unit, the Corley Lake member, can be traced along the McLeod Road Fault (Bailes, 1980), suggesting that it also formed as an early

brittle thrust that was later reactivated as a major ductile thrust zone.

A few km south of Snow Lake, the VMS Lalor deposit occurs in metavolcanic rocks offset by an early brittle fault. The Lalor Fault displaces folded and steeply-dipping metavolcanic rocks overlying the deposit from recumbent, shallowly-dipping, folded volcanic rocks hosting the deposit (Bailes et al., 2013). The fault is locally exposed underground as a chlorite schist (Caté et al., 2014; Caté, 2016) but it lacks expression along strike suggesting that it experienced no or minimal hydrothermal alteration during faulting and was completely recrystallized during regional deformation and metamorphism. Early map-scale isoclinal folds, overprinted by the regional S2 cleavage and lacking an axial planar cleavage, have been described by Stewart et al. (2018) in the Lalor deposit area. Those early folds presumably formed during the same early thrusting event as the Bounter Fault.

In the absence of early hydrothermal alteration, identification of metamorphosed brittle thrust faults is difficult, especially in metavolcanic rocks, which are typically more massive and which do not record tectonic structures as well as well-bedded sedimentary rocks. Early brittle thrust faults are likely more common than recognized and may be responsible for the initial stacking and repetition of metavolcanic and metasedimentary units. Lister and Williams (1983) explained that the presence of planar anisotropies favors non-coaxial ductile flow of rocks under any imposed stresses, and thus the formation of shear zones, and once formed, any internal material heterogeneities within the shear zones would cause continuous re-partitioning of flow over time. By juxtaposing volcanic rocks against weaker turbiditic sandstones, the early brittle thrust faults acted as strong planar anisotropies that created the boundary constraints that localized

subsequent deformation and enabled the rocks to deform by non-coaxial flow during the formation of the later ductile thrust faults.

The age of the early brittle thrust faults is bracketed between ca. 1.855 Ga, the maximum depositional age of the Burntwood Group turbidites, and ca. 1.830 Ga to ca. 1.840 Ga, the age of small, calc-alkaline, dioritic to granitic stocks which cross or lack D2 structures and therefore must be younger than the D1 structures. These include: 1) the 1834 +8/-6 Ma Wekusko Lake pluton on the SW shore of Wekusko Lake, east of Snow Lake, which lacks a tectonic fabric (Gordon et al., 1990); and 2) the 1832 ±2 Ma Nelson Bay pluton, north of File Lake and northwest of Snow Lake, which has a strong S2 gneissic banding folded around the Nelson Bay gneiss dome (David et al., 1996). The faults either formed during the accretion of the Snow Lake arc to the Amisk collage along the Morton Lake Fault (Fig. 3.2; Syme et al., 1995), or more likely, as they are roughly parallel to the D2 ductile thrust faults, they likely formed during early SW-directed thrusting of the Kisseynew domain over the FFGC (Syme et al., 1995; Connors, 1996; Zwanzig, 1999).

Progressive development of the sheath-like Herblet Lake and Pulver Lake gneiss domes during thrusting

During the D2 deformation event, (Fig. 3.16b), a regional cleavage formed axial planar to isoclinal folds (Nor Acme Anticline), was folded by isoclinal folds (McLeod Lake synform), and these structures were refolded around the Herblet Lake and Pulver Lake gneiss domes, forming concentric rings of isoclinally folded metasedimentary and metavolcanic rocks with a contact-parallel gneissic foliation, surrounding the granitic core of the gneiss domes. As the regional L2

stretching lineation is roughly parallel to the axis of the F2 to F4 folds and to the stretching lineation along the shear zones, this suggests that these structures formed during the same progressive deformation event and were rotated into near-parallelism with the tectonic transport direction, during a non-coaxial deformation that produced three generations of folds and ductile shear zones (G2 to G4).

The Herblet Lake and Pulver Lake gneiss domes (Fig. 3.15) are doubly plunging folds or domes cored by central massive plutons surrounded by banded gneisses. The domes are highly non-cylindrical with 60°-70° hinge angles between their NNE-plunging and SE-plunging fold axes. As their hinge angles are less than 90°, they classify as sheath folds (Skjernaa, 1989). Sheath folds typically form by the rotation of the fold axes (or hinges) of drag folds or pre-existing folds, towards the shear or transport direction, during a progressive non-coaxial deformation (Cobbold and Quinquis, 1980). Previous work by Mandal et al., (2009) indicates that only small initial irregularities in the orientation of the hinge line are needed for a sheath like structure to form. Therefore, the massive competent central plutons coring the domes presumably created the instabilities and irregularities in the hinge line orientation required for sheath fold generation during ductile flow of the rocks. These irregularities were amplified and led to the formation of sheath folds as the foliation wrapped around the strong central plutons. Ductile thrust faults later formed during the same progressive deformation event as deformation became partitioned or localized within narrow shear zones.

Formation of an orogen-parallel stretching lineation

The trajectories of stretching lineations have been used to interpret the relative motion of plates

in orogens including, for example, the Variscides (Alps), Caledonides of Europe, Himalayas, the Pan African fold belt (Shackleton and Ries, 1984), or zones within orogens such as the Alborán domain in the central Betic Cordillera in Spain (Williams and Platt, 2017), or within orogenic plateaux or hot orogens (Cagnard et al., 2006; Chardon et al., 2011) to name a few. Changes in the rate and angle of plate convergence, or abrupt changes in plate margin geometries (ie, promontories and reentrants) as, for example, along the Superior boundary zone (White et al., 2002), may result in the lateral extrusion of crustal material (Kuiper et al., 2011), the rotation of the colliding plates, or to oblique collisions between the plates (Ellis and Watkinson, 1987; Holdsworth and Strachan, 1991; Styron et al., 2011; Fernández -Diez and Catalán, 2012), all of which can produce lineation trajectories varying in orientation from orogen-transverse to orogen-parallel.

More specifically, a number of mechanisms have been suggested for the generation of orogen-parallel stretching lineations. They may form as a result of syn-orogenic collapse during thickening of the crust (Burg et al., 1994; Coleman, 1996; Frisch et al., 2000; Indares et al., 2000; Matte, 2007; Styron et al., 2011; -Diez and Catalán, 2012), partitioning of the deformation during oblique continental collision (Ellis and Watkinson 1987; Holdsworth and Strachan, 1991), and mid to lower crustal flow of laterally restricted hot crust against cold rigid cratons (Poli and Oliver, 2001; Gapais et al., 2005; Cagnard et al., 2006; Chardon et al., 2011).

On the scale of individual high strain zones or shear zones, the orientation and development of stretching lineations are affected by many factors, including rock composition, presence of pre-existing planar fabrics, boundary conditions, bulk strain imposed on the rock, partitioning of this

strain, and intensity of metamorphic and strain-induced recrystallization (Lister and Williams, 1983; Lin and Williams, 1992; Tikoff and Greene, 1997; Goodwin and Tikoff, 2002; Piazolo and Passchier, 2002; Miller et al., 2006). Although all these factors likely affected the development of the regional stretching lineation in the Snow Lake area, its consistent regional orientation suggests that the bulk strain during crustal flow controlled its development. The stretching lineation is coaxial to the Nor Acme anticline, the sheath-like Pulver Lake and Herblet Lake gneiss domes, and thrust faults that formed during D2 transport of the FFGC and Kisseynew Domain over the Sask craton (Fig. 3.16b). It is also coaxial to F5 fold axes and parallel to the S5 cleavage (Froese and Moore, 1980; Kraus and Williams, 1999), which overprints, and formed during sinistral and dextral reactivation of the MRT and the Cleaver Lake Fault, respectively, during ENE to WSW D3 shortening (Fig. 3.16c). This suggests that F5 fold axes, as did F2, F3 and F4 fold axes, rotated into near-parallelism with the stretching lineation during NE-SW ductile flow of the rocks. Thus, the formation of G5 structures overlapped with that of the stretching lineation. Our interpretation of the overprinting S5 cleavage differs from that of Kraus and Williams (1999), who attributed the formation of the cleavage to ductile thrusting along the MRT. The high angle (>45°) of the cleavage to the MRT and overprinting of the shear zone foliation along the MRT and Cleaver Lake Fault by the S5 cleavage, suggest that the D3 deformation event either occurred after or overlapped both in time and space with the D2 deformation event.

The S5 cleavage wraps around staurolite and garnet porphyroblasts which grew early during the development of the cleavage (Kraus and Menard, 1997; Menard and Gordon, 1997; Kraus and Williams, 1999). The cleavage formed at ca. 1.82 Ga – ca. 1.81 Ga (David et al., 1996) at peak

metamorphic temperatures and pressures (Menard and Gordon, 1997) which outlasted the development of the cleavage (Kraus and Williams, 1999). In the Wekusko Lake area, 10 km to the east of Snow Lake, a similar cleavage wraps around staurolite porphyroblasts and is locally overgrown by garnet, suggesting that it formed at peak metamorphic conditions (Connors et al., 2002), similar to the S5 cleavage in Snow Lake. The cleavage is axial planar to regional NE-trending folds and becomes more pronounced in parallel, steeply-dipping, sinistral and east-side-up shear zones. These shear zones have complex stretching lineation patterns, varying in orientation from gently NE-plunging to steeply SE-plunging. The formation of these structures and changes in the orientation of the stretching lineation, are interpreted to reflect spatially and temporally overlapping southwest-directed thrusting of the Kisseynew basin and FFGC over the Sask craton and sinistral transpression related to collision of the FFGC with the Superior craton (Connors et al., 2002). To the north of the FFGC in the Kisseynew Domain and Superior Boundary Zone, other workers have demonstrated that thrust-imbrication of Burntwood Group turbidites with gneisses of the Superior craton and their Paleoproterozoic cover sequence began at ca. 1.83 Ga (Percival et al., 2005; 2006; Zwanzig and Murphy, 2009; Couëslan et al., 2013). Interaction between the Superior Boundary Zone and Kisseynew Domain was a long-lasting event (Bleeker, 1990; Fueten and Robin, 1989; Gapais et al., 2005) that changed to transpressive tectonics at ca. 1.77 Ga and continued to ca. 1.72 Ga (Bleeker, 1990; Machado et al., 2011; Couëslan et al., 2013).

A similar interpretation is proposed here. Southwest-directed thrusting of the Kisseynew basin over the FFGC during collision with the Sask craton is recorded by the imbrication of metavolcanic rocks of the Snow Lake arc with metasedimentary rocks of the Burntwood and

Missi groups (Fig. 3.16 a, b). Continued thrusting produced thrust stacks of F2 - F3 isoclinal folds and sheath-like F4 gneiss domes bounded by ductile thrust faults. A regional stretching lineation formed during thrusting and continued to develop during collision of the FFGC-Kisseynew domain with the Superior craton (Fig. 3.16c). Crustal flow of the laterally restricted hot FFGC and Kisseynew Domain against the cold Archean Superior craton accentuated the development of the stretching lineation parallel to the Superior craton boundary, and reactivated the thrust faults as dextral and sinistral transcurrent faults during the formation of the S5 cleavage. The development of the orogen-parallel stretching lineation is therefore the result of a continuous, overlapping, two-stage collision involving early collision of the FFGC and Kisseynew Domain with the Sask craton at ca. 1.84 Ga to ca. 1.82 Ga followed later by collision with the Superior craton at ca. 1.83 Ga – ca. 1.80 Ga, whilst collision with the Sask craton was ongoing. Those continuous and progressive D2 and D3 events began after the deposition of the Burntwood Group at ca. 1855 Ma to 1840 Ma and during the emplacement of ca. 1840 Ma and ca. 1830 Ma calc-alkaline plutons. It continued with the formation of the S5 cleavage at ca. 1.82 Ga to ca. 1810 Ma during peak metamorphism in the Snow Lake and Wekusko Lake areas (David et al., 1996) and with overprinting of the McLeod Road thrust system and the sheath-like Pulver Lake and Herblet Lake gneiss domes by the Threehouse syncline and other NE-trending F6 folds. These folds plunge parallel to the regional stretching lineation and thus were rotated into the tectonic transport direction during lateral crustal flow of the FFGC and Kisseynew Domain against the Archean Superior craton.

As opposed to the Wekusko Lake area where transpressional deformation dominated during Superior craton collision (Connors et al., 2002), the Snow Lake area, which is located closer to

the centre of the Trans-Hudson Orogen, deformed by more pervasive crustal flow during lateral extrusion of the FFGC and Kisseynew Domain. As strain and shear became localized along major transcurrent faults near the Superior craton margin (Connors et al. 2002; Gapais et al. 2005), deformation and strain was more homogeneously distributed closer to the center of the orogen and resulted in the progressive rotation and reorientation of all linear structural features parallel to the regional stretching lineation and Superior craton margin.

The present triangular map pattern of the Herblet Lake gneiss dome and the elongate map pattern of its flanking Pulver Lake gneiss dome formed by refolding of the gneiss domes by a NE-trending F6 fold (Fig. 3.15). East-west trending metamorphic isograds (Kraus and Menard, 1997 and references therein) through the Snow Lake area are not affected by the Threehouse syncline and other F6 folds (Fig. 3.3) (Kraus and Williams, 1999) but, north of Wekusko Lake, they are folded by NE-trending folds similar in orientation to the F6 folds. This suggests that the folds formed after ca. 1.82 Ga shortly before and after peak metamorphism in response to continued convergence between the FFGC-Kisseynew and the Superior craton.

3.6. Conclusions

Ductile deformation of rocks of the SLA assemblage and Kisseynew basin began during a progressive deformation event, which involved the formation of a regional foliation, two generations of isoclinal folds, and sheath-like gneiss domes bounded by major ductile thrust faults. During this event, volcanic rocks of the Snow Lake arc were imbricated with younger sedimentary rocks of the Burntwood and Missi groups, as this crustal thrust stack was transported in a southwesterly direction over the Sask craton. A regional stretching lineation

formed transverse to the Snow Lake – Kisseynew orogenic front and, together with the fold axes of the isoclinal folds and gneiss domes, it was rotated into the southwesterly direction of tectonic transport. The southwest transport of the Snow Lake – Burntwood crustal stack continued as the west-converging Superior craton began interacting with the Sask craton and overlying crustal stack. This caused west-northwest shortening across the Snow Lake area, the formation of a second regional cleavage, and the reactivation of earlier formed thrust faults as dextral and sinistral transcurrent shear zones, all during the same progressive and overlapping D2 and D3 deformational events. The convergence of the Superior craton towards the Sask craton and overlying Snow Lake – Kisseynew crustal stack forced the latter to flow laterally parallel to the cold Archean Superior craton enhancing the development of the northeast-plunging regional stretching lineation. Thus, an orogen-parallel stretching lineation formed, as the deformation progressed from transverse ductile flow, parallel to the tectonic transport direction, to lateral crustal flow against a rigid orogenic boundary, during two spatially and temporally overlapping collisional events.

Ductile thrusting was preceded by early brittle thrust faulting, either at the beginning of the same continued deformation or during early accretion of the Snow Lake arc to the FFGC. These brittle thrust faults are characterized by structural juxtaposition of older volcanic rocks above younger sedimentary rocks, overprinting of the faults by regional foliations, and by metamorphic recrystallization of previously hydrothermally altered damage zones. Juxtaposition of rocks of contrasting strengths, across the brittle thrust faults, created the boundary constraints that forced the rocks to deform by non-coaxial flow during later ductile thrusting. Previously unrecognized in the FFGC and in many other metamorphic orogenic belts, early brittle thrust faults may have

played an important role in establishing the early crustal architecture, which later controlled ductile thrust faulting in these belts.

3.7. Acknowledgments

A Collaborative Research and Development (CRD) grant established between the Natural Sciences and Engineering Research Council of Canada (NSERC) and QMX Gold Corporation provided funding for the project, and the Manitoba Geological Survey kindly provided full logistical field support and field assistants. The authors would like to thank S. Gagné for his ongoing support and advice and A. Bailes for useful discussions both in and out of the field during numerous field trips in the study area. Field assistants: S. Kushner, C. Hanasyk, S. Bawden, E. Reimer, and E. Tetlock, were invaluable in completion of the field work and their hard work and enthusiasm was greatly appreciated. We would also like to thank all the QMX Gold Corporation geologists; with special thanks to D. Rigg, who supplied additional field support when required and provided useful discussions during the project.

3.8. References

Ansdell, K.M., 2005. Tectonic evolution of the Manitoba–Saskatchewan segment of the Paleoproterozoic Trans-Hudson Orogen, Canada. Canadian Journal of Earth Sciences 42, 741–759. doi:10.1139/e05-035.

Ansdell, K.M., Connors, K.A., 1995. Geochemistry of mafic volcanic rocks, east Wekusko Lake, Manitoba. In Trans-Hudson Orogen Transect, Report of 5th Transect Meeting, 1995, Regina, Sask. Edited by Z. Hajnal and J. Lewry. Lithoprobe Report 48: 198–205.

Ansdell, K.M., Norman, A.R., 1995. U-Pb geochronology and tectonic development of the sourhtern flank of the Kisewynew Domain, Trans-Hudson Orogen, Canada. Precambrian Research 72, 147 – 167.

Ansdell, K.M., Lucas, S.B., Connors, K.A., Stern, R., 1995. Kisseynew metasedimentary gneiss belt, Trans-Hudson orogen (Canada): Back-arc origin and collisional inversion. Geology 23, 1039–1043.

Ashton, K.E., Heaman, L.M., Lewry, J.F., Hartlaub, R.P., Shi, R., 1999. Age and origin of the Jan Lake Complex: a glimpse at the buried Archean craton of the Trans-Hudson Orogen. Canadian Journal of Earth Sciences 36, 185–108.

Ashton, K.E., Lewry, J.F., Heaman, L.M., Hartlaub, R.P., Stauffer, M.R., Tran, H.T., 2005. The Pelican thrust zone: basal detachment between Sask craton and the Paleoproterozoic Flin Flon–Glennie Complex, western Trans-Hudson Orogen. Canadian Journal of Earth Sciences 42, 685–706.

Babechuk, M. G., & Kamber, B. S., 2013. The Flin Flon paleosol revisited. Canadian Journal of Earth Sciences, 50, 1223–1243.

Bailes, A. H., 1975. Geology of the Guay-Wimapedi Lakes Area. Manitoba Department of Mines, Resources and Environmental Management. Mineral Resources Division Geological

Services Branch Publication 75–2, pp. 1–104.

Bailes, A.H., 1980. Geology of the File Lake area: Manitoba Department of Energy and Mines Geological Report 78–1, pp. 1–134.

Bailes, A. H., 1997. Geochemistry of Paleoproterozoic volcanic rocks in the Photo Lake area, Flin Flon Belt (parts of NTS 63 K/16). In: Manitoba Energy and Mines, Mineral Resources Division, Report of Activities, 1997, pp. 61-62.

Bailes, A. H., Galley, A. G., 1996. Setting of Paleoproterozoic volcanic-hosted massive base metal sulphide deposits, Snow Lake, Manitoba. In: EXTECH I: a multidisciplinary approach to massive sulphide research in the Rusty Lake– Snow Lake greenstone belts, Manitoba. Edited by G.F. Bonham- Carter, A.G. Galley and G.E.M. Hall. Geological Survey of Canada, Bulletin 426, pp. 105–138.

Bailes, A.H., Galley, A.G. 1999. Evolution of the Paleoproterozoic Snow Lake arc assemblage and geodynamic setting for associated volcanic-hosted massive sulphide deposits, Flin Flon Belt, Manitoba, Canada. Canadian Journal of Earth Sciences, 36: 1789–1805. doi:10.1139/e98-111.

Bailes, A.H., Schledewitz, D.C.P., 1998. Geology and geochemistry of the Paleoproterozoic volcanic rocks between the McLeod Road and Birch Lake faults, Snow Lake area, Flin Flon belt (parts of NTS 63K/16 and 63J/13). In: Manitoba Energy and Mines, Geological services, Report of Activities, 1998, pp. 4 -13.

Bailes, A., Rubingh, K., Gagné, S., Taylor, C., Galley, A., Bernaeur, S., Simms, D., 2013. Volcanological and Structural Setting of Paleoproterozoic VMS and Gold deposits at Snow Lake, Manitoba; Geological Association of Canada–Mineralogical Association of Canada Joint Annual Meeting, Field Trip Guidebook FT-A2. Manitoba Innovation, Energy and Mines, Manitoba Geological Survey, Open File Report OF2013-3, pp. 1 - 73.

Beaumont-Smith, C.J., Gagné, S., 2008. Structural geology of the Snow Lake–Squall Lake area, Manitoba (parts of NTS 63K16, 63J13); Manitoba Science, Technology, Energy and Mines, Manitoba Geological Survey, Preliminary Map PMAP2008-1, scale 1:20 000.

Bickford, M.E., Collerson, K.D., Lewry, J.F., Van Schmus, W.R., Chiarenzelli, J.R., 1990. Proterozoic collisional tectonism in the Trans-Hudson Orogen, Saskatchewan. Geology 18, 14-18.

Bickford, M.E., Mock, T.D., Steinhart, W.E., III, Collerson, K.D., Lewry, J.F., 2005. Origin of the Archean Sask Craton and its extent within the Trans-Hudson orogen: evidence from Pb and Nd isotopic compositions of basement rocks and post-orogenic intrusions. Canadian Journal of Earth Sciences 42, 659–684.

Bleeker, W., 1990. New structural-metamorphic constraints on Early Proterozoic oblique collision along the Thompson Nickel Belt, Manitoba, Canada. In: The Early Proterozoic Trans-Hudson Orogen of North America. Edited by J.F. Lewry, and M.R. Stauffer. Geological

Association of Canada, Special Paper 37, pp. 57–73

Brun, J.P., Burg, J.P., 1982. Combined thrusting and wrenching in the Ibero-Amorican arc: a corner effect during continental collision. Earth and Planetary Science Letters 651, 319–332.

Burg, J.P., Bale, P., Brun, J.P., Giradeau, J., 1987. Stretching lineation and transport direction in the lbero-Armorican arc during the siluro-devonian collision. Geodinamica Acta (Paris) 1987, 1, 1, 71–87.

Burg, J. P., Van Den Driessche, J., Brun, J.-P., 1994. Syn to post-thickening extension in the Variscan Belt of Western Europe: Modes and structural consequences. Geology of France 3, 33–51.

Bryant, B., Reed, J.C., 1969. Significance of lineation and minor folds near major thrust faults in the southern Appalachians and the British and Norwegian Caledonides. Geological Magazine 106, 412 – 429.

Caine, J.S., Evans, J.P., Forster, C.B., 1996. Fault zone architecture and permeability structure. Geology 24, 1025–1028.

Cagnard, F., Durrieu, N., Gapais, D., Brun, J., Ehlers, C., 2006. Crustal thickening and lateral flow during compression of hot lithospheres, with particular reference to Precambrian times. Terra Nova 18, 72–78.

Caté, A., 2016. Geology of the Paleoproterozoic Zn-Cu-Au Lalor volcanogenic massive sulphide deposit and its gold-rich lenses, Snow Lake, Manitoba. Unpublished PhD thesis, Université du Québec, Institut National de la Recherche Scientifique, Centre Eau Terre Environnement., 430 pp.

Caté, A., Mercier-Langevin, P., Ross, P.-S., and Simms, D. (2014b) Structural controls on geometry and ore distribution in the Lalor volcanogenic massive-sulphide deposit, Snow Lake, west-central Manitoba (part of NTS 63K16): preliminary results from underground mapping. Report of Activities 2014, Manitoba Mineral Resources, Manitoba Geological Survey, p 104-115.

Chardon, D., Jayananda, M., Peucat, J., 2011. Lateral constrictional flow of hot orogenic crust: Insights from the Neoarchean of south India, geological and geophysical implications for orogenic plateaux. Geochemistry, Geophysics, Geosystems 12, Q02005. doi:10.1029/2010GC003398

Chester, F. M., and Logan, J. M., 1986. Composite planar fabric of gouge from the Punchbowl fault, California. Journal of Structural Geology 9, 621–634.

Chiarenzelli, J., Aspler, L., Villeneuve, M., Lewry, J., 1998. Early Proterozoic Evolution of the Saskatchewan Craton and its Allochthonous Cover, Trans-Hudson Orogen. The Journal of Geology 106, 247 – 268.

Choukrane, P., Ballévre, M., Cobbold, P., Gautier, Y., Merle, O., Vuichard, J.P., 1986. Deformation and motion in the western Alpine arc. Tectonics 5, 215 – 216.

Clowes, R. M., White, D. J., Hajnal, Z., 2010. Mantle heterogeneities and their significance: results from Lithoprobe seismic reflection and refraction – wide – angle reflection studies. Canadian Journal of Earth Sciences 47, 409 - 443.

Cobbold, P.R., Quinquis, H., 1980. Development of sheath folds in shear regimes. Journal of Structural Geology 2, 119 – 126.

Coleman, M. E., 1996. Orogen-parallel and orogen-perpendicular extension in the central Nepalese Himalayas. Geological Society of America Bulletin 108, 1594–1607.

Connors, K.A., 1996. Unravelling the boundary between turbidites of the Kisseynew belt and volcano-plutonic rocks of the Flin Flon belt, Trans-Hudson Orogen, Canada. Canadian Journal of Earth Sciences 33, 811–829.

Connors, K.A. and Ansdel1, K.M., 1994. Transition between the Flin Flon and Kisseynew domains of the Trans-Hudson Orogen, File Lake-Limestone Point Lake area, northern Manitoba. In: Current Research 1994-C. Geological Survey of Canada, p. 183–1 92.

Connors, K.A., Ansdell, K.M., Lucas, S.B., 1999. Coeval sedimentation, magmatism, and fold-

thrust development in the Trans- Hudson Orogen: propagation of deformation into an active continental arc setting, Wekusko Lake area, Manitoba. Canadian Journal of Earth Sciences 36, 275–291.

Connors, K.A., Ansdell, K.M., Lucas, S.B., 2002. Development of a transverse to orogen parallel extension lineation in a complex collisional setting, Trans-Hudson Orogen, Manitoba, Canada. Journal of Structural Geology 24, 89–106.

Corrigan, D., Hajnal, Z., Németh, B., Lucas, S.B., 2005. Tectonic framework of the Paleoproterozoic arc-continent collision zone, Trans-Hudson Orogen, from geological and seismic reflection studies. Canadian Journal of Earth Sciences 42, 421–434.

Corrigan, D., Galley, A.G., Pehrsson, S., 2007. Tectonic evolution and metallogeny of the southwestern Trans-Hudson Orogen. In: Goodfellow, W. D. (ed.) Mineral Deposits of Canada: A Synthesis of Major Deposit-types, District Metallogeny, the Evolution of Geological Provinces, and Exploration Methods. Geological Association of Canada, Mineral Deposits Division, Special Publication, 5, 881–902.

Corrigan, D., Pehrsson, S., Wodnicka, N., De Kemp, E., 2009. The Palaeoproterozoic Trans-Hudson Orogen: A prototype of modern accretionary processes. Geological Society of London Special Publications 327, 457–479. doi:10.1144/SP327.19.

Couëslan, C.G., Pattison, D.R.M, Dufrane, S.A., 2013. Paleoproterozoic metamorphic and

deformation history of the Thompson Nickel Belt, Superior Boundary Zone, Canada, from in situ U-Pb analysis of monazite. Precambrian Research 237, 13-35.

Culshaw, N. G., Beaumont, C., Jamieson, R.A., 2006. The orogenic superstructure-infrastructure concept: Revisited, quantified, and revived. Geology 34, 733–736. doi:10.1130/g22793.1.

David, J., Bailes, A.H., Machado, N., 1996. Evolution of the Snow Lake portion of the Paleoproterozoic Flin Flon and Kisseynew belts, Trans-Hudson Orogen, Manitoba Canada. Precambrian Research 80, 107–124.

Dewey, J., F., Shackleton, R.M., Chang, C., Sun, Y., 1988. The tectonic evolution of the Tibetan Plateau. Philosophical Transactions of the Royal Society A 327, 379 – 413. doi:10.1098/rsta.1988.0135.

Duclaux, G., Rey, P., Guillot, S., Ménot, R.P., 2007. Orogen-parallel flow during continental convergence: Numerical experiments and Archean field examples. Geology 35, 715–718.

Duebendorfer, E. M., 2003. The interpretation of stretching lineations in multiply deformed terranes: An example from the Hualapai Mountains, Arizona, USA. Journal of Structural Geology 25, 1393–1400.

Ellis, M., Watkinson, A. J., 1987. Orogen-parallel extension and oblique tectonics: The relation between stretching lineations and relative plate motions. Geology 15, 1022–1026.

Escher, A., Watterson, J., 1974. Stretching fabrics, folds and crustal shortening. Tectonophysics 22, 223 – 231.

Fernández-Díez, R., Catalán, J.R.M., 2012. Stretching lineations in high-pressure belts: The fingerprint of subduction and subsequent events (Malpica–Tui Complex, NW Iberia). Journal of Geological Society of London 169, 531–543.

Fernández-Díez, R., Pereira, M.F., 2016. Extensional orogenic collapse captured by strike-slip tectonics: Constraints from structural geology and U\Pb geochronology of the Pinhel shear zone (Variscan orogen, Iberian Massif). Tectonophysics 691, 290–310

Fueten, F., Robin, P.Y., 1989. Structural petrology along a transect across the Thompson Nickel Belt, Manitoba: dip slip at the western Churchill–Superior boundary. Canadian Journal of Earth Sciences 26, 1976–1989. doi:1139/e89-167.

Frisch, W., Kuhlemann, J., Dunkl, I., Brugel, A., 1998. Palinspastic reconstruction and topographic evolution of the Eastern Alps during late Tertiary tectonic extrusion. Tectonophysics 297, 1–15

Frisch, W., Dunkl, I., Kuhlemann, J., 2000. Post-collisional orogen parallel large-scale extension in the Eastern Alps. Tectonophysics 327, 239–265

Froese, E., Moore, J.M., 1980. Metamorphism in the Snow Lake area, Manitoba Geological

Survey of Canada, pp. 78-27.

Gagné, S., 2009. Geological investigation of the McLeod Road- Birch Lake allochthon east of Snow Lake, Manitoba (part of NTS 63J13). In: Report of Activities 2009, Manitoba Innovation, Energy and Mines, pp. 58–68.

Gagné, S. 2010: Update on geological investigations in the Snow Lake–Squall Lake–Herblet Lake area, west-central Manitoba (parts of NTS 63J13, 63K16); in Report of Activities 2010, Manitoba Innovation, Energy and Mines, Manitoba Geological Survey, p. 118–128.

Gagné, S. and Beaumont-Smith, C.J. 2010: Geology of the Snow Lake–Squall Lake–Herblet Lake area, Manitoba (parts of NTS 63K16, 63J13); Manitoba Innovation, Energy and Mines, Manitoba Geological Survey, Preliminary Map PMAP2010-3, scale 1:20 000.

Gapais, D., Potrel, A., Machado, N., and Hallot, E. 2005. Kinematics of long-lasting Paleoproterozoic transpression within the Thompson Nickel Belt, Manitoba, Canada. Tectonics 24, 1– 16. doi:10.1029/2004TC001700.

Goodwin, L. B., Tikoff, B., 2002. Competency contrast, kinematics, and the development of foliations and lineations in the crust. Journal of Structural Geology 24, 1065–1085.

Gordon, T.M., Hunt, P.A., Bailes, A.H., and Syme, E.C. 1990. U– Pb ages from the Flin Flon and Kisseynew belts, Manitoba: chronology of crust formation at an Early Proterozoic

accretionary margin. In The Early Proterozoic Trans-Hudson Orogen of North America. Edited by J.F. Lewry and M.R. Stauffer. Geological Association of Canada, Special Paper 37, pp. 177–199.

Goscombe, B., Trouw, R., 1999. The geometry of folded tectonic shear sense indicators. Journal of Structural Geology 21, 123–127.

Fumerton, S.L., Stauffer, M.R., Lewry, J.F., 1984. The Wathaman Batholith; largest known Precambrian pluton. Canadian Journal of Earth Sciences 21, 1082-1097.

Growdon, M., 2010. Crustal development and deformation of Laurentian during the Trans-Hudson and Alleghenian orogenies. Unpublished PhD thesis, Indiana University, U.S.A., 221 pp.

Growdon, M.L., Percival, J.A., Rayner, N., Murphy, L., 2006. Regional granulite- facies metamorphism in the northeastern Kisseynew Domain, Manitoba (parts of NTS 63O). In: Report of Activities 2006, Manitoba Science, Technology, Energy and Mines, Manitoba Geological Survey, p. 104–115.

Growdon, M., Percival, J., Rayner, N., Wintsch, R., 2008. Rapid loading and heating to granulite facies in the eastern Trans-Hudson Orogen, Manitoba, Canada. Geological Society of America, 2008 Annual Meeting, October 5–9, 2008, Houston, TX, Abstracts with Programs, v. 40, no. 6, p. 204.

Hajnal, Z., Lucas, S.B., White, D.J., Lewry, J., Bezdan, S., Stauffer, M.R., Thomas, M.D. 1996. Seismic reflection images of strike-slip faults and linked detachments in the Trans-Hudson Orogen. Tectonophysics 15, 427–439.

Hajnal, Z., Lewry, J., White, D., Ashton, K., Clowes, R., Stauffer, M., Gyorfi, I. Takacs, E., 2005. The Sask Craton and Hearne Province margin: seismic reflection studies in the western Trans- Hudson Orogen. Canadian Journal of Earth Sciences, 42, 403–419.

Harrison, J.M. 1949. Geology and mineral deposits of File - Tramping Lakes area, Manitoba. Geological Survey of Canada, Memoir 250, 92p

Hoffman, P. F., 1988. United Plates of America, the birth of a craton-Early Proterozoic assembly and growth of Laurentia. Annual Review of Earth and Planetary Sciences 16, 543-603.

Holdsworth, R.E., Strachan, R.A., 1991. Interlinked system of ductile strike slip and thrusting formed by Caledonian sinistral transpression in northeastern Greenland. Geology 19, 510 – 513.

Holland, H. D., Feakes, C. R., and Zbinden, E. A., 1989. The Flin Flon paleosol and the composition of the atmosphere 1.8 BYBP. American Journal of Science, 289, 362–389.

Indares, A., Dunning, G., Cox, R., 2000. Tectono-thermal evolution of deep crust in a Mesoproterozoic continental collision setting: the Manicouagan example. Canadian Journal of Earth Sciences 37, 325–340.

Jessup, M. J., Newell, D. L., Cottle, J. M., Berger,A. L., Spotila, J. A., 2008. Orogen-parallel extension and exhumation enhanced by denudation in the trans-Himalayan Arun River gorge, Ama Drime Massif, Tibet-Nepal. Geology 36, 587–590. doi:10.1130/G24722a.1.

Jessup, M. J., Cottle, J. M., 2010. Progression from south-directed extrusion to orogen-parallel extension in the southern margin of the Tibetan Plateau, Mount Everest Region. Tibet Journal of Geology 118, 467–486. doi:10.1086/655011.

Kisters, A.F.M., Jordaan, L.S., Neumaier, K., 2004. Thrust-related dome structures in the Karibib district and the origin of orthogonal fabrics in the south Central Zone of the Pan-African Damara belt, Namibia. Precambrian Research 133, 283–303.

Kraus, J., 1998. Structural and metamorphic studies in the Snow Lake area, Trans-Hudson Orogen, Manitoba, central Canada Ph.D. thesis, University of New Brunswick, Fredericton, New Brunswick.

Kraus, J., Menard, T., 1997. A thermal gradient at constant pressure: implications for low- to medium-pressure metamorphism in a compressional tectonic setting, Flin Flon and Kisseynew domains, Trans-Hudson Orogen, central Canada. The Canadian Mineralogist 35, 1117–1136.

Kraus, J., Williams, P.F., 1999. Structural development of the Snow Lake allochthon and its role in the evolution of the southeastern Trans-Hudson Orogen in Manitoba, central Canada. Canadian Journal of Earth Sciences 36, 1881–1899.

Kuiper, Y.D., Lin, S., Böhm, C.O., 2011. Himalayan-type escape tectonics along the Superior Boundary Zone in Manitoba, Canada. Precambrian Research 187, 248–262.

Kvale, A., 1953. Linear structures and their relation to movement in the Caledonides of Scandinavia and Scotland. Quarterly Journal of the Geological Society London 109, 51-74.

Lewry, J.F., Collerson, K.D. 1990. The Trans-Hudson Orogen: extent, subdivisions and problems. In The Early Proterozoic Trans-Hudson Orogen of North America. Edited by J.F. Lewry, M.R. Stauffer, P.C. Thurston, and K.D. Card. Geological Association of Canada, Special Paper 37, pp. 1–14.

Lin, S., Williams, P.F., 1992. The geometrical relationship between the stretching lineation and the movement direction of shear zones. Journal of Structural Geology 14, 491–497.

Lister, G.S., Williams, P.F., 1983. The partitioning of deformation in flowing rock masses. Tectonophysics 92, l-33.

Lucas, S.B., Green, A., Hajnal, Z., White, D., Lewry, J.F., Ashton, K.E., Weber, W., Clowes, R., 1993. Deep seismic profiles across a Proterozoic collision zone: surprises at depth. Nature (London), 363, 339–342.

Lucas, S.B., White, D., Hajnal Z., Lewry, J., Green, A., Clowes, R., Zwanzig, H., Ashton, K.,

Schledewitz, D., Stauffer, M., Norman, A., Williams, P.F., Spence, G., 1994. Three-dimensional collisional structure of the Trans-Hudson Orogen, Canada. Tectonophysics 232, 161-178.

Lucas, S.B., Stern, R.A., Syme, E.C., Reilly, B.A., Thomas, D.J., 1996. Intraoceanic tectonics and the development of continental crust: 1.92–1.84 Ga evolution of the Flin Flon Belt, Canada. Geological Society of America Bulletin 108, 602–629.

Lucas, S.B., Stern, R.A., Syme, E.C., Zwanzig, H, Bailes, A.H., Ashton, K.E., Maxeiner, R.O., Ansdell, K.M., Lewry, J.F., Ryan, J.J., and Kraus, J. 1997. Tectonics of the southeastern Reindeer Zone, Trans-Hudson Orogen (Manitoba, and Saskatchewan). Geological Association of Canada – Mineralogical Association of Canada, Program with Abstracts, v. 22: p. A93.

Machado, N., Zwanzig, H.V., and Parent, M. 1999. U–Pb ages of plutonism, sedimentation, and metamorphism of the Paleoproterozoic Kisseynew metasedimentary belt, Trans- Hudson Orogen (Manitoba, Canada). Canadian Journal of Earth Sciences, 36: 1829–1842.

Machado, N., Gapais, D., Potrel, A., Gauthier, G., Hallot, E., 2011. Chronology of transpression, magmatism and sedimentation in the Thompson Nickel Belt (Manitoba, Canada) and timing of Trans-Hudson Orogen – Superior Province collision. Canadian Journal of Earth Sciences 48, 295 – 324. doi:10.1139/E10-040.

Mandal, N., Kumar Mitra, A., Sarkar, S., Chakraborty, C., 2009. Numerical estimation of the initial hinge-line irregularity required for the development of sheath folds: A pure shear model. Journal of Structural Geology 31, 1161–1173.

Matte, P., 2007. Variscan thrust nappes, detachments, and strike-slip faults in the French Massif Central: Interpretation of the lineations. The Geological Society of America Memoir 200, 391 – 402.

Menard, T., Gordon, T.M., 1997. Metamorphic P-T paths from the eastern Flin Flon Belt, and Kisseynew Domain, Snow Lake, Manitoba. The Canadian Mineralogist 35, 1093–1115.

Miller, R. B., Paterson, S.R., Lebit, H., Alsleben, H., Lüneburg, C., 2006. Significance of composite lineations in the mid-to deep crust: A case study from the North Cascades, Washington. Journal of Structural Geology 28, 302–322.

Moores, E. M., Twiss, R.J. 1995. Tectonics. W.H. Freeman and Company, New York, 415 pp.

Murphy, M. A., Copeland, P., 2005. Transtensional deformation in the central Himalaya and its role in accommodating growth of the Himalayan orogen. Tectonics, 24, TC4012, doi: 10.1029/2004TC001659.

Nagy, C., Godin, L., Antolín, B. Cottle, J., Archibald, D., 2015. Mid-Miocene initiation of orogen-parallel extension, NW Nepal Himalaya Lithosphere 7, 483 – 502. doi:10.1130/l425.1.

NATMAP Shield Margin Project Working Group. 1998. Geology, NATMAP Shield Margin Project area (Flin Flon Belt), Manitoba–Saskatchewan. Geological Survey of Canada Map 1968A, Manitoba Energy and Mines Map A-98-2, sheets 1–7, Saskatchewan Energy and Mines

Map 258A-1, scale 1: 100 000.

Nemeth, B., Clowes, R., Hajnal, Z., 2005. Lithospheric structure of the Trans-Hudson Orogen from seismic refraction—wide-angle reflection studies. Canadian Journal of Earth Sciences 42, 435–456. doi: 10.1139/e05-032.

Neves, S. P., da Silva, J. M. R., Mariano, G., 2005. Oblique lineations in orthogneisses and supracrustal rocks: Vertical partitioning of strain in a hot crust (eastern Borborema Province, NE Brazil). Journal of Structural Geology 27, 1513–1527.

Norman, A.R., Williams, P.F., Ansdell, K.M., 1995. Early Proterozoic deformation along the southern margin of the Kisseynew gneiss belt, Trans-Hudson Orogen: a 30 Ma progressive deformation cycle. Canadian Journal of Earth Sciences 32: 875–894.

Northrup, C.J., Burchfiel, B.C., 1996. Orogen-parallel transport and vertical partitioning of strain during oblique collision, Efjorden, north Norway. Journal of Structural Geology 18, 1231–1244.

Percival, J.A., Whalen, J.B., Rayner, N., 2005. Pikiwitonei-Snow Lake Manitoba transect (parts of NTS 63J, 63O and 63P), Trans-Hudson Orogen-Superior Margin Metallotect Project: new results and tectonic interpretation. In: Report of Activities 2005, Manitoba Industry, Economic Development and Mines, Manitoba Geological Survey, pp. 69–91.

Percival, J.A., Zwanzig, H.V., Rayner, N., 2006. New tectonostratigraphic framework for the

northeastern Kisseynew Domain, Manitoba (parts of NTS 63O). In: Report of Activities 2006, Manitoba Science, Technology, Energy and Mines, Manitoba Geological Survey, pp. 74–84.

Piazolo, S., Passchier, C.W., 2002. Controls on lineation development in low to medium grade shear zones: A study from the Cap de Creus peninsula, NE Spain. Journal of Structural Geology 24, 25–44.

Poli, L.C., Oliver, G.J.H., 2001. Constrictional deformation in the central zone of the Damara Orogen, Namibia. Journal of African Earth Sciences 33, 303-321.

Ratschbacher, L., Frisch, W., Linzer, H.G., Merle, O., 1991. Lateral extrusion in the eastern Alps. Part 2: Structural analysis, Tectonics, 10, 257–271, doi: 10.1029/90TC02623.

Rayner, N., Stern, R.A., Bickford, M.E., 2005b. Tectonic implications of new SHRIMP and TIMS U–Pb geochronology of rocks from the Sask Craton, Peter Lake Domain, and Hearne margin, Trans-Hudson Orogen, Saskatchewan. Canadian Journal of Earth Sciences 42, 635–657.

Rey, P., Vanderhaeghe, O., Teyssier, C., 2001. Gravitational collapse of the continental crust: definition, regimes and modes. Tectonophysics 342, 435–449.

Ring, U., Ratschbacher, L., Frisch, W., 1988. Plate boundary kinematics in the Alps: Motion in the Arosa suture zone. Geology 16, 696 – 698.

Rossetti, F., Faccenna, C., Crespo-Blanc, A., 2005. Structural and kinematic constraints to the

exhumation of the Alpujarride Complex (Central Betic Cordillera, Spain). Journal of Structural Geology 27, 199–216. doi:10.1016/j.jsg.2004.10.008.

Rubingh, K.E., 2011. Stratigraphy of the McLeod Road–Birch Lake thrust panel, Snow Lake, west-central Manitoba (parts of NTS 63K16 and 63J13). In: Report of Activities 2011 Manitoba Innovation, Energy and Mines, pp. 68–78.

Rubingh, K.E., Lafrance, B., Gibson, H.L., Gagné, S., 2012a. Preliminary lithostratigraphic map of the McLeod Road– Birch Lake thrust panel, Snow Lake, west-central Manitoba (parts of NTS 63K16, 63J13). In: Report of Activities 2012a, Manitoba Innovation, Energy and Mines, Preliminary Map PMAP2012-7, 1:5000 scale.

Rubingh, K.E., Lafrance, B., Gibson, H.L., 2012b. Lithostratigraphy and structural geology of the McLeod Road–Birch Lake thrust panel, Snow Lake, west-central Manitoba (parts of NTS 63K16, 63J13). In: Report of Activities 2012b, Manitoba Innovation, Energy and Mines, pp. 104–114.

Rubingh, K.E., Gibson, H.L., Lafrance, B., 2017. Evidence for voluminous, bimodal pyroclastic volcanism, during rifting of a Paleoproterozoic Arc at Snow Lake, Manitoba. Canadian Journal of Earth Sciences 54, 654–676.

Seyferth, M., Henk, A., 2004. Syn-convergent exhumation and lateral extrusion in continental collision zones—Insights from three-dimensional numerical models. Tectonophysics 382, 1–29.

doi:10.1016/j.tecto.2003.12.004.

Scharf, A., Handy, M.R., Favaro, S., Schmid, S.M, Bertrand, A., 2013. Modes of orogen-parallel stretching and extensional exhumation in response to microplate indentation and roll-back subduction (Tauern Window, Eastern Alps). International Journal of Earth Sciences 102, 1627 – 1654. doi 10.1007/s00531-013-0894-4.

Schneider, D.A., Heizler, M.T., Bickford, M.E., Wortman, G.L., Condie, K.C., Perilli, S., 2007. Timing constraints of orogeny to cratonization: thermochronology of the Paleoproterozoic Trans-Hudson orogen, Manitoba and Saskatchewan, Canada. Precambrian Research 153, 65–95.

Shackleton, R. M., and Ries, A.C., 1984. The relation between regionally consistent stretching lineations and plate motions. Journal of Structural Geology6(1), 111–117.

Sibson, R. H., 1977. Fault rocks and fault mechanisms. Geological Society of London Journal 133, 191–231.

Skjernaa, L., 1989. Tubular folds and sheath folds: definitions and conceptual models for their development, with examples from the Grapesvare area, northern Sweden. Journal of Structural Geology 11, 689-703.

Staples, R.D., Gibson, H.D., Colpron, M., Ryan, J.J., 2016. An orogenic wedge model for diachronous deformation, metamorphism, and exhumation in the hinterland of the northern

Canadian Cordillera. Lithosphere 8, 165–184. doi:10.1130/L472.1

Stauffer, M. R. 1984. Manikewan and early Proterozoic ocean in central Canada, its igneous history and orogenic closure. Precambrian Research, 25, 257–281.

Stern, R.A., Syme, E.C., Bailes, A.H., Galley, A.G., Thomas, D.J., and Lucas, S.B. 1992. Nd-isotopic stratigraphy of the Early Proterozoic Amisk Group metavolcanic rocks from the Flin Flon
belt. In Radiogenic age and isotopic studies. Geological Survey of Canada, Report 5, Paper 92-2, pp. 73–84.

Stewart, M., Lafrance, B., Gibson, H.L., 2018. Early thrusting and folding in the Snow Lake camp, Manitoba: Tectonic implications and their effects on volcanogenic massive sulphide deposits. Canadian Journal of Earth Sciences 55, 935–957.

Styron, R. H., Taylor, M.H., Murphy M.A., 2011. Oblique convergence, arc-parallel extension, and the role of strike-slip faulting in the High Himalayan, Geosphere, 7, 582–596.

Syme, E.C, Bailes, A.H., Lucas, S.B., 1995. Geology of the Reed Lake area (parts of NTS 63K/9 and 10). In: Report of Activities, 1995. Manitoba Energy and Mines, Geological Services, pp. 42–60.

Syme, E.C., Lucas, S.B., Bailes, A.H., Stern, R.A., 1999. Contrasting arc and MORB-like

assemblages in the Paleoproterozoic Flin Flon Belt, Manitoba, and the role of intra-arc extension in localizing volcanic-hosted massive sulphide deposits. Canadian Journal of Earth Sciences 36, 1767–1788. doi:10.1139/cjes- 36-11-1767.

Tikoff, B., Greene D., 1997. Stretching lineations in transpressional shear zones: An example from the Sierra Nevada Batholith, California. Journal of Structural Geology 19, 29–39.

White, D.J., Lucas, S.B., Bleeker, W., Hajnal, Z. Lewry, J.F., Zwanzig, H.V., 2002. Suture-zone geometry along an irregular Paleoproterozoic margin: the Superior Boundary Zone, Manitoba, Canada. Geology 30, 735–738.

White, D.J., Thomas, M.D., Jones, A.G., Hope, J., Németh, B. and Hajnal, Z. 2005. Geophysical transect across a Paleoproterozoic continent-continent collision zone: the Trans-Hudson Orogen, Canadian Journal of Earth Sciences 42, 385–402.

Williams, P.F., and Jiang, D., 2005. An investigation of lower crustal deformation: evidence for channel flow and its implications for tectonics and structural studies. Journal of Structural Geology 27, 1486–1504.

Williams, J.R., and Platt, J.P., 2017. Superposed and refolded metamorphic isograds and superposed directions of shear during late orogenic extension in the Alborán Domain, southern Spain. Tectonics 36, 756 – 786. doi: 10.1002/2016TC004358.

Zaleski, E., Froese, E., Gordon, T.M., 1991. Metamorphic petrology of Fe–Zn–Mg–Al alteration

at the Linda volcanogenic massive sulfide deposit, Snow Lake, Manitoba. Canadian Mineralogist 29, 995–1017.

Zwanzig, H.V., 1990. Kisseynew gneiss belt in Manitoba: stratigraphy, structure, and tectonic evolution; in The Early Proterozoic Trans- Hudson Orogen of North America, J.F. Lewry and M.R. Stauffer (ed.), Geological Association of Canada, Special Paper 37, p. 95–120.

Zwanzig, H.V., 1999. Structure and stratigraphy of the south flank of the Kisseynew Domain in the Trans-Hudson Orogen, Manitoba: implications for 1.845–1.77 Ga collision tectonics; in NATMAP Shield Margin Project, Volume 2. Canadian Journal of Earth Sciences 36, 1859 – 1880.

Zwanzig, H.V., Bailes, A.H., 2010. Geology and geochemical evolution of the northern Flin Flon and southern Kisseynew domains, Kississing – File lakes area, Manitoba (parts of NTS 63K, N). Manitoba Innovation, Energy and Mines, Manitoba Geological Survey, Geoscientific Report GR2010-1, pp. 1–135.

Zwanzig, H.V., Murphy, L.A., 2009. Geometry and history of the Notigi Lake structure (parts of NTS 63O14, 63B3). In: Report of Activities, Manitoba Innovation, Energy and Mines, Manitoba Geological Survey, pp. 85–93.

	Snow Creek sequence
Birch Lake Basalts: Aphyric pillowed flows with thin pillow selvages (Bailes and Schledewitz, 1998).	**Snow Creek basalts:** Aphyric pillowed lavas with thin selvages and interpillow hyaloclastite (Bailes and Galley, 1996).
MB sequence	**Chisel sequence**
Unit 5: **Mafic volcaniclastic and lava lithofacies:** Mafic volcaniclastic rocks and lava flows with coarse pyroxene phenocrysts ranging in size from 0.5 - 1 cm in diameter.	**(Upper Chisel sequence) Porphyritic pillowed lavas:** Pyroxene and pyroxene - plagiolase phyric mafic flows similar to Threehouse pillowed flows.
Unit 4: Felsic lava lithofacies: Aphyric, coherent, rhyolite flow lobes and flow top breccias with locally well developed columnar jointing and quartz filled amygdules.	**Undivided felsic units of the upper and lower Chisel volcanic rocks**: Typically coherent aphyric felsic lavas, locally containing remnant quartz phenocrysts.
Unit 3: Mafic volcanic and volcaniclastic lithofacies: Well-bedded, heterolithic mafic volcaniclastic rocks with bombs and lapilli and block sized fragments of aphyric to plagioclase-porphyritic mafic flow, aphyric to plagioclase-porphyritic felsic flow, scoriaceous mafic rock, and plagioclase and pyroxene-porphyritic mafic flow; plagioclase-porphyritic pillowed flows.	**Threehouse mafic volcaniclastic rocks and pillowed lavas**: Well-bedded, fine grained, mafic volcaniclastic rocks represented by scoria-rich mafic lapilli tuff and tuff breccias, with well-preserved bomb sags, ripples and rip up clasts; pyroxene-plagioclase phyric pillowed basaltic andesitic lavas.
Unit 2: **Felsic lavas and volcaniclastic lithofacies:** Plagioclase-porphyritic, flow-banded, rhyolite flows with flow yop breccias; felsic volcaniclastic rocks with quartz and feldspar porphyritic felsic fragments.	**(Lower Chisel sequence) Ghost and Photo Lake rhyolite:** Rhyolite flows with lobe features and flow top breccias.
Unit 1: Heterolithic felsic volcaniclastic lithofacies. Pyroclastic flows composed of fine tuff (ash sized material), intact and broken plagioclase crystals (1-2mm), dark wispy fragments, mafic lithic fragments and plagioclase-porphyritic felsic fragments.	**(Lower Chisel sequence) Powderhouse dacite like unit**: Plagioclase and locally quartz phenocrystic dacitic tuff and lapillit tuffs with dark wispy fragments and mafic lithic clasts.

Table 3. 1: Physical attributes and correlation of units in the Snow Lake area.

Kraus and Williams (1999) Snow Lake area	**Connors et al. (1999, 2002)** Wekusko lake area	**Rubingh, et al. (2017)** Snow Lake area
D3 **F3 folds** (Macroscopic NNE trending Threehouse synform) S3 spaced fracture cleavage **F2 shear zones** **McLeod Road Thrust fault, Birch Lake Fault** N to NNE trend; moderate dip, and a down dip stretching lineation with sinistral transcurrent shear sense **S2** crenulation cleavage / schistosity, porphyroblasts have pressure shadows aligned parallel to S2 porphyroblasts	**D3** **F3 folds** **D3 faults** **Crowduck Bay fault** S3 cleavage (NNE to N trending) wraps around staurolite but is overgrown by garnet. L3 (SE to NE plunging) extension lineation (defined by stretched clasts and elongate minerals) overprints F2a and F2b folds and D2 thrusts	**D3** **G6** **F6 fold** (Macroscopic NNE trending Threehouse synform) **S6 foliation** NNE to ENE, steeply dippping, weakly spaced fracture cleavage, which is axial planar to z folds, and the Threehouse synform **G5** **S5 overprinting cleavage**, sinistral reactivation of the MRT fault and dextral reactivation of the Cleaver Lake fault
F2 isoclinal folds **(McLeod Lake fold)** Low - angle shear zones and reactivation of F1 shear zones Composite **L1 - L2** stretched quartz aggregates, elongate amygdales and clasts **S1 parallel to S0** in the the Burntwood Group rocks and the volcanic rocks S1 is preserved as a mesoscopic pervasive fabric in porphyroblasts. **F1** isoclinal folds in Burntwood group rocks and low - angle shear zones; Snow Lake Fault	**D2** **D2 faults** Faults are subparallel to the S2a cleavage and truncate the hinge of F2a folds. Other faults are folded by later generation F2 folds. **F2 folds** Map scale tight to isoclinal folds. The folds plunge sub parallel to the extension lineation, fold the S2a fabric and contain a weak axial planar cleavage. S2a is defined by alignment of phyllosilicates in the Missi Group	**D2** **G4** **McLeod Road Thrust fault**, (N to NNE trending fault). F4 folds - Herblet Lake and Pulver Lake Gneiss domes, Whitefish Bay synform, Herblet Lake fold **G3** **Cleaver Lake fault, Birch Lake fault,** **F3 McLeod Lake fold** **G2** Stretching lineation (elongation of volcanic clasts, amygdules) **S2 defined by the flattening of clasts** in the volcaniclastic rocks **F2 Nor Acme fold** F2 tight to isoclinal folds in the Burntwood Group rocks
D1 and D2 Sedimentation of Missi and Burntwood groups	**D1** Not recognised	**D1** **G1** **Brittle faults and folds** Bounter Fault and lower fault of the MB panel. Sedimentation of Missi and Burntwood groups

Table 3. 2: Comparison of deformational events identified by various authors in the McLeod Road-Birch Lake thrust panel. Bold face indicates principle structures formed during each deformational event.

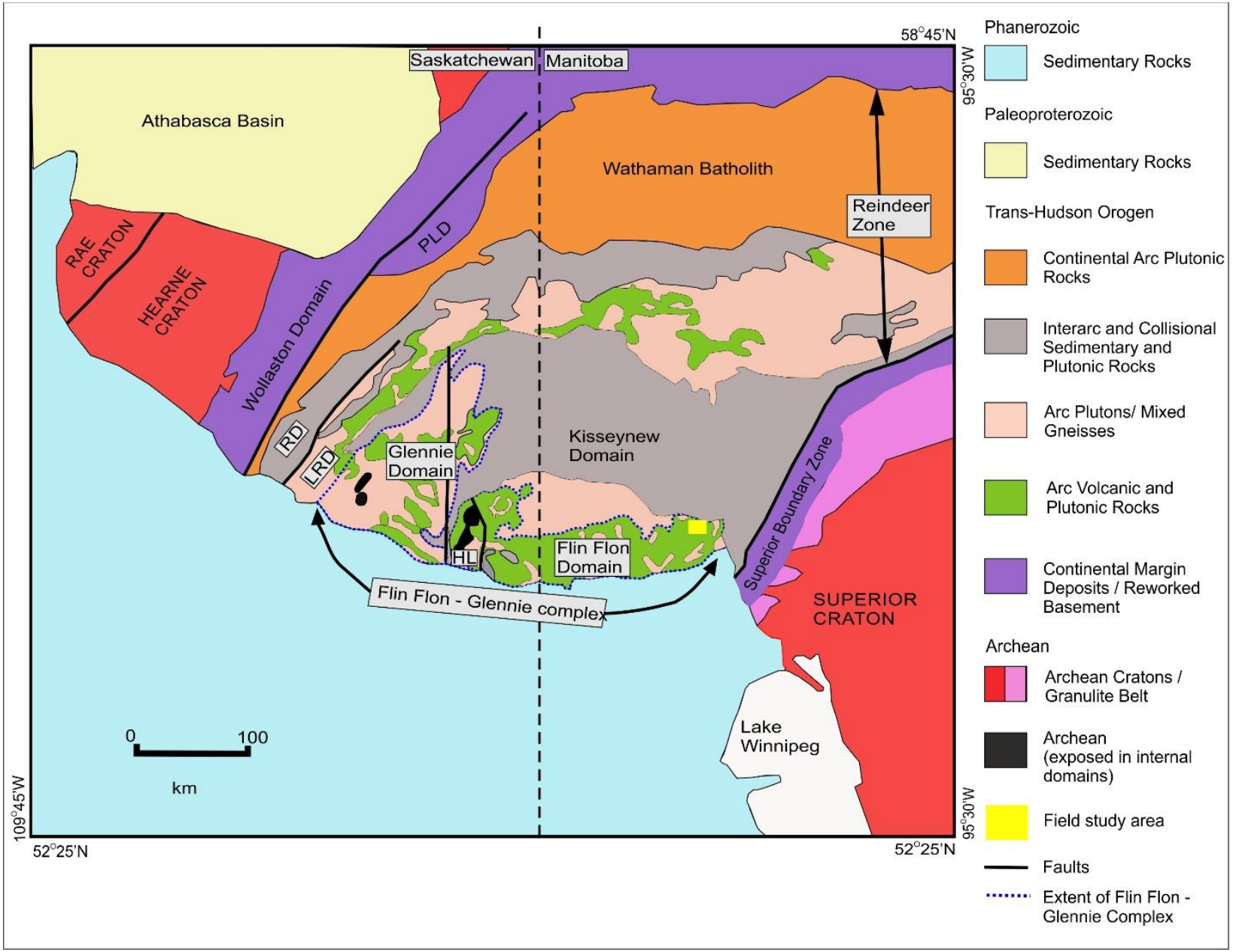
58°45'N
95°30'W
Saskatchewan
Manitoba
Athabasca Basin
Wathaman Batholith
Reindeer Zone
RAE CRATON
HEARNE CRATON
Wollaston Domain
PLD
RD
LRD
Glennie Domain
Kisseynew Domain
Superior Boundary Zone
HL
Flin Flon Domain
Flin Flon - Glennie complex
SUPERIOR CRATON
Lake Winnipeg
0
100
km
109°45'W
52°25'N
95°30'W
52°25'N
Phanerozoic
Sedimentary Rocks
Paleoproterozoic
Sedimentary Rocks
Trans-Hudson Orogen
Continental Arc Plutonic Rocks
Interarc and Collisional Sedimentary and Plutonic Rocks
Arc Plutons/ Mixed Gneisses
Arc Volcanic and Plutonic Rocks
Continental Margin Deposits / Reworked Basement
Archean
Archean Cratons / Granulite Belt
Archean (exposed in internal domains)
Field study area
Faults
Extent of Flin Flon - Glennie Complex

Figure 3. 1. Simplified domain map of the Saskatchewan – Manitoba portion of the Trans-Hudson Orogen (THO) and location of the Archean cratons. The extent of the Sask Craton (Ashton et al 2005) and the Flin – Flon Glennie complex (Ashton, 1999) is outlined. The latter comprises the Glennie Domain, Hanson Lake block and the Flin Flon Domain. HL, Hanson Lake block; RD, Rottenstone Domain; LRD, La Ronge Domain; PLD, Peter Lake Domain. The location of the Snow Lake study area is shown. Figure modified after Lucas et al. (1993).

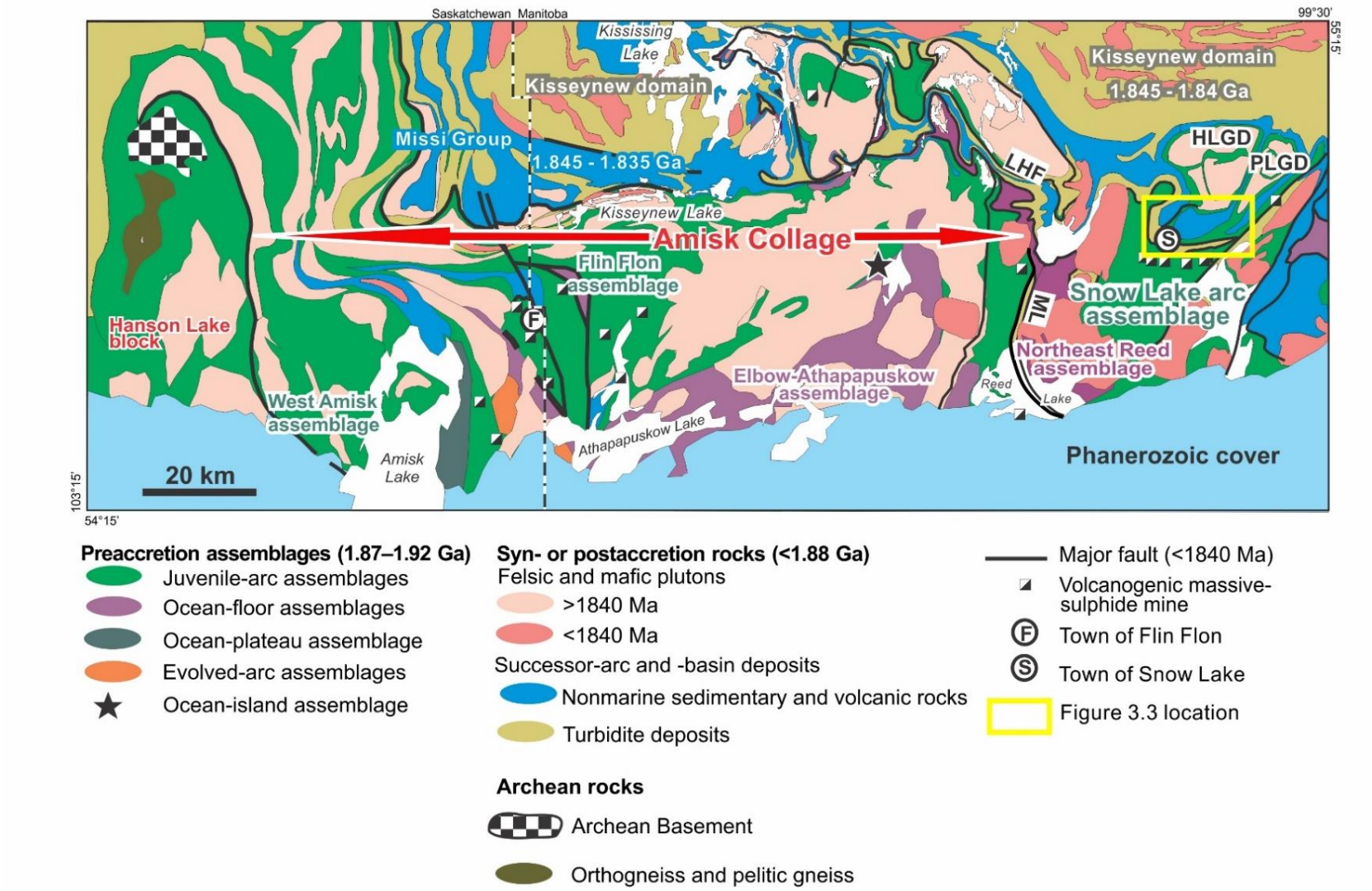

Figure 3. 2. Regional geology of the Flin Flon – Snow Lake belt, of Manitoba (modified after Syme et al. 1999). Abbreviations: HLGD, Herblet Lake gneiss dome; LHF, Loonhead Lake fault; ML, Morton Lake Fault; PLGD, Pulver gneiss dome. Extent of field study area is highlighted by the yellow box.

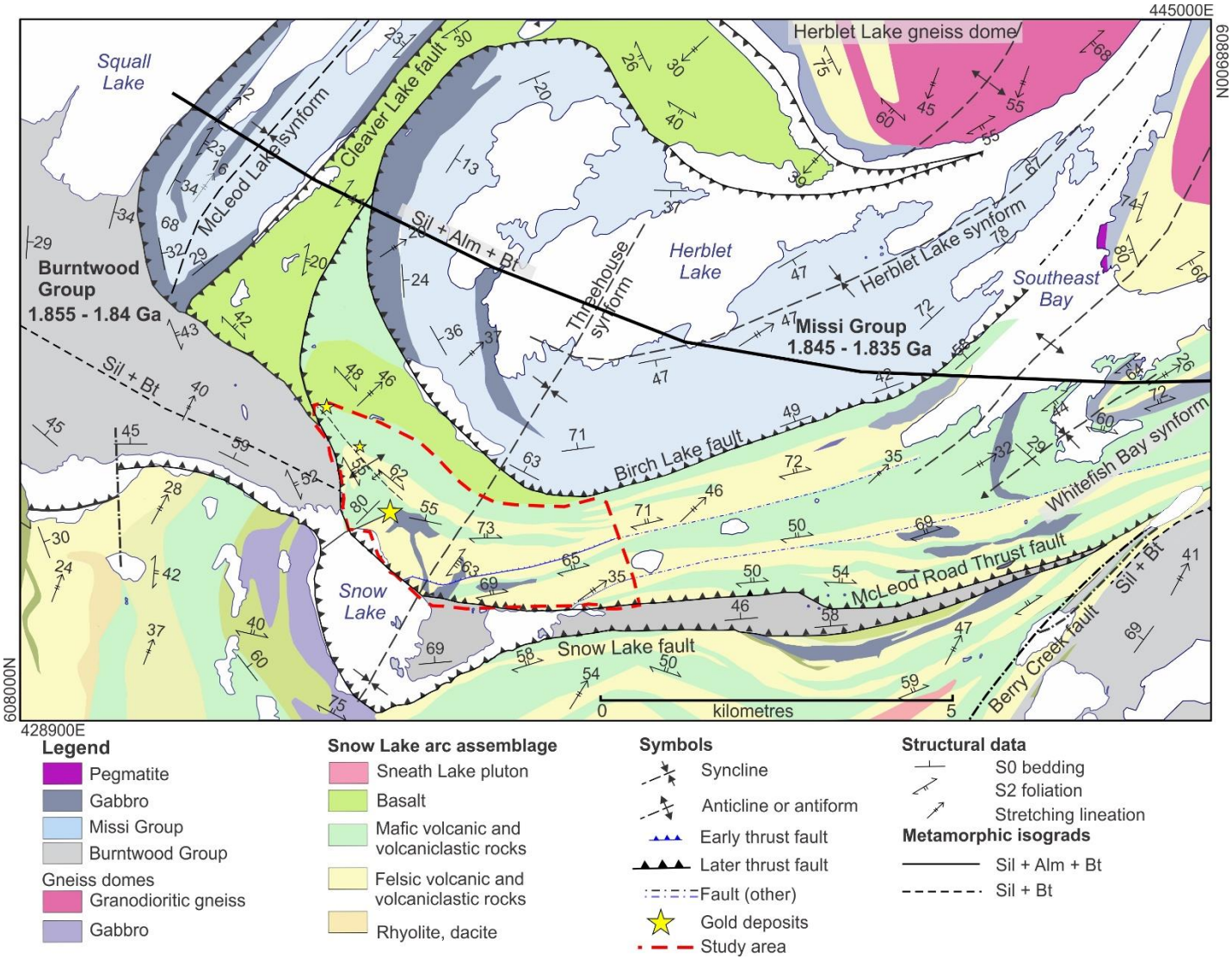

Figure 3. 3. Regional geology of the Snow Lake area and location of the McLeod Road - Birch Lake thrust panel study area. Modified after Gagné and Beaumont-Smith (2010). Regional data compilation from Froese and Moore (1980), Kraus and Williams (1999), Beaumont-Smith and Gagné (2008).

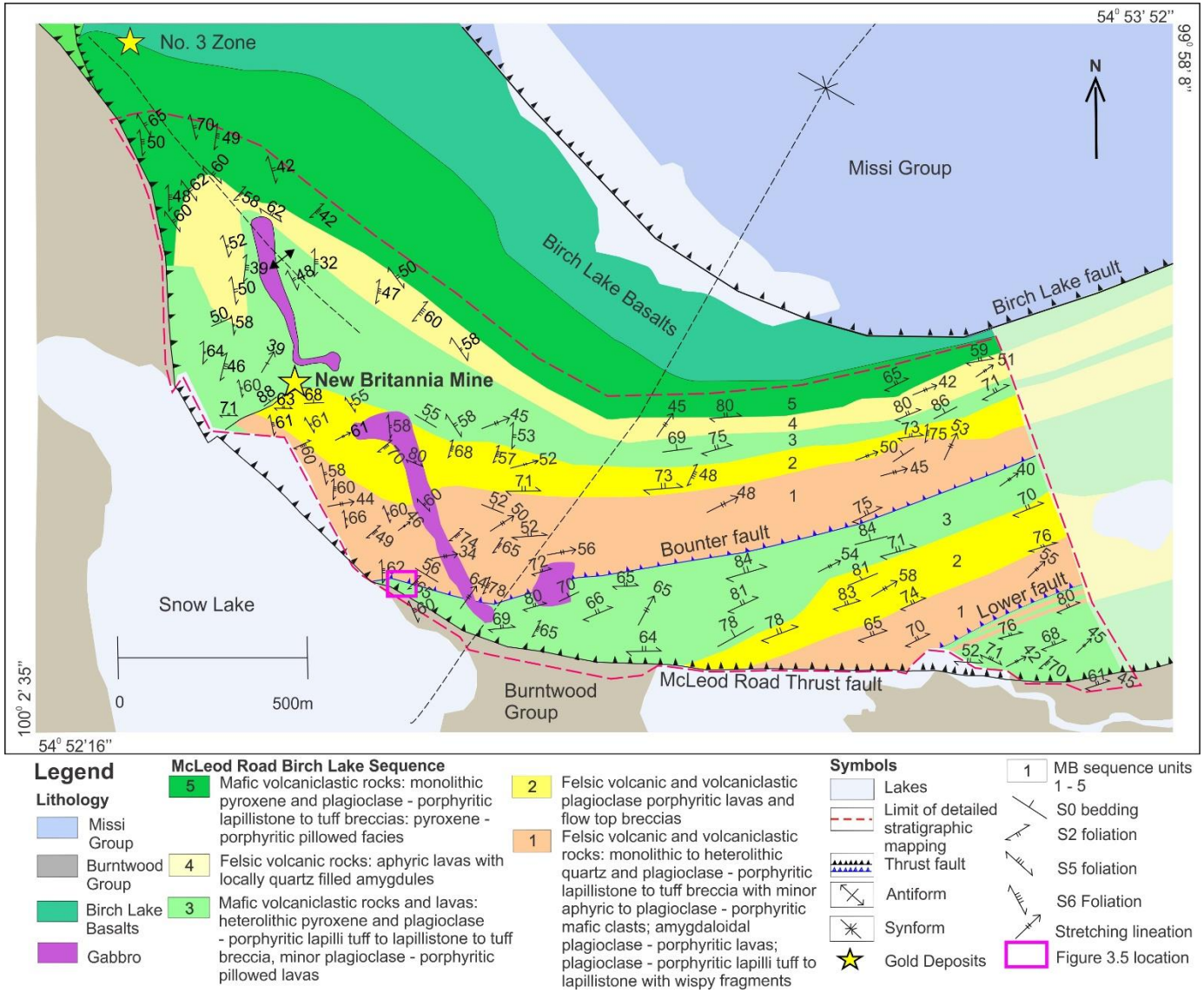

Figure 3. 4. Geology of the McLeod Road - Birch Lake thrust panel, (1:7000 scale; modified after Rubingh et al. 2012a and base geology map from Beaumont-Smith and Gagné 20010).

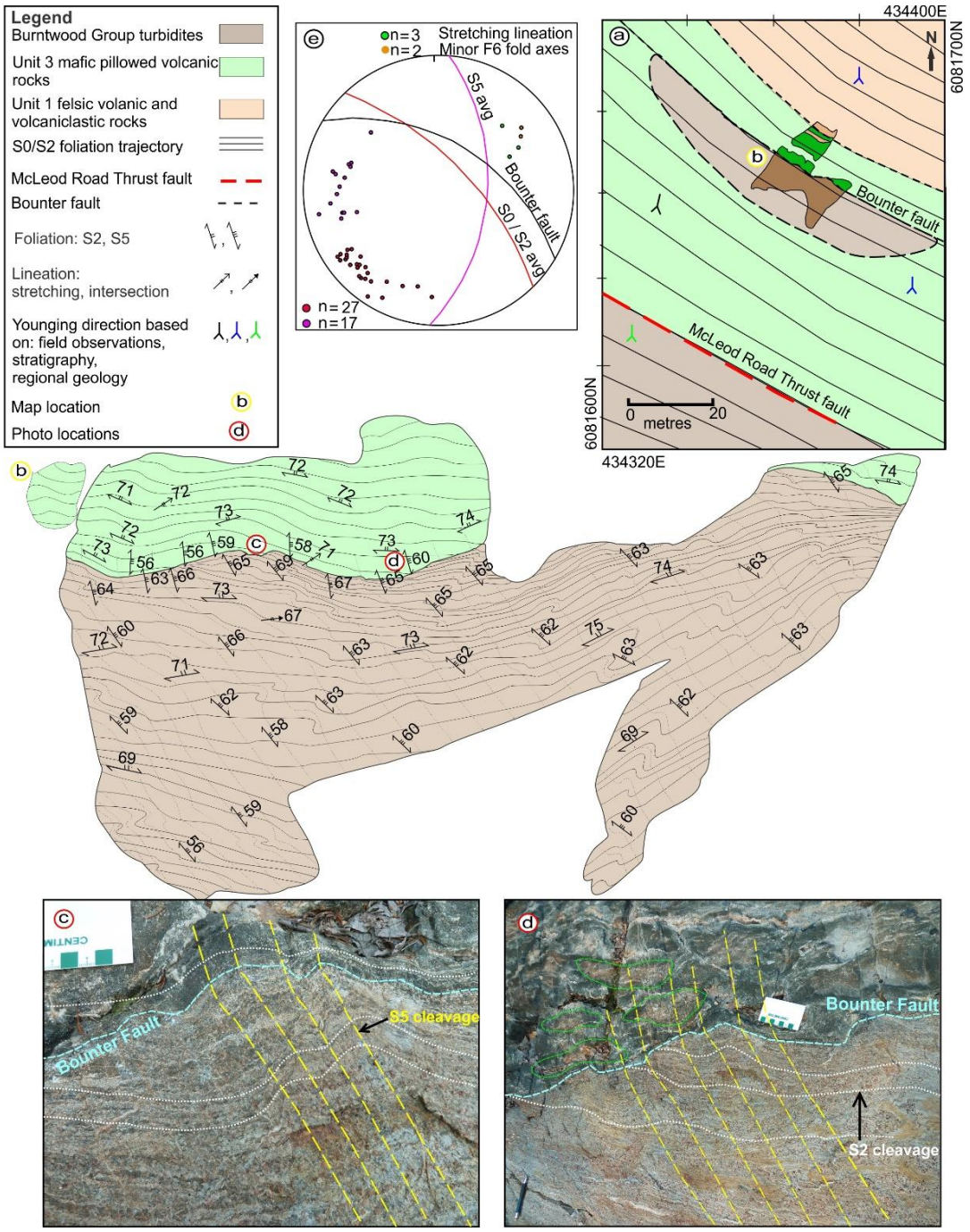

Figure 3. 5. (a) Form surface map of the S2 cleavage at the Bounter Fault, with detailed outcrop location (b) and the McLeod Road Thrust inferred location. (b) Detailed map of the Bounter Fault with the S2 foliation trajectory, S5 cleavage relationships and field photograph locations. (c) Folded contact (light blue) and the overprinting S5 cleavage (yellow) which refracts as it passes from the Burntwood Group turbidites, into the pillowed mafic volcanic rocks of unit 3. (d) Outline of deformed pillowed volcanic rocks (green) and relationship between the S2 cleavage (white) and the contact (blue). Photo card (9 cm in length for scale). (e) Equal area, lower hemisphere projection of structural data from the Bounter fault location. Number of measurements indicated by "N=numerical value".

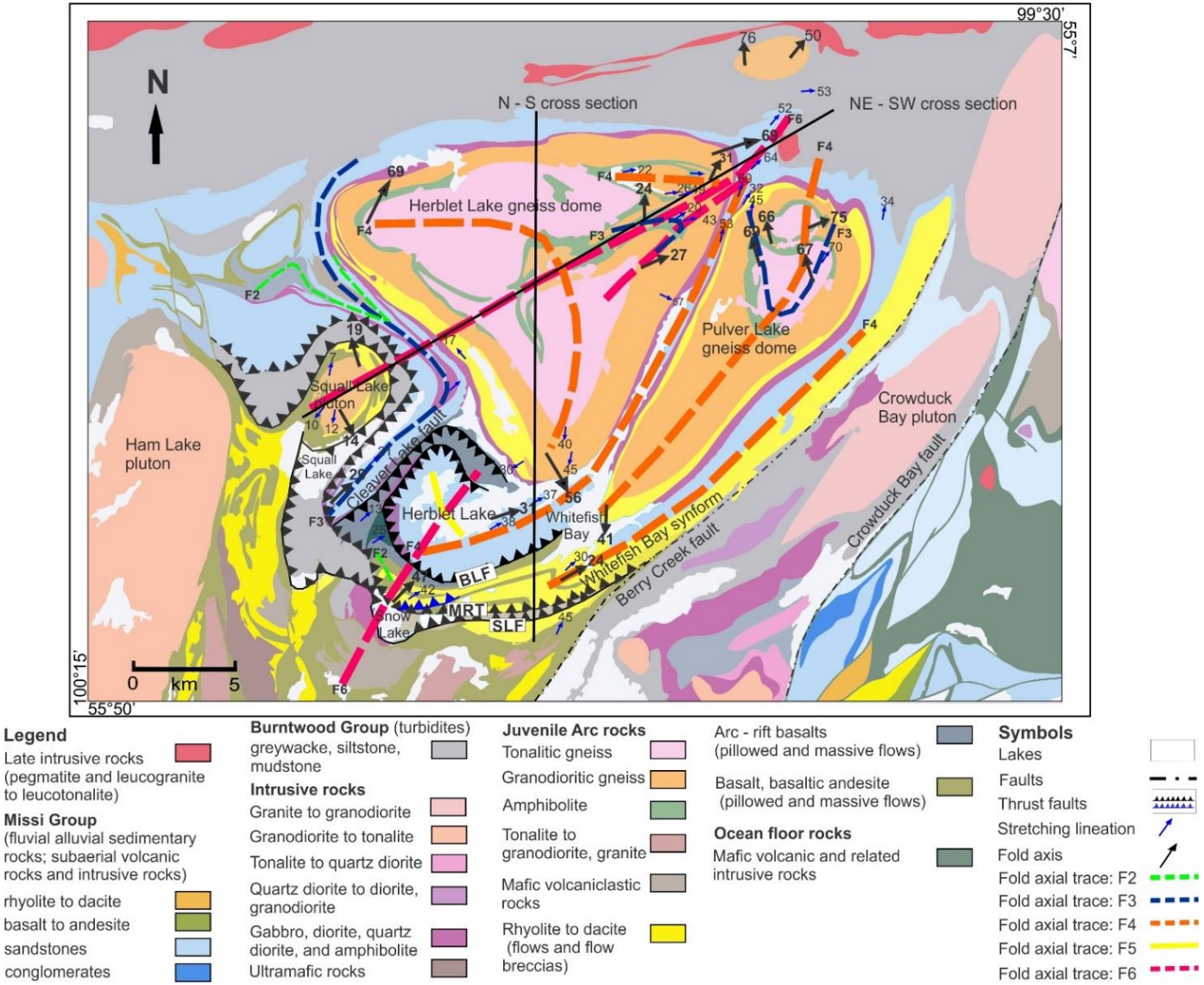

Figure 3. 6. Regional geological map showing the regional faults and interpretation of fold generations in the Snow Lake area. The N-S and NE-SW cross section locations are shown (solid black lines) which are illustrated in Figure 3.15. Abbreviations: MRT, McLeod Road Thrust Fault; BLF, Birch Lake Fault; SLF, Snow Lake Fault. Modified after Natmap Shield Margin Project Working Group

(1998).

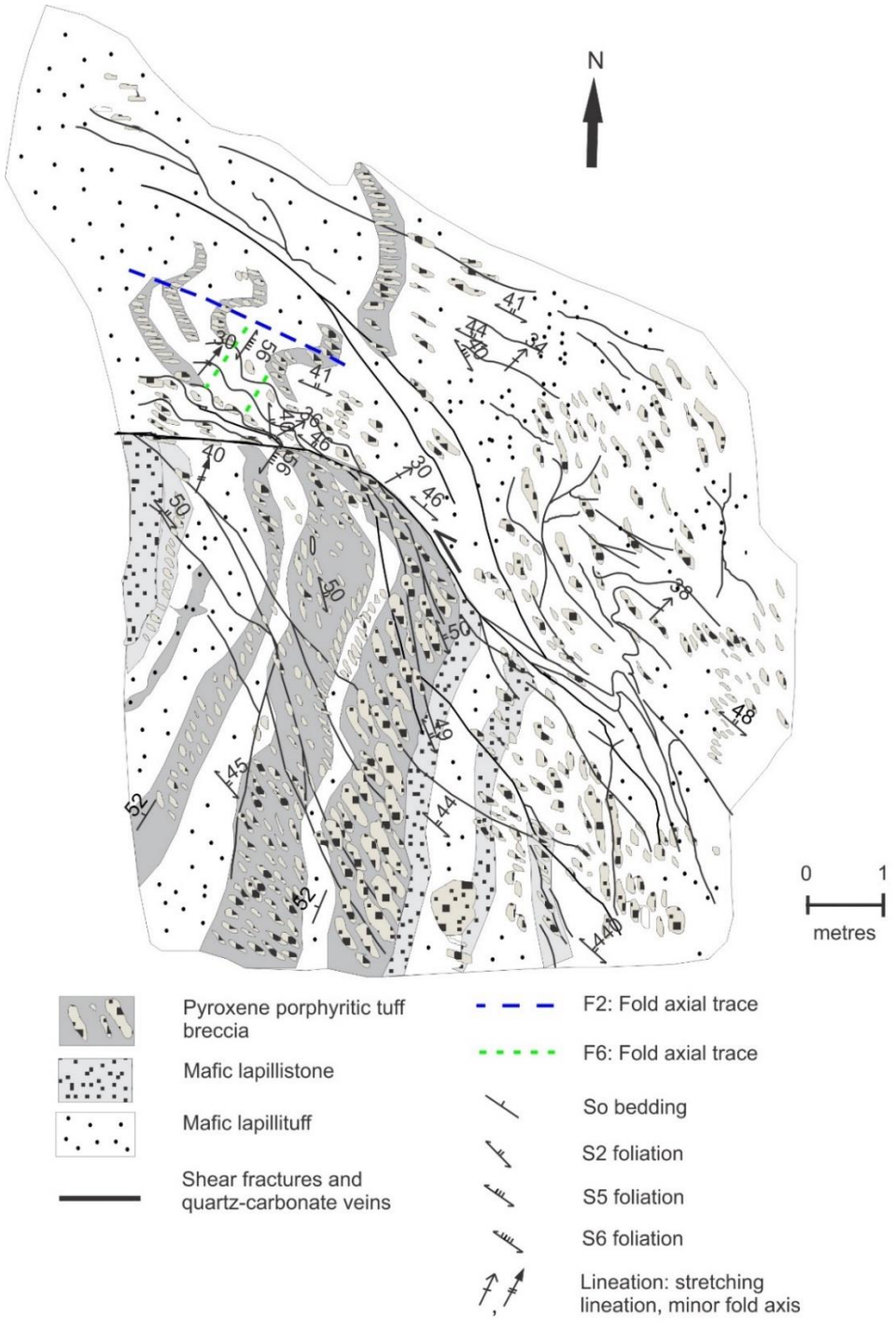

Figure 3. 7. Detailed outcrop geological map of the No 3 Zone outcrop illustrating the relationship between bedding and S2 in the hinge area of the F2 Nor-Acme Anticline, within the mafic volcaniclastic rocks of Unit 5. The latter consists of lapilli tuff, lapillistone and tuff breccia. Beds are 1-2 m thick and the matrix is crystal rich and composed of pyroxene and plagioclase with monolithic clasts that are 3 – 80 cm in size. The clasts are similar in composition and texture to the matrix. The clasts are characterized by 15% pyroxene (3-25 mm) and 5-7% plagioclase (2-4 mm) phenocrysts.

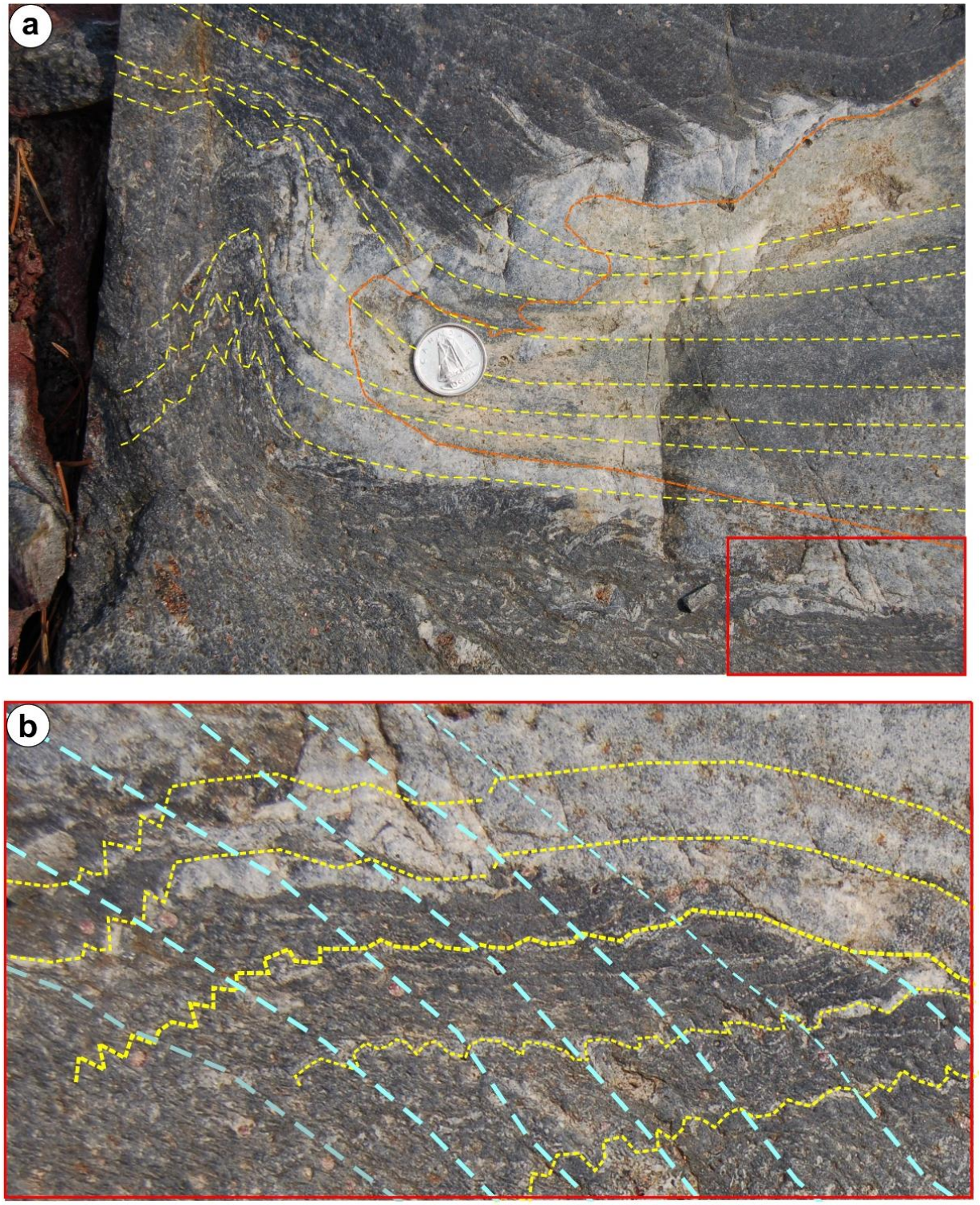

Figure 3. 8. Field photographs of an isoclinal F2 fold in turbiditic sandstone of the Burntwood Group within the Town of Snow Lake. (a) F2 fold hinge (orange) with axial planar S2 cleavage, (yellow), and red box outline indicating location of photograph (b) (b) Close up photograph of (a) (indicated by red box outline) showing microfolding of the S2 cleavage and S5 crenulation

cleavage (blue) along the lower limb of the isoclinal F2 fold. Coin (1.8 cm in diameter) for scale.

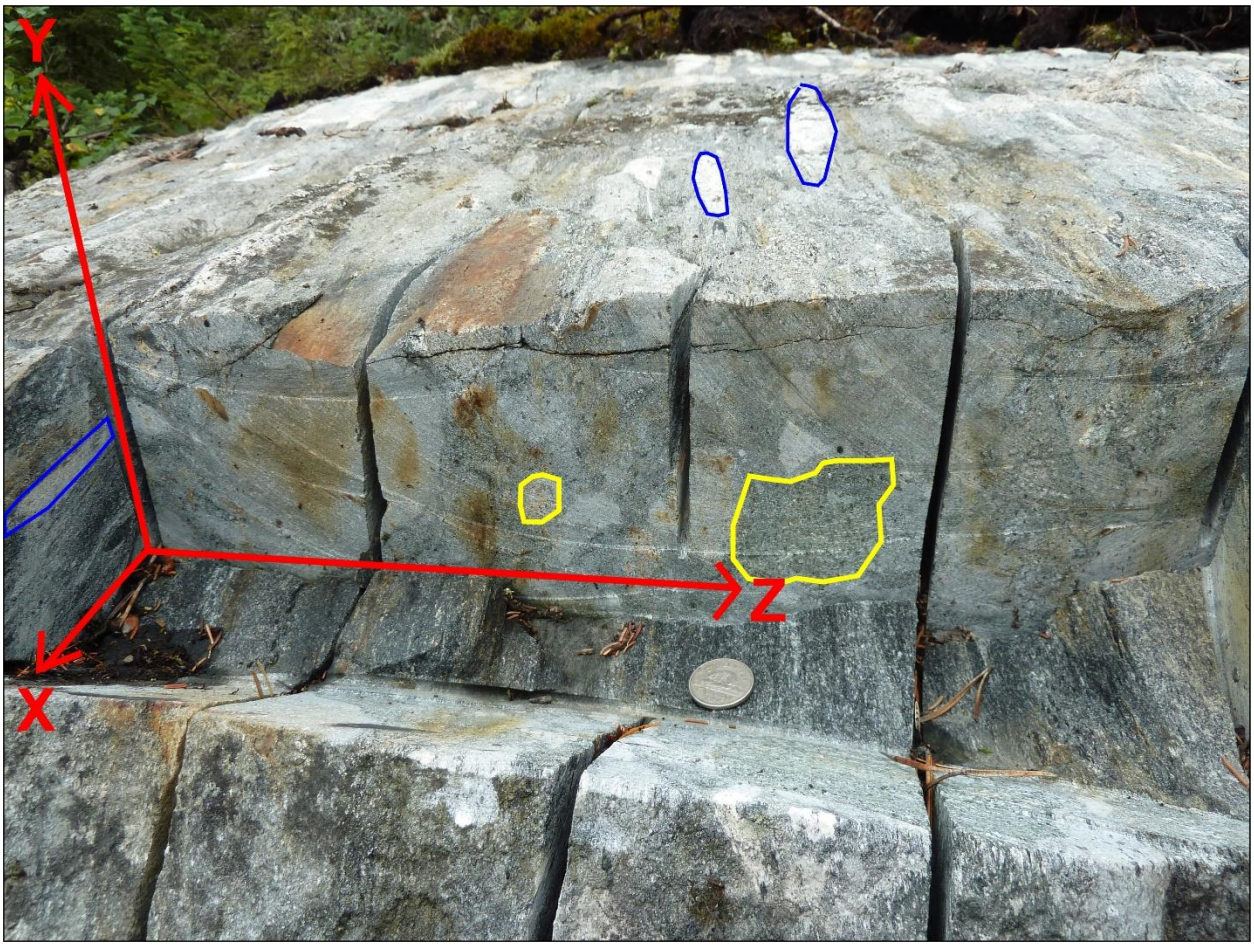

Figure 3. 9. Field photograph of the regional stretching lineation looking to the north east. The lineation is defined by the elongation of volcanic clasts (outlined in blue) in a heterolithic mafic volcaniclastic rock within the hinge area of the Whitefish Bay synform. Its location is given in Figure 3.3. X, Y, Z represent spatial axes. The lineation is plunging 26° to the NE parallel to the X axis. The surface of the outcrop is approximately horizontal and is perpendicular to the YZ surface and parallel to the XZ plane. YZ is a cut surface approximately perpendicular to the flat horizontal outcrop surface. Because the lineation is plunging 26° to the NE and parallel to the X axis, the clasts appear elongate on the outcrop surface (outlined in blue) but near circular on the YZ section (outlined in yellow) as this surface is near perpendicular to the lineation. Coin (1.8 cm in diameter) for scale.

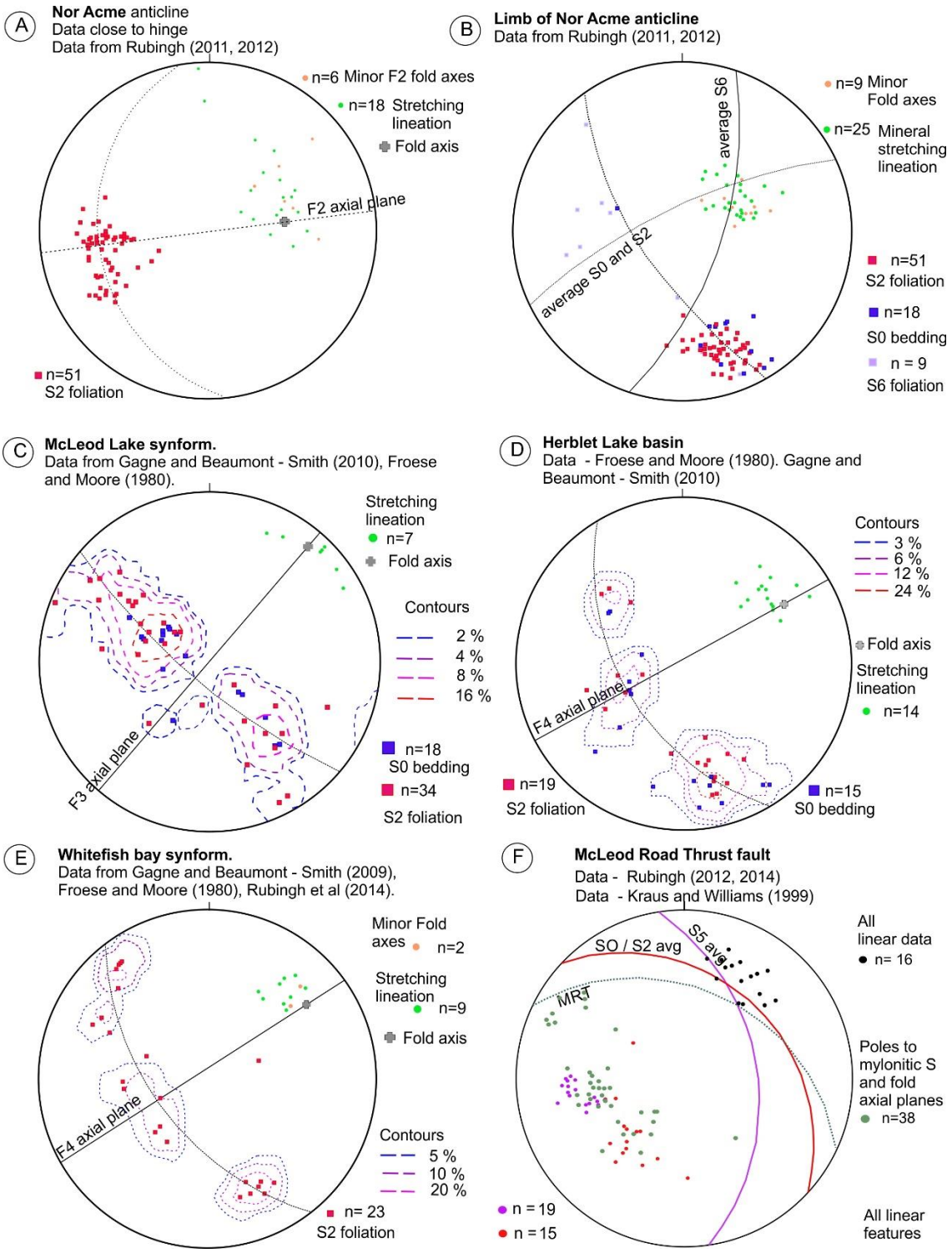

Figure 3. 10. Equal area projections, lower hemisphere projection of structural measurements from: (a) Hinge of the Nor Acme Fold, (b) Limbs of the Nor Acme Fold, (c) McLeod Lake synform, (d) Herblet Lake Basin, (e) Whitefish bay synform, (f) McLeod Road Thrust fault. Planes are plotted as great circles and poles; fold axes and lineations are plotted as lines. Number of measurements indicated by "N=numerical value".

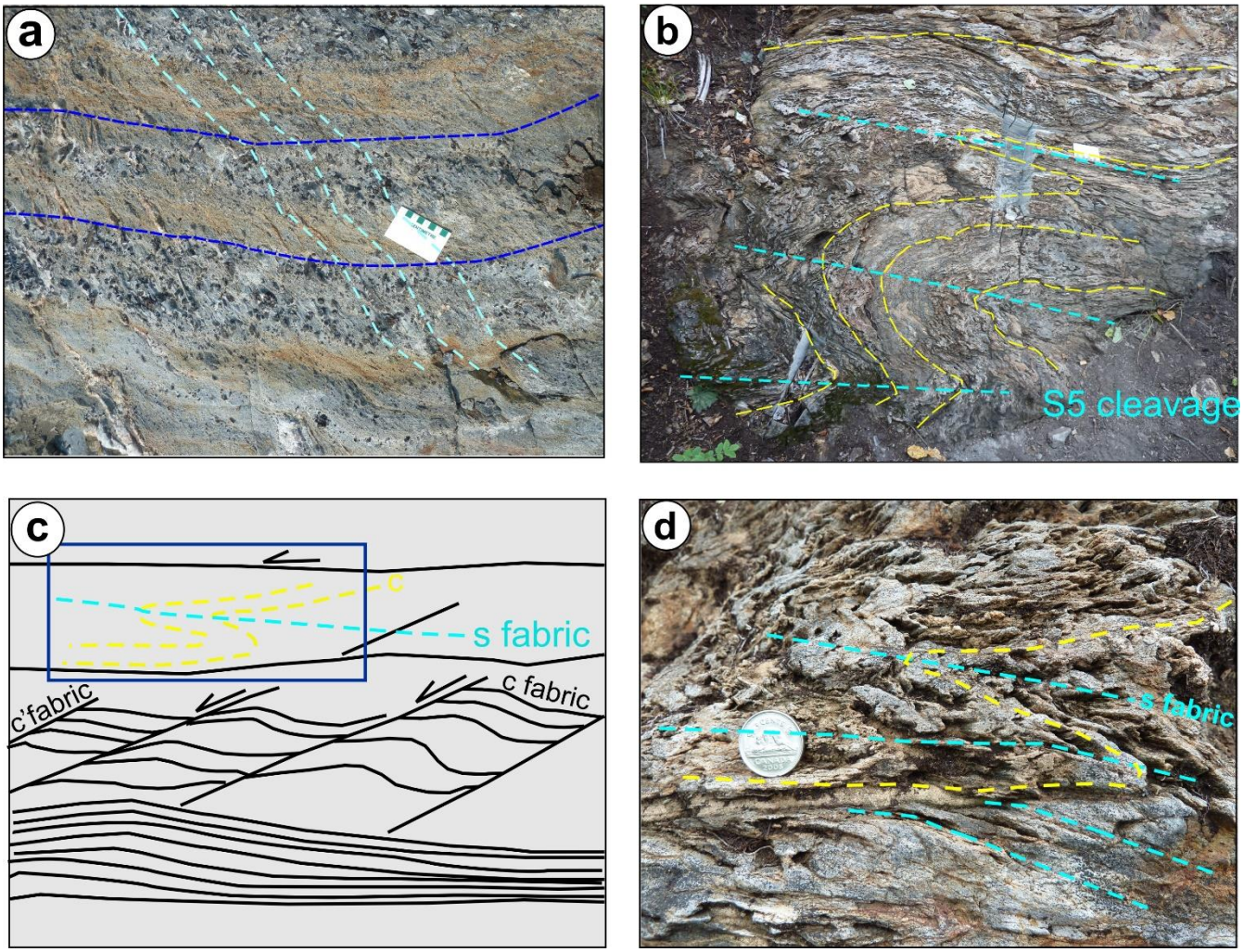

Figure 3. 11. Field photographs of structural features along the McLeod Road Thrust: (a) Sinistral refraction of S5 (light blue) across beds (dark blue) within turbidites of the Burntwood Group. Photo card (9 cm in length) for scale. (b) S-shaped F5 fold with axial planar S5 cleavage, overprinting the shear foliation. Photo card (9 cm in length) for scale. (c) Line diagram from outcrop showing sinistral C-C' fabrics and overprinting S-shaped F5 fold, (d) s-shaped F5 folds from blue rectangular area in Figure 3.13c. Coin (1.8 cm in diameter) for scale.

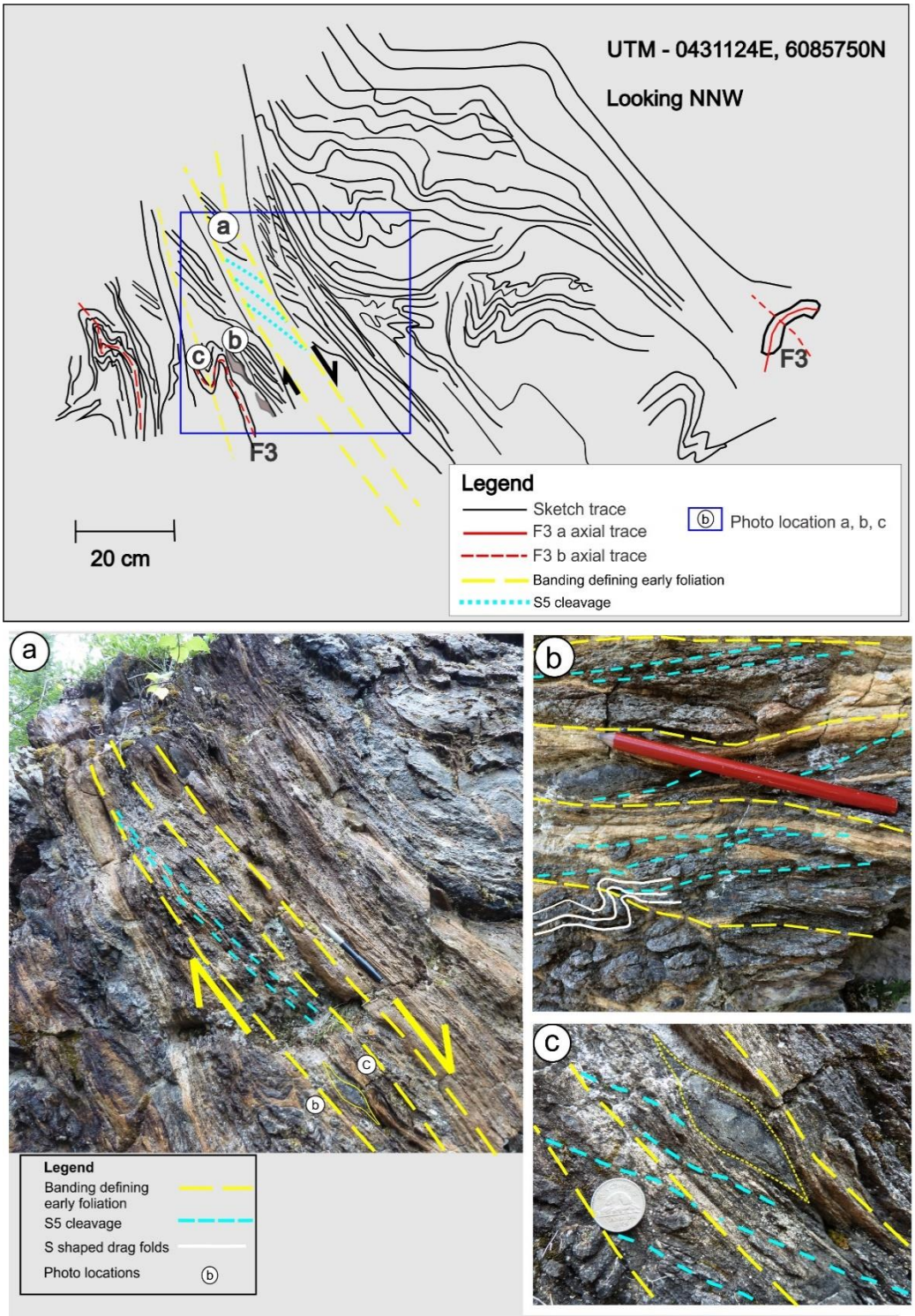

Figure 3. 12. Line diagram of vertical SSE-facing (NNW-looking) vertical outcrop surface of the Cleaver Lake Fault. Location of field photographs are shown by letters a, b, c. (a) S-C fabrics indicating normal fault movement. The photo is looking NNW. Pencil (16 cm in length) for scale, (b) overprinting of early S-shaped drag folds by the S-C fabric. Photo location B is rotated clockwise; such that top is now to the left. Pencil (16 cm in length), (c) back-rotated mafic boudins also indicating normal movement on this fault. Coin (1.8 cm in diameter) for scale.

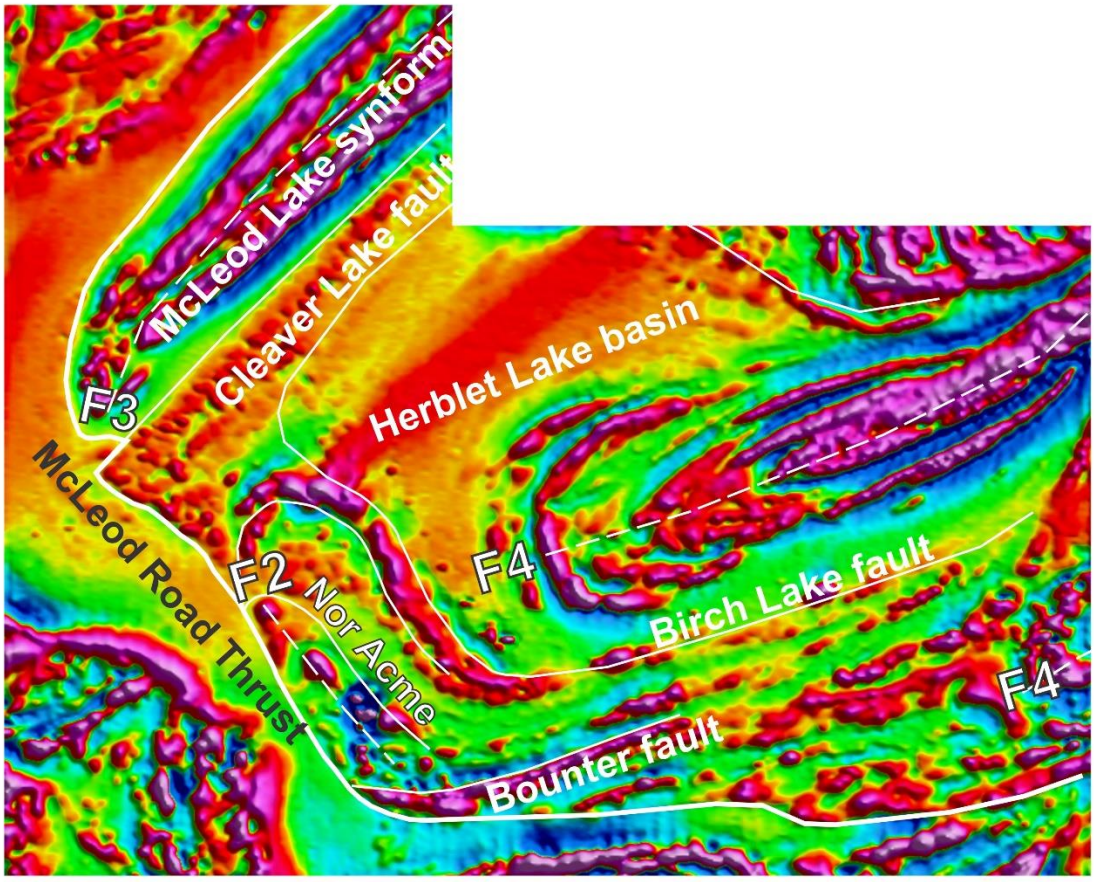

Figure 3. 13. Goldak Geophysical airborne EM survey (2008), first derivative of magnetic data is shown, with line work drawn in white to illustrate the outline of the main structures in the Snow Lake area. Dashed white lines represent fold axial traces and solid white lines define the thrust faults.

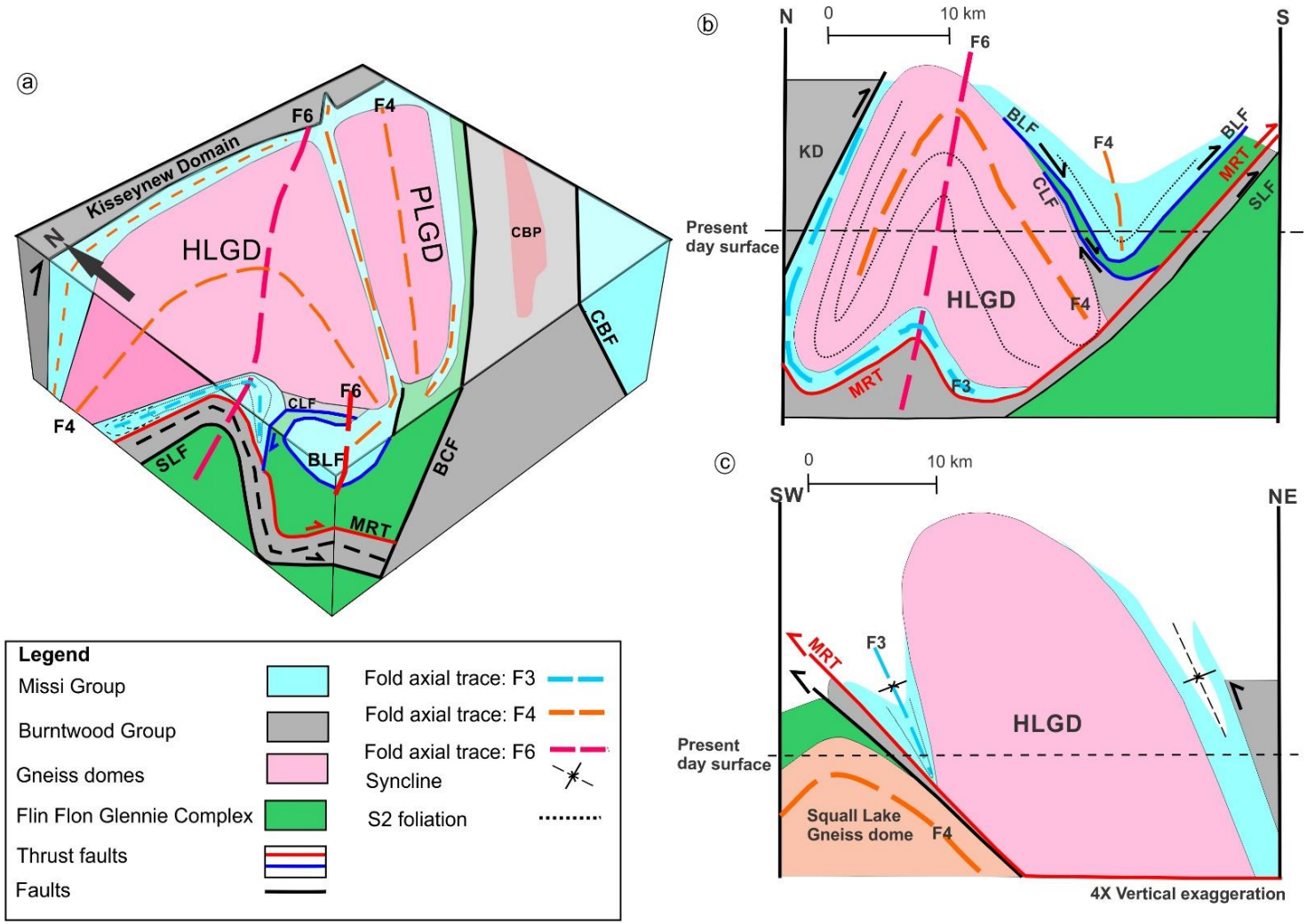

Figure 3. 14. (a) Geological block model of the Snow Lake area. Abbreviations: KD, Kisseynew Domain, HLGD, Herblet Lake gneiss dome; PLGD, Pulver Lake gneiss dome; CBP, Crowduck bay pluton; CBF, Crowduck Bay fault; MRT, McLeod Road Thrust fault; SLF, Snow Lake fault; BLF, Birch Lake fault; CLF, Cleaver Lake fault; BCF, Berry Creek fault. (b) North-south cross section with four times vertical exaggeration across the Herblet Lake and Pulver Lake gneiss domes, (c) E-W cross section with four times vertical exaggeration across the Herblet Lake and Pulver Lake gneiss. Locations of cross sections are shown on Figure 3.6.

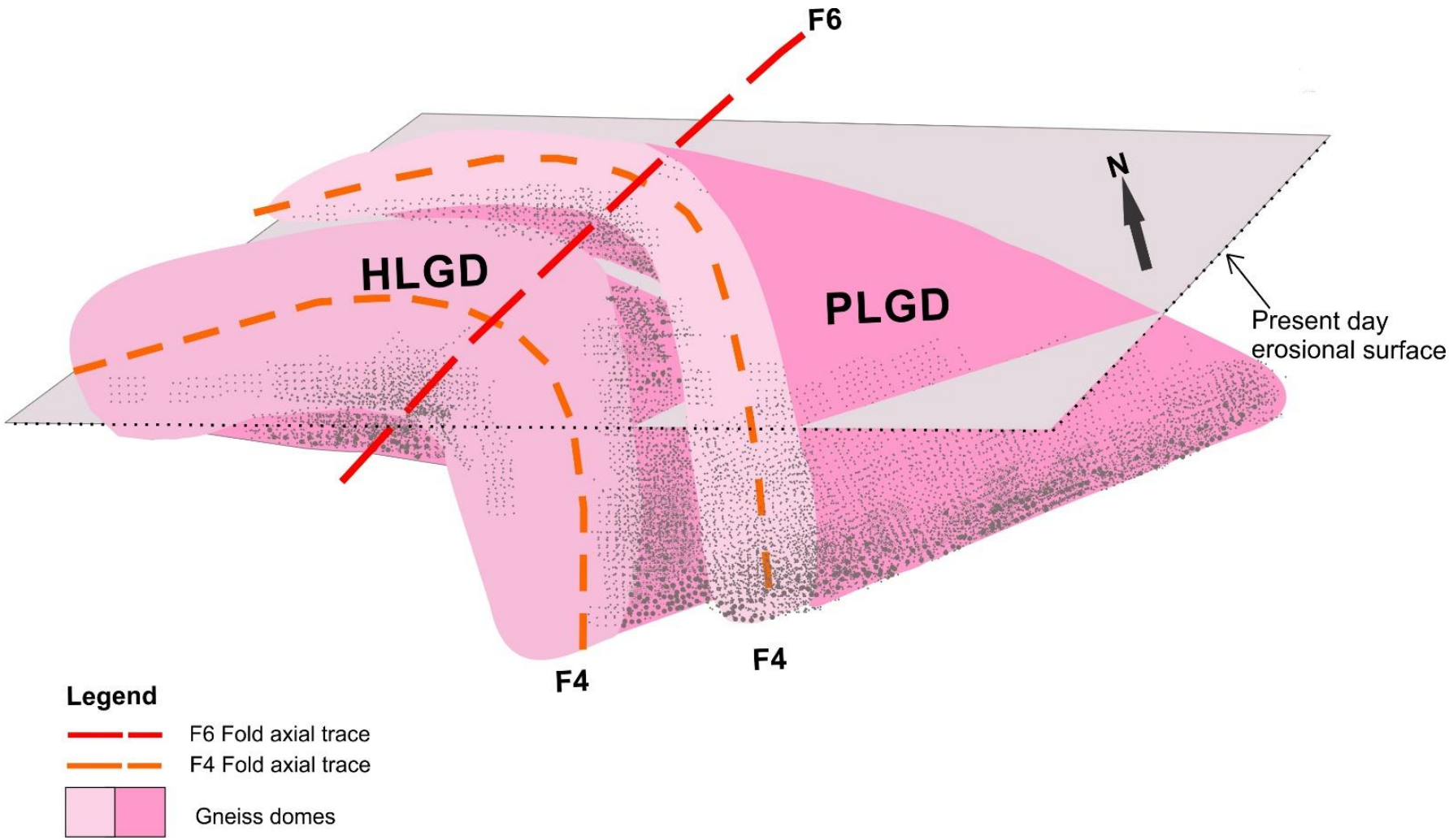

Figure 3. 15. Schematic 3D diagram of the F4 sheath-like gneiss domes overprinted by NE-plunging F6 folds. Abbreviations: HLGD, Herblet Lake gneiss dome; PLGD, Pulver Lake gneiss dome.

D1 (1.84 - 1.83 Ga)
Early thrusting within the MB sequence (Bounter Fault and the MRT)
Emplacement of granitic plutons along the structural - stratigraphic transition zone

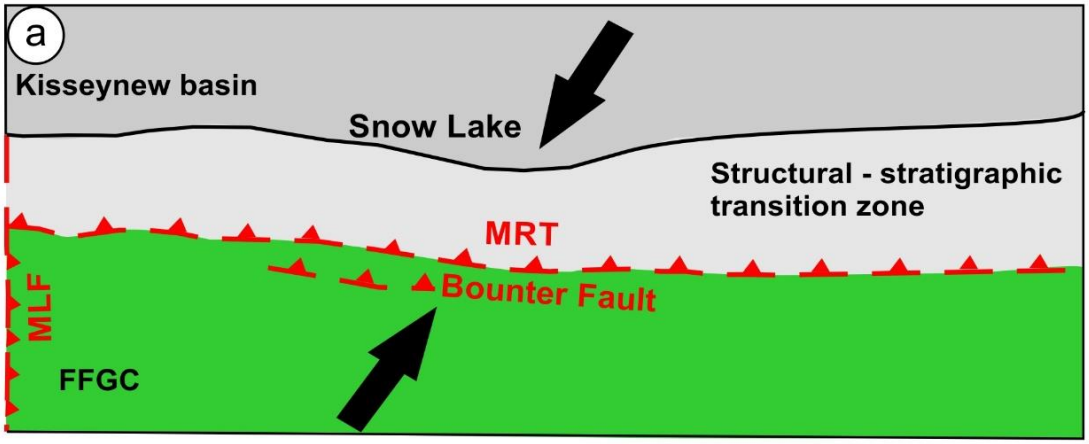

D2 (1.84 - 1.82 Ga)
Sask craton collision. Formation of ductile thrust fault regional foliation and lineation.

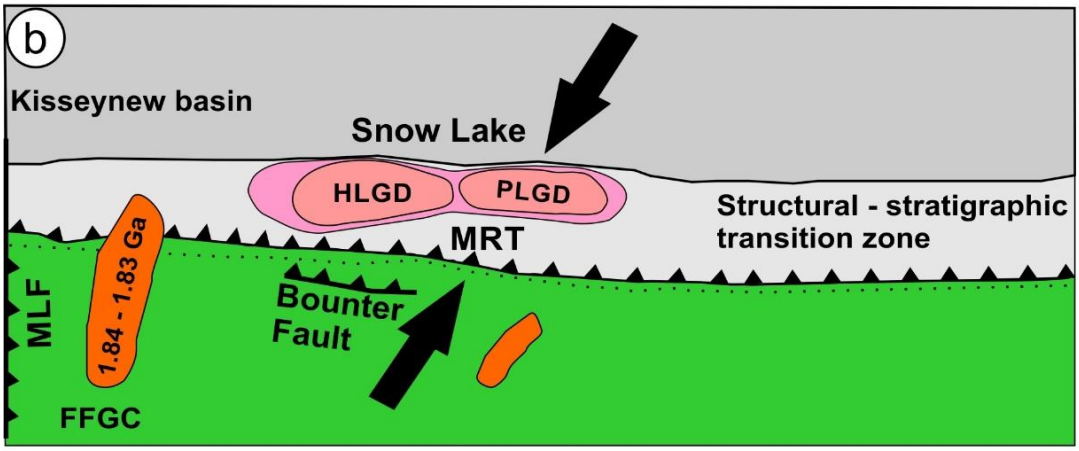

D3 (1.83 - 1.80 Ga)
Superior craton collision and formation of the S5 cleavage (purple) and S6 cleavage (red). Refolding of gneiss domes into their present shape

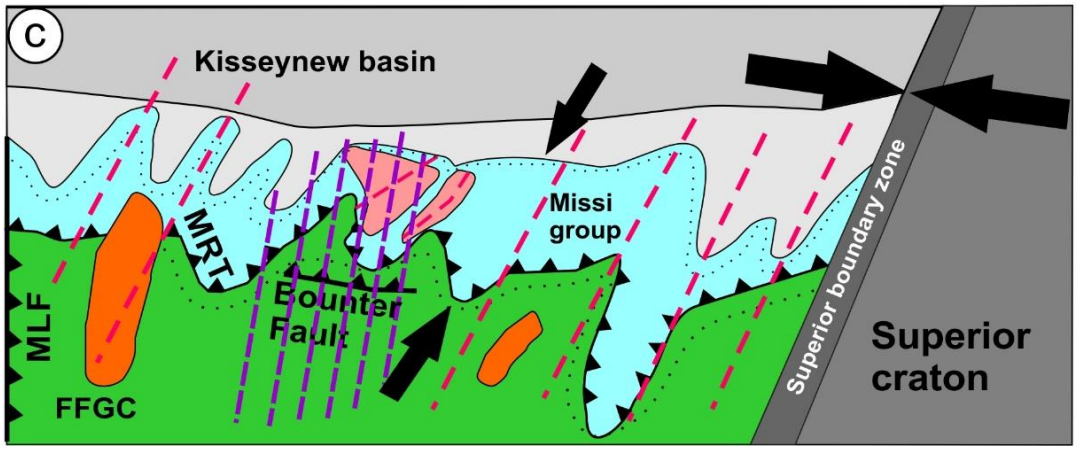

Figure 3. 16. Graphic representation and summary of the D1 to D3 deformation events in the southeastern Trans Hudson orogen: (a) D1 (1.84 – 1.83 Ga) represents early brittle thrusting (Bounter Fault and the MRT Fault) of the Kisseynew Domain over the FFGC during collision with the Sask craton; (b) D2 (1.84 – 1.82 Ga) ductile thrusting and formation of sheath-like gneiss domes (1889 +/- 5 Ma) during ongoing southwest-directed transport of the Kisseynew basin over the FFGC and emplacement of late successor arc plutons (1.84 – 1.83 Ga). Dashed black line represents the regional S2 foliation parallel to the tectonic front. (c) D3 (1.82 – 1.80 Ga) collision with the Superior craton during ongoing southwest directed thrusting. Domal structures are refolded and new S5 (purple dashed lines) and S6 (orange dashed lines) cleavages form overprinting the older structures and reactivating the thrust faults as dextral and sinistral shear zones.

Chapter 4 - The amphibolite facies Paleoproterozoic Snow Lake gold deposits: Formation and modification of orogenic gold deposits during early thrusting in the Paleoproterozoic Trans Hudson Orogen, Manitoba

4.1 Abstract

The Snow Lake camp is located in the ca. 1.89 Ga Flin Flon – Glennie Complex (FFGC) in the Paleoproterozoic Trans Hudson Orogen, Manitoba, Canada. The FFGC is bordered by the ca. 1.855 Ga-1.84 Ga metasedimentary Kisseynew Domain to the north, by the Archean Superior craton to the east, and is underlain by the Archean Sask microcraton. It hosts several orogenic gold deposits, including the No. 3 zone, Boundary zone, and New Britannia deposit, which itself consists of five ore zones (Toots, Dick, Hogg, Ruttan, Mine East). The No. 3 zone extends over 150 meter across the hinge of a major fold, the Nor-Acme Anticline. It consists of gold-bearing quartz-carbonate veins within a 24 m wide zone of altered mafic volcaniclastic rocks overprinted by a biotite-hornblende foliation which is axial planar to the D2 Nor-Acme Anticline. The Boundary zone consists of folded gold-bearing quartz veins in biotite- and carbonate-altered felsic rhyolite in the hinge of a parasitic fold to the Nor-Acme Anticline. The New Britannia ore zones are characterized by biotite, hornblende, plagioclase, carbonate, ilmenite ± diopside ± orthoclase ± garnet mineral assemblages. They are folded and overprinted by the Nor-Acme foliation, and transposed together with quartz-carbonate veins into a shear zone, the Howe Sound fault, which cuts across the hinge of the Nor- Acme Anticline.

The ore zones underwent mass gains in K_2O, CO_2, S and As, which are represented by increased abundance of biotite, carbonate (ferroan dolomite-ankerite-calcite), arsenopyrite and pyrrhotite, and are characterized by strong correlations between Au and trace indicator metals Ag, Bi, Sb. Laser ablation inductively coupled plasma mass spectrometry element maps of arsenopyrite shows: 1) an antithetic relationship between Au and Sb in zoned arsenopyrite from the No. 3, Boundary and Toots zones, 2) an absence of invisible Au in arsenopyrite grains from the Dick, Ruttan and Mine East zones, and 3) an enrichment in Co, Ni, Pb, Bi in transgranular fractures and along the grain margins. The incorporation of gold during the growth of arsenopyrite at the No. 3, Boundary and Toots zone and its absence in arsenopyrite at the Ruttan, Dick and Mine East zones, suggest that gold was released from arsenopyrite during overprinting and shearing of the ore zones along the Howe Sound fault.

The Snow Lake deposits formed during a major collisional event between the FFGC and the Sask microcraton at ca. 1.84 Ga – ca. 1.82 Ga. Gold was introduced in the hinge of the early Nor-Acme anticline during southwest-directed thrusting and imbrication of the Kisseynew Domain and FFGC, and was remobilized along the Howe Sound fault, which likely formed as a transfer fault during the same event. The deposits formed at amphibolite facies temperatures prior to peak metamorphism (540–600°C, 4-6 kbars) during a prograde and progressive orogenic event, and thus share elements of both metamorphic devolatilization and crustal continuum models for the formation of orogenic gold deposits.

4.2 Introduction

Orogenic gold deposits typically occur in lower to middle greenschist facies terranes of Archean

and Proterozoic greenstone belts and Phanerozoic orogenic belts. Two models have been influential in explaining their formation: the metamorphic devolatilization model of Phillips and Groves (1983) and Phillips and Powell (2010), and the crustal continuum model of Colvine et al. (1988), Colvine (1989), and Groves (1993). The metamorphic model cites the generation of gold-bearing hydrothermal fluids by metamorphic devolatilization at the greenschist-amphibolite facies transition, followed by the upward migration of those fluids along major structures, and the deposition of gold and veins in the brittle-ductile transition zone at lower to middle greenschist facies crustal levels. The continuum model invokes a deeper source for the ore fluids, that is, subduction zones (Goldfarb et al., 2001) or the anatectic granitic lower crust (Groves, 1993), followed by the upward migration of the ore fluids along transcrustal structures, and formation of the gold deposits over a 25 km crustal depth from granulite to greenschist crustal levels. In the continuum model, amphibolite to granulite facies orogenic gold deposits formed during shearing at peak metamorphic conditions, whereas in the metamorphic model, the same deposits formed at greenschist crustal levels and were then tectonically buried and metamorphosed at amphibolite to granulite crustal levels.

The two models can be tested on orogenic gold deposits hosted by amphibolite or higher grade metamorphic rocks: did they form during peak metamorphism (continuum model)? Or are they pre-peak metamorphic metamorphosed deposits (metamorphic model)? Phillips and Powell (2010) argued that because of the high temperature associated with granulite-facies conditions the ore fluids would cause partial melting of the host rocks, and would be absorbed by the melts instead of acting as transporting agents for gold. Orogenic gold deposits at amphibolite facies are more problematic (Phillips and Powell, 2010) because the deposits could possibly form at the

greenschist-amphibolite transition zone, but at temperatures and crustal levels insufficient for partial melting. The problem is compounded in polyphase, deformed and metamorphosed terranes which underwent several orogenic events, as deposits may have formed during one orogenic event, and subsequently underwent deformation and metamorphism during a second orogenic event.

Gold deposits in the Paleoproterozoic Snow Lake camp in the Trans-Hudson orogen, Canada, are good examples of amphibolite grade orogenic gold deposits that formed at pre-peak metamorphic temperatures and pressures during a prograde and progressive orogenic event. The deposits had been previously intrepreted to have formed prior to regional deformation and metamorphism (Gale, 2002), in early pre peak metamorphic shear zones (Fieldhouse, 1999), or in post peak metamorphic retrograde shear zones (Galley et al., 1986, 1988). The aims of this study are to (1) document the nature of gold mineralization in the Snow Lake camp, (2) determine the timing of gold mineralization during the structural and metamorphic evolution of the camp, (3) compare the formation of the Snow Lake gold deposits to that of other deposits in the Trans-Hudson Orogen, and (4) discuss the applicability of the metamorphic and continuum models to the formation of the Snow Lake deposits.

4.3 Geology of the Trans-Hudson Orogen and Snow Lake camp

The Trans-Hudson Orogen comprises a Paleoproterozoic collision zone, called the Reindeer Zone, separating the Archean Hearne and Superior cratons from the Archean Sask micro craton (Fig. 4.1). The Reindeer Zone includes the Flin Flon Glennie Complex (FFGC), which represents an intraoceanic volcanic terrane that was accreted at ca. 1.88 Ga – 1.87 Ga prior to

craton collision and final closure of the ancestral Manikewan Ocean (Ashton, 1999; Ansdell, 2005). The FFGC consists of ca. 1.92 – 1.88 Ga ocean floor and island arc assemblages (Ashton et al., 1999; Bickford et al., 2005) and ca. 1.89 – 1.88 Ga synvolcanic plutons (David et al., 1996). It is bounded to the north by a large sedimentary basin, represented by the Kisseynew Domain, which comprises marine turbiditic sandstones of the ca. 1.855– 1.84 Ga Burntwood Group. Slightly younger alluvial-fluvial sandstones and conglomerates of the ca. 1.845 – 1.835 Ga Missi Group unconformably overlie the FFGC (Ansdell et al., 1995; Lucas et al., 1996).

In the Snow Lake area, the FFGC is represented by the Snow Lake arc assemblage (Fig. 4.2), which contains strata recording the evolution of a primitive arc (Anderson sequence), to a mature arc (Chisel sequence) to an evolved arc rift setting (Snow Creek sequence) (Bailes and Galley, 1996; Bailes, 1997; Bailes and Schledewitz, 1998; Syme et al., 1999). A structural sliver of the Chisel sequence and Snow Creek sequence, named the McLeod Road Birch Lake thrust panel (MB panel) (Rubingh 2011; Rubingh et al., 2012a, b, 2017), is bounded to the north and south by the Birch Lake fault and McLeod Road Thrust (MRT), respectively (Fig. 4.3). This panel hosts the main gold deposits in the Snow Lake camp.

Rubingh et al. (2017) divided the MB panel into five distinct lithological units correlating with similar units in the Chisel sequence (Fig. 4.4), and an additional unit, the Birch Lake basalts, correlating with the Snow Creek sequence. Unit 1 is up to 450 m thick and consists of heterolithic, plagioclase and quartz-porphyritic felsic volcaniclastic rocks, with flattened, dark, wispy fragments, interpreted as altered and deformed pumice. Unit 2 is up to 110 m thick and consists of felsic volcaniclastic rocks and plagioclase-porphyritic rhyolitic lavas exhibiting

characteristic flow lobe structures and flow top breccias. Unit 3 is up to 250 meters thick and consists of mafic lapilli tuff to tuff breccia with minor plagioclase porphyritic mafic pillowed lavas. Unit 4 is up to 155 m thick and is represented by massive coherent rhyolitic flows that are similar to unit 2 rhyolitic flows but that differ by their lack of phenocrysts and by the presence of columnar cooling joints and quartz filled amygdules. Unit 5 is up to 90 m thick and consists of mafic volcaniclastic rocks and pillowed to massive flows with distinct coarse relict pyroxene crystals (0.5 cm to 1 cm), replaced by amphibole. The Birch Lake basalts were defined by Bailes and Schledewitz (1998) as massive to pillowed aphyric lavas.

Three deformation events affected the Snow Lake area (Chapter 3 of this thesis, and Rubingh et al., in prep.). During the first deformation event (D_1), units 1 to 3 were thrust-imbricated and repeated across brittle thrust faults now represented by the Bounter and Lower faults (Fig. 4.4). The thrust faults either formed during early accretion of the Snow Lake arc assemblage to the FFGC at ca. 1.84 Ga (Lucas et al., 1996), or during south-directed thrusting of the Kisseynew basin and Snow Lake Arc assemblage above the colliding Sask craton during a prograde and progressive D1-D2 deformation event. During the ca. 1.84 – 1.82 Ga D_2 event (David et al 1996; Lucas et al 1996; Kraus and Williams, 1999; Rubingh et al., in prep), a regional foliation expressed by the alignment of amphibole and biotite (Fig. 4.5a) and by the flattening of clasts in volcaniclastic units (Fig. 4.5b) formed parallel to the axial plane of isoclinal regional folds (e.g. Nor Acme anticline in Fig. 4.4). The foliation and folds were stretched parallel to a NE-plunging regional lineation, were truncated by ductile thrust faults (MRT, Birch Lake fault), and were refolded around gneissic domes (Herblet gneiss dome in Figure 4.3) that formed as sheath folds along the Kisseynew – FFGC boundary during southwest-directed thrusting of the Kisseynew

basin and Snow Lake arc assemblage above the Sask craton. The third and last deformation event (D3) records the final, ca. 1.82 – 1.80 Ga, collision of the Sask craton, FFGC and Kisseynew basin with the Superior craton to the east (David et al., 1996; Kraus and Williams, 1999). D2 thrust faults, folds and gneiss domes were overprinted by D3 structures, including the NE-striking Threehouse synform and its axial plane cleavage (Fig. 4.3).

Metamorphic isograds in metasedimentary rocks are defined by the appearance of staurolite + biotite, sillimanite + biotite, sillimanite + almandine + biotite, and sillimanite + melt (Froese and Moore, 1980; Menard and Gordon, 1997; Kraus and Menard, 1997). They are traced across the limbs and axial plane of the Threehouse synform suggesting that peak metamorphic conditions were attained late during the D3 event. The MB panel, which lies between the staurolite + biotite isograd and the sillimanite + almandine + biotite isograd, underwent peak metamorphic temperatures of 540°C – 600°C and pressures of 4 kbar – 6 kbar (Fig. 4.3) (David et al., 1996; Menard and Gordon, 1997; Kraus and Menard, 1997).

4.4 Gold mineralization

The Snow Lake camp hosts several gold deposits including the New Britannia (Nor-Acme) deposit, the No. 3 Zone and the Boundary Zone (Figure 4.4). The New Britannia deposit is the largest gold deposit in the Trans Hudson Orogen in Manitoba and Saskatchewan. It was discovered in 1927 and was first in production from 1949 to 1958. During this first phase of production, it produced 5,394,000 tons at an average grade of 0.142 oz Au/ton for a total of 763,000 oz of gold. It was dormant for the next ~40 years prior to the re-opening of the mine in 1995. During this second phase of production which ended in 2005, it produced 6,480,266 tons

at an average grade of 0.132 oz/ton for a total of 858,075 oz of gold. The No. 3 Zone was in production in 1995 and 1996. Its ore was processed at the New Britannia mill and during these two years, it produced 241,574 tons at a grade of 0.126 oz/ton gold for a total of 30,335 oz of gold. The Boundary Zone is a zone of low grade mineralization exposed at surface. It was the target of several exploration drilling programs, which failed to delineate more mineralization at depth.

Several interpretations have been previously proposed for the formation of the Snow Lake deposits. Galley et al. (1986, 1988) suggested that the deposits formed in late retrograde shear zones that cut across the hinge of the Nor Acme Anticline and merge with the McLeod Road Thrust. Fieldhouse (1999) suggested a similar interpretation but thought that the mineralization was pre-peak metamorphism based on the presence of arsenopyrite inclusions in garnet porphyroblasts. Gale (2002) also thought that the deposits were pre-peak metamorphism but further argued that the deposits formed prior to regional deformation. Thus, no concensus exists on the origin of the deposits.

4.5 No. 3 Zone

4.5.1 Lithology and field structural relationships

The No. 3 Zone is located in the hinge of the F2 Nor-Acme Anticline, close to the contact between mafic volcaniclastic rocks (unit 5 of Rubingh et al., 2017) and mafic pillowed flows of the Birch Lake basalts (Figure 4.4). The mafic volcaniclastic rocks are lapillistone and tuff breccia consisting of monolithic fragments that are similar in composition to a surrounding crystal-rich matrix composed of plagioclase and coarse relict pyroxene replaced by amphibole.

The mineralized zone was previously exposed in underground workings (Fig. 4.6a) and was described as a S-shaped, up to 150 m long structure, dipping 45° to 50° to the north and striking 260° and 285° across the north limb and south limb of the Nor-Acme anticline, respectively (Galley et al., 1986; Fieldhouse, 1999). The trace of the mineralized zone is shown in Figure 4.6b. It extends from the north limb of the fold, where the syn-folding regional S2 cleavage is oriented clockwise to lithological contacts and mineralized veins, across the axial plane of the fold, to the south limb of the fold, where the S2 cleavage is oriented anticlockwise to bedding (Fig. 4.6c). A detailed surface map of the mineralized veins is shown on Figure 4.7, where the mineralized zone crosses the north limb of the fold.

Where exposed at surface, the mineralized zone is hosted by mafic volcaniclastic rocks of unit 5 within a 9-meter-wide alteration zone surrounding mineralized quartz veins (Fig. 4.7). The alteration zone is defined by strong biotite and carbonate alteration and by the presence of fine, disseminated grains of arsenopyrite. It is overprinted by the S2 cleavage, which strikes NW and refracts in anticlockwise manner as it passes from the unaltered mafic volcaniclastic rocks into the alteration zone (Fig. 4.7). The S2 cleavage is defined by aligned amphibole, biotite, and flattened clasts and contains a NE-plunging stretching lineation (L2) expressed by the elongation and alignment of the same fabric elements. The S2 cleavage is axial planar to the F2 Nor-Acme anticline (Fig. 4.7), and the L2 stretching lineation is parallel to the fold axis of the anticline.

Four types of veins are present (Fig. 4.7), from older to younger: 1) early massive ‘bull’ quartz veins with tourmaline; 2) pale pink quartz – carbonate breccia veins with fragments of altered mafic volcaniclastic rocks; 3) white quartz – carbonate breccia veins with similar slivers of wall

rock; and 4) late iron carbonate veins. The early massive quartz veins consist of two thick quartz veins that are up to 75 cm and 200 cm in thickness, and several, parallel, narrower quartz veins with an average thickness of 5 cm (Fig. 4.7). The veins are gently folded and the S2 cleavage is axial planar to the folds (Fig. 4.8a). The surfaces of the veins are corrugated and shaped into ridges and grooves that are parallel to the stretching L2 lineation (Fig. 4.8b). The massive quartz veins are locally brecciated and crossed by the pale pink quartz – carbonate breccia veins, which are themselves truncated by the white quartz – carbonate breccia veins (Fig. 4.7). These truncations resulted in the enclosure of angular and foliated wallrock slivers within the veins (Figs. 4.8c, d). One of the slivers contains a folded, narrow, quartz vein with the cleavage axial planar to the fold (Fig. 4.8d). This suggests that vein emplacement and the formation of the foliation occurred during the same progressive event.

Coarse visible gold is associated with the white quartz-carbonate veins and with fine-grained arsenopyrite needles either in the adjacent wallrocks of the veins or in wall rock fragments within the veins (Galley et al., 1991). Samples of the pink and white breccia veins, containing fragments of altered wallrocks with fine-grained arsenopyrite, returned gold values of 4.39 to 29.3 g/t (Fig. 4.7). A sample of the massive quartz-tourmaline vein yielded a gold value of 0.023 g/t and a second sample of its arsenopyrite-speckled wallrocks had a gold value of 1.4 g/t (Fig 4.6).

4.5.2. Petrography

Mafic volcaniclastic rocks in the alteration zone surrounding the veins consist of magnesiohornblende + biotite + almandine garnet + oligoclase/andesine + orthoclase + quartz +

calcite + ferroan dolomite + ilmenite + sulphides +/- ankerite +/- cummingtonite (Fig. 4.9a, b, c). Sulphide minerals include arsenopyrite with minor pyrrhotite, pyrite and chalcopyrite. Arsenopyrite occurs as aggregates with triple point junctions and as single, euhedral lath and rhomboid crystals. Pyrite occurs as euhedral cubic grains in contact with arsenopyrite and interstitial pyrrhorite and chalcopyrite, and as irregular grains with corroded grain boundaries intergrown with chalcopyrite. A single grain of loellingite was found along silicate grain boundaries.

The S2 foliation is defined by flattened clasts, deformed quartz-carbonate lenses, and by magnesiohornblende and biotite that wrap around garnet (Fig. 4.9d) and hornblende porphyroblasts. The garnet porphyroblasts contain inclusions of gold and silicate (biotite, plagioclase), sulphide (arsenopyrite, chalcopyrite) and oxide (ilmenite) minerals (Fig. 4.9e). Similar gold as well as silicate and oxide mineral inclusions are observed in arsenopyrite, which is also present as euhedral grains in the strain shadows of garnet porphyroblasts (Fig. 4.9c). Late very-fine-grained brown carbonate and chlorite overprint the S2 foliation and the porphyroblasts.

4.6 Boundary Zone

4.6.1 Lithology and field structural relationships

The Boundary zone (Fig. 4.4) is located near the hinge of the Nor-Acme Anticline along its north limb. The zone is adjacent to the folded contact between felsic (unit 4) and mafic (unit 5) volcanic and volcaniclastic rocks (Fig. 4.10). The felsic rocks consist of a massive coherent quartz amygdaloidal rhyolite flow with in situ flow top breccia and overlying felsic flank breccia. The fragments in both breccias are monotlithic and derived from autobrecciation and

mass wasting of the coherent rhyolite dome, suggesting younging to the north (Bailes et al., 2013). The felsic rocks are overlain by mafic volcanic and volcaniclastic rocks that are similar to those described at the No. 3 zone.

Beds and lithological contacts dip to the NE and N, and they vary in strike from NW to WSW as they sweep around a gentle, outcrop-scale, S-shaped fold (Fig. 4.10). The latter has a strong axial plane cleavage (S2), which is defined by the alignment of biotite and hornblende and by flattened clasts and quartz-filled amygdules. The S2 cleavage is steeply-dipping and changes in orientation from NW- to WNW-striking due to strong anticlockwise refraction as it passes from the rhyolite flow into the less competent overlying felsic breccias (Fig. 4.10). Similar anticlockwise cleavage refraction is observed between finer- and coarser-grained beds in the breccias (Fig. 4.11a) and along a sinistral shear zone along the margin of a pyroxene porphyritic mafic dyke (Fig. 4.11b, c). A stretching lineation (L2) is defined by the elongation of the clasts. It lies along the S2 cleavage and has an average plunge and trend of 47° to the NE.

Mineralization is associated with massive white quartz veins and quartz-carbonate veins, varying in thickness from 0.3 m to 0.75 m (Fig. 4.11d). The veins are in the coherent rhyolite dome within a 10-meter-wide biotite and carbonate alteration zone, containing 5-7% fine-grained, acicular arsenopyrite, pyrrhotite, and pyrite. The veins are folded and the S2 cleavage is axial planar to the folds (Fig. 4.11e). Small, en échelon, quartz-filled, tension gashes are perpendicular to the cleavage and are gently folded (Fig. 4.11f). One of the massive white quartz vein yielded a gold assay value of 1.54 g/t, but the highest gold assay values (8.61 and 5.44 g/t) are from altered rhyolite adjacent to the veins (Figure 4.10). Gold assay values of 4.22 and 2.17 g/t were obtained

from samples of the felsic flank breccias along the east limb of the S-shaped fold, where the S2 cleavage has been strongly refracted into near parallelism with lithological contacts. Other samples collected a few meters north of the felsic flow-breccia contact yielded anomalous gold assay values of 0.26 and 0.22 g/t, and samples of rusty monolithic rhyolite tuff breccias farther away from this contact returned very low gold values of 0.06 g/t.

4.6.2 Petrography

The S2 cleavage in the alteration zone within the coherent rhyolite dome is expressed by a weak alignment of biotite locally surrounding garnet porphyroblasts. The abundance of biotite increases within the biotite- and sulphide-rich selvedges of the veins, where biotite laths are oriented parallel to crystal faces of pyrite cubes. The selvedges are 1 cm to 5 cm thick and remain similar in width regardless of the thickness of the veins. In addition to sulphide minerals and biotite, which make up to 75% of the vein selvedges, other minor minerals are present, including oligoclase, orthoclase, garnet, calcite, ferroan dolomite – ankerite, and +/- sericite. The sulphide minerals consist of fine arsenopyrite needles and euhedral rhomboid crystals (8-10%), pyrrhotite (1-3%), pyrite (2-3 %) and chalcopyrite (<1%). Gold, pyrrhotite and ilmenite occur as inclusions within arsenopyrite grains. Feldspars are partially altered to fine-grained brown carbonate and chlorite.

4.7 New Britannia mine mineralization

4.7.1 Lithology and field relationships

The New Britannia mine comprises five ore zones, including from west to east, the Toots, Dick, Ruttan, Hogg and Mine East zones. Ore was extracted from the first four zones at the time the

mine was in operation and the Mine East zone was delineated several years after cessation of mining activities. The zones form distinct lenses ranging in width from 1 to 30 meters over a combined strike length of 300 m. The Toots and Dick zones are located near surface and were exposed in historic trenches; the Hogg and Ruttan zones were only exposed underground. The ore zones are located in the hinge area and along the north limb of the F2 Nor-Acme Anticline (Fig. 4.4). Outlines of the ore zones on mine level plans from the 320 feet to 1780 feet levels show that the ore zones are folded and moderately plunging (42°) towards to NE, which is consistent with the trend and plunge of both the Nor-Acme anticline and the regional stretching lineation (Fig. 4.12).

At surface, Unit 3 mafic volcaniclastic rocks make up the hanging wall of the ore zones (Fig. 4.13). Beds are normally graded and north-younging. They are folded by meter-scale folds with orientations and axial plane cleavage of second-order parasitic folds to the Nor-Acme Anticline. Units 1 to 3 make up the footwall of the ore zones. The units are upright, strike NW (~335°), and dip ~60° to the NE. Unit 1 is a densely packed volcaniclastic rock with a light-colored felsic matrix surrounding mafic and felsic lithic fragments and flattened pumice. Unit 2 consists of coherent massive rhyolite flows. Unit 3 is the same as described above and is separated from structurally overlying Unit 1 volcaniclastic rocks by the D1 Bounter Fault (Fig. 4.13).

A ductile shear zone, called the Howe Sound fault (Figs. 4.4, 4.12), separates Unit 3 in the folded hanging wall from the NW-striking footwall units. The fault strikes 260° to 300° and has an average dip of 45° to the NE. Within two meters of the fault, the axial plane S2 cleavage of the Nor-Acme Anticline abruptly changes orientation and is deflected in anticlockwise manner into

parallelism with the strike of the fault (Fig. 4.13). The latter can be traced by the deflection or dragging of the S2 cleavage, but is only exposed at its western extremity, where it offsets the McLeod Road Thrust by 60 to 70 m, as indicated by underground mapping and drilling (QMX Gold Corporation, 2013). Underground, the fault is expressed by multiple, roughly parallel, stepping faults, varying in orientation from WSW to NNW (Fig. 4.14). Where it is exposed at surface near the lakeshore of Snow Lake (Fig. 4.15), the fault is characterized by a strong, WSW-striking, hornblende and biotite foliation, a shallowly-plunging striation defined by hornblende (Fig. 4.15b), and S-shaped drag folds defined by folded quartz-carbonate veins (Fig. 4.15a). Large, broken and displaced blocks of mineralized fault breccia are observed in close proximity to the fault (Fig. 4.15). Along the projected extension of the Bounter Fault (Fi. 4.15) strong silicification is present within altered felsic volcanic rocks of unit 2 at its inferred contact with mafic volcaniclastic rocks of unit 3. Ten meters south of this outcrop, shear sense indicators related to the NNW-striking McLeod Road Thrust are exposed in the hanging wall of the fault within strongly biotite-altered and carbonatized mafic volcaniclastic rocks (Unit 3) with disseminated pyrite and arsenopyrite (Fig. 4.15c). The fault itself is not exposed and is located roughly ten meters west of this outcrop along the contact between the volcanic rocks and Burntwood Group turbidities (Fig. 4.13, 15). The altered mafic volcaniclastic rocks have a strong biotite cleavage that wraps around flattened clasts and is axial planar to S-folded pyroxene phyric (now amphibole) dikes (Fig. 4.16). Iron carbonate veins transect the folds (Fig. 4.16), are themselves S-folded, and overprinted by SE-side-up sinistral shear bands (Fig. 4.15d). Late chlorite-filled fractures overprint these structures (Fig. 4.16).

4.7.2 Petrography

Unmineralized Unit 3 mafic volcaniclastic rocks consist of ferrohornblende and magnesiohornblende (20-50%), andesine-oligoclase (10-20%), quartz (5-15%), biotite (5-15%), calcite (5 - 10%), chlorite (3-5%), ilmenite (1-3%), titanite (<1%), and sulphide minerals (<1%) including pyrite, chalcopyrite and galena. They have a weak to moderate foliation (S2) defined by hornblende and biotite (50-75 μm grain size) and by deformed quartz-feldspar and quartz-carbonate microlayers, wrapping around large (600-700 μm) hornblende porphyroblasts. Pyrite and chalcopyrite occur as fine-grained disseminations along silicate grain boundaries. Minor calcite replaces the deformed margins of feldspar grains, and biotite is locally chloritized.

Dick, Ruttan, Mine East zones

The Dick, Ruttan, and Mine East zones are overprinted by the Howe Sound fault. They are not exposed at surface and the following description of the ore zones is from drill core samples. The Dick, Ruttan and Mine East zones are characterized by a strong increase in the intensity of the foliation, by a gradual increase in the abundance of biotite and concurrent decrease in the abundance of hornblende, by the presence of ferroan dolomite and ankerite in addition to calcite, increased total abundance of carbonate and sulphide minerals, more sodic plagioclase compositions, and by the appearance of pyrrhotite-arsenopyrite-dominated sulphide assemblages. The mineralized zones typically consist of 20-25% biotite, 10-15% oligoclase-albite, 3-5% orthoclase, 12%-15% ankerite-ferroan dolomite (+/- calcite), 12-15% quartz, 5-10% magnesiohornblende (+ /- paragasite), 5-7% arsenopyrite-pyrrhotite-pyrite (+/- chalcopyrite), 3-5% chlorite, 1-2% ilmenite, and <1% titanite, garnet, scheelite, epidote and native gold. They have a strong foliation defined by the alignment of biotite and hornblende, by deformed and boudinaged quartz-carbonate veins with altered wallrock fragments, and by the preferred

elongation of carbonate minerals and amphibole nd plagioclase porphyroblasts. The foliation deflects around the plagioclase, amphibole, and garnet porphyroblasts. The latter contain internal inclusion trails that are parallel to the external biotite-amphibole foliation (Fig. 4.17a). The plagioclase porphyroblasts (400 – 500 μm) are replaced along their margins and transgranular microfractures by small recrystallized grains (30 – 50 μm) with irregular grain boundaries. The small recrystallized grains are similar in size to subgrains within the porphyroblasts.

Sulphide minerals occur as anhedral grains with aspect ratios of 4:1 (chalcopyrite, pyrrhotite) and as euhedral prisms and needles (arsenopyrite) oriented parallel to foliation. Arsenopyrite grains are surrounded by strain shadows parallel to foliation (Fig. 4.17b) and contain internal inclusion trails of ilmenite, pyrrhotite and biotite also parallel to foliation. Inclusions of arsenopyrite are present in pyrrhotite and both arsenopyrite and pyrrhotite occur as inclusions in deformed and partially recrystallized plagioclase, amphibole, and garnet porphyroblasts. Pitted pyrite grains with irregular grain boundaries are in contact with silicate, carbonate and sulphide (arsenopyrite, chalcopyrite) grains. Native gold is observed along sulphide and silicate grain boundaries (Fig. 4.17c, d) and is also present in association with fine arsenopyrite needles in altered fragments within the quartz-carbonate veins (Galley et al., 1986, 1991).

Toots Zone

The Toots zone is poorly exposed at surface and is described from drill core samples. It differs in modal mineralogy from that of the other mineralized zones, notably by the absence of carbonate minerals and the presence of diopside (20 - 25%), actinolite (15 - 20%) and orthoclase (3-5%), in addition to oligoclase (15 - 20%), quartz (10- 15%), biotite (5 - 7%), chlorite (2-3%), pyrrhotite-

arsenopyrite-pyrite-chalcopyrite (2 - 3%), and titanite (<1%). It has a weak foliation defined by diopside, actinolite, biotite, and by trains of sulphide grains. Diopside forms large (200μm – 800μm) poikiloblastic porphyroblasts with inclusions of sulphides (pyrrhotite, pyrite and arsenopyrite) and gold (Fig. 4.18a, b). Large plagioclase grains (400μm - 500 μm) are recrystallized into small grains (20 μm-30 μm), which are similar in size to matrix plagioclase grains (Fig. 4.18c). Older zoned pyrite grains with corroded rims are replaced by arsenopyrite (Fig. 4.18d), which is typically intergrown with pyrrhotite (Fig. 4.18e). Younger pyrite grains with sharp grain boundaries are in contact with pyrrhotite. Native gold is observed along silicate-only grain boundaries (Fig. 4.18 f).

Summary

The minerals present in the host mafic volcaniclastic rocks and mineralized zones are summarized in Figure 4.19. The mineralized zones are associated with metamorphic minerals (hornblende, biotite, plagioclase, ilmente, ± garnet) similar to those in the unmineralized mafic metavolcaniclastic host rocks. They are characterized by an increase in the total abundance of biotite, carbonates and sulphides, the addition of K-feldspar, and by changes in mineral chemistry from calcite to ankerite - ferroan dolomite. Arsenopyrite and pyrrhotite are the dominant sulphide minerals; they replace early pyrite with irregular corroded grain boundaries. Where overprinted by the Howe Sound fault, the mineralized zones (Dick, Ruttan, Mine East) are further characterized by the recrystallization of plagioclase (andesine) to oligoclase – albite and by the alignment of acicular arsenopyrite grains and their strain shadows parallel to the shear zone foliation. The Toots zone differs from the other mineralized ore zones by the near absence of carbonate minerals, the presence of diopside and actinolite, and lesser abundance of biotite.

Late carbonate, chlorite, and sericite overprint all mineralized zones.

4.8 Geochemistry

4.8.1 Whole rock geochemistry

Analytical methods

Fifty-four samples were collected from drill cores across the New Britannia mine mineralized zones (37 from Toots, Hogg, Ruttan, Mine East zones), the Boundary Zone (5) and the No. 3 Zone (12). They consist of non-mineralized to strongly mineralized mafic volcanic and volcaniclastic rocks (New Britannia mine, No. 3 zone) and felsic volcanic rocks (Boundary zone). Representative whole rock analyses are listed in Table 4-1. Samples were pulverized using an agate mill at the Ontario Geoscience Laboratories (OGL) in Sudbury, Ontario. Major element analyses were done at Activation Laboratories in Ancaster, Ontario, using a split sample of the pulp. Fused disks of the sample, prepared in platinum crucibles using lithium metaborate and lithium tetraborate with lithium bromide as releasing agents, were then analyzed for major elements on a Panalytical Axios Advanced wavelength dispersive XRF. Precision and accuracy were calculated using certified reference standards AN-G, BE-N, AC-E, and NCSDC73304. Precision is better than 5% for the major elements SiO_2, Al_2O_3, MnO, K_2O, and TiO_2. All other major elements are precise to 20% or greater. Accuracy is better than 10% for all major elements except P_2O_5 and MgO.

Trace elements were analyzed (Ba, Be, Bi, Cd, Co, Cr, Cs, Cu, Ga, Hf, In, Li, Mo, Nb, Ni, Pb,

Rb, Sb, Sn, Sr, Ta, Th, Ti, Tl, U, V, W, Zn, Zr, including rare earth elements Ce, Dy, Er, Eu, Gd, Ho, La, Lu, Nd, Pr, Sm, Sc, Tb, Tm, Yb, Y) using the ICP-MS at the OGL on samples prepared by closed vessel multi-acid digestion. Precision and accuracy were calculated using known international standards; AGV-2, BHVO-2, GSP-2 and in-house standard MRB-29. Trace elements are more precise than 10% except for Mo, Ce, Co, Ni, Zr, Ta, Sn and Sc which are precise to 20%.

The data accuracy is better than 10% for all trace elements except for Co, Cr, Ni, Sc, Ta, Th and Sn. CO_2 and S concentrations were measured by infrared energy absorption on combusted samples. The precision for CO_2 and S analyses are better than 5% and 20%, respectively, and data accuracy is better than 10% for both CO_2 and S analyses. A subset of 33 mineralized samples were dissolved in an Aqua Regia solution and analyzed for Au, Ag, As, W, Zn, Cu, Pb, Bi, Te, Mo, Sb, Sn and Se using the ICP–MS at the OGL.

Fifteen surface samples were collected across the Boundary Zone (8) and the No. 3 Zone (7). The Boundary zone samples were analyzed at Activation Laboratories in Ancaster, Ontario, Canada and the No. 3 zone samples were analyzed at ALS laboratories in Sudbury, Ontario, Canada. Au was analyzed by fire assay at both labs.

Mass balance changes

The best-fit isocon method of Grant (1986) was used to determine the gains and losses of major oxides and trace elements for the mineralized samples relative to that of their least-altered precursors (units 3 to 5), which were collected located roughly 900 metres away from the New Britannia mine. No suitable least-altered precursor was found for the Boundary Zone. Element

mobility was assessed using the following immobile elements: Zr, Nb, Ta, La, Yb, V, Sc which were assessed using binary plots of Zr vs each element. The mass factor was calculated using these elements and then used to calculate mass changes, which are displayed on % mass change histograms (Figs. 4.20a, b).

Strong mass gains (>150%) in K_2O, Ba, Cs, Pb, Rb, Sb, Tl, W, S and CO_2 are observed at the No. 3 Zone in altered mafic volcaniclastic host rocks (Fig. 4.20a), and similar strong mass gains in K_2O, Rb, Tl, W, Cs, Pb, S, and CO_2 and variable mass gains (100% - 150%) in Na_2O, Cr, Be, Ni, and Sb are observed in mafic volcaniclastic rocks from the mineralized zones at the New Britannia mine (Fig. 4.20b). The strong mass gains in K_2O, S, CO_2 correspond to increases in biotite, orthoclase, sulphides (arsenopyrite, pyrrhotite), and carbonates (ankerite and ferroan – dolomite) in the ore zones, and the more variable mass gain in Na_2O correspond to the increased sodic composition of plagioclase from andesine to oligoclase-albite in the ore zones. Mass gains in Ba, Cs, Rb, Tl, reflect the same increase in biotite and orthoclase in the ore zones because these elements substitute for K (Heinrichs et al., 1980; Shaw and Penczak., 1996; Wood and Blundy., 2003). Ba can subsititute for Ca in carbonates, whereas Rb only occupies interstitial positions in the crystal structure of calcite and doesn't substitute for Ca (Okumura and Kitano., 1986). Be substitutes for Si in K feldspar in a simultaneous reaction typically with La which substitutes for K (Ross, M., 1964). Mass gains in metals W, Sb, Pb, Cr, Ni are explained by the deposition of new sulphide minerals (i.e. scheelite, galena) and their incorporation in inclusions (i.e, pyrrhotite, ilmenite, scheelinte, galena) and lattice-bound elements within arsenopyrite and pyrrhotite.

Metal association

Correlations between Au and other indicator metals at the New Britannia Mine (Dick, Ruttan, Mine East) are calculated using the Pearson correlation coefficient (r) (Pearson, 1895). Correlations are considered significant for r > 0.64 and r < - 0.64, or r^2 > 0.41, using a significance level (p) of < 0.01 for a two – tailed test where the degrees of freedom (df) = N-2 = 13, and N = number of pairs of data. Because of the limited number of samples, significant correlations could not be determined for the No. 3 Zone, Boundary Zone and Toots zone.

Gold concentrations show strong positive correlations (0.73 < r^2 < 0.85) with S, Ag, Bi and Sb concentrations (Table 4-2). Arsenic concentrations are above their upper detection limit (>500 ppm) which preclude calculations of their correlation coefficients. Copper correlates positively with Se (r^2 > 0.41) and similar positive correlations exist between Cr, Ni, Zn, Ti and Sn (Table 4-2).

4.8.2 In situ trace element analysis

Analytical methods

Element maps of arsenopyrite grains from the New Britannia mine, No. 3 Zone and the Boundary zone were done in situ by laser ablation (LA) inductively coupled plasma mass spectrometry (ICP-MS) at the Chemical Fingerprinting Laboratory, Laurentian University. Operating conditions and data collection and reduction specifications are given in Table 4-3 and are described in Gourcerol et al. (2015).

LA-ICP-MS maps

A total of 36 arsenopyrite grains were analysed by LA-ICP-MS. Complete element maps were

done on 16 of the larger grains (200 - 2000 µm) and 20 line scans were done across smaller (10 – 80 µm) arsenopyrite needles. The larger grains were selected based of features observed under the SEM and optical microscope, including growth sector zoning, core-rim zoning, textural relationships with other sulfide minerals, and the presence of gold inclusions. The rim of the larger arsenopyrite grains is typically richer in iron (1 – 2 %) and sulphur (2-3%) and poorer in As (2 - 3%) relative to the core of the grains.

Arsenopyrite element maps for the No. 3 Zone (Fig. 4.21a) show an inverse relationship between Au and Sb, elevated Co, Ni, Pb, and Bi concentrations along the margin of the grain, and point concentrations of Ti and W in the grain, representing inclusions of ilmenite and scheelite. At the Boundary Zone (Fig. 4.22a), the same strong inverse correlation between Au and Sb is observed and defines a sector zoning expressed by Au-poor and Sb-rich triangular areas within a nearly uniformly Au-rich and Sb-poor arsenopyrite grain. Elevated Co, Pb, and Bi are observed along the margin of the grain and Bi and Ag form point concentrations corresponding with pyrrhotite inclusions within the arsenopyrite grain.

Arsenopyrites at the Dick, Ruttan, and Mine East zones are devoid of gold. Arsenopyrite at the Dick zone contains inner areas enriched in Sb (Fig. 4.23a). The margin of the grain and microfractures cutting across the grain are enriched in Co, Ni, Pb, Bi and Te. Two W point concentrations represent scheelite inclusions. Arsenopyrite at the Toots zone differs from that at the Dick zone. It is enriched in Au and shows an inverse correlation between Au and Sb similar to that observed at the No. 3 zone (Fig. 4.24a). Otherwise, it shows similar enrichments in Co, Ni, Pb, and Bi along the grain margin and along crosscutting microfractures, as well as a single

W point concentration representing an inclusion of scheelite.

4.9 Discussion

4.9.1 Formation of the ore zones

An important question is the timing of mineralization with respect to deformation and metamorphism. The chronology of gold mineralization at the No. 3 zone can be interpreted from field relationships and petrographic observations. The No. 3 Zone consists of quartz-carbonate veins within a 9 m wide alteration zone in the hinge of the Nor-Acme anticline. On one hand, the alteration zone is overprinted by the regional foliation, which is axial planar to both the Nor-Acme Anticline and the folded veins, suggesting that the veins and gold were emplaced either pre- or syn-Nor Acme folding. On the other hand, the veins and alteration zone truncate and can be traced over 150 m across the nose of the Nor-Acme Anticline (Fig. 4.6b; Galley et al., 1986, 1991; Fieldhouse, 1999), and altered and foliated wallrock slivers are present in the veins (Fig.4.8c, d), suggesting that the veins and gold are either syn- or post Nor-Acme folding. Thus, these mutually overprinting relationships collectively suggest that the veins and gold mineralization were emplaced during Nor-Acme folding. Within the alteration zone, the foliation is defined by magnesiohornblende and biotite deflecting around garnet porphyroblasts containing inclusions of arsenopyrite, pyrrhotite, and gold. This texture is consistent with the crystallization of arsenopyrite, pyrrhotite, and gold before the growth of garnet followed by their enclosure as inclusions during the continued growth of the garnet porphyroblast and progressive formation of the foliation (Passchier and Trouw, 1996). The metamorphic minerals (hornblende, biotite, oligoclase, garnet) in the mineralized zone are indicative of amphibolite grade conditions during

the formation of the foliation and gold mineralization.

A similar interpretation is proposed for the Boundary Zone, which is located along the north limb and near the hinge of the Nor-Acme Anticline. The Boundary Zone is characterized by gold-bearing quartz veins and small arrays of extensional veins that are oriented at high angles to the foliation, which is consistent with their emplacement during shortening across the foliation planes. Their orientation, together with the strong sinistral refraction of the foliation and gentle S-shaped folding of the veins and lithological contacts, suggests that the gold-bearing veins were emplaced, and the foliation formed, during shortening and flexural slip along the north limb of the Nor-Acme Anticline.

At the New Britannia Mine, all ore zones are located either within or near the hinge area of the Nor-Acme Anticline (Fig. 4.12). The Toots zone and Dick zone are folded and occupy the hinge of minor parasitic folds associated with the Nor-Acme Anticline (Harrison, 1947; Hogg, 1957). This suggests that mineralization was initially emplaced in fractures and/or dilational sites that formed early during Nor-Acme folding as proposed for the No. 3 and Boundary zones. Arsenopyrite at the Toots zone and at the No. 3 and Boundary zones contains invisible gold with an antithetic relationship to Sb. Invisible gold occurs either as lattice-bound gold or as nanoparticles less than 250 nm in size (Cabri et al., 1989; Cook and Chryssoulis, 1990). Sector-zoned Sb-rich arsenopyrite, as observed at the Boundary zone, has also been described at the Roudný gold deposit in the Bohemian Massif (Zachariáš et al., 2004). The inclusion of invisible gold, Sb-Au sector zoning, and more general antithetic Au-Sb relationships, are primary features that formed during the crystallization and growth of arsenopyrite in the presence of a gold-rich

ore fluid. At the Toots zone, arsenopyrite is intergrown with pyrrhotite and oligoclase, orthoclase, actinolite and diopside porphyroblasts. The latter grew along the foliation and contain inclusions of sulphide minerals and gold, suggesting that the porphyroblasts and arsenopyrite grew as pulses of gold-rich fluids migrated along the foliation during Nor-Acme folding.

The presence of zoned pyrite with corroded rims, and the growth of arsenopyrite and pyrrhotite across these grains, suggests that pyrite crystallized first and was replaced by arsenopyrite and pyrrhotite during reactions with an evolving ore fluid during a single mineralization event, or during reactions with different ore fluids during separate mineralization events. If the latter, then an early mineralization and alteration event may have preceded the formation of the Nor Acme S2 foliation and associated gold mineralization. Fulton (1999) found invisible gold in pyrite from the New Britannia Mine using secondary ion mass spectrometry. Although speculative, if this gold-bearing pyrite grew during an early gold mineralization and alteration event, this may explain the presence of native gold inclusions in silicate porphyroblasts as these inclusions may represent early gold that was liberated from the pyrite grains and then incorporated in the porphyroblasts during their growth. This may also explain why the Toots zone differs in modal mineralogy from other zones at the New Britannia mine, as superposed alteration events differing spatially in intensity may result in different mass changes and modal mineralogy. Alternatively, the same explanations would apply if pyrite grew, and the host rocks were altered, during an early pulse of gold-rich fluids during a prolonged mineralization event that started early during Nor Acme folding.

Relative to the No. 3, Boundary and Toots zone, the Dick, Ruttan and Mine East zones are

characterized by textural changes indicative of increased strain, including: (1) decreases in grain size of feldspar porphyroclasts and matrix quartz and feldspar due to recrystallization, (2) the development of high strain zones with a strong foliation defined by biotite, hornblende and elongate carbonate minerals surrounding lower strain lenses with a weak foliation, (3) the rotation or growth of arsenopyrite needles parallel to foliation and the elongation of pyrrhotite grains parallel to foliation, and (4) the development of strain shadows around the arsenopyrite needles. These textural changes are spatially associated both in drill core and outcrop with abrupt changes in the orientation of the Nor-Acme foliation as it rotates into the Howe Sound fault, suggesting that they are related to shearing along the Howe Sound fault. A compilation of underground maps by T. Flemming, (2012), who was Chief Mining Geologist when the mine was last in production, shows that the Howe Sound fault consists of several discrete segments that do not all coincide with mineralized zones (Fig. 4.14), which is consistent with overprinting of earlier mineralized zones by later shearing.

The textural relationships between gold and arsenopyrite further suggest that the strong shearing associated with the Howe Sound fault is superposed on earlier mineralized zones. At the No. 3, Boundary and Toots zone, arsenopyrite contains primary invisible gold. With the exception of the Toots zone, arsenopyrite at the New Britannia mine is devoid of gold, which occurs as free gold along silicate-sulphide grain boundaries, as inclusions in metamorphic minerals, and in association with fine arsenopyrite needles. This suggests that gold was liberated from early-formed, Au-bearing, arsenopyrite, as present at the Toots zone, and precipitated as visible gold together with fine arsenopyrite needles during shearing along the Howe Sound fault (e.g. Mumin et al., 1994; Larocque et al., 1995; Wagner et al., 2007). Gold may have expelled and

remobilized from early gold-bearing arsenopyrite either by hydrothermal fluids infiltration during shearing (e.g. Morey et al., 2008; Sung et al., 2009; Cook et al., 2013; Lawley et al., 2015; Li et al., 2018) or by melting of arsenopyrite in the presence of pyrite to produce an As-melt and pyrrhotite (Frost et al., 2002; Tomkins et al., 2006, 2007). This melting reaction occurs at temperatures of ~560°C at 5 Kbars (*ibid*) similar to the peak metamorphic temperatures and pressures determined for Snow Lake (Fig. 4.3) (Menard and Gordon, 1997; Kraus and Menard, 1997). The single grain of lollingite at the No.3 Zone may be due to solid state transformation of arsenopyrite to lollingite and pyrrhotite at low sulphur fugacity insufficient to cause arsenopyrite melting (Tomkins et al., 2006, 2007). The enrichment in Co, Ni, Pb, Bi ± Te along arsenopyrite margins and transgranular fractures, which is observed at all ore zones, likely result from a late metal-rich fluid that infiltrated the ore zones and interacted with arsenopyrite.

The Howe Sound fault cuts across the nose of the Nor-Acme Anticline and offsets the McLeod Road Thrust. The latter formed by the intensification of the Nor-Acme foliation in ductile shear zones during southwest-directed D2 thrusting and imbrication of metasedimentary rocks of the Kisseynew Domain with metavolcanic rocks of the Snow Lake Arc Assemblage (Connors, 1996; Connors et al 1999; 2002; Kraus and Williams, 1999; Norman et al 1995). Because the Howe Sound fault has a similar strong ductile biotite-hornblende fabric produced by the dragging and intensification of the Nor-Acme foliation, it likely formed later during the same D2 deformation event, possibly as a transfer fault during thrusting. A retrograde fluid circulated along the Howe Sound fault and resulted in the late chlorite, carbonate and albite alteration observed along the fault.

4.9.2 Discussion of the continuum and metamorphic models for the formation of the Snow Lake deposits

The Snow Lake deposits share many common features with orogenic gold deposits (Böhlke (1982), Groves et al. (1998), Goldfarb et al. (2005) and Phillips and Powell (2010) for descriptions of orogenic gold deposits). They are gold-only deposits that formed during a major orogenic event from fluids of presumably metamorphic origin as inferred by their lack of temporal and spatial association with intrusions. They have similar bulk metal associations (Au, Ag, Bi, Sb) as orogenic gold deposits, their wallrocks underwent similar mass gains in S, CO_2, K, ± Na ± Rb, Ba, Pb, Cs, and they have alteration assemblages similar to higher temperature orogenic deposits.

Of the two models invoked to explain the formation of orogenic gold deposits, neither the continuum model nor the metamorphic model fully explains all the features observed in the Snow Lake deposits. The latter formed at temperatures above the greenschist-amphibolite transition, thus they are not metamorphosed deposits that formed at middle greenschist facies temperatures and that were later buried and metamorphosed at amphibolite temperatures as demanded by the metamorphic model. Nor did they form during the metamorphic peak of the Trans-Hudson Orogeny as required by the continuum model. The Snow Lake deposits formed in the hinge of the Nor-Acme Anticline early during the D2 deformation event and were later sheared along the Howe Sound Fault during the same deformation event. The D2 event records the southwest-directed overthrusting of the Flin Flon belt by the Kisseynew basin during their collision with the Archean Sask craton at ca. 1.84 Ga - ca. 1.82 Ga, prior to D3 collision at ca. 1.83 Ga. - 1.80 Ga of these terranes with the Archean Superior craton approaching from the east

(Kraus and Williams, 1999). Metamorphic isograds in the Kisseynew basin and Flin Flon belt are broadly parallel to the boundary between the Kisseynew and Flin Flon belt terranes (Kraus and Menard, 1997) and thus largely formed in response to tectonic burial and crustal thickening during the D2 event with heating of the crust continuing, and peak metamorphic conditions (540–600°C, 4-6 kbars) being attained, during the D3 event (Menard and Gordon, 1997; Kraus and Menard, 1997; Kraus and Williams, 1999). Thus, the deposits formed early during a prograde metamorphic path that began during D2 thrusting and that peaked during D3 collision of the Kisseynew basin and Flin Flon belt with the Superior craton.

The Snow Lake deposits exemplify how orogenic deposits in high-temperature metamorphic terranes may have complex relationships with their host rocks and host structures. Deposits that form early during a progressive prograde deformation event may be later deformed and modified during the same event obscuring early primary features of the deposits.

4.9.3 Comparison to other gold deposits in the Manitoba and Saskatchewan segment of the Trans- Hudson Orogen

Contrary to the New Britannia deposits, where gold was emplaced during an early orogenic phase of thrusting (the D2 deformation event), most other Trans-Hudson gold deposits in Saskatchewan and Manitoba (Fig. 4.1) are associated with steeply-dipping, syn- to post-peak metamorphic, transcurrent or reverse shear zones. For example, the Seabee Mine in the metavolcanic Glennie Domain, Saskatchewan, is hosted by post-peak metamorphic, dextral transpressional or dextral-oblique slip, shear zones with biotite-actionolite-epidote-sericite±calcite alteration assemblage (Schultz, 1990, 1996; Tourigny, 2003). The nearby Santoy

deposits are hosted in similar post-peak metamorphic, dextral oblique-slip, shear zones with diopside-quartz-K-feldspar-plagioclase-titanite-actinolite alteration assemblages (Wood, 2016). The Seabee and Santoy gold deposits (Fig. 4.1) are the only current producing gold deposits in the Trans Hudson Orogen in Manitoba and Saskatchewan, and collectively they produced over 1.2 million ounces of gold (reported from Claude Resources, 2016) and, as of December 31st 2016, another 360,000 ounces of gold at an average grade of 8.19g/t of proven and probable mineral reserves has been delineated (www.ssrmining.com). The setting of these deposits is similar to that of the Tartan Lake gold deposit (Fig. 4.1) in the Flin Flon Domain, which is another example of a post-peak metamorphic gold deposit, which formed at greenschist facies conditions in a transpressional setting within shear zones that overprint peak metamorphic fabrics (Fedorowich et al., 1991).

Other gold deposits in the metavolcanic La Ronge-Lynn Lake Domain (Fig. 4.1) formed earlier during the Trans Hudson Orogeny along near-to syn-peak metamorphic fault zones. The deposits are characterized by biotite-Fe-carbonate-chlorite-pyrite alteration assemblages and are hosted by late, large scale structures, including the oblique-slip reverse Byers fault zone in Saskatchewan (Lafrance and Heaman, 2004) and the dextral transpressional Johnson Shear Zone in Manitoba (Beaumont-Smith et al. 2001; Jones et al., 2006).

The Puffy Lake deposit (Fig. 4.1) is the only other past-producing deposit (34,957 ounces' gold from December 1987 to March 1991; Gagné et al., 2006) with an early deformation history similar to that of the Snow Lake deposits. The deposit is located in the Kisseynew basin near its contact with the FFGD. It is characterized by a diopside-biotite-hornblende-feldspar alteration

assemblage. Mineralization was emplaced either before or during the development of the main bedding-parallel foliation (Ostry and Halden, 1995) during southwest-directed overthrusting of the FFGC by the Kisseynew basin (Norman et al., 1995). Thus, the deposit is thought to have formed early during the Trans-Hudson Orogeny and to have been later metamorphosed, and gold remobilized, during peak metamorphism at temperatures of 650-700°C and pressures of 3.5 to 6.5 kbar (Gagné et al., 2006).

4.10. Conclusions

The Snow Lake deposits, with New Britannia as the main deposit, produced more gold than any other present or past producing gold mines in the Trans Hudson Orogen of Manitoba and Saskatchewan. Gold mineralization was emplaced early in the hinge of a major fold, the Nor-Acme Anticline, during a major orogenic event that began with the formation of a regional foliation axial planar to the Nor Acme Anticline and culminated with the formation of major thrust faults (MRT) and gneiss domes along the boundary between the FFGD and Kisseynew basin. The Howe Sound Fault offsets the MRT and likely formed as a transfer fault during thrusting. It cuts across the hinge of the Nor Acme Anticline and overprints the main ore zones at the New Britannia Mine, resulting in ore zones that differ from the No. 3 Zone and Boundary Zone by the formation of a strong biotite shear zone foliation surrounding deformed quartz-carbonate veins, and by the presence of remobilized free gold along grain boundaries associated with fine acicular arsenopyrite aligned parallel to foliation.

With the exception of the Puffy Lake deposit, other deposits across the orogen differ from the Snow Lake deposits by their association with late, syn- to post-peak metamorphic, transcurrent

transpressional or oblique-slip fault zones. The Snow Lake deposits formed at amphibolite temperatures during a progressive and prograde deformation event and thus have elements of both metamorphic and continuum models.

4.11. References

Ansdell, K.M. 2005. Tectonic evolution of the Manitoba–Saskatchewan segment of the Paleoproterozoic Trans-Hudson Orogen, Canada. Canadian Journal of Earth Sciences, **42**: 741–759. doi:10.1139/e05-035.

Ansdell, K.M., Lucas, S.B., Connors, K.A., Stern, R., 1995. Kisseynew metasedimentary gneiss belt, Trans-Hudson orogen (Canada): Back-arc origin and collisional inversion. Geology 23, 1039–1043.

Ashton, K.E., Heaman, L.M., Lewry, J.F., Hartlaub, R.P. Shi, R., 1999. Age and origin of the Jan Lake Complex: a glimpse at the buried Archean craton of the Trans-Hudson Orogen. Canadian Journal of Earth Sciences 36, 185–108.

Bailes, A. H. 1997. Geochemistry of Paleoproterozoic volcanic rocks in the Photo Lake area, Flin Flon Belt (parts of NTS 63 K/16). In Manitoba Energy and Mines, Mineral Resources Division, Report of Activities, 1997, pp. 61-62.

Bailes, A.H. and Galley, A.G. 1996. Setting of Paleoproterozoic volcanic-hosted massive base metal sulphide deposits, Snow Lake, Manitoba; in EXTECH I: A Multidisciplinary Approach to Massive Sulphide Research in the Rusty Lake– Snow Lake Greenstone Belts, Manitoba, G.F.

BonhamCarter, A.G. Galley and G.E.M. Hall (ed.), Geological Survey of Canada, Bulletin 426, p. 105–138.

Bailes, A.H. and Galley, A.G. 1999. Evolution of the Paleoproterozoic Snow Lake arc assemblage and geodynamic setting for associated volcanic-hosted massive sulphide deposits, Flin Flon Belt, Manitoba, Canada; Canadian Journal of Earth Sciences, v. 36, p. 1789–1805.

Bailes, A.H. and Schledewitz, D.C.P. 1998. Geology and geochemistry of the Paleoproterozoic volcanic rocks between the McLeod Road and Birch Lake faults, Snow Lake area, Flin Flon belt (parts of NTS 63K/16 and 63J/13); in Report of Activities 1998, Manitoba Energy and Mines, Geological Services, p. 4–13.

Bailes, A., Rubingh, K., Gagné, S., Taylor, C., Galley, A., Bernaeur, S. and Simms, D. 2013. Volcanological and Structural Setting of Paleoproterozoic VMS and Gold deposits at Snow Lake, Manitoba; Geological Association of Canada–Mineralogical Association of Canada Joint Annual Meeting, Field Trip Guidebook FT-A2. Manitoba Innovation, Energy and Mines, Manitoba Geological Survey, Open File Report OF2013-3, pp. 1 - 73.

Beaumont-Smith, C.J. and Lavigne, J. 2008. Structural geology and gold metallogenesis of the New Britannia Mine area, Snow Lake, Manitoba (NTS 63K16); in Report of Activities 2008, Manitoba Science, Technology, Energy and Mines, Manitoba Geological Survey, p. 7–17.

Beaumont-Smith, C.J., Anderson, S.D., and Böhm, C.O. 2001. Structural analysis and

investigations of shear-hosted gold mineralization in the southern Lynn Lake greenstone belt (parts of NTS 64C/11, /12, /15, /16). In Report of activities 2001. Manitoba Industry, Trade, and Mines, Manitoba Geological Survey, pp. 67–75.

Bickford, M.E., Mock, T.D., Steinhart, W.E., III, Collerson, K.D., Lewry, J.F., 2005. Origin of the Archean Sask Craton and its extent within the Trans-Hudson orogen: evidence from Pb and Nd isotopic compositions of basement rocks and post-orogenic intrusions. Canadian Journal of Earth Sciences 42, 659–684.

Böhlke, J.K., 1982. Orogenic (metamorphic-hosted) gold-quartz veins. in Erickson, R. L., ed., Characteristics of Mineral Deposit Occurrences: U.S. Geological Survey Open-File Report 82-795, p. 70-76.

Cabri, L.J., Chryssoulis, S.L., De Villiers, J.P.R., Laflamme, J.H.G. and Buseck, P.R. 1989. The nature of “invisible” gold in arsenopyrite. The Canadian Mineralogist. 27, 353- 362.

Colvine, A.C. 1989. An empirical model for the formation of Archaean gold deposits: products of final cratonization of the Superior Province, Canada. Econ. Geol., Mono. 6:37-53

Colvine, A.C., Fyon, J.A., Heather, K.B., Marmont, S., Smith, P.M., Troop, D.G., 1988. Archean lode gold deposits in Ontario. Ontario Geological Survey Miscellaneous Paper 139. 136 pp.

Connors, K.A., 1996. Unravelling the boundary between turbidites of the Kisseynew belt and

volcano-plutonic rocks of the Flin Flon belt, Trans-Hudson Orogen, Canada. Canadian Journal of Earth Sciences 33, 811–829.

Connors, K.A., Ansdell, K.M., Lucas, S.B., 1999. Coeval sedimentation, magmatism, and fold-thrust development in the Trans- Hudson Orogen: propagation of deformation into an active continental arc setting, Wekusko Lake area, Manitoba. Canadian Journal of Earth Sciences 36, 275–291

Connors, K.A., Ansdell, K.M., Lucas, S.B., 2002. Development of a transverse to orogen parallel extension lineation in a complex collisional setting, Trans-Hudson Orogen, Manitoba, Canada. Journal of Structural Geology 24, 89–106.

Cook, N.J., and Chryssoulis, S.L., 1990. Concentrations of "invisible gold" in the common sulphides: Canadian Mineralogist, v. 28, p. 1–16.

Cook, N.J., Ciobanu, C.L., Mewria, D., Silcock, D., and Wade, B., 2013. Arsenopyrite-pyrite association in an orogenic gold ore: Tracing mineralization history from textures and trace elements: Economic Geology, v. 108, p. 1273–1283.

David, J., Bailes, A.H. and Machado, N. 1996. Evolution of the Snow Lake portion of the Paleoproterozoic Flin Flon and Kisseynew belts, Trans-Hudson Orogen, Manitoba Canada. Precambrian Research, 80: 107–124.

Fedorowich, J., Stauffer, M., and Kerrich, R., 1991. Structural Setting and Fluid Characteristics of the Proterozoic Tartan Lake Gold Deposit, Trans-Hudson Orogen, Northern Manitoba. Economic Geology, v. 86, p. 1434–1467.

Fieldhouse, I. 1999. Geological setting of gold mineralization in the vicinity of the New Britannia mine, Snow Lake, Manitoba; M.Sc. thesis, University of Manitoba, Winnipeg, Manitoba, 136 p

Froese, E. and Moore, J.M. 1980. Metamorphism in the Snow Lake area, Manitoba; Geological Survey of Canada, Paper 78-27, 16 p.

Frost, B.R., Mavrogenes, J.A. and Tomkins, A.G. 2002. Partial melting of sulfide ore deposits during medium- and high-grade metamorphism. The Canadian Mineralogist, 40: 1-18.

Gagné, S. 2009. Geological investigation of the McLeod Road Birch Lake allochthon east of Snow Lake, Manitoba (part of NTS 63J13); in Report of Activities 2009, Manitoba Innovation, Energy and Mines, Manitoba Geological Survey, p. 58–68.

Gagné, S., Beaumont-Smith, C.J., William-Jones, A.E., Hynes, A. 2006. Metallogenic and metamorphic study of selected deposits from the Snow Lake area and the southern flank of the Kisseynew Domain, Manitoba (NTS 63K16 and 63N2); in Report of Activities 2006, Manitoba Science, Technology, Energy and Mines, Manitoba Geological Survey, p. 42–48.

Galley, A.G., Ziehlke, D.V., Franklin, J.M., Ames, D.E. and Gordon, T.M. 1986. Gold

mineralization in the Snow Lake–Wekusko Lake region, Manitoba; in Gold in the Western Shield, A.L. Clark (ed.), Canadian Institute of Mining and Metallurgy, Special Volume 38, p. 379–398.

Galley, A.G., Bailes, A.H., Syme, E.C., Bleeker, W., Macek, J.J. and Gordon, T.M. 1991. Geology and mineral deposits of the Flin Flon and Thompson belts, Manitoba (Field Trip 10); Geological Survey of Canada, Open File 2165, 8th IAGOD Symposium Field Trip Guidebook, 137 p.

Goldfarb, R. J., Baker, T., Dube, B., Groves, D. I., Hart, C. J., and Gosselin, P., 2005. Distribution, character, and genesis of gold deposits in metamorphic terranes: Economic Geology 100th Anniversary Volume, p. 407–450.

Goldfarb, R.J., Groves, D.I., and Gardoll, S., 2001. Orogenic gold and geologic time: A global synthesis: Ore Geology Reviews, v. 18, p. 1–75.

Gourcerol, B., Thurston, P.C., Kontak, D.J., Côté-Mantha, O., 2015. Interpretations and implications of preliminary LA ICP-MS analysis of chert for the origin of geochemical signatures in banded iron formations (BIFs) from the Meadowbank gold deposit, Western Churchill Province, Nunavut. Chem. Geol. 410, 89–107.

Grant, J. A.,1986. The Isocon diagram—A simple solution to Gresen's equation for metasomatic alteration. Econ. Geol. 81, 1976–1982.

Groves, D.I., 1993. The crustal continuum model for late Archaean lode-gold deposits of the Yilgarn Block, Western Australia. Mineralium Deposita, 28, 366–374.

Groves, D.I., Goldfarb, R.J., Gebre-Mariam, M., Hagemann, S.G., and Robert, F., 1998. Orogenic gold deposits: A proposed classification in the context of their crustal distribution and relationship to other gold deposit types: Ore Geology Reviews, v. 13, p. 7–27.

Harrison, J.M. 1949. Geology and Mineral Deposits of FileTramping Lakes area, Manitoba; Geological Survey of Canada Memoir 250, 92 p.

Heinrichs, H., Schulz-Dobrick, B., Wedepohl, K. H. 1980. Terrestrial geochemistry of Cd, Bi, Tl, Zn and Rb. Geochim. Cosmochim. Acta, 44, 1519−1533.

Hogg, N. 1957. Nor-Acme Mine. Structural Geology of Canadian Ore deposits. Canadian Institute of Mining and Metallurgy. Sixth Commonwealth Mining and Metallurgical Congress, Vol. 2, pp.262-275

Jones, L.R., Lafrance, B. and Beaumont-Smith, C.J. 2006. Structural Controls on Gold Mineralization at the Burnt Timber Mine, Lynn Lake Greenstone Belt, Trans-Hudson Orogen, Manitoba, in Exploration and Mining Geology, Vol. 15, pp.89-100.

Kraus, J. and Menard, T. 1997. A thermal gradient at constant pressure: implications for low- to

medium-pressure metamorphism in a compressional tectonic setting, Flin Flon and Kisseynew domains, Trans-Hudson Orogen, central Canada. The Canadian Mineralogist, 35: 1117–1136.

Kraus, J. and Williams, P.F. 1999. Structural development of the Snow Lake allochthon and its role in the evolution of the southeastern Trans-Hudson Orogen in Manitoba, central Canada; Canadian Journal of Earth Sciences, v. 36, p. 1881–1899.

Lafrance, B., and Heaman, L.M. 2004. Structural controls on hypozonal orogenic gold mineralization in the La Ronge Domain, Trans-Hudson Orogen, Saskatchewan. Canadian Journal of Earth Sciences 41, 1453–1471.

Larocque, A.C.L., Hodgson, C.J., Cabri, L.J., and Jackman, J.A., 1995. Ion microprobe analysis of pyrite, chalcopyrite and pyrrhotite from the Mobrun VMS deposit in northwestern Quebec: Evidence for metamorphic remobilization of gold. The Canadian Mineralogist 33, 373-388.

Lawley, C.J.M., Creaser, R., Jackson, S., Yang, Z., Davis, B., Pehrsson, S., Dubé, B., Mercier-Langevin, P., and Vaillancourt, D., 2015. Unravelling the Western Churchill Province Paleoproterozoic Gold Metallotect: Constraints from Re-Os arsenopyrite and U-Pb xenotime geochronology and LA-ICP-MS arsenopyrite geochemistry at the BIF-hosted Meliadine gold district, Nunavut, Canada: Economic Geology, v. 110, p. 1425–1454.

Li, W., Cook, N.J., Xie, G.-Q., Mao, J.-W., Ciobanu, C.L., Li, J.-W., and Zhang, Z.-Y., 2018. Textures and trace element signatires of pyrite and arsenopyrite from the Gutaishan Au-Sb

deposit, South China. Mineralium Deposita https://doi.org/10.1007/s00126-018-0826-0

Lucas, S.B., Green, A., Hajnal, Z., White, D., Lewry, J.F., Ashton, K.E., Weber, W., Clowes, R., 1993. Deep seismic profiles across a Proterozoic collision zone: surprises at depth. Nature (London), 363, 339–342.

Lucas, S.B., Stern, R.A., Syme, E.C., Reilly, B.A. and Thomas, D.J. 1996. Intraoceanic tectonics and the development of continental crust: 1.92–1.84 Ga evolution of the Flin Flon Belt, Canada; Geological Society of America Bulletin, v. 108, p. 602–629.

Menard, T., Gordon, T.M., 1997. Metamorphic P-T paths from the eastern Flin Flon Belt, and Kisseynew Domain, Snow Lake, Manitoba. The Canadian Mineralogist 35, 1093–1115.

Mikucki, E.J. and Ridley, J.R., 1993. The hydrothermal fluid of Archaean lode-gold deposits at different metamorphic grades: compositional constraints from ore and wallrock alteration assemblages. Mineralium Deposita, 28, 469–481.

Morey, A.A., Tomkins, A.G., Bierlein, F.P., Weinberg, R.F., and Davidson, G.J., 2008. Bimodal distribution of gold in pyrite and arsenopyrite: Examples from the Archean Boorara and Bardoc shear systems, Yilgarn craton, Western Australia: Economic Geology, v. 103, p. 599–614.

Mumin, A.H., Fleet, M.E., and Chryssoulis, S.L., 1994. Gold mineralization in As-rich mesothermal gold ores of the Bogosu-Prestea mining district of the Ashanti gold belt, Ghana: Remobilization of “invisible” gold: Mineralium Deposita, v. 29, p. 445–460.

Norman, A.R., Williams, P.F., Ansdell, K.M., 1995. Early Proterozoic deformation along the southern margin of the Kisseynew gneiss belt, Trans-Hudson Orogen: a 30 Ma progressive deformation cycle. Canadian Journal of Earth Sciences, 32: 875–894.

Okumura, M., and Y. Kitano. 1986. Coprecipitation of alkali metal ions with calcium carbonate, Geochim. Cosmochim. Acta, 50, 49–58.

Ostry, G. and Halden, N.M. 1995. Geology of the Puffy Lake Au deposit, Sherridon district, Manitoba; Exploration and Mining Geology, v. 4, p. 51–63.

Passchier C. W and Trouw. R.A.J. 1996. Microtectonics. Springer-Verlag, Berlin. 289 p.

Paton, C., Hellstrom, J., Paul, B., Woodhead, J. and Hergt, J. 2011. “Iolite: Freeware for the visualisation and processing of mass spectrometric data.” Journal of Analytical Atomic Spectrometry. doi:10.1039/c1ja10172b.

Pearson, K., 1895. Royal Society Proceedings, 58, 241. (1920), "Notes on the History of Correlation," Biometrika, 13, 25-45.

Phillips, G.N. and Groves, D.I., 1983. The nature of Archaean gold-bearing fluids as deduced from gold deposits of Western Australia. Journal Geological Society Australia, 30, 25–39.

Phillips, G.N. and Powell, R., 2010. Formation of gold deposits: a metamorphic devolatilization

model. Journal of Metamorphic Geology, 28, 689–718.

Ross, M. 1964. Crystal chemistry of beryllium. U.S. Geological Survey Professional Paper 468, 30 p.

Rubingh, K.E 2011. Stratigraphy of the McLeod Road–Birch Lake thrust panel, Snow Lake, west-central Manitoba (parts of NTS 63K16 and 63J13). In Report of Activities, 2011 Manitoba Innovation, Energy and Mines, 2011, pp. 68–78.

Rubingh, K.E., Lafrance, B., Gibson, H.L. and Gagné, S. 2012a. Preliminary lithostratigraphic map of the McLeod Road– Birch Lake thrust panel, Snow Lake, west-central Manitoba (parts of NTS 63K16, 63J13). In Report of Activities 2012a, Manitoba Innovation, Energy and Mines, Preliminary Map PMAP2012-7, 1:5000 scale.

Rubingh, K.E., Lafrance, B. and Gibson, H.L. 2012b. Lithostratigraphy and structural geology of the McLeod Road–Birch Lake thrust panel, Snow Lake, west-central Manitoba (parts of NTS 63K16, 63J13). In Report of Activities 2012b, Manitoba Innovation, Energy and Mines, pp. 104–114.

Rubingh, K.E., Gibson, H.L., Lafrance, B., 2017. Evidence for voluminous, bimodal pyroclastic volcanism, during rifting of a Paleoproterozoic Arc at Snow Lake, Manitoba. Canadian Journal of Earth Sciences 54, 654–676.

Schultz, D.J., 1996. The fluid history of the Seabee mesothermal gold deposit, northern Saskatchewan; M.Sc. thesis, University of Saskatchewan, Saskatoon, 122p.

Schultz, D.J., 1990. Reconnaissance geological study of the Seabee gold deposit, Glennie Domain. in Summary of investigations 1990, Saskatchewan Geological Survey, Saskatchewan Energy and Mines, Miscellaneous Report 90-4, p. 70-73.

Shaw, C.S.J., and Penczak, R.S., 1996. Barium- and titanium-rich biotite and phlogopite from the western and eastern gabbro, Coldwell alkaline complex, northwestern Ontario. The Canadian Mineralogist, 34, 967-975.

Sung, Y.H., Brugger, J., Ciobanu, C.L., Pring, A., Skinner, W., and Nugus, M., 2009. Invisible gold in aresenian pyrite and arsenopyrite from a multistage Archean gold deposits: Sunrise Dam, Eastern Goldfield Province, western Australia. Mineralium Deposita, 44: 765-791.

Syme, E.C, Bailes, A.H. and Lucas, S.B. 1995. Geology of the Reed Lake area (parts of NTS 63K/9 and 10); in Report of Activities 1997, Manitoba Energy and Mines, Geological Services, Report of Field Activities, p. 42–60.

Syme, E.C., Bailes, A.H. and Lucas, S.B. 1996. Tectonic assembly of the Paleoproterozoic Flin Flon belt and setting of VMS deposits; Geological Association of Canada– Mineralogical Association of Canada, Joint Annual Meeting, Winnipeg, Manitoba, May 27–29, 1996, Field Trip Guidebook B1, 131 p.

Syme, E.C., Lucas, S.B., Bailes, A.H., and Stern, R.A. 1999. Contrasting arc and MORB-like assemblages in the Paleoproterozoic Flin Flon Belt, Manitoba, and the role of intra-arc extension in localizing volcanic-hosted massive sulphide deposits. Canadian Journal of Earth Sciences, 36: 1767–1788. doi:10.1139/cjes- 36-11-1767.

Tomkins, A.G., Frost, B.R., and Pattison, D.R.M., 2006. Arsenopyrite melting during metamorphism of sulfide ore deposits. The Canadian Mineralogist, 44: 1045-1062.

Tomkins, A.G., Pattison, D.R.M., and Frost, B.R., 2007. On the initiation of metamorphic sulfide anatexis. Journal of Petrology, 48: 511-535.

Tourigny, G. 2003. Preliminary structural study of the gold-bearing shear zone system at the Seabee mine, northern Saskatchewan; in Summary of Investigations 2003, Volume 2, Saskatchewan Geological Survey, Sask. Industry and Resources, Misc. Rep. 2003-4.2, CD-ROM, Paper B-1, 11p.

Wagner, T., Klemd, R., Wenzel, T., and Mattsson, B., 2007. Gold upgrading in metamorphosed massive sulfide ore deposits: Direct evidence from laser-ablation–inductively coupled plasma–mass spectrometry analysis of invisible gold; Geology, V. 35, p. 775-778)

Wood, B.J., Blundy, J.D., 2003. Trace element partitioning under crustal and uppermost mantle conditions: the influences of ionic radius, cation charge, pressure, and temperature. In: Carlson,

R.W. (Ed.), Treatise on Geochemistry. Elsevier, Amsterdam, pp. 395–425.

Wood, C.R., 2016. Structural study of the auriferous Santoy shear zone, northeastern Glennie domain, Saskatchewan, MSc. Thesis, University of Regina, 154 p.

Woodhead, J., Hellstrom, J., Hergt, J., Greig, A. & Maas, R.,2007. Isotopic and elemental imaging of geological materials by laser ablation Inductively Coupled Plasma mass spectrometry. Journal of Geostandards and Geoanalytical Research, 31, p. 331-343.

Zacharias, J., Fryda, J., Paterova, B., and Mihaljevik, M., 2004. Arsenopyrite and As-bearing pyrite from the Roudny deposit, Bohemain Massif. Mineralogical Magazine, Vol. 68 (1), pp. 31 – 46.

Table 4- 1: Concentration data for major and trace elements for representative samples from the New Britannia Mine mineralization, No.3 Zone and the Boundary Zone.

Sample No. Alteration zone		12KR080A01 LAP-MV (unit3)	KR11-090 LAP-FV (unit 4)	KR11-037 LAP-MV (unit5)	C12KR049 MM - SMZ (unit 3)	C12KR129 BZ - SMZ (unit 4)	C12KR112 3Z - SMZ (unit 5)
Major oxides	Method	Lithium metaborate and tetraborate fusion XRF					
SiO_2	FUS-XRF	49.88	74.64	46.06	45.10	68.10	45.03
Al_2O_3	FUS-XRF	16.47	9.56	12.24	18.22	14.38	17.12
Fe_2O_3(T)	FUS-XRF	13.14	3.70	13.00	8.22	6.66	14.77
MnO	FUS-XRF	0.19	0.09	0.20	0.16	0.10	0.26
MgO	FUS-XRF	5.29	0.47	9.34	6.13	1.40	11.53
CaO	FUS-XRF	10.49	3.59	12.21	13.24	2.12	6.61
Na_2O	FUS-XRF	2.11	1.30	0.92	4.24	3.94	1.21
K_2O	FUS-XRF	0.41	1.87	0.27	2.91	2.36	2.72
TiO_2	FUS-XRF	0.59	0.21	0.32	0.40	0.30	0.57
P_2O_5	FUS-XRF	0.10	0.03	0.12	0.20	0.01	0.05
Cr_2O_3	FUS-XRF	nd	nd	nd	0.01	0.01	0.02
V_2O_5	FUS-XRF	nd	nd	nd	0.08	0.00	0.08
LOI	FUS-XRF	1.42	4.02	4.53	8.77	2.26	5.01
Total		100.20	99.48	99.21	98.90	99.38	99.96
CO_2	IRC	1.043	2.38	0.31	8.03	1.1	3.46
S	IRC	0.01	0.003	0.009	0.29	1.67	0.37
Trace elements	Method	Closed vessel multi acid total digestion and ICP-MS finish					
Li	TD - ICPMS	21.30	26.60	21.90	34.30	16.60	38.20
Be	TD - ICPMS	0.22	0.65	0.43	0.44	1.04	0.71
Bi	TD - ICPMS	0.15	0.15	0.15	<0.15	0.26	0.19
Cr	TD - ICPMS	52.00	34.00	491.00	93.00	18.00	88.00
Ni	TD - ICPMS	19.00	1.80	91.40	27.40	2.80	27.20
Sc	TD - ICPMS	44.90	11.10	60.10	48.00	17.50	58.70
Ti	TD - ICPMS	3338.00	1045.00	1750.00	2071.00	1727.00	3136.00
V	TD - ICPMS	359.80	1.30	307.80	>370	9.70	370.00
Cu	TD - ICPMS	112.80	21.90	94.80	16.90	184.00	130.60
Co	TD - ICPMS	39.88	1.34	53.74	18.40	2.20	49.72

Table 4-1. Concentration data for major and trace elements for representative samples from the New Britannia Mine mineralization, No.3 Zone and the Boundary Zone. (Continued)

Sample No. Alteration zone		12KR080A01 LAP-MV (unit3)	KR11-090 LAP-FV (unit 4)	KR11-037 LAP-MV (unit5)	C12KR049 MM - SMZ (unit 3)	C12KR129 BZ - SMZ (unit 4)	C12KR112 3Z - SMZ (unit 5)
Trace elements	Method	Closed vessel multi acid total digestion and ICP-MS finish					
Pb	TD - ICPMS	1.30	2.70	2.80	4.10	32.20	18.40
Zn	TD - ICPMS	84.00	70.00	76.00	41.00	233.00	117.00
Ga	TD - ICPMS	13.35	9.09	9.49	14.13	16.59	17.42
Rb	TD - ICPMS	5.10	23.45	1.42	35.74	25.87	34.30
Mo	TD - ICPMS	0.88	1.51	0.37	0.40	1.92	0.36
Cd	TD - ICPMS	0.06	0.10	0.07	0.07	0.34	0.15
In	TD - ICPMS	0.05	0.06	0.03	0.03	0.11	0.06
Sn	TD - ICPMS	0.41	0.96	0.38	0.55	1.53	0.56
Sb	TD - ICPMS	0.58	0.38	0.55	1.05	2.93	5.90
Cs	TD - ICPMS	0.21	0.73	0.02	0.54	0.22	1.21
Ba	TD - ICPMS	311.60	159.60	69.60	401.20	872.40	611.60
Sr	TD - ICPMS	173.10	54.10	284.00	192.50	118.50	219.10
Nb	TD - ICPMS	1.67	4.71	1.11	0.40	6.43	0.76
Hf	TD - ICPMS	0.81	2.70	0.47	0.24	3.94	0.45
Zr	TD - ICPMS	28.00	96.00	16.00	8.00	143.00	15.00
Y	TD - ICPMS	11.87	30.08	6.05	4.17	40.92	11.90
Th	TD - ICPMS	0.55	1.93	0.61	0.17	2.63	0.32
U	TD - ICPMS	0.24	0.86	0.30	0.15	1.32	0.19
La	TD - ICPMS	3.34	12.62	4.10	1.06	14.86	4.55
Ce	TD - ICPMS	7.70	28.03	8.76	2.65	33.29	9.52
Pr	TD - ICPMS	1.08	3.69	1.19	0.40	4.52	1.34
Nd	TD - ICPMS	5.13	16.11	5.34	1.82	19.79	6.62
Sm	TD - ICPMS	1.39	4.25	1.36	0.50	5.14	1.89
Eu	TD - ICPMS	0.49	1.04	0.44	0.36	1.21	0.79
Gd	TD - ICPMS	1.73	5.05	1.30	0.61	5.75	2.33
Tb	TD - ICPMS	0.30	0.85	0.19	0.10	0.96	0.35
Dy	TD - ICPMS	2.02	5.58	1.17	0.68	6.71	2.14
Ho	TD - ICPMS	0.43	1.15	0.24	0.15	1.44	0.42

Table 4-1: Concentration data for major and trace elements for representative samples from the New Britannia Mine mineralization, No.3 Zone and the Boundary Zone. (Continued)

Sample No. / Alteration zone		12KR080A01 LAP-MV (unit3)	KR11-090 LAP-FV (unit 4)	KR11-037 LAP-MV (unit5)	C12KR049 MM - SMZ (unit 3)	C12KR129 BZ - SMZ (unit 4)	C12KR112 3Z - SMZ (unit 5)
Trace elements	Method	Closed vessel multi acid total digestion and ICP-MS finish					
Er	TD - ICPMS	1.35	3.41	0.69	0.46	4.64	1.19
Tm	TD - ICPMS	0.20	0.51	0.10	0.07	0.71	0.16
Yb	TD - ICPMS	1.39	3.31	0.66	0.47	4.78	1.07
Lu	TD - ICPMS	0.21	0.49	0.10	0.08	0.75	0.16
Ta	TD - ICPMS	0.08	0.26	0.06	<0.023	0.36	0.03
W	TD - ICPMS	0.38	0.47	0.15	>141	11.56	7.51
Tl	TD - ICPMS	0.04	0.11	0.01	0.17	0.10	0.14
Trace elements	Method		Aqua regia digestion ICP-MS				
Li	AR-ICPMS	10.87	14.73	7.37	36.93	14.76	28.74
Be	AR-ICPMS	0.03	0.19	0.11	0.08	0.15	0.26
Bi	AR-ICPMS	0.01	0.03	0.00	0.05	0.06	0.10
Cr	AR-ICPMS	13.35	15.30	36.73	81.00	6.00	50.00
Ni	AR-ICPMS	4.30	1.50	8.30	34.30	7.80	32.50
Sc	AR-ICPMS	6.88	4.77	4.10	>20	12.05	20.00
Ti	AR-ICPMS	454.30	391.40	172.00	1703.10	832.90	1671.90
V	AR-ICPMS	63.96	0.13	26.57	>80	8.00	80.00
Cu	AR-ICPMS	117.50	22.20	96.40	16.80	170.70	121.10
Co	AR-ICPMS	7.24	1.17	4.45	17.55	2.11	44.19
Pb	AR-ICPMS	0.35	0.85	1.52	1.00	27.90	10.40
Zn	AR-ICPMS	14.80	72.90	7.20	40.22	238.47	71.94
Ga	AR-ICPMS	3.15	3.87	2.69	9.10	6.19	10.05
Rb	AR-ICPMS	3.47	9.74	0.56	31.60	13.68	31.13
Mo	AR-ICPMS	0.45	1.02	0.30	0.29	1.42	0.19
Cd	AR-ICPMS	0.02	0.05	0.01	0.02	0.39	0.11
In	AR-ICPMS	0.01	0.04	0.00	0.03	0.09	0.03

Table 4-1: Concentration data for major and trace elements for representative samples from the New Britannia Mine mineralization, No.3 Zone and the Boundary Zone. (Continued)

Sample No.		12KR080A01	KR11-090	KR11-037	C12KR049	C12KR129	C12KR112
Alteration zone		LAP-MV (unit3)	LAP-FV (unit 4)	LAP-MV (unit5)	MM - SMZ (unit 3)	BZ - SMZ (unit 4)	3Z - SMZ (unit 5)
Trace elements	Method	Aqua regia digestion ICP-MS					
Sn	AR-ICPMS	0.06	0.39	0.03	0.40	0.85	0.18
Sb	AR-ICPMS	0.13	0.19	0.08	0.87	2.65	4.19
Cs	AR-ICPMS	0.18	0.38	0.01	0.51	0.17	1.12
Ba	AR-ICPMS	145.28	56.25	21.39	334.80	126.90	558.70
Sr	AR-ICPMS	48.50	12.91	212.94	30.77	11.19	96.89
Nb	AR-ICPMS	0.05	0.34	0.03	0.03	0.49	0.03
Hf	AR-ICPMS	0.01	0.14	0.00	<0.05	0.50	0.05
Zr	AR-ICPMS	0.54	6.13	0.20	0.37	19.50	0.68
Y	AR-ICPMS	2.46	17.72	0.82	3.63	8.60	6.54
Th	AR-ICPMS	0.45	1.68	0.58	0.16	2.26	0.29
U	AR-ICPMS	0.16	0.44	0.21	0.11	0.40	0.09
La	AR-ICPMS	2.98	12.35	3.72	0.95	14.18	4.38
Ce	AR-ICPMS	6.55	26.92	7.68	2.40	31.40	9.20
Pr	AR-ICPMS	0.83	3.56	0.96	0.36	4.09	1.23
Nd	AR-ICPMS	3.31	15.57	3.70	1.69	17.08	5.82
Sm	AR-ICPMS	0.65	4.05	0.61	0.44	4.05	1.49
Eu	AR-ICPMS	0.17	0.80	0.14	0.23	0.65	0.53
Gd	AR-ICPMS	0.53	4.49	0.33	0.55	3.83	1.89
Tb	AR-ICPMS	0.08	0.69	0.04	0.09	0.47	0.24
Dy	AR-ICPMS	0.46	3.95	0.18	0.57	2.17	1.35
Ho	AR-ICPMS	0.09	0.72	0.03	0.13	0.35	0.24

Table 4-1: Concentration data for major and trace elements for representative samples from the New Britannia Mine mineralization, No.3 Zone and the Boundary Zone. (Continued)

Sample No.		12KR080A01	KR11-090	KR11-037	C12KR049	C12KR129	C12KR112
Alteration zone		LAP-MV (unit3)	LAP-FV (unit 4)	LAP-MV (unit5)	MM - SMZ (unit 3)	BZ - SMZ (unit 4)	3Z - SMZ (unit 5)
Trace elements	Method	Aqua regia digestion ICP-MS					
Er	AR-ICPMS	0.28	1.88	0.09	0.38	0.95	0.57
Tm	AR-ICPMS	0.04	0.23	0.01	0.06	0.13	0.07
Yb	AR-ICPMS	0.28	1.40	0.07	0.40	0.87	0.43
Lu	AR-ICPMS	0.04	0.20	0.01	0.07	0.13	0.06
Ta	AR-ICPMS	0.00	0.00	0.00	<0.004	0.00	0.00
W	AR-ICPMS	0.74	0.09	0.04	>90	8.20	4.40
Tl	AR-ICPMS	0.03	0.05	0.00	0.17	0.07	0.14
Hg	AR-ICPMS	0.01	0.01	0.01	<0.01	0.01	0.02
Pt	AR-ICPMS	0.00	0.00	0.00	0.00	0.00	0.01
Se	AR-ICPMS	0.07	0.05	0.07	<0.4	0.50	0.50
Te	AR-ICPMS	0.02	0.00	0.00	0.03	0.02	0.05
Ag	AR-ICPMS	0.01	0.02	0.01	0.02	0.26	8.10
As	AR-ICPMS	0.68	0.95	0.48	>500	>500	>500
Au	AR-ICPMS	0.01	0.00	0.00	0.12	1.12	100.00

Note: Samples chosen were to illustrate the most representative analysis from each zone and compared with the least altered precursor; LAP-MV, least altered precursor for the mafic volcaniclastic rocks; LAP-FV, least altered precursor for the felsic volcanic rocks; MM-SMZ, New Britannia mine strongly mineralized zone; 3Z-SMZ, No. 3 Zone strongly mineralized zone; BZ- SMZ, Boundary zone strongly mineralized zone. Major elements in wt.%; trace elements in ppm; total Fe as Fe_2O_3; LOI, loss on ignition; FUS–XRF, Lithium metaborate and tetraborate fusion follwed by XRF; FUS–MS, lithium metaborate and tetraborate fusion ICP–MS; IRC, combustion and analysis by infrared absorption; TD–ICPMS, Closed vessel multi acid total digestion and ICP-MS finish; AR–ICPMS, aqua regia digestion with an ICP–MS finish.

Table 4- 2. Table for the coefficient of determination, referred to as the square of the Pearson correlation coefficient, (r^2) which represents the proportion of the variance shared by both elements. The table illustrates the combined analysis between mineralized samples from all of the zones (except the Toots zone), to determine the metal association between gold, base metals and selective trace elements. Data was selected for; CO_2, S, LOI, Ag, As, Au, Bi, Se and Te from the AR-ICPMS analysis and all other data was used from the TD-ICPMS analysis. Critical values, which represent a strong significant correlation between two variables are represented where r^2 >0.411.

	CO2	S	LOI	Ag	Au	Bi	Ba	Co	Cr	Cs	Cu	Mo	Ni	Pb	Sb	Se	Sn	Te	Ti	W	Zn
CO2	1	0.36	0.96	0.30	0.34	0.31	0.01	0.23	0.28	0.03	0.03	0.01	0.17	0.04	0.30	0.03	0.01	0.00	0.37	0.14	0.32
S		1	0.43	0.55	0.73	0.68	0.07	0.04	0.25	0.04	0.03	0.00	0.13	0.02	0.75	0.12	0.13	0.16	0.19	0.00	0.10
LOI			1	0.29	0.39	0.40	0.01	0.17	0.23	0.02	0.02	0.00	0.16	0.02	0.34	0.03	0.01	0.01	0.36	0.13	0.21
Ag				1	0.85	0.52	0.16	0.07	0.11	0.20	0.08	0.04	0.03	0.39	0.75	0.20	0.08	0.02	0.18	0.03	0.18
Au					1	0.83	0.23	0.09	0.13	0.17	0.01	0.01	0.05	0.15	0.84	0.10	0.07	0.05	0.17	0.03	0.12
Bi						1	0.17	0.03	0.15	0.18	0.02	0.03	0.03	0.00	0.68	0.11	0.09	0.04	0.14	0.01	0.09
Ba							1	0.15	0.00	0.17	0.20	0.02	0.00	0.09	0.25	0.13	0.08	0.04	0.00	0.02	0.02
Co								1	0.24	0.04	0.21	0.00	0.29	0.20	0.11	0.20	0.01	0.07	0.18	0.33	0.26
Cr									1	0.07	0.03	0.20	0.59	0.01	0.14	0.06	0.13	0.00	0.44	0.04	0.63
Cs										1	0.02	0.00	0.03	0.12	0.25	0.05	0.12	0.01	0.08	0.03	0.18
Cu											1	0.08	0.03	0.01	0.00	0.91	0.13	0.00	0.05	0.00	0.07
Mo												1	0.00	0.19	0.02	0.04	0.00	0.13	0.01	0.00	0.13
Ni													1	0.00	0.09	0.01	0.09	0.02	0.43	0.04	0.28
Pb														1	0.19	0.00	0.04	0.00	0.01	0.10	0.06
Sb															1	0.05	0.08	0.10	0.15	0.02	0.13
Se																1	0.13	0.03	0.06	0.00	0.05
Sn																	1	0.01	0.43	0.10	0.18
Te																		1	0.01	0.02	0.27
Ti																			1	0.10	0.49
W																				1	0.07
Zn																					1

Table 4- 3: LA-ICP-MS Operating Conditions

LA	
Model	Resonetics Resolution M-50
Type	ArF excimer
Wavelength (nm)	193 nm
Pulse duration (ns)	20
Gas flows: (ml/min)	
1) Helium carrier gas	650
2) Argon neb gas flow	780
d) Nitrogen additional gas	6
ICP - MS	
Model	Thermo X-series II Quadrupole ICP-MS
Plasma	Argon
Forward Power (W)	1470
Oxide production (ThO+/Th+ of NIST612)	< 1%
Th/U signal of NIST612	~ 1
Data acquisition and Reduction	
Scanning parameters:	
Spot diameter (µm)	ranges from 8 - 14
Speed (um/s)	ranges from 3 - 9
Fluence [J/cm^2]	4
Repetition rate [Hz]	8
Dwell time per isotope (ms)	10
External standard	NIST610, GSE
Internal standard	Fe
Data reduction	Iolite v.3 after Woodhead et al., (2007); Patron

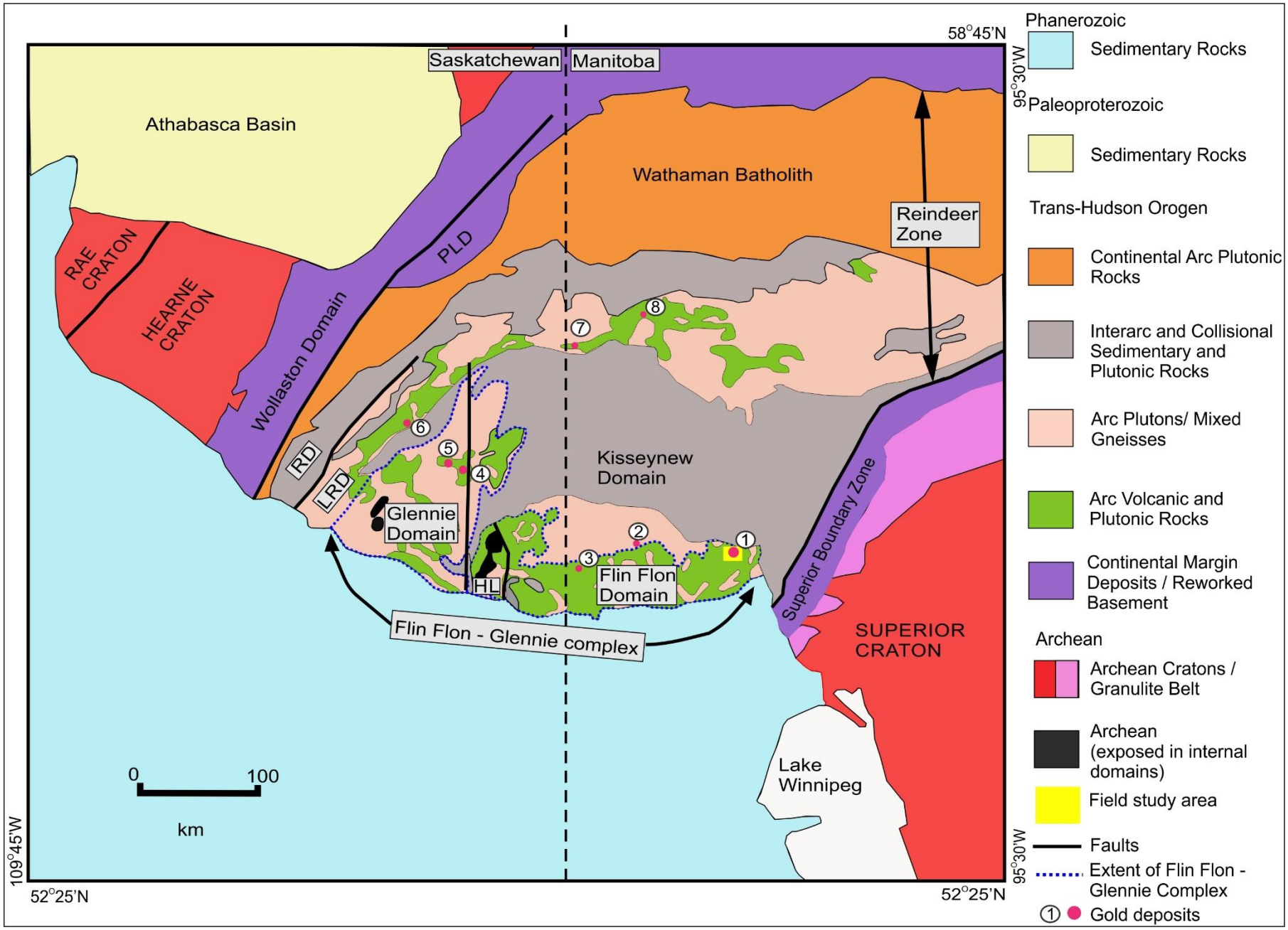
58°45'N
Saskatchewan
Manitoba
Athabasca Basin
Wathaman Batholith
Reindeer Zone
RAE CRATON
HEARNE CRATON
Wollaston Domain
PLD
RD
LRD
Kisseynew Domain
Glennie Domain
Flin Flon Domain
HL
Flin Flon - Glennie complex
Superior Boundary Zone
SUPERIOR CRATON
Lake Winnipeg
0
100
km
109°45'W
52°25'N
95°30'W
Phanerozoic
Sedimentary Rocks
Paleoproterozoic
Sedimentary Rocks
Trans-Hudson Orogen
Continental Arc Plutonic Rocks
Interarc and Collisional Sedimentary and Plutonic Rocks
Arc Plutons/ Mixed Gneisses
Arc Volcanic and Plutonic Rocks
Continental Margin Deposits / Reworked Basement
Archean
Archean Cratons / Granulite Belt
Archean (exposed in internal domains)
Field study area
Faults
Extent of Flin Flon - Glennie Complex
Gold deposits

Figure 4.1. Simplified domain map of the Saskatchewan – Manitoba portion of the Trans-Hudson Orogen (THO) and location of the Archean cratons. The Flin – Flon Glennie complex (Ashton, 1999) include the Glennie Domain, Hanson Lake block and Flin Flon Domain. The location of the Snow Lake camp is indicated by a yellow rectangle. The location of gold deposits discussed in the text are numbered and represented by red circles: 1, New Britannia Mine; 2, Puffy Lake Mine; 3, Tartan Lake deposit; 4, Santoy depsoits; 5, Seabee Mine; 6, Komis Mine; 7, Burnt Timber Mine; 8, Lynn Lake area deposits. Domain names: HL, Hanson Lake block; RD, Rottenstone Domain; LRD, La Ronge Domain; PLD, Peter Lake Domain. Modified after Lucas et al. (1993).

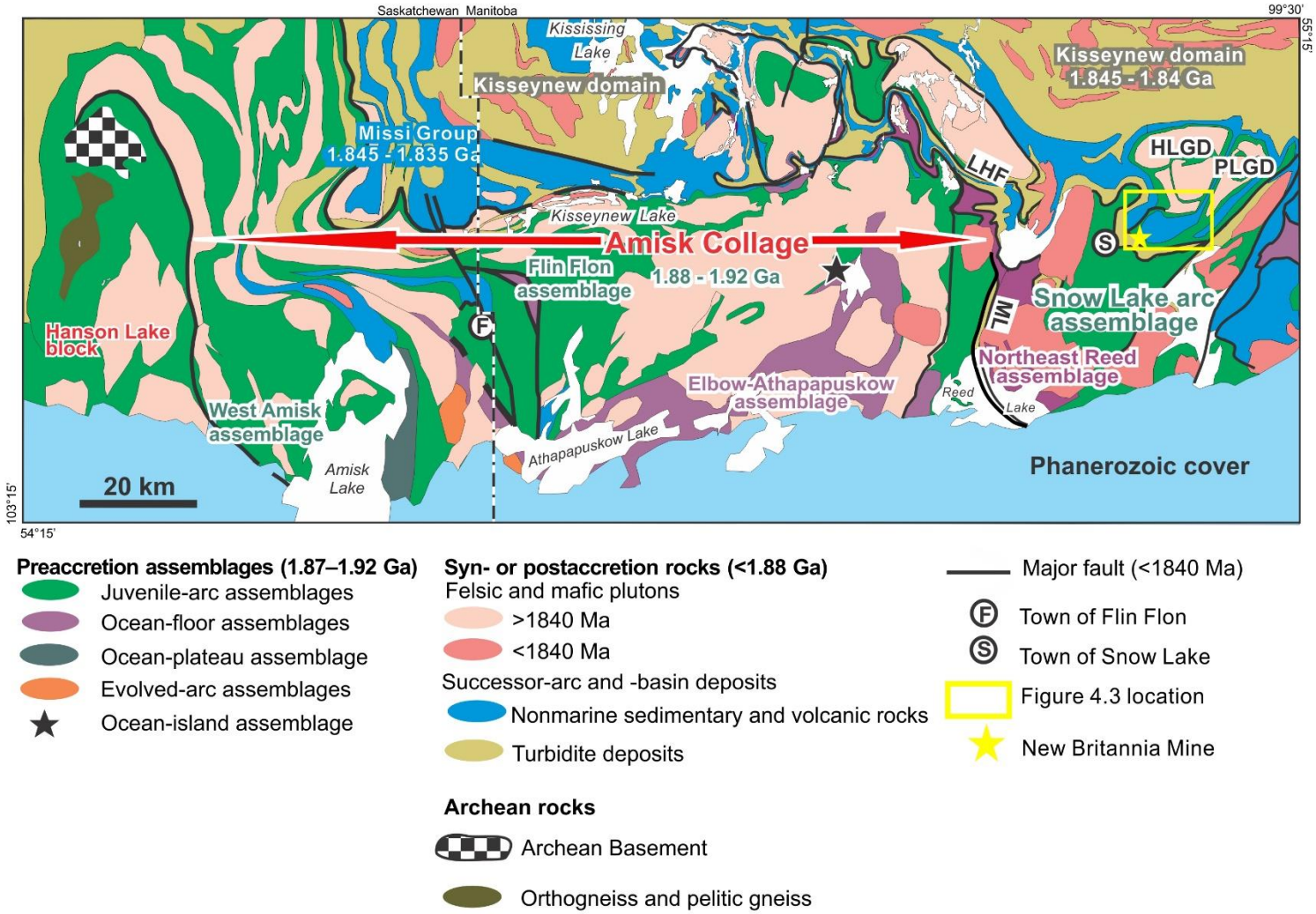

Figure 4.2. Regional geology of the Flin Flon Glennie Complex (excluding the Glennie Domain). Abbreviations: HLGD, Herblet Lake gneiss dome; LHF, Loonhead Lake fault; ML, Morton Lake Fault; PLGD, Pulver Lake gneiss dome. Snow Lake area is highlighted by the yellow box. Modified after Syme et al. (1999).

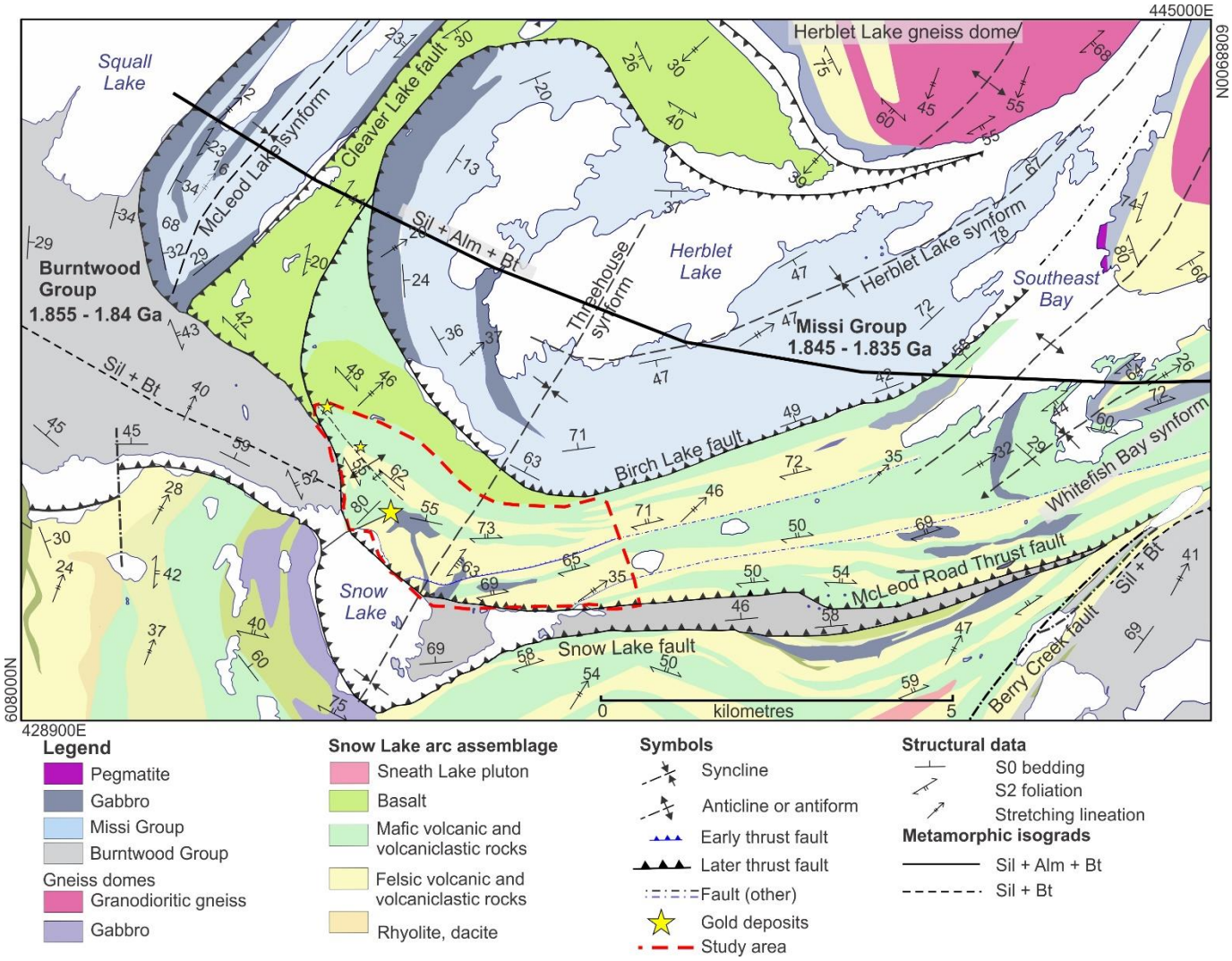

Figure 4.3: Regional geology of the Snow Lake area. The McLeod Road - Birch Lake thrust panel is bounded to the south by the McLeod Road Thrust fault and to the north by the Birch Lake fault. Modified after Gagné (2009). Regional data compilation from Froese and Moore (1980), Kraus and Williams (1999), Beaumont-Smith and Gagné (2010) and Rubingh et al. (2017).

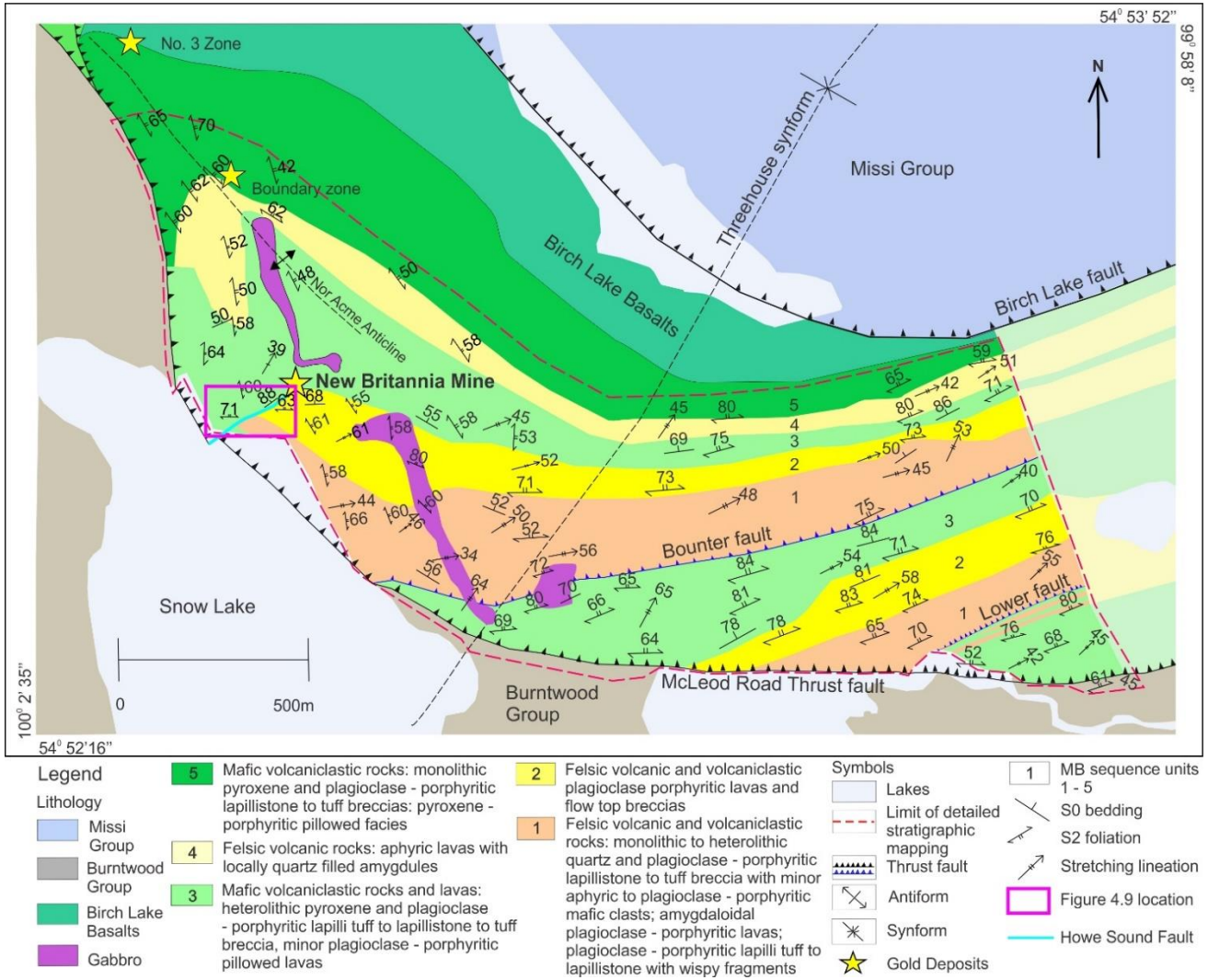

Figure 4.4. Geology of the central McLeod Road - Birch Lake thrust panel, including location of the New Britannia Mine, Boundary Zone and the No. 3 Zone. Modified after Beaumont-Smith and Gagné (2008) and Rubingh et al. (2012a).

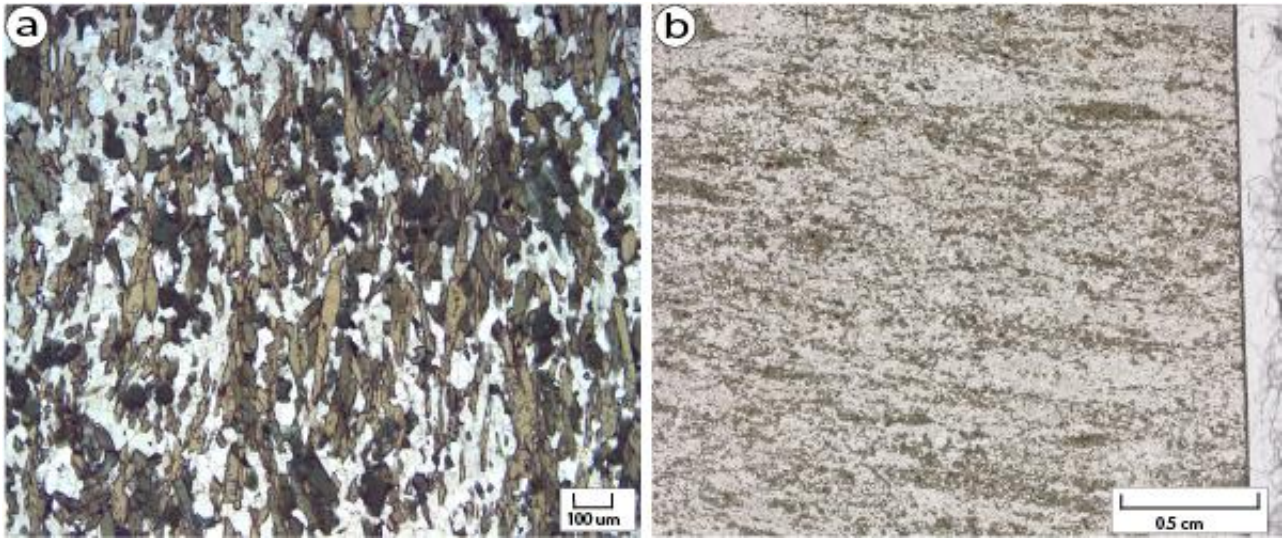

Figure 4.5: a) Plane polarized light photomicrograph of Nor-Acme S2 cleavage defined by amphibole and biotite in mafic volcaniclastic rocks of Unit 3. b) Plane polarized light photomicrograph of S2 cleavage defined by amphibole and biotite, in mafic volcaniclastic rocks of Unit 3.

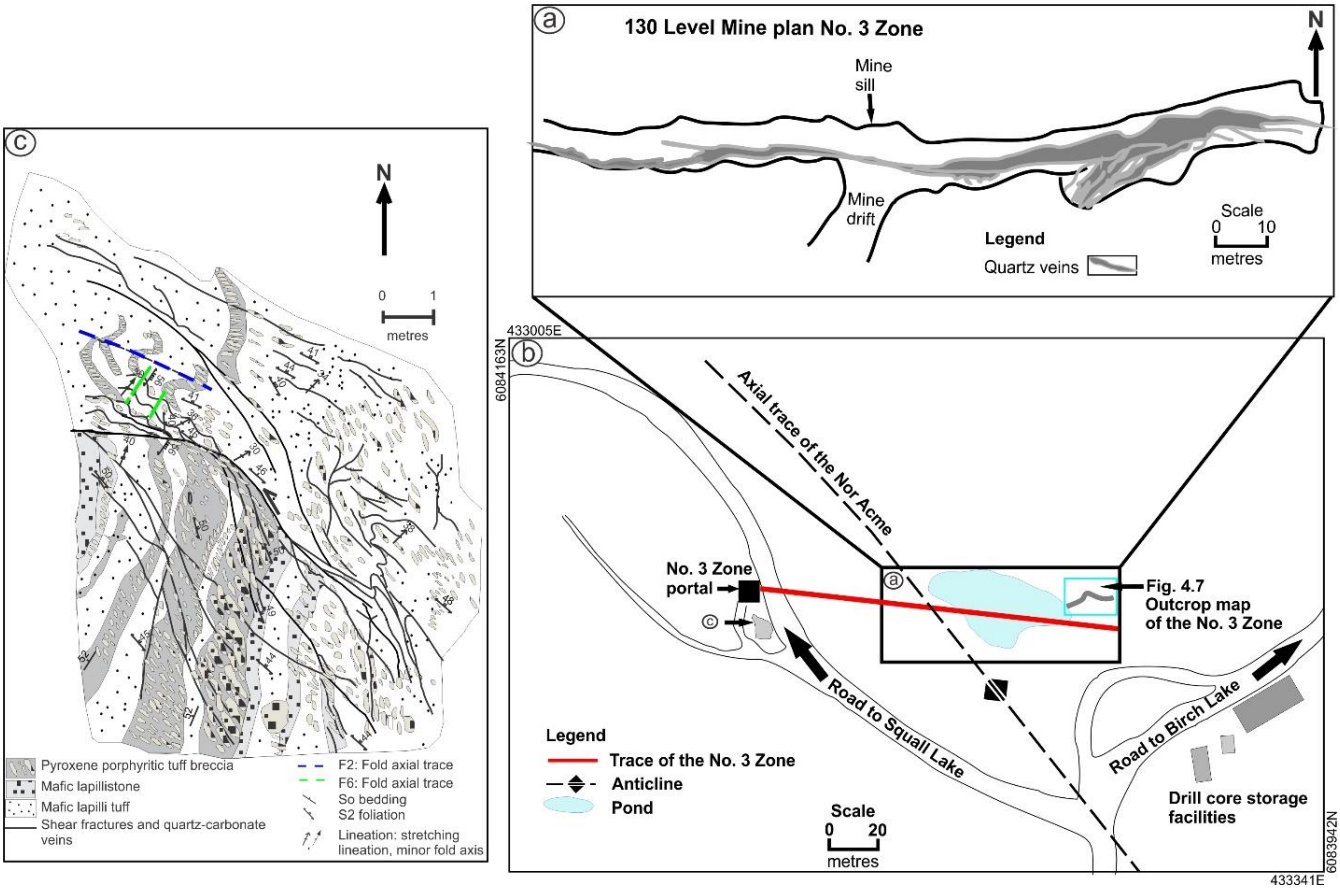

Figure 4.6: No. 3 Zone field relationships: a) Underground mine level plan of the No. 3 Zone (modified after Fieldhouse, 1999), b) Geographical location map showing location of (a) and (c) and Figure 4.7, c) No. 3 Zone field outcrop map in proximity to the No. 3 Zone portal to illustrate the relationship of bedding to the regional foliation on the west limb of the Nor Acme anticline. Unit 5 mafic volcaniclastic rocks of unit 5 consist of lapillituff, lapillistone and tuff breccia. They have a crystal-rich matrix of pyroxene and plagioclase surrounding monolithic fragments of similar mineralogy and composition.

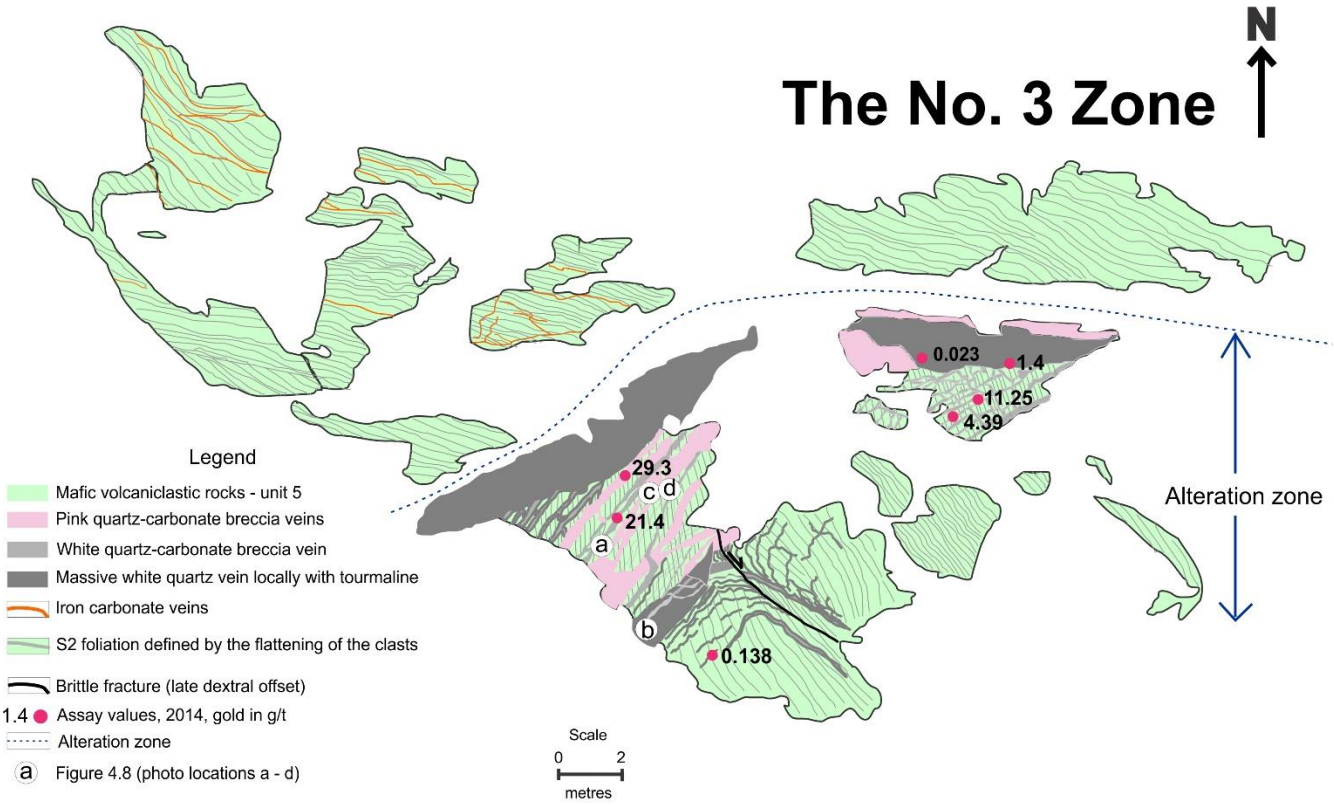

Figure 4.7. Outcrop map of the No. 3 Zone, illustrating the relationship between the S2 cleavage and folded quartz veins. Gold assay values in g/t.

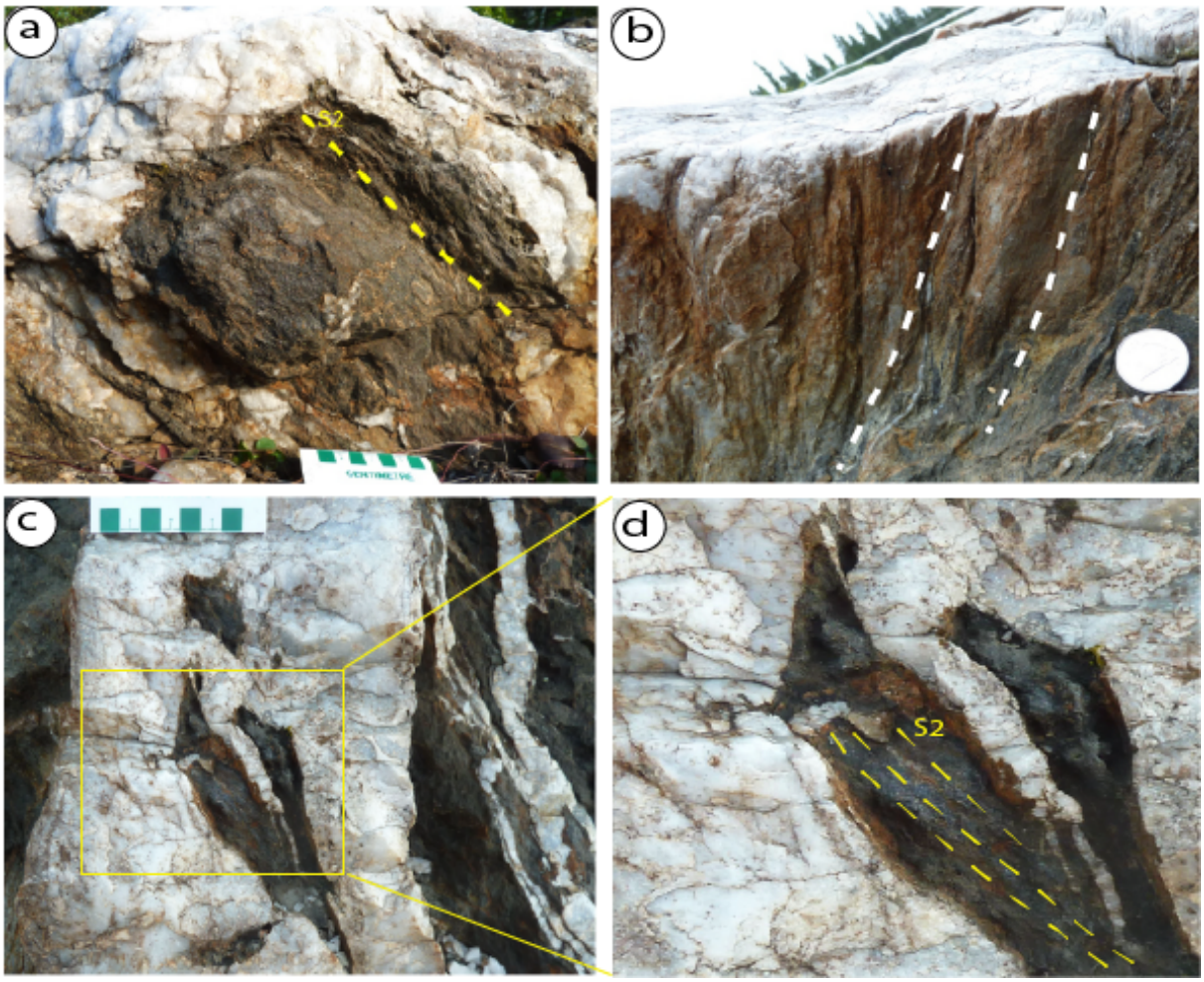

Figure 4.8. Field photographs of the No.3 Zone: a) S2 cleavage in altered mafic volcanic rock adjacent to vein. b) Stretching lineation expressed as a corrugation along the margin of vein. c) Foliated fragments of altered mafic volcanic rock in vein. d) Close up of foliated fragment in (c) showing small folded quartz vein with axial planar S2 cleavage. Note: S2 cleavage and L2 stretching lineation shown by broken yellow and white lines, respectively.

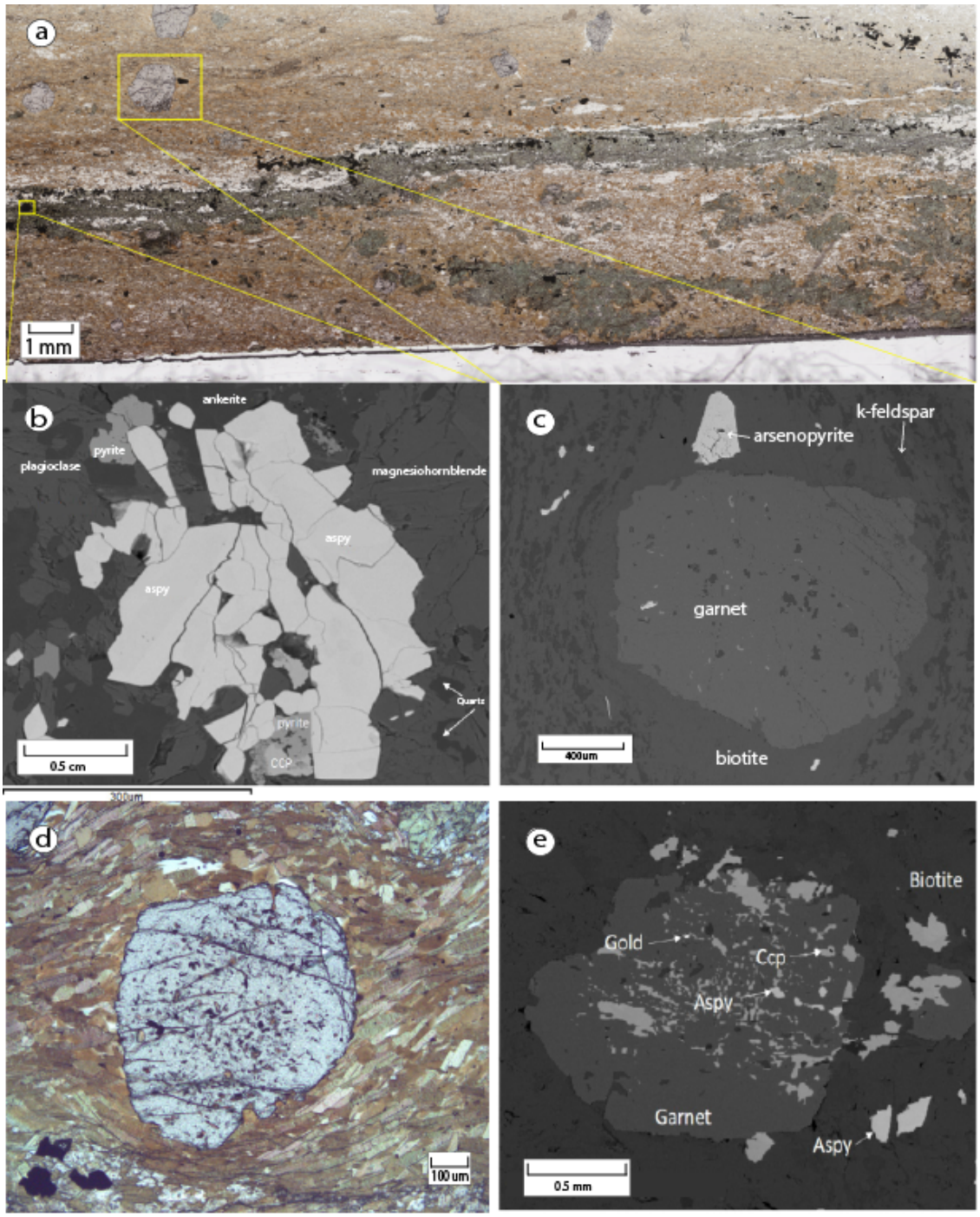

Figure 4.9. Photomicrographs and SEM images from the No. 3 Zone: a) Plane polarized light photomicrograph showing the strong amphibole and biotite S2 cleavage, and location of Figures 4.8b, and (c). b) SEM backscattered image showing aggregate of arsenopyrite with early pyrite and chalcopyrite surrounded by magnesiohornblende, ankerite and plagioclase. c) SEM backscattered image showing arsenopyrite in the strain shadow of garnet with inclusions of biotite and ilmenite. d) Plane polarized light photomicrograph of garnet porphyroblast surrounded by strong biotite S2 cleavage. e) SEM backscattered image of garnet porphyroblast with inclusions of arsenopyrite (Aspy), chalcopyrite (Ccp) and gold.

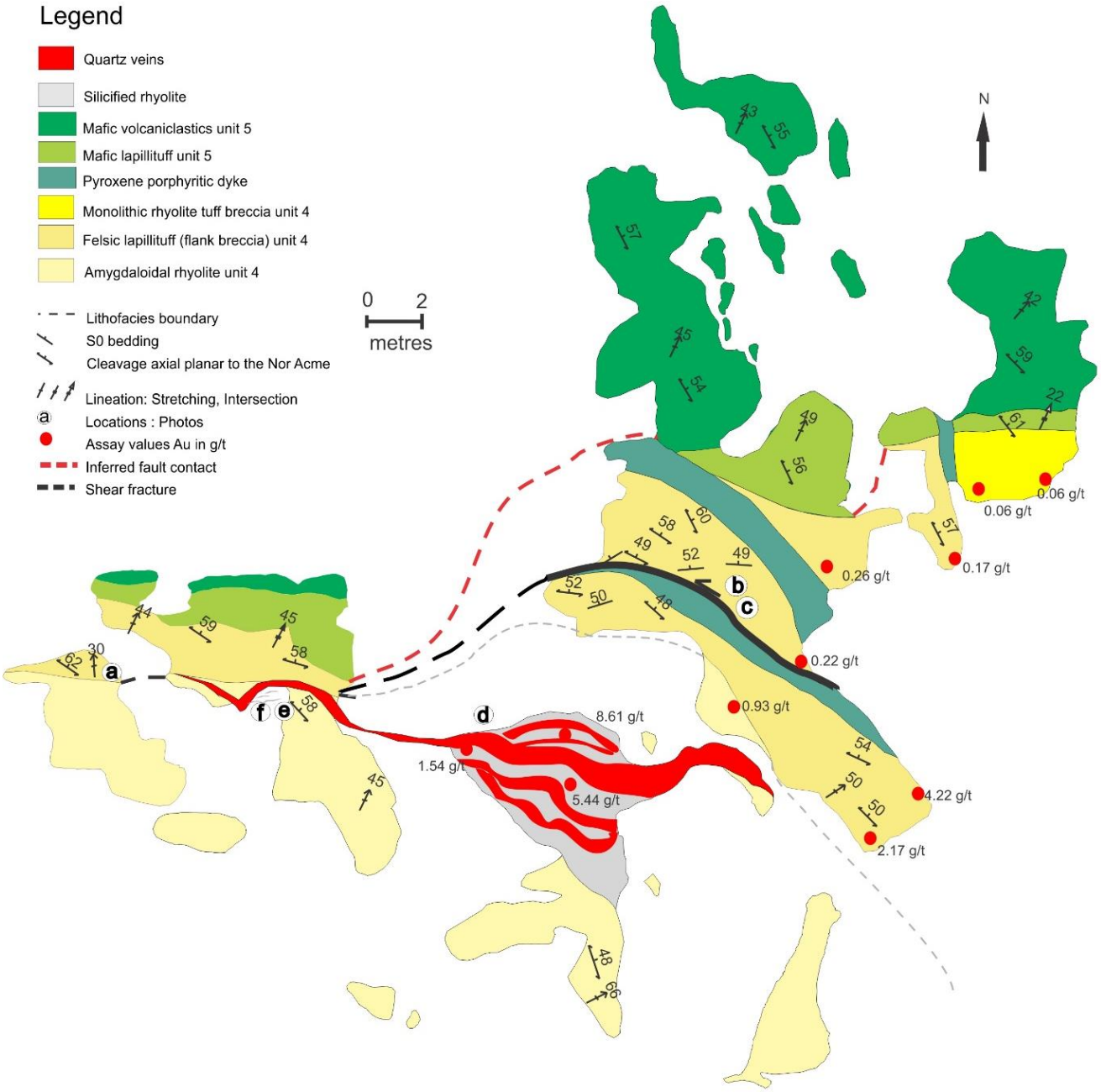

Figure 4.10. Outcrop map of the Boundary Zone, showing gold assay locations (red circle) and values in g/t. Letters a to f within white circles refer to locations of field photographs in Figure 4.11.

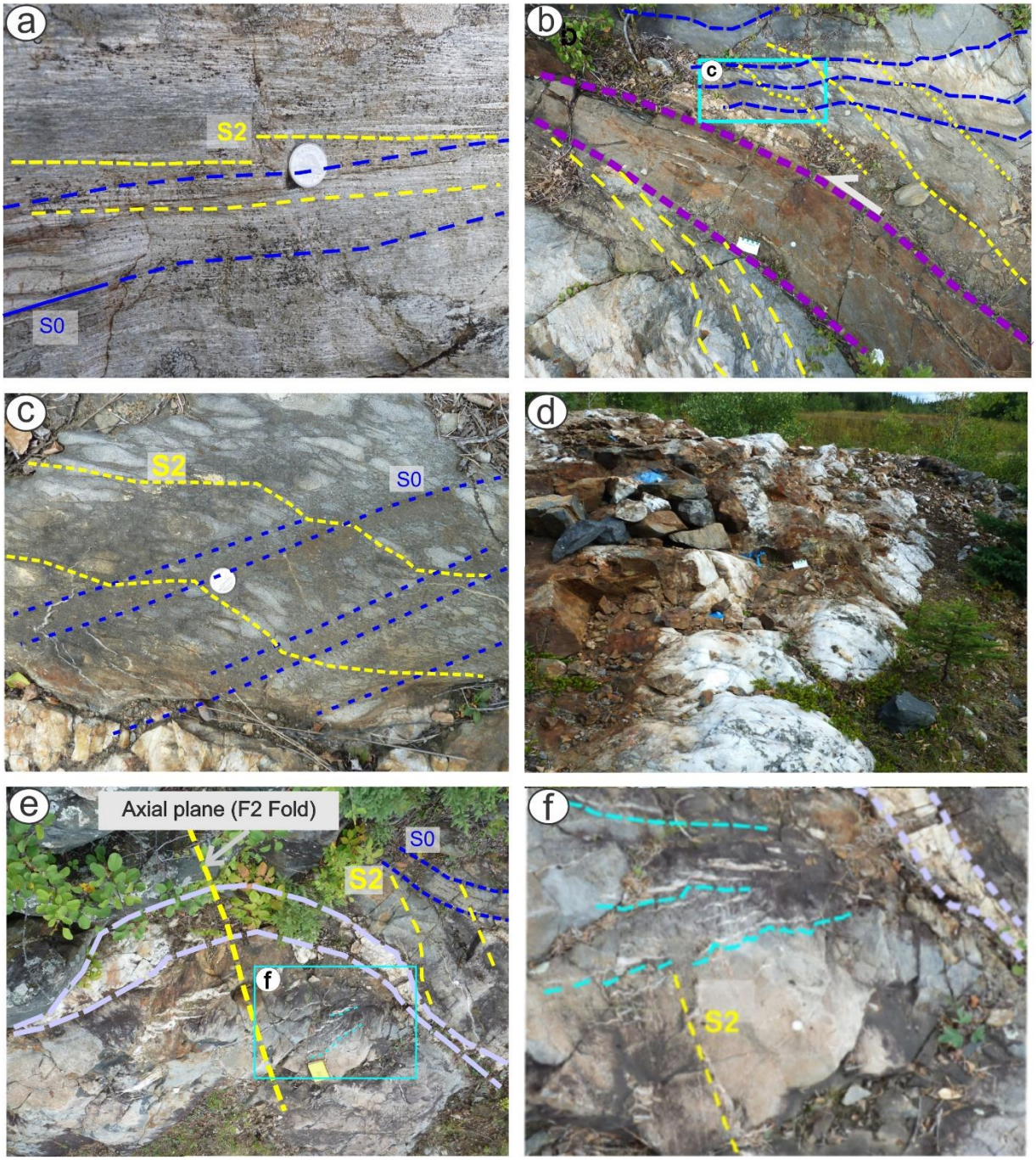

Figure 4.11. Field photographs from the Boundary Zone: (a) Strong S2 cleavage defined by flattening and transposition of clasts adjacent to massive felsic dome (20 mm diameter coin for scale). (b) Strong sinistral refraction of the S2 cleavage along mafic dyke and between felsic tuff and lapilli tuff beds (10 cm photo card for scale). (c) Close up of S2 cleavage refraction in felsic tuff and lapilli tuff beds (20 mm diameter coin for scale). (d) Thick, massive, white quartz vein in massive rhyolite flow (10 cm photo card for scale). (e) Folded quartz vein in massive rhyolite flow with axial plane S2 cleavage (19 cm tall notebook for scale). (f) Close up from Figure 4.11e of narrow, en echelon, extensional, white quartz veins oriented perpendicular to S2 cleavage in the hinge of folded thick quartz vein in massive rhyolite flow (20 mm coin for scale).

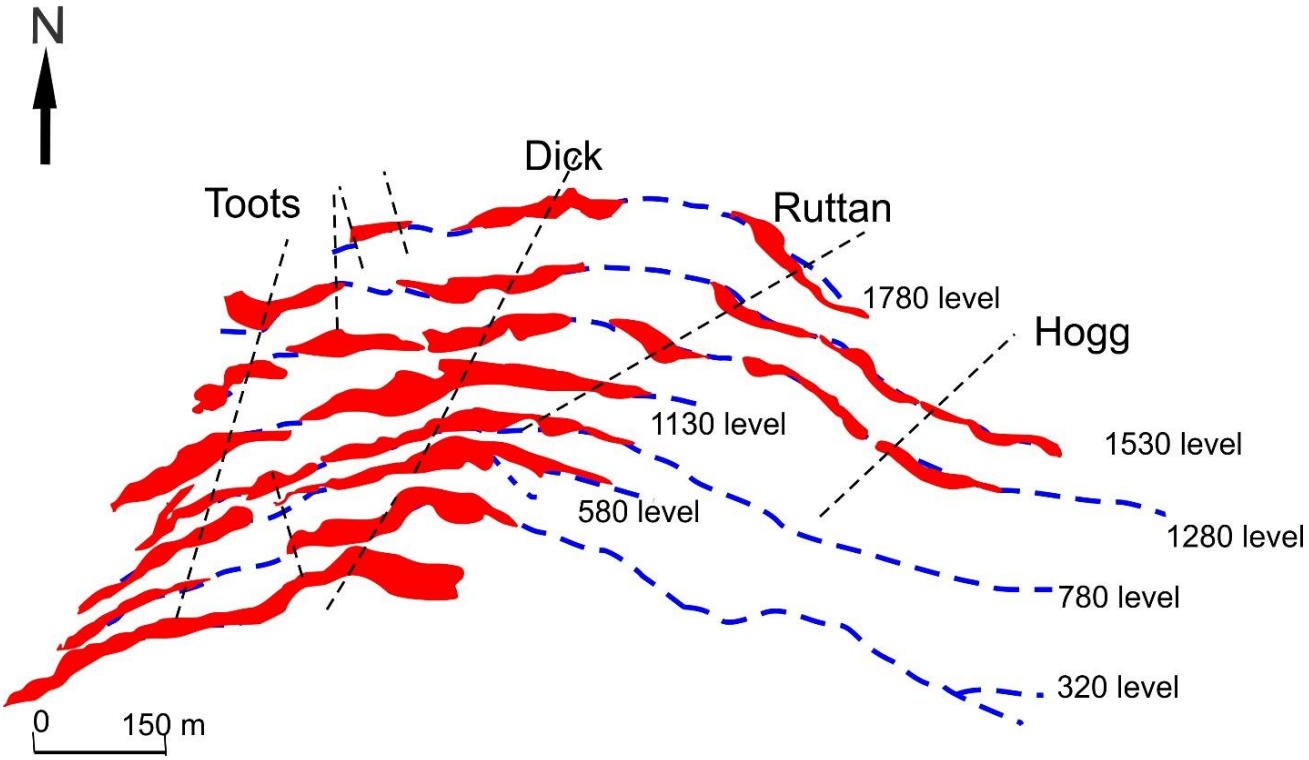

Figure 4.12. Down plunge projection of the ore zones at the New Britannia mine, showing the folded mineralization in red and previously interpreted trace of the Howe Sound fault in blue. Mine levels are in feet. Modified after Hogg (1957).

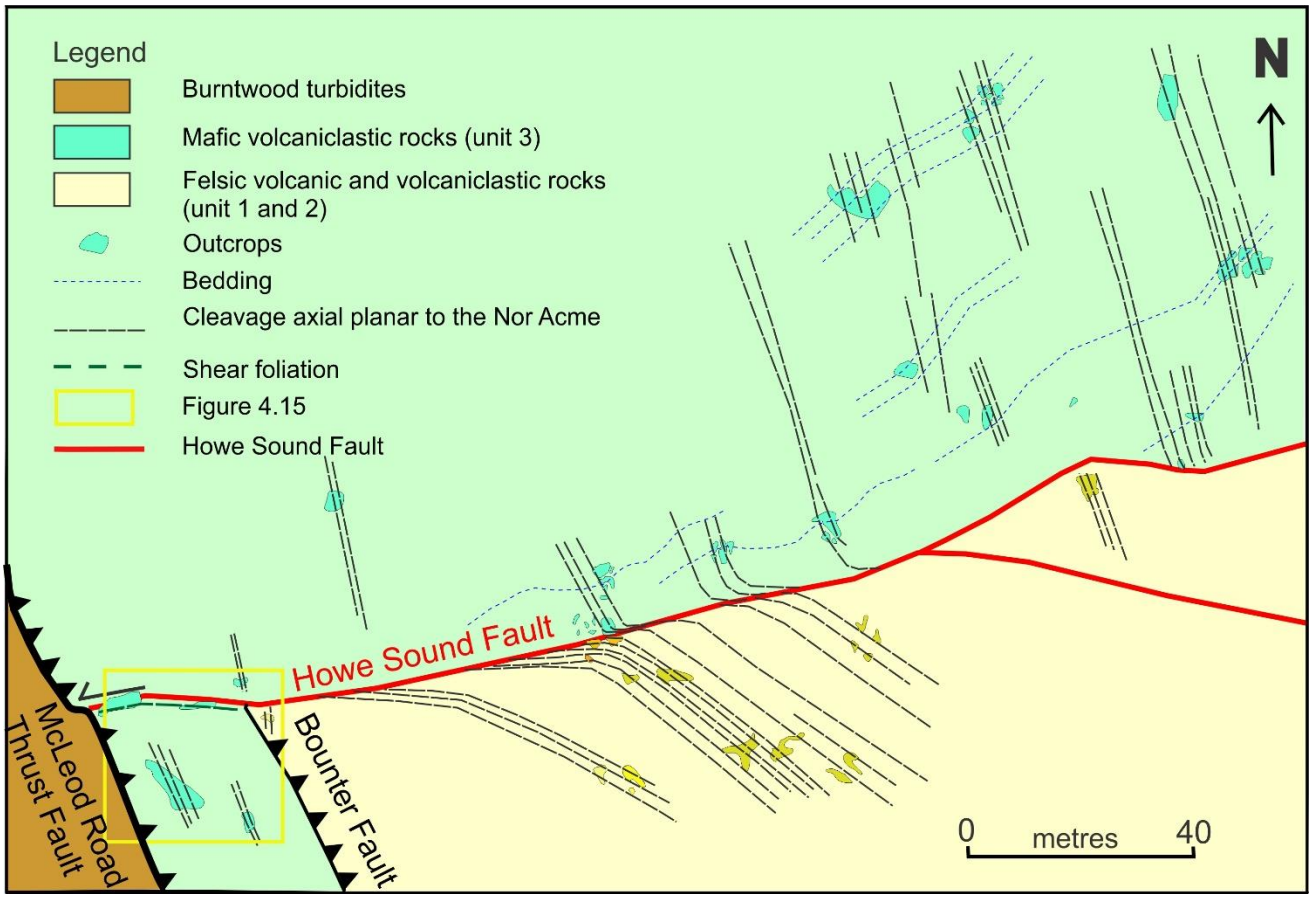

Figure 4.13. Simplified geologic map of the Howe Sound Fault. Note the location of the Bounter Fault at the contact between unit 3 and units 1 and 2 and its termination against the Howe Sound Fault, the dragging of the S2 cleavage along the Howe Sound Fault, and the offset of the McLeod Road Thrust by the Howe Sound Fault. Location Figure 4. 15 represented by yellow box.

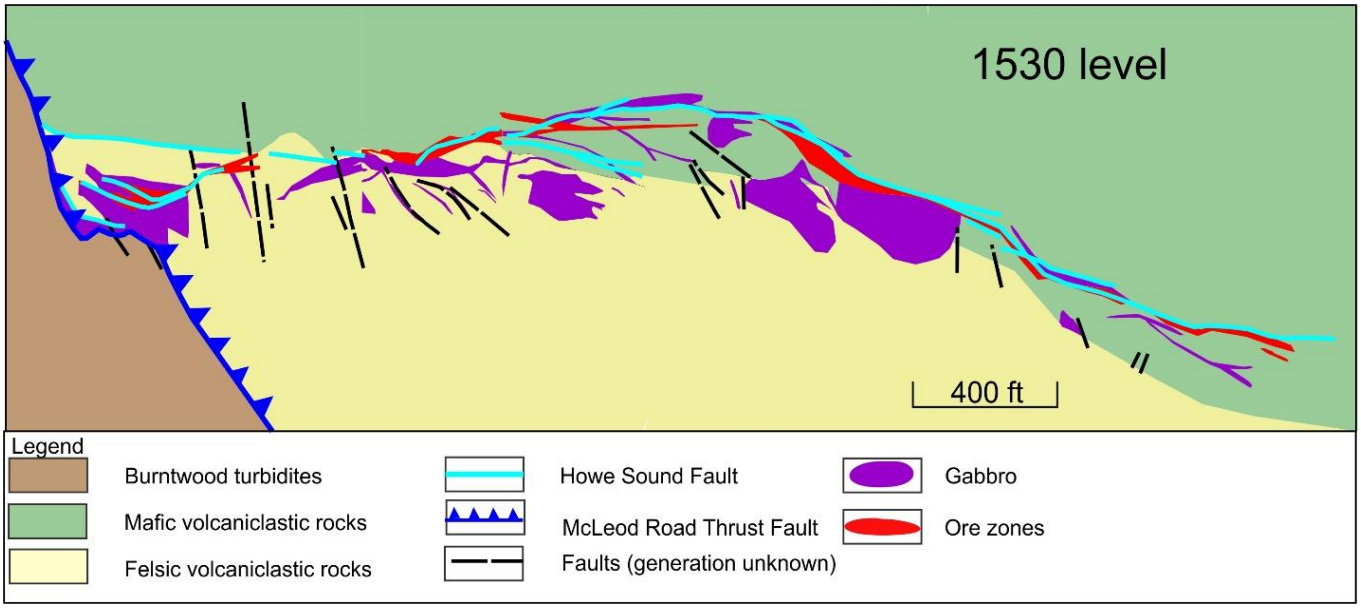

Figure 4.14. Underground geologic compilation map of the New Britannia Mine ore zones on the 1530 mine level (level plans are in feet). Map was compiled by Tom Fleming, who was the chief geologist when the mine was in production. Ore zones in red and trace of the Howe Sound fault in pale blue.

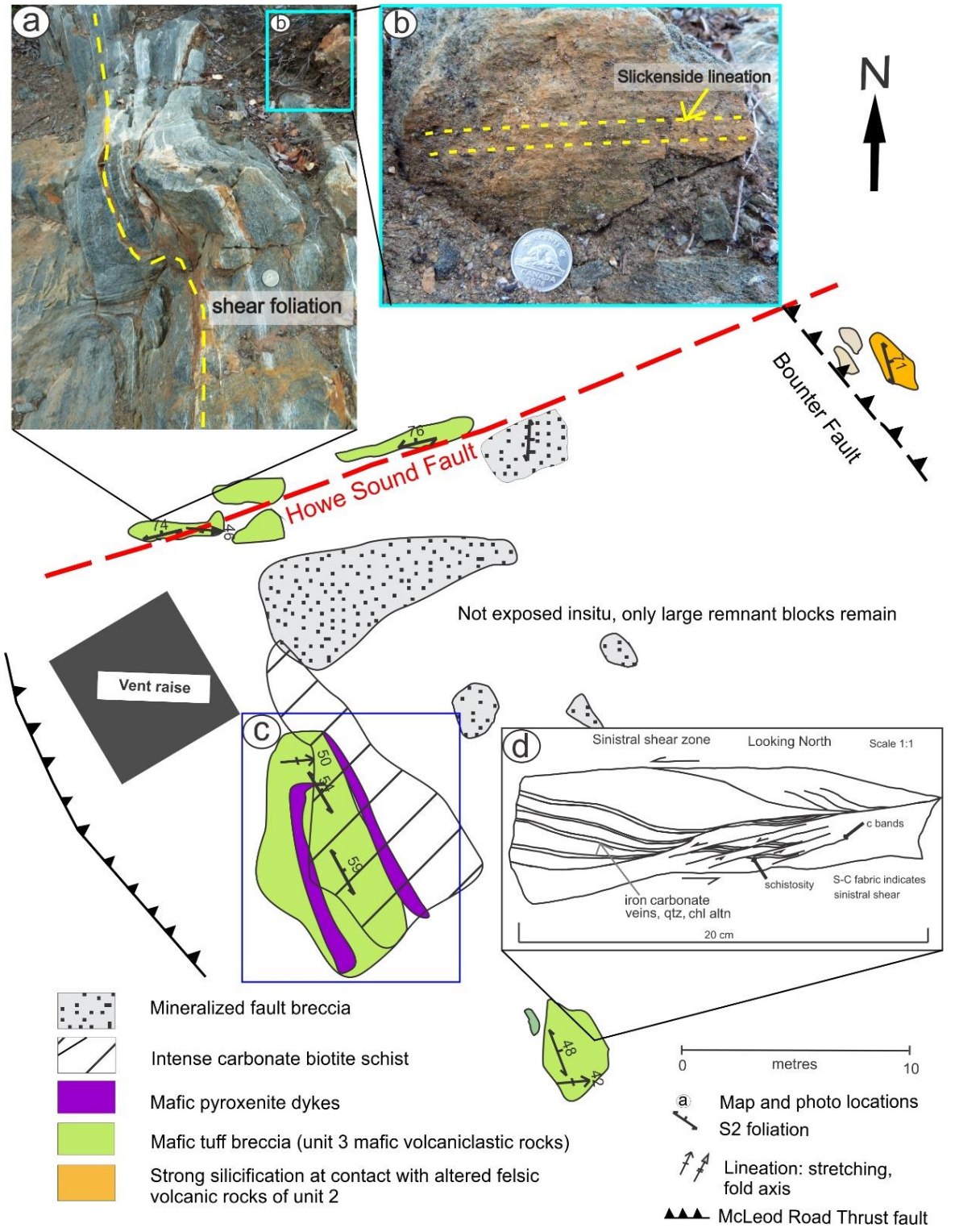

Figure 4.15. Simplified detailed surface map of the Toots zone; (a) Shear zone foliation and S-shaped drag fold along the Howe Sound fault. Coin (20 mm diameter) for scale. (b) Horizontal mineral lineation along the shear zone foliation. Coin (20 mm diameter) for scale. (c) Location of detailed map on Figure 4.16 (d) East-side-up sinistral S-C shear sense indicators in hanging wall of McLeod Road Thrust.

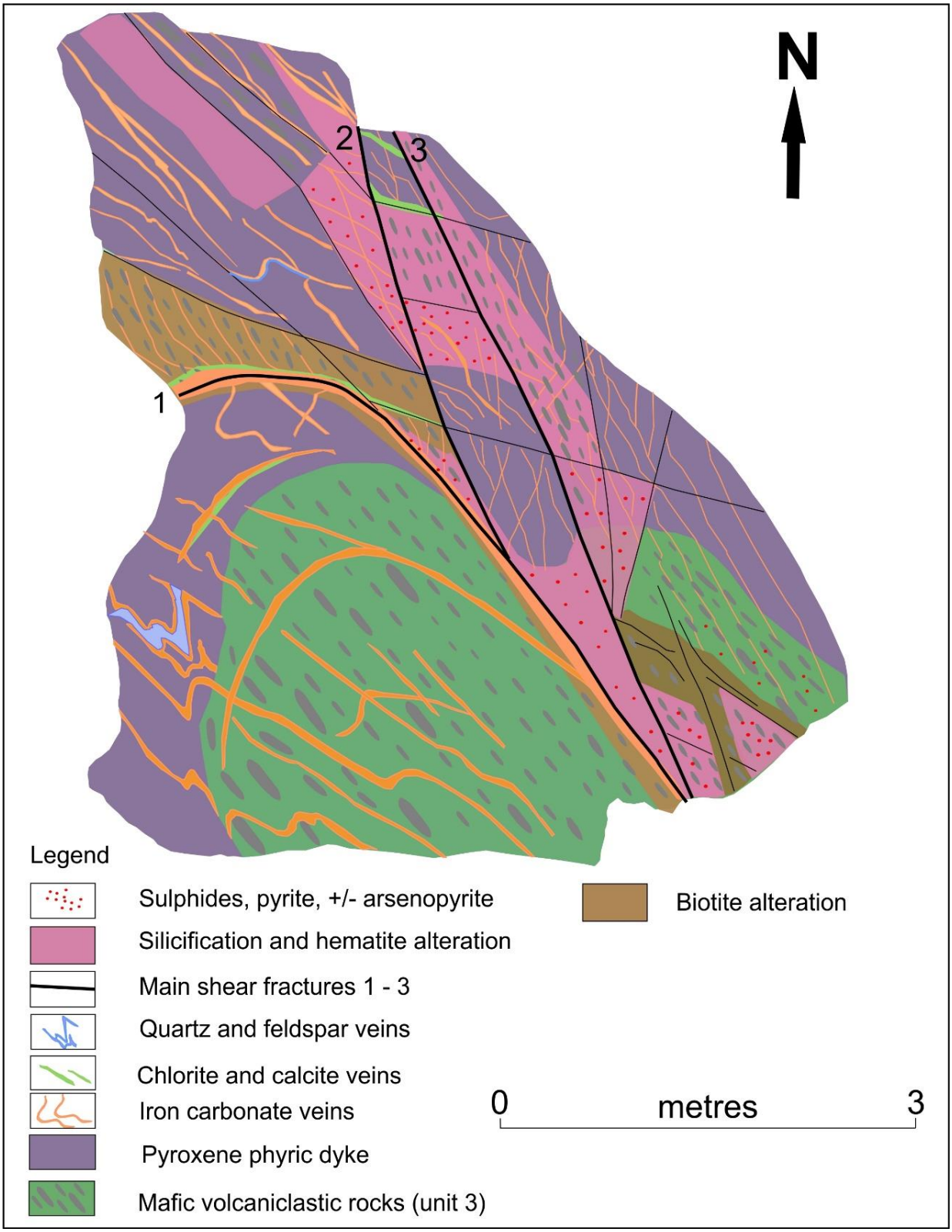

Figure 4.16. Alteration, structure and mineralization at the McLeod Road Thrust Fault.

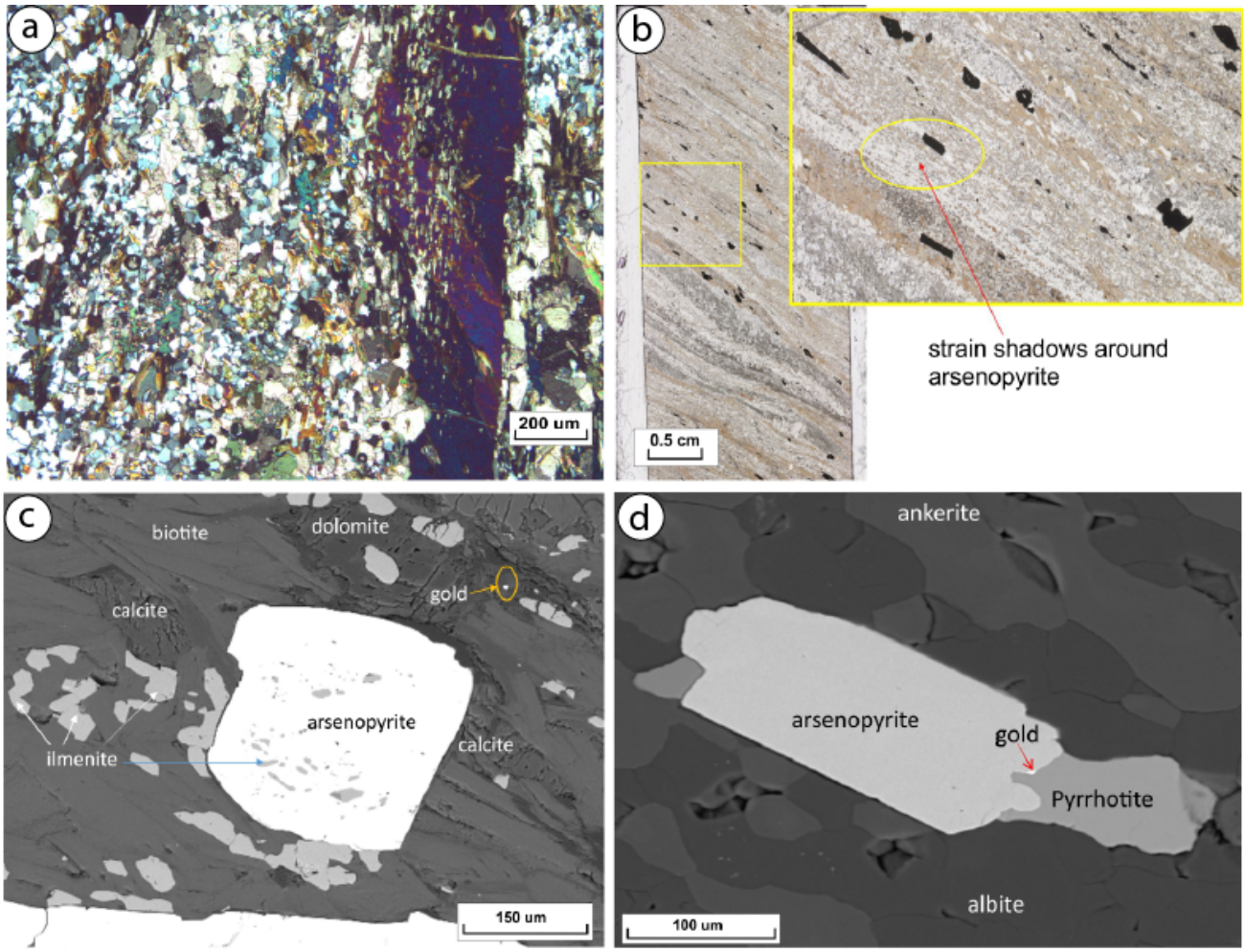

Figure 4.17. Photomicrographs and SEM images from the Ruttan zone, Mine East and Dick Zones of the New Britannia Mine. a) crossed polarized transmitted light photomicrograph of the inclusion trails in an amphibole porphyroblast. Both the inclusion trails and porphyroblast are parallel to the external S2 foliation, b) plane polarized transmitted light photomicrograph of thin section showing strongly deformed arsenopyrite parallel to the regional (S2) foliation with strain shadows around the deformed sulphides highlighted by the yellow circle, c) SEM backscattered image showing foliation defined by biotite with calcite in the strain shadows of an arsenopyrite grain and native gold, highlighted by the yellow circle, along silicate grain boundaries, d) SEM backscattered image of arsenopyrite and pyrrhotite with gold located at the sulphide grain boundary.

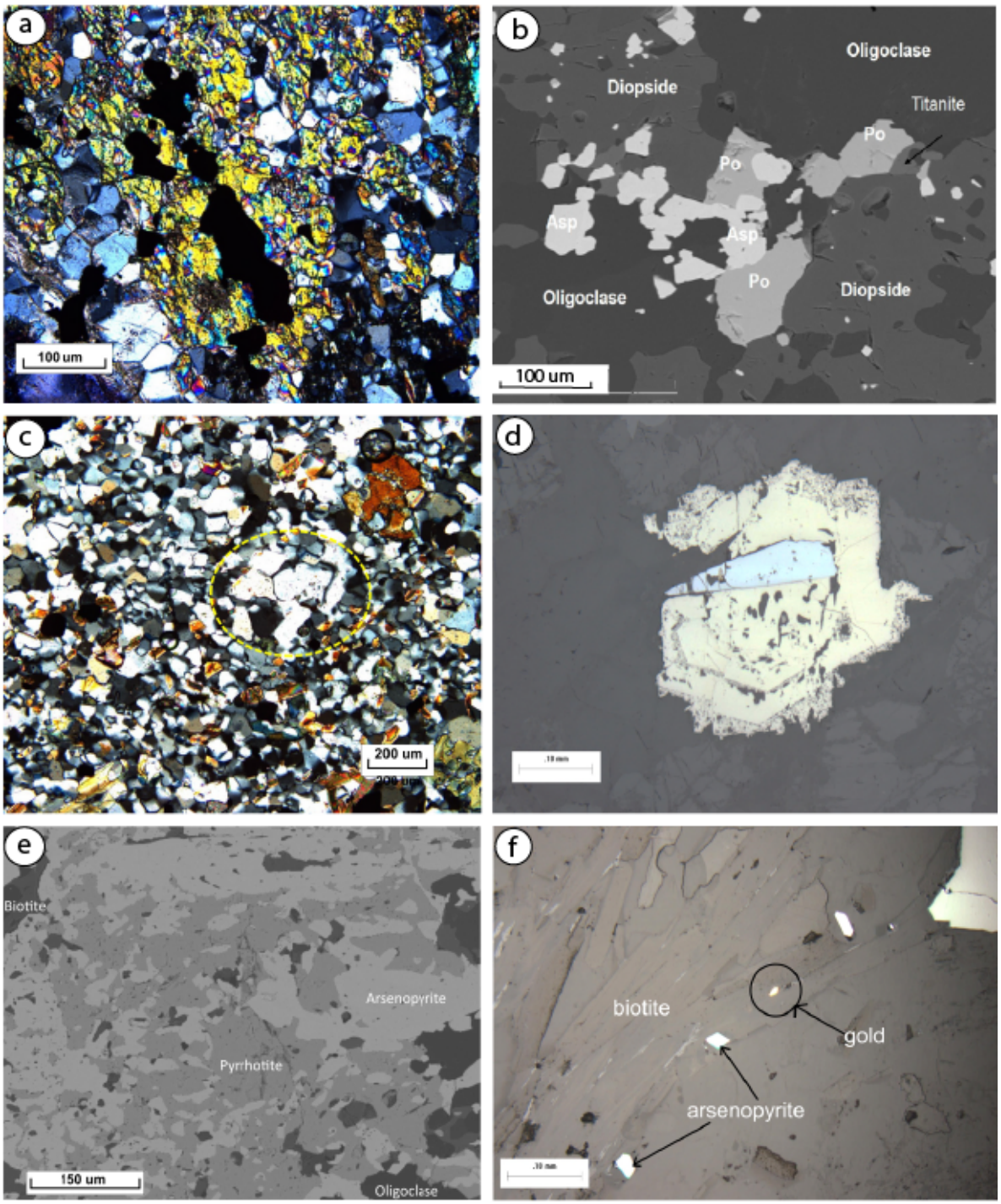

Figure 4.18. Photomicrographs and SEM backscattered images from the Toots Zone of the New Britannia Mine: a) crossed polarized transmitted light photomicrograph showing sulphides enclosed within clinopyroxene and amphiboles, b) SEM backscattered image illustrating arsenopyrite enclosed within diopside, c) crossed polarized transmitted light photomicrograph showing strongly recrystallized plagioclase grains, dashed yellow line, along the Howe Sound Fault, d) reflected light photomicrograph showing oscillatory zoned pyrite being replaced by arsenopyrite, e) SEM backscattered image of intergrown arsenopyrite and pyrrhotite, f) reflected light photomicrograph showing native gold and arsenopyrite along biotite grain boundaries.

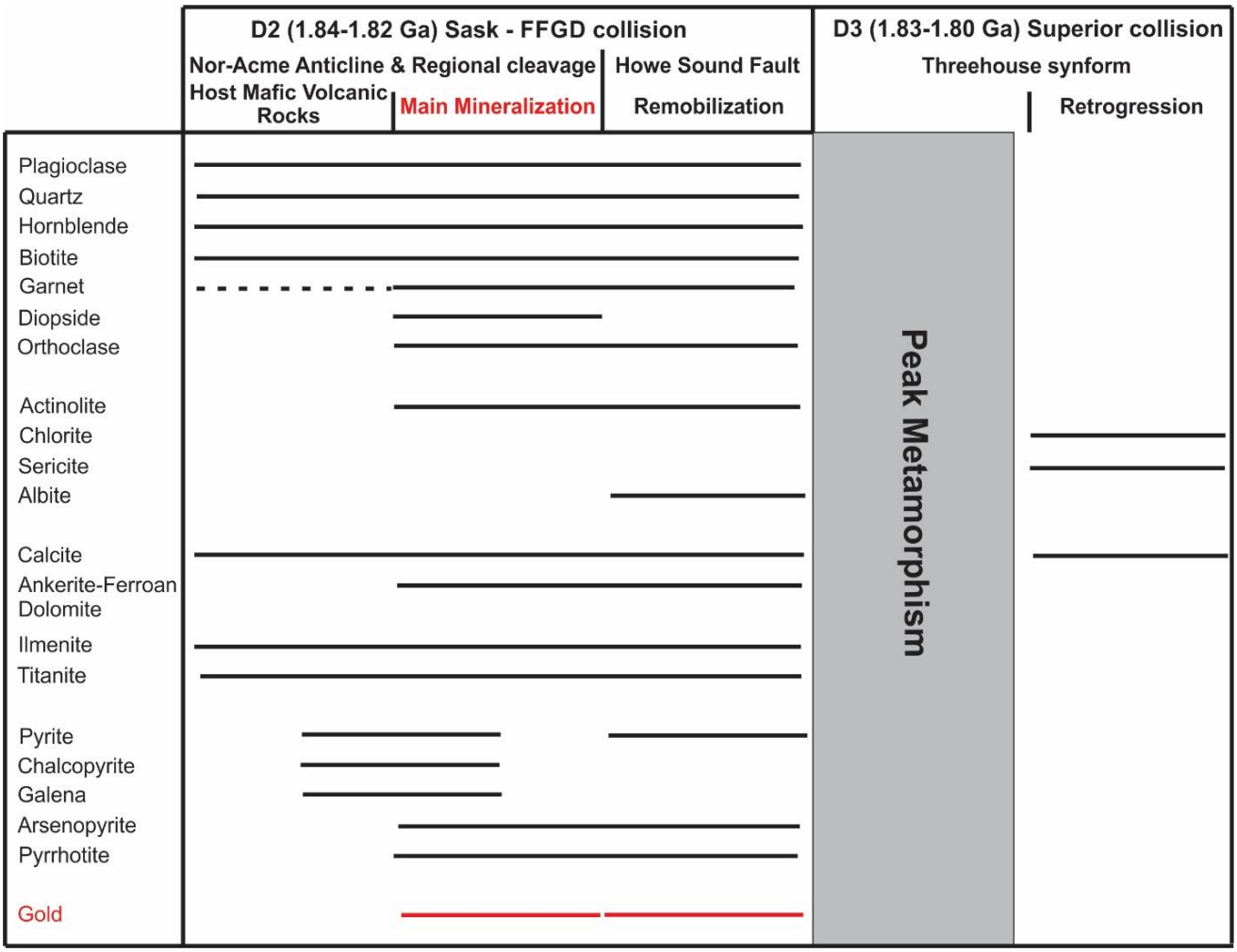

Figure 4.19: Paragenesis table of the minerals present in the host mafic volcaniclastic rocks and mineralized zones relative to deformation events and peak metamorphism.

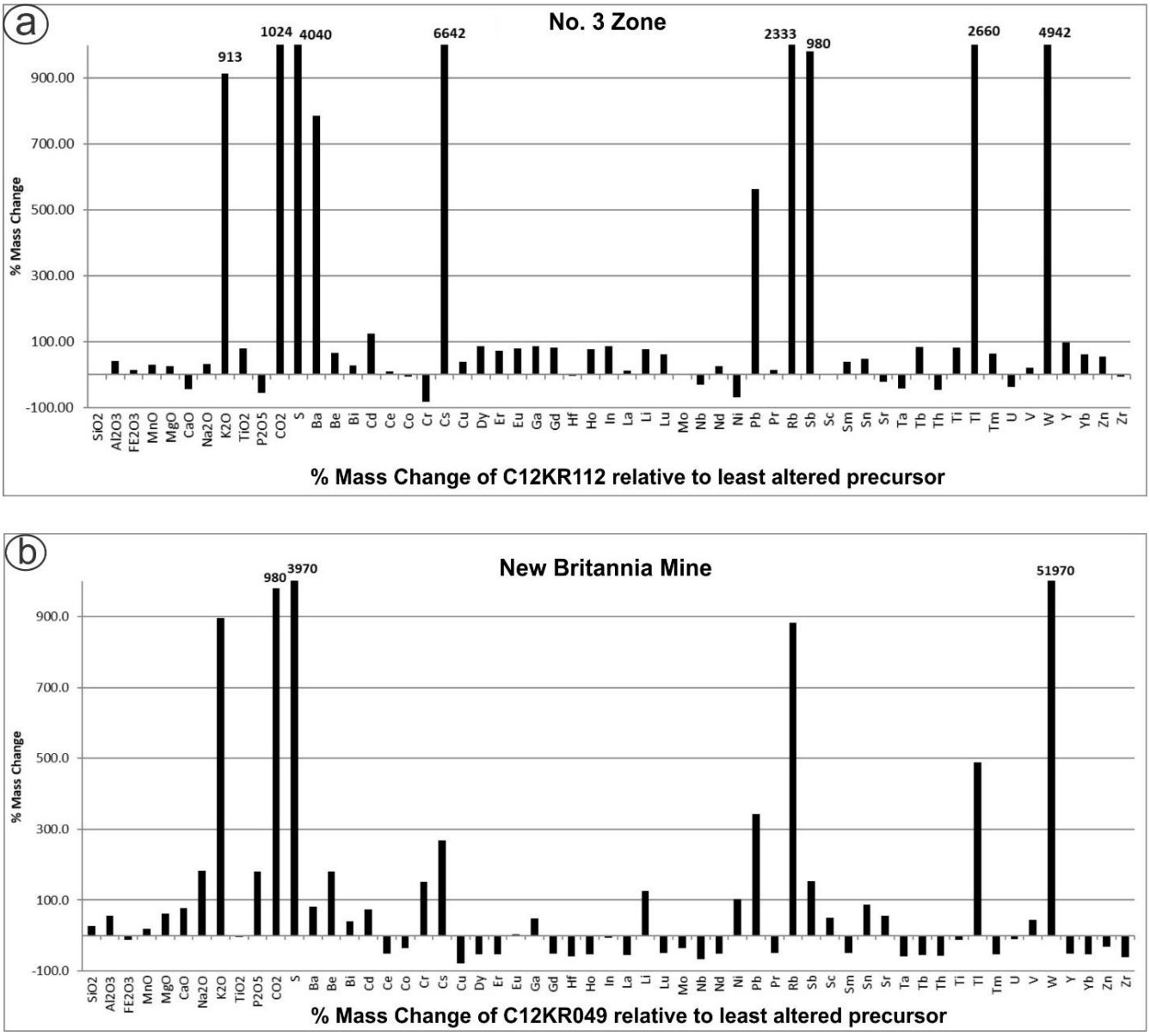

Figure 4.20: Mass change histograms: a) No. 3 Zone mineralized mafic volcaniclastic rocks (C12KR112) relative to least altered precursor (KR11037). (b) New Britannia mine, mineralized mafic volcaniclastic rocks (C12KR049) relative to least altered precursor – (12KR080A01).

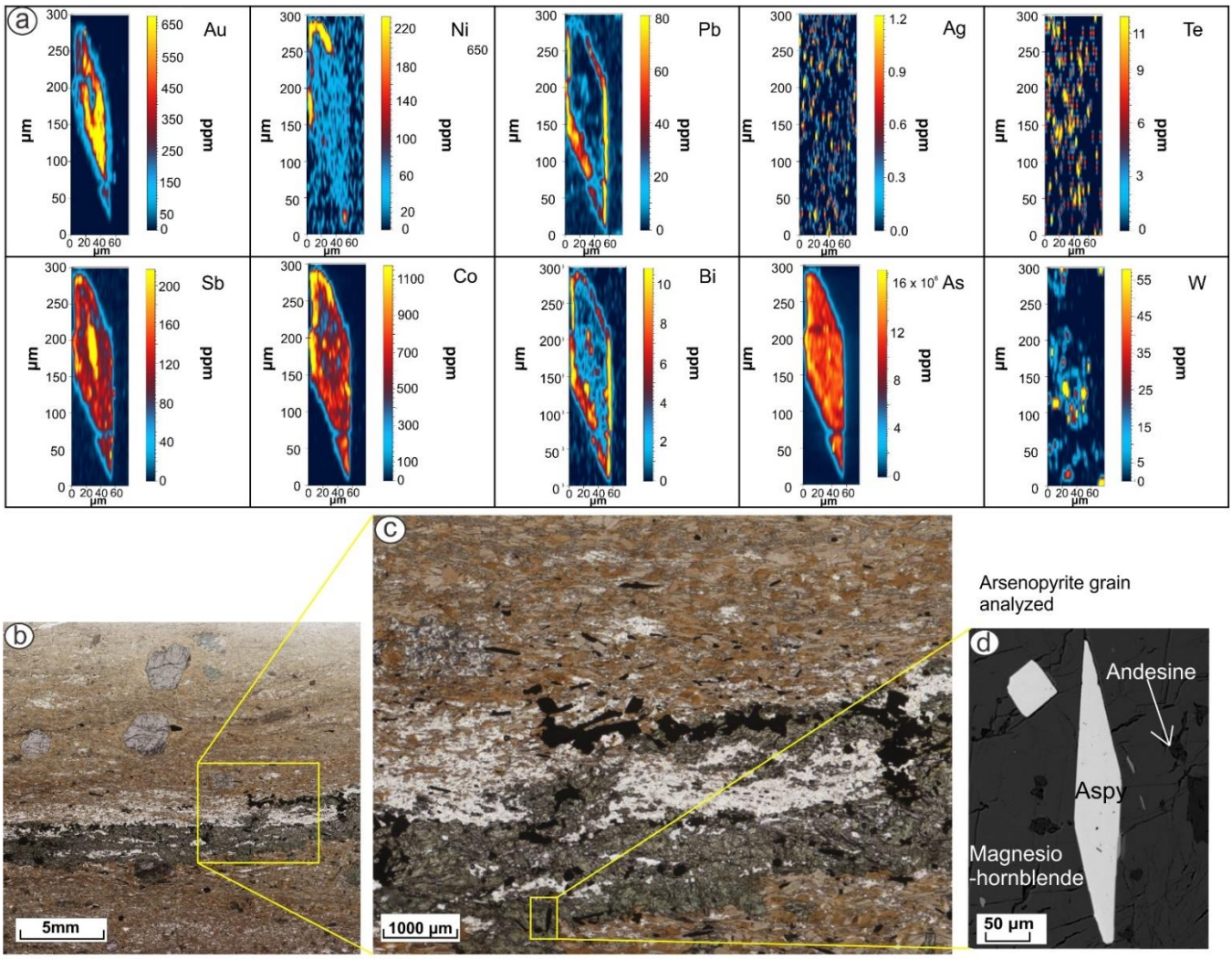

Figure 4.21: LA-ICP-MS map and photomicrographs from the No. 3 Zone, a) The No.3 Zone LA-ICP-MS element maps of an arsenopyrite grain, with concentrations in ppm, b) – c) plane polarized transmitted light photomicrograph to show the location of the arsenopyrite grain, d) SEM backscattered image of mapped arsenopyrite grain.

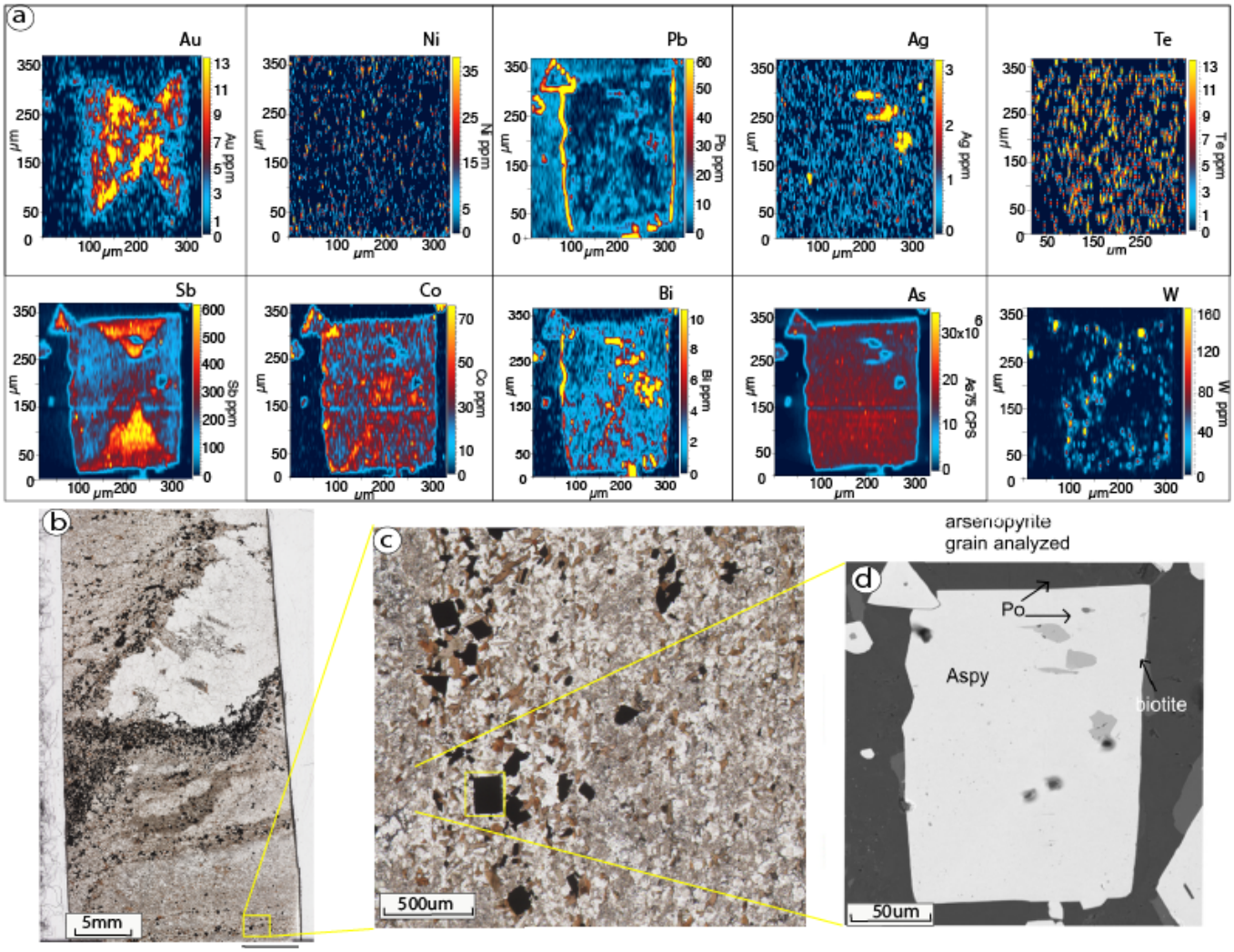

Figure 4.22: LA-ICP-MS maps amd photomicrographs for the Boundary Zone. a) The Boundary Zone LA-ICP-MS element maps of an arsenopyrite grain, with concentrations in ppm, b) – c) plane polarized transmitted light photomicrograph to show the location of the arsenopyrite grain, d) SEM backscattered image of mapped arsenopyrite grain.

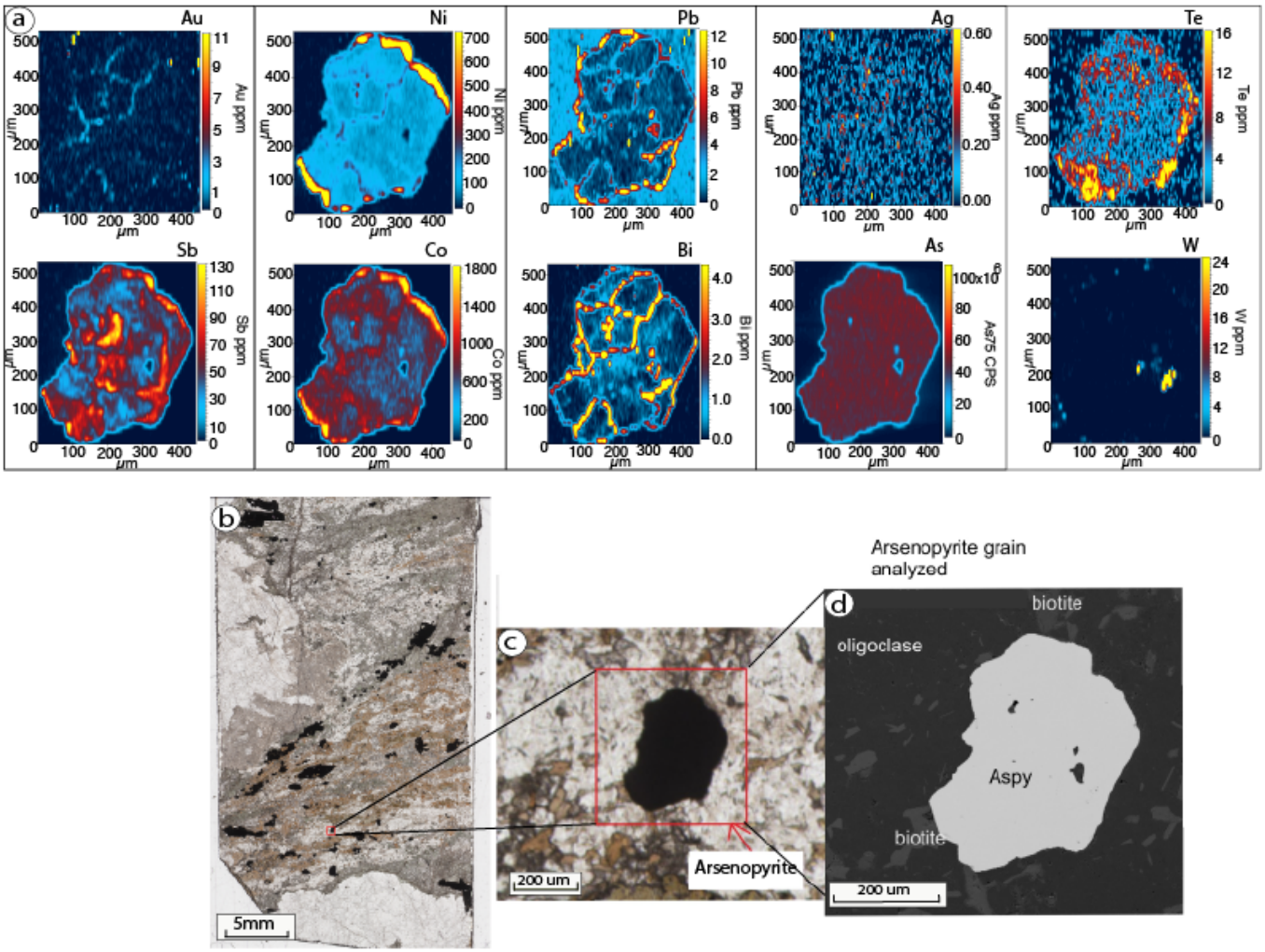

Figure 4.23: LA-ICP-MS element map and photomicrographs for the Dick Zone representing the New Britannia Mine mineralized zone. a) The Dick Zone LA-ICP-MS element maps of an arsenopyrite grain, with concentrations in ppm, b) – c) plane polarized transmitted light photomicrograph to show the location of the arsenopyrite grain, d) SEM backscattered image of mapped arsenopyrite grain.

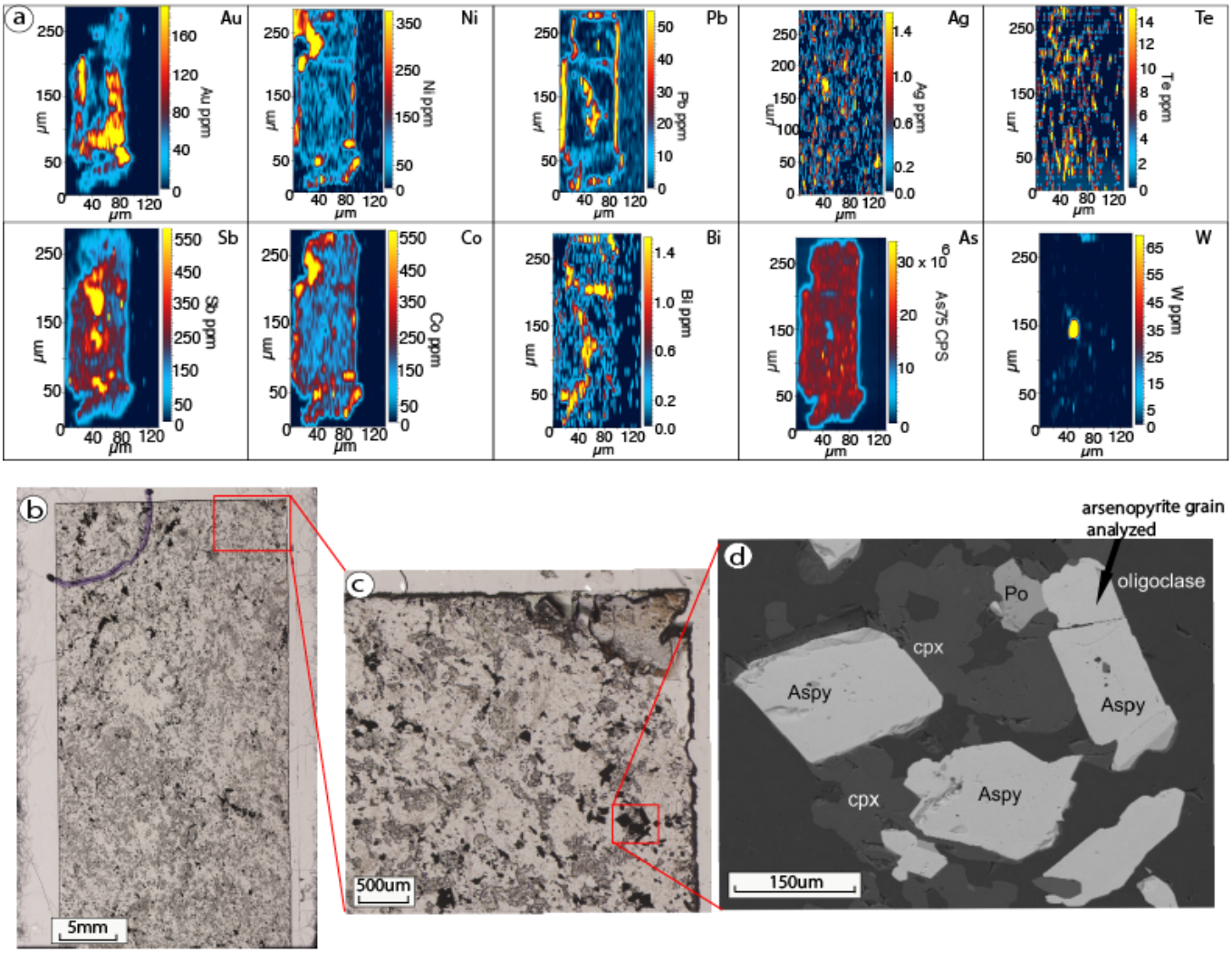

Figure 4.24: LA-ICP-MS element maps and photomicrographs for the Toots Zone, a) The Toots Zone LA-ICP-MS element maps of an arsenopyrite grain, with concentrations in ppm, b) – c) plane polarized transmitted light photomicrograph to show the location of the arsenopyrite grain, d) SEM backscattered image of mapped arsenopyrite grain.

Chapter 5

Conclusions

5.1. Summary

The New Britannia Mine, is the most important past-producing gold mine of the southeastern Trans Hudson Orogen. The sequence of depositional, structural and mineralizations events leading to the formation of the deposit are summarized in Figure 5.1. The deposit is located within the McLeod Road Birch Lake (MB) sequence (Rubingh et al., 2017) of the Paleoproterozoic Snow Lake arc (SLA) assemblage (Bailes and Schledewitz, 1998; Bailes and Galley, 1999). The SLA formed as part of a larger oceanic microcontinent, the Flin Flon Glennie Complex (FFGC) which amalgamated at ca. 1.88 – 1.87 Ga (Lucas et al., 1996). The FFGC lies within the internal juvenile zone of the Trans Hudson Orogen and is structurally juxtaposed to the younger Kisseynew basin to the north, the La Ronge – Lynn Lake greenstone belt to the west, the Archean Superior craton to the east, and is underlain by the Archean Sask micro craton.

A new stratigraphy is proposed for the volcanic rocks of the MB sequence, which correlates with volcanic strata of the Chisel Lake and Snow Creek sequences to the south. It includes a significantly greater volume of submarine pyroclastic flow deposits than previously recognized across the SLA. These pyroclastic units were deposited in a single basin or series of nested basins during initial arc rifting and subsidence of the SLA. This explosive volcanic episode was shortly followed by the deposition of the VMS deposits of the Chisel sequence, which have yet to be found in the MB sequence.

The new proposed stratigraphy revealed repetitions in MB volcanics units across hitherto

unrecognized metamorphosed brittle thrust faults. These faults formed during a D1 event, which occurred after the deposition of ca. 1.855 – 1.84 Ga Burntwood turbidites in the Kisseynew basin and before the formation of ductile fabrics at < ca. 1.845 – 1.835 Ga. These early D1 thrust fault either formed during collision of the Sask craton with the Kisseynew basin and FFGC, or during accretion of the SLA to the FFGC.

The early brittle thrust faults established the boundary conditions that facilitated southwest-directed ductile thrusting during overthrusting of the Kisseynew basin and FFGC above the colliding Sask micro craton during the ca. 1.84 Ga – ca. 1.82 Ga D2 deformation event. The D2 event began with the formation of a regional foliation axial planar to map-scale isoclinal folds and culminated with the formation of sheath-like gneiss domes along the Kisseynew-FFGC boundary and regional ductile thrust faults, such as the McLeod Road Thrust and the Snow Lake fault. The McLeod Road Thrust is shouldered by metamorphosed alteration assemblages similar to those observed in the damage zones of the early D1 thrust faults and thus initially formed as a brittle thrust fault. Correlation of stratigraphy across the SLA assemblage from the Snow Lake area (MB sliver) to the Chisel basin area suggest that major thrust faults, such as the McLeod Road Thrust (MRT) fault and the Snow Lake fault, may have less regional significance and displacements than previously thought.

D3 collision between the eastern Flin Flon Glennie Complex and Superior craton began at ca. 1.83-1.80 Ga during continued southwest-directed thrusting of the Kisseynew and FFGC over the Sask craton. This northwest-directed collisional event reactivated the ductile thrust faults as sinistral and dextral shear zones, produced NE-trending folds overprinting the sheath-like gneiss

domes, and enabled the Kisseynew and FFGC to flow laterally parallel to the cold Archean Superior craton, thus accentuating the development of an orogen-parallel regional stretching lineation that initially formed during southwest-directed D2 thrusting.

The New Britannia Mine and associated gold deposits were emplaced in the hinge of an isoclinal fold, the Nor-Acme Anticline, early during the D2 event. The ore zones were folded during tightening of the fold, and ore zones at the New Britannia Mine were transposed together with gold-bearing quartz-carbonate veins into the Howe Sound fault, a transfer fault which cuts across the hinge of the Nor-Acme Anticline and offsets the McLeod Road Thrust. The plunge of the ore bodies and folds in the SLA assemblage consistently plunge to the NE parallel to the tectonic transport direction represented by the regional stretching lineation.

The New Britannia Mine and associated gold deposits formed at amphibolite facies conditions early during the Trans-Hudson Orogen. They formed prior to the peak of a prograde metamorphic event and thus their formation includes elements of both metamorphic and continuum models for the formation of orogenic gold deposits. Other gold deposits across the Trans Hudson Orogen, with the sole exception of the Puffy Lake gold deposit (Gagne et al., 2006), are conspicuously different from the New Britannia mine deposits. Unlike the New Britannia mine deposits, they are associated with syn- to post-peak metamorphic, transcurrent, transpressional, or oblique-slip fault zones, which formed late during the Trans Hudson Orogeny (Schultz, 1990, 1996; Fedorowich et al., 1991; Tourigny, 2003; Jones et al, 2006; Lafrance and Heaman, 2004; Wood, 2016).

5.2. Future Work and Outstanding Problems

The goal of this thesis was to present a comprehensive study of the stratigraphy and structural history of the rocks hosting the New Britannia Mine and nearby deposits and to explore how these gold deposits formed within this framework. As the deposits formed at amphibolite facies conditions, it also provided an opportunity to contribute to the continuum versus metamorphic debate on the formation of orogenic gold deposits.

Further insights would result from a study of the Bounter gold occurrence, which is located along the early brittle Bounter thrust fault. Galley et al. (1986) correlated the style of gold mineralization at the Bounter occurrence with that of New Britannia Mine. Yet, it may have formed earlier and may represent an early mineralizing event that was coeval with greenschist facies metamorphism.

The absolute timing of gold mineralization has not been determined. Thus, U-Pb dating of accessory minerals (titanite and rutile) associated with gold mineralization at the New Britannia main mine ore bodies (Toots, Dick, Ruttan and Mine East) could provide further constraints on the formation of the deposits.

Finally, published metamorphic temperatures and pressures in the Snow Lake area are from studies on pelite (Froese and Moore, 1980; Kraus and Menard, 1997) and metamorphosed argillic alteration envelopes of VMS deposits (Zaleski et al., 1991; Menard and Gordon, 1997). Recent advances in thermodynamic models for the formation of metamorphic minerals in mafic volcanic rocks would provide better constraints on the metamorphic history of the volcanic rocks

hosting the deposits.

5.3 Implications for Mineral Exploration

The research has highlighted the importance of early regional structures, such as the Nor Acme anticline, as hosts for gold mineralization in the Trans Hudson Orogen, as well as the modification and beneficiation of the ore zones during later shearing and peak metamorphism. Shearing of the ore zones along the Howe Sound fault and their recrystallization during peak metamorphism liberated gold from refractory arsenopyrite and remobilized it as free gold, thereby facilitating its extraction during metallurgical processes. These early structures are important targets for regional gold exploration which have in the past focussed on late transpressional shear zones and retrograde faults.

5.4. References

Bailes, A.H. and Galley, A.G. 1999: Evolution of the Paleoproterozoic Snow Lake arc assemblage and geodynamic setting for associated volcanic-hosted massive sulphide deposits, Flin Flon Belt, Manitoba, Canada; Canadian Journal of Earth Sciences, v. 36, p. 1789–1805.

Bailes, A.H. and Schledewitz, D.C.P. 1998: Geology and geochemistry of the Paleoproterozoic volcanic rocks between the McLeod Road and Birch Lake faults, Snow Lake area, Flin Flon belt (parts of NTS 63K/16 and 63J/13); in Report of Activities 1998, Manitoba Energy and Mines, Geological Services, p. 4–13.

Froese, E. and Moore, J.M. 1980. Metamorphism in the Snow Lake area, Manitoba; Geological Survey of Canada, Paper 78-27, 16 p.

Gagné, S., Beaumont-Smith, C.J., William-Jones, A.E., Hynes, A. 2006: Metallogenic and metamorphic study of selected deposits from the Snow Lake area and the southern flank of the Kisseynew Domain, Manitoba (NTS 63K16 and 63N2); in Report of Activities 2006, Manitoba Science, Technology, Energy and Mines, Manitoba Geological Survey, p. 42–48.

Galley, A.G., Ziehlke, D.V., Franklin, J.M., Ames, D.E. and Gordon, T.M. 1986: Gold mineralization in the Snow Lake–Wekusko Lake region, Manitoba; in Gold in the Western Shield, A.L. Clark (ed.), Canadian Institute of Mining and Metallurgy, Special Volume 38, p. 379–398.

Jones, L.R., Lafrance, B. and Beaumont-Smith, C.J. 2006. Structural Controls on Gold Mineralization at the Burnt Timber Mine, Lynn Lake Greenstone Belt, Trans-Hudson Orogen, Manitoba, in Exploration and Mining Geology, Vol. 15, pp.89-100.

Kraus, J., Menard, T., 1997. A thermal gradient at constant pressure: implications for low- to medium-pressure metamorphism in a compressional tectonic setting, Flin Flon and Kisseynew domains, Trans-Hudson Orogen, central Canada. The Canadian Mineralogist 35, 1117–1136.

Lafrance, B., and Heaman, L.M. 2004. Structural controls on hypozonal orogenic gold mineralization in the La Ronge Domain, Trans-Hudson Orogen, Saskatchewan. Canadian Journal of Earth Sciences 41, 1453–1471.

Lucas, S.B., Stern, R.A., Syme, E.C., Reilly, B.A. and Thomas, D.J. 1996. Intraoceanic tectonics and the development of continental crust: 1.92–1.84 Ga evolution of the Flin Flon Belt, Canada; Geological Society of America Bulletin, v. 108, p. 602–629.

Menard, T., Gordon, T.M., 1997. Metamorphic P-T paths from the eastern Flin Flon Belt, and Kisseynew Domain, Snow Lake, Manitoba. The Canadian Mineralogist 35, 1093–1115.

Rubingh, K.E., Gibson, H.L., Lafrance, B., 2017. Evidence for voluminous, bimodal pyroclastic volcanism, during rifting of a Paleoproterozoic Arc at Snow Lake, Manitoba. Canadian Journal of Earth Sciences 54, 654–676.

Schultz, D.J, 1990, Reconnaissance geological study of the Seabee gold deposit, Glennie Domain. in Summary of investigations 1990, Saskatchewan Geological Survey, Saskatchewan Energy and Mines, Miscellaneous Report 90-4, p. 70-73.

Schultz, D.J. 1996: The fluid history of the Seabee mesothermal gold deposit, northern Saskatchewan; M.Sc. thesis, University of Saskatchewan, Saskatoon, 122p.

Tourigny, G. 2003. Preliminary structural study of the gold-bearing shear zone system at the Seabee mine, northern Saskatchewan; in Summary of Investigations 2003, Volume 2, Saskatchewan Geological Survey, Sask. Industry and Resources, Misc. Rep. 2003-4.2, CD-ROM, Paper B-1, 11p.

Wood, C.R., 2016. Structural study of the auriferous Santoy shear zone, northeastern Glennie domain, Saskatchewan, MSc. Thesis, University of Regina, 154 p.

Zaleski, E., Froese, E., Gordon, T.M., 1991. Metamorphic petrology of Fe–Zn–Mg–Al alteration at the Linda volcanogenic massive sulfide deposit, Snow Lake, Manitoba. Canadian Mineralogist 29, 995–1017.

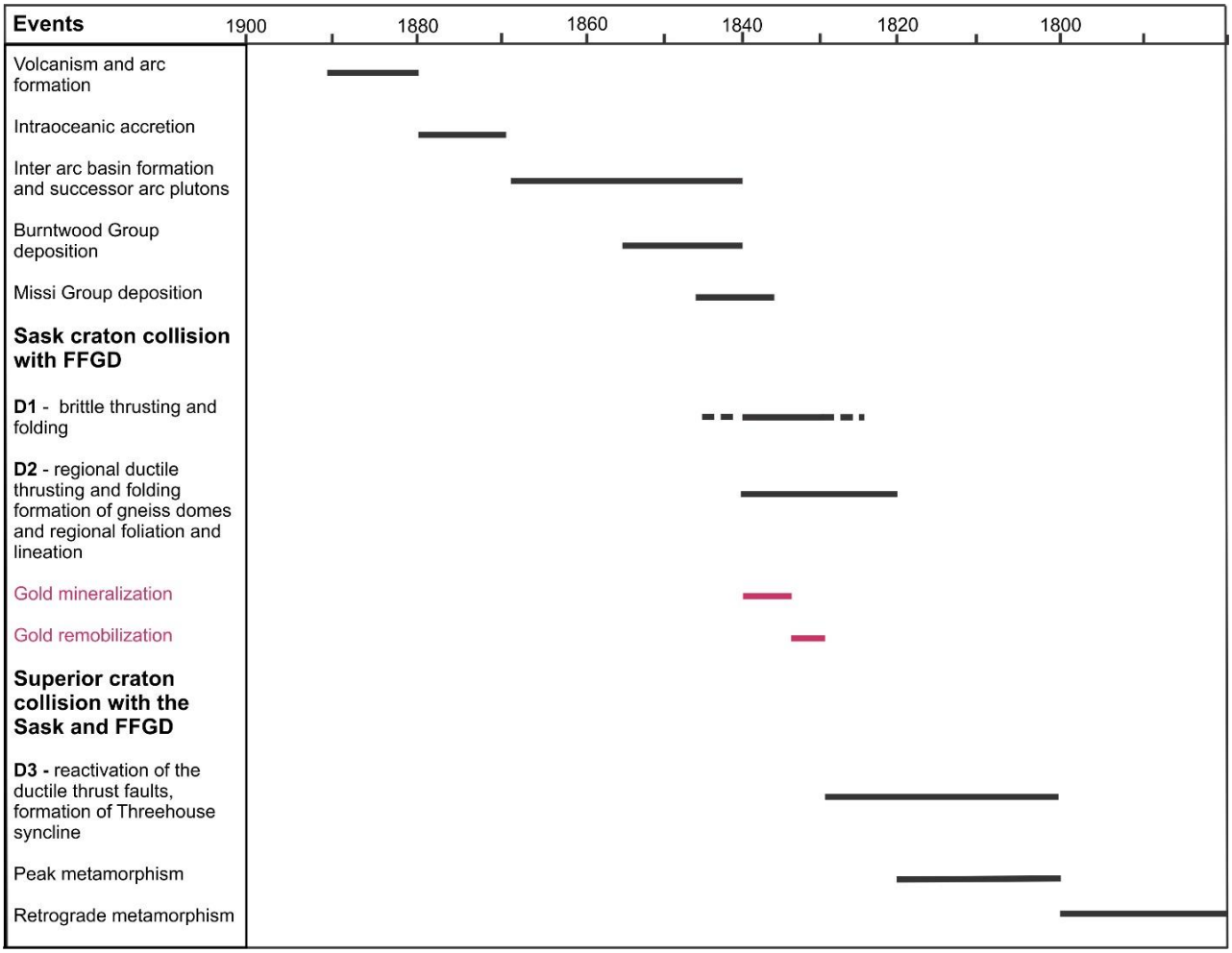

Figure 5. 1: Depositional, structural and mineralization events in the Snow Lake area.

Appendices

Appendix A

Appendix A. Rubingh, K.E. 2011: Stratigraphy of the McLeod Road–Birch Lake thrust panel, Snow Lake, west-central Manitoba (parts of NTS 63K16 and 63J13); in Report of Activities 2011, Manitoba Innovation, Energy and Mines, Manitoba Geological Survey, p. 68–78.

GS-7 Stratigraphy of the McLeod Road–Birch Lake thrust panel, Snow Lake, west-central Manitoba (parts of NTS 63K16 and 63J13)

by K.E. Rubingh[1]

Rubingh, K.E. 2011: Stratigraphy of the McLeod Road–Birch Lake thrust panel, Snow Lake, west-central Manitoba (parts of NTS 63K16 and 63J13); *in* Report of Activities 2011, Manitoba Innovation, Energy and Mines, Manitoba Geological Survey, p. 68–78.

Summary

During the 2011 field season, lithostratigraphic mapping was undertaken within the McLeod Road–Birch Lake thrust panel near the town of Snow Lake, Manitoba. The objective of the 2011 field season was to outline and define early regional structure through the repetition of structure by folding or thrusting, which would have implications on the understanding of gold mineralization at the New Britannia mine. Stratigraphy was defined across the upper portion of the thrust panel, which was then correlated across three transects to the east of Snow Lake. The transects covered a strike length of 3 km and no repetition of units was observed. This work suggests that the upper portion of the McLeod Road–Birch Lake thrust panel represents a homoclinal sequence that consistently youngs to the north.

Introduction

The McLeod Road–Birch Lake thrust panel is a fault-bounded package of mafic and felsic volcanic and volcaniclastic rocks, which is host to three gold deposits in the vicinity of the town of Snow Lake including the Nor-Acme (New Britannia) deposit, which produced 43 694 kg (1 404 950 oz.) gold over the lifetime of the mine. These deposits are located in the hangingwall of the McLeod Road Thrust, at the contact between lithological units. Rocks from the McLeod Road–Birch Lake thrust panel are geochemically similar to those of the Snow Lake arc assemblage (Bailes and Schledewitz, 1998), which contains several volcanogenic massive sulphide (VMS) deposits. The upper panel, as described in this paper, is the part of the thrust panel, which is north of Bud Lake. The goal of this paper is to provide a detailed description of each of the lithofacies through the upper part of the thrust panel without interpretation of paleoenvironment.

The structural controls on gold mineralization in the area are not well understood, although several studies have been conducted to classify the style and setting of the gold and the nature of the structures controlling the mineralization within the McLeod Road–Birch Lake thrust panel and more specifically the New Britannia deposit (Harrison, 1949; Hogg, 1957; Galley et al., 1986; Galley et al., 1988; Galley et al., 1991; Gale, 1997; Schledewitz, 1997; Schledewitz, 1998; Fieldhouse, 1999; Fulton, 1999; Gale, 2002; Beaumont-Smith and Lavigne, 2008). The gold mineralization is hosted by quartz and quartz carbonate replacements and veins in both mafic and felsic volcaniclastic and volcanic rocks. Fieldhouse (1999) and Galley et al. (1991) proposed that the New Britannia gold mineralization was associated with early structures that predate peak metamorphic conditions. Galley et al. (1991) associated the gold mineralization with the intersection of fluid-bearing faults with a secondary structure (i.e., a fold hinge), which allowed a sudden pressure release and in situ brecciation of the wallrocks and flooding of the zone containing the mineralizing fluids. Previous work on the mineralization at the New Britannia mine considered the possibility that the gold had a syngenetic origin and was later remobilized (Froese and Moore, 1980).

The fieldwork initiated in 2011 is part of a multiyear project, which is supported by the Manitoba Geological Survey and Alexis Minerals Corporation as a research project conducted at Laurentian University. The study is multidisciplinary and will use lithostratigraphy, geochemistry, structural geology and geochronology, with the main goal being to investigate the geological controls on gold mineralization at the New Britannia mine, Snow Lake. The focus of this first field season was to establish a detailed lithostratigraphy of the McLeod Road–Birch Lake thrust panel to test for the presence of structurally repeated lithofacies.

An improved understanding of the geometry of lithological units and a complete lithostratigraphy will aid in determining the internal geometry of the McLeod Road–Birch Lake thrust panel and in defining the structural controls on gold mineralization.

Regional geology

The Flin Flon–Snow Lake greenstone belt (Figure GS-7-1) is in the internides of the Trans-Hudson Orogen. It is bounded to the east by the Superior Boundary Zone, to the west by the Wollaston fold belt, to the north by metaturbidite and sandstone of the Kisseynew basin and to the south it is buried beneath a Paleozoic basin. The belt consists of an amalgamation of several tectonic domains that are distinct in terms of geochemistry, metamorphism and structural history (Lucas et al., 1996; Syme et al., 1996).

[1] Department of Earth Sciences and Mineral Exploration Research Centre, Laurentian University, 935 Ramsey Lake Road, Sudbury, Ontario, P3E 2C6

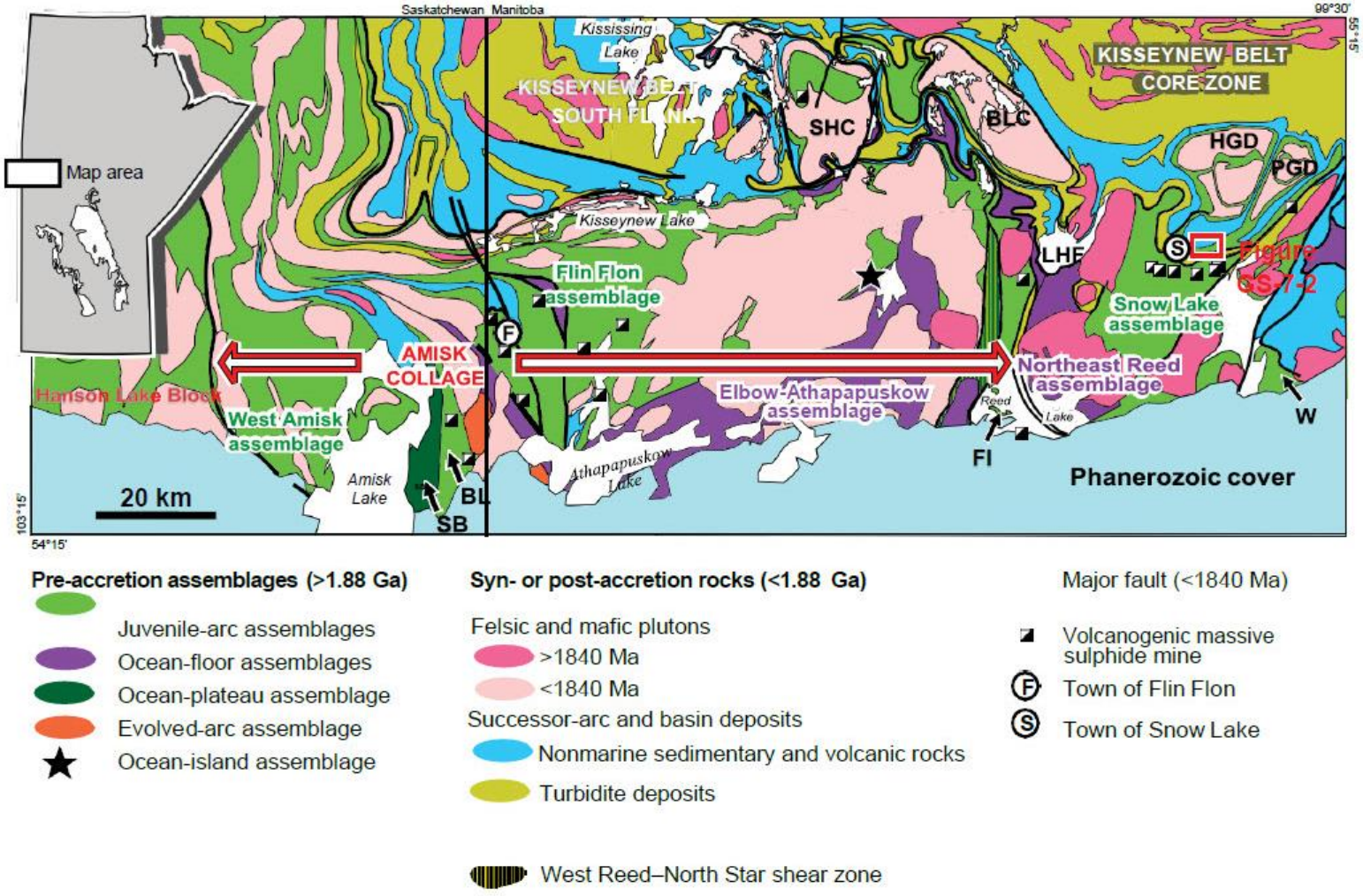

***Figure GS-7-1**: Geology of the Flin Flon–Snow Lake greenstone belt in west-central Manitoba, showing the location of Figure GS-7-2. Abbreviations: BL, Birch Lake; BLC, Batty Lake complex; FI, Fourmile Island; HGD, Herblet gneiss dome; LHF, Loonhead Lake Fault; PGD, Pulver gneiss dome; SB, Sandy Bay; SHC, Sherridon–Hutchinson Lake complex.*

In the Snow Lake area, the deformation was determined to be that of a fold and thrust belt (Connors et al., 1996; Kraus, 1998; Zwanzig, 1999), producing a tectonically imbricated package of volcanic (ca. 1.89 Ga) and metasedimentary rocks (ca. 1.84–1.86 Ga; Syme et al., 1995; Kraus and Williams, 1999). The main panel of volcanic rocks, located south of Snow Lake, forms a 6 km thick succession referred to as the Snow Lake assemblage. This assemblage is subdivided into three sequences based on their unique geochemistry and lithological variation (Bailes and Galley, 1996, 1999, 2007). This geochemical variation reflects the evolution of the Snow Lake assemblage from a primitive arc (e.g., Anderson sequence: mafic and felsic flows), to a mature arc (e.g., Chisel sequence: mafic volcaniclastic rocks with minor felsic volcanic and volcaniclastic rocks), to an evolved arc rift environment (e.g., Snow Creek sequence: mafic flows and pillows). The McLeod Road–Birch Lake thrust panel was attributed to D_2 regional deformation, whereby D_2 thrust faults imbricate thrust slices of the volcanic rocks with younger Burntwood and Missi sedimentary rocks, which were then folded by the large-scale D_3 Threehouse synform (Beaumont-Smith and Lavigne, 2008; Gagné, 2009).

Stratigraphy

The McLeod Road–Birch Lake thrust panel is defined as a north-dipping homoclinal sequence of mafic and felsic volcanic and volcaniclastic rocks. The sequence is bounded by the McLeod Road Thrust to the south and the Birch Lake Fault to the north. Both of these faults are considered to be thrusts. The McLeod Road Thrust moves the older Snow Lake Arc rocks (Bailes and Galley, 2007) on top of the younger Burntwood Group turbidite. The Birch Lake Fault, which juxtaposes younger Missi Group sedimentary rocks on top of older Snow Lake assemblage volcanic rocks, is also interpreted as a thrust fault (Beaumont-Smith and Lavigne, 2008).

Lithostratigraphic mapping was conducted within the McLeod Road–Birch Lake thrust panel at a scale of 1:500 for stratigraphic logs and 1:1000 for outcrop mapping along three measured sections (T1, T2 and T3; Figure GS-7-2), which were then used to correlate

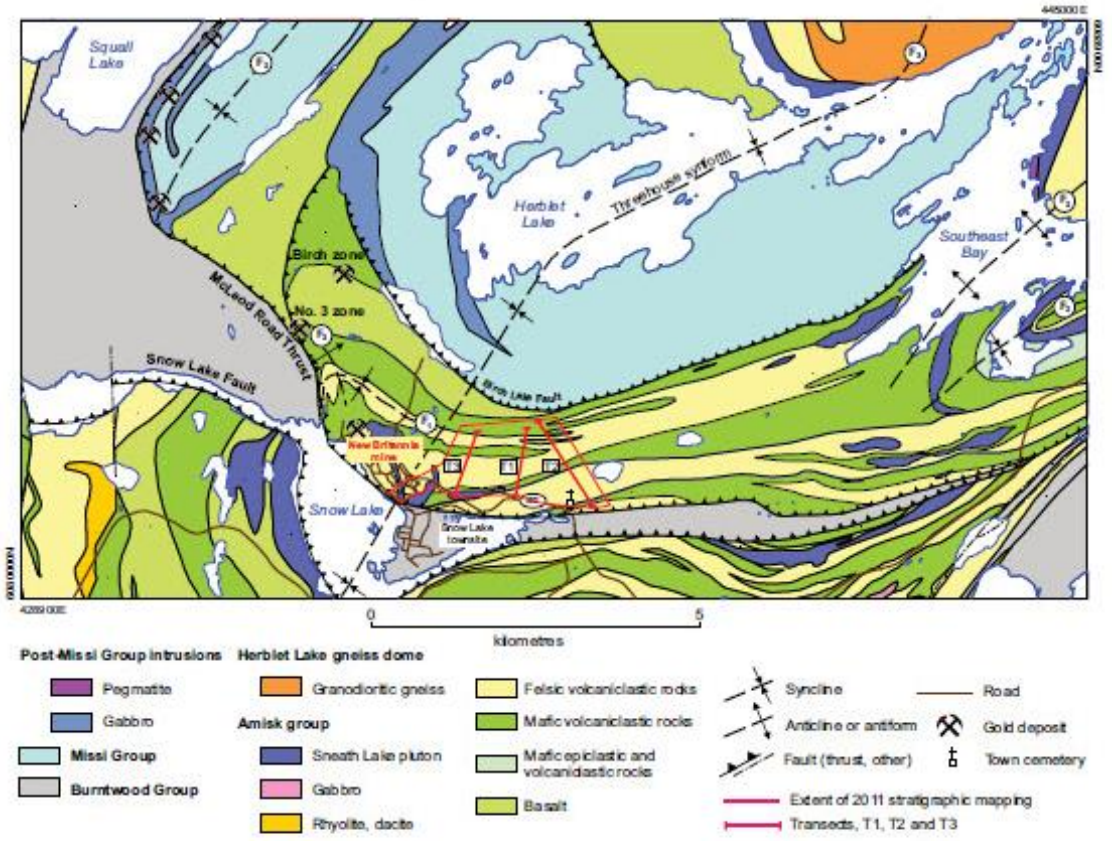

Figure GS-7-2: Geology of the McLeod Road–Birch Lake thrust panel (modified from Gagné, 2009). The 2011 lithostratigraphic mapping is overlain to show the locations of each transect and the location of stratigraphic units across the upper part of the thrust.

the stratigraphy from the town cemetery to the town centre of Snow Lake (Figure GS-7-3). The sections were chosen for the best outcrop exposure and thus two transects run parallel to the main power lines to the east of Snow Lake. Along each stratigraphic section, detailed mapping of surface outcrops, sampling of the hostrock for lithogeochemistry and relogging of drillcore was performed. The purpose of the fieldwork was to collect a set of representative samples from each lithofacies for detailed textural and geochemical analyses, to correlate the lithofacies from each transect and to form the basis for the geological context of the mineralization.

The following section provides a detailed description, from oldest to youngest, of each lithofacies within the stratigraphy defined for the upper panel of the McLeod Road–Birch Lake thrust panel (Figure GS-7-4). Each lithofacies has been grouped into units that represent lithofacies that share common characteristics; some of the units described comprise several lithofacies, whereas others contain only one. In the descriptions that follow, all primary pyroxene phenocrysts have been pseudomorphed by hornblende due to peak amphibolite facies metamorphism; therefore, the pyroxene phenocrysts described refer only to relict pyroxene.

Unit 1: Mafic flows and volcaniclastic rocks

This unit can be correlated along a strike length of more than 3 km. The most distinctive lithofacies within this unit are the plagioclase-phyric pillows and scoriaceous volcaniclastic rocks. The entire package ranges in thickness from 150 to 200 m thick and can be subdivided into the following six lithofacies. No repetition of facies has been observed through unit 1 and a consistent north-younging direction was determined.

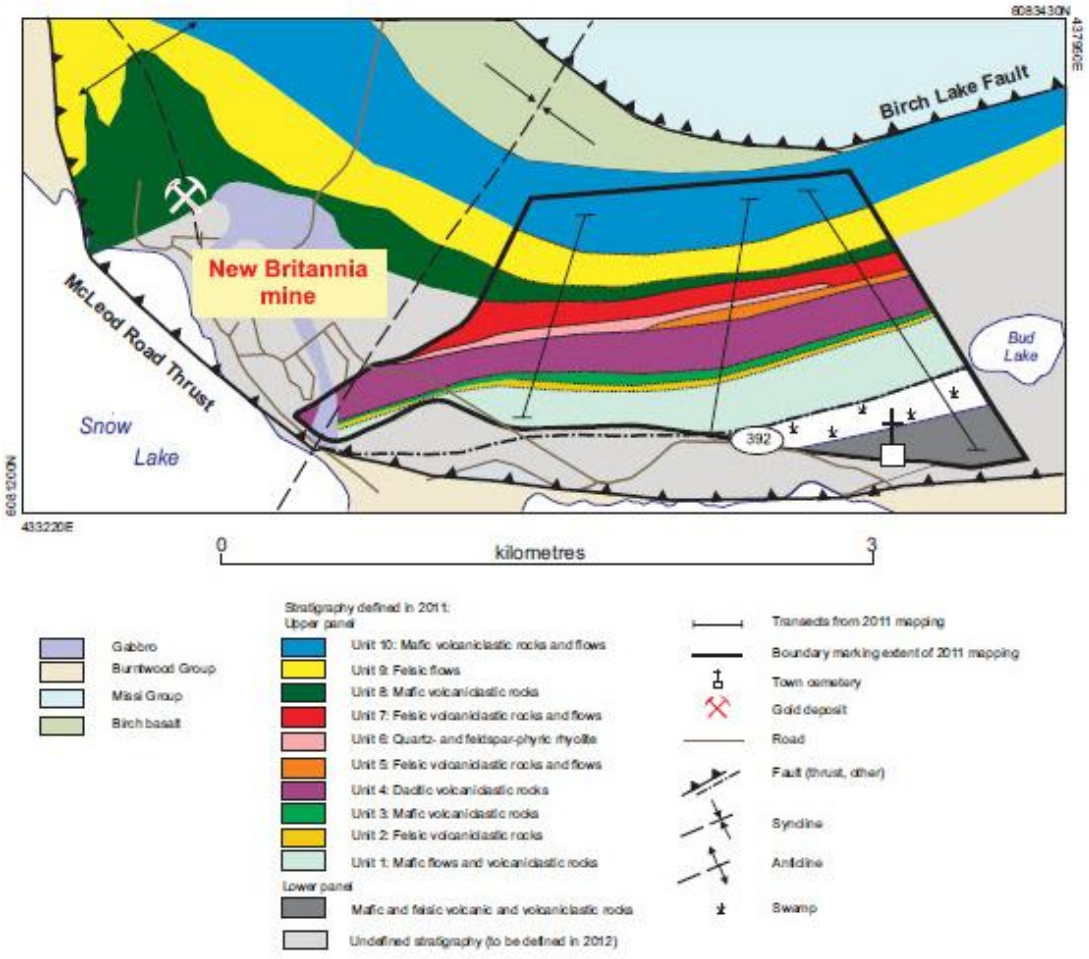

Figure GS-7-3: Lithostratigraphic mapping from 2011 showing the stratigraphic units across the upper panel of the McLeod Road–Birch Lake thrust panel.

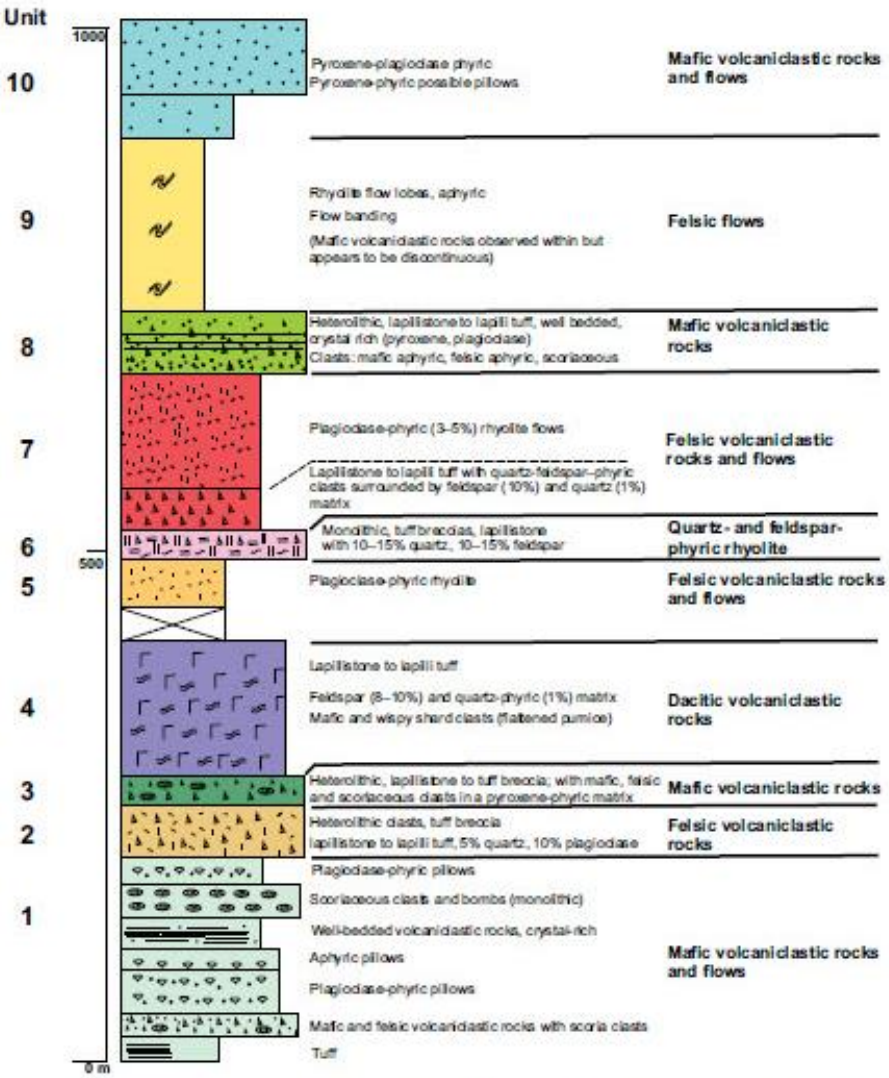

Figure GS-7-4: Stratigraphy of the upper panel of the McLeod Road–Birch Lake thrust panel as defined from the 2011 fieldwork.

1) Mafic tuff

The mafic tuff lithofacies varies from 2 to 25 m in thickness; it is finely laminated to thinly bedded and is interbedded with felsic tuff. The mineralogy includes hornblende, biotite, plagioclase and garnet. A strong foliation, defined by hornblende and plagioclase, is pervasive throughout the facies. Hornblende also defines a well-developed mineral lineation. Garnet grains are flattened parallel to foliation and preferential growth occurs parallel to the lineation and within the foliation surfaces. The contact is sharp with the overlying lithofacies and a narrow tuff bed is observed at the contact. Alteration is low to moderate, early patchy hornblende alteration is observed throughout and late hematite staining and K-feldspar alteration occur locally.

2) Mafic and felsic volcaniclastic rocks with scoriaceous clasts

This lithofacies is 5–45 m thick and is present on all three transects. It is well bedded and comprises heterolithic felsic and mafic volcaniclastic rocks with lesser mafic scoriaceous clasts (Figure GS-7-5a), and is commonly intruded by basaltic dikes. Rocks from this lithofacies typically are framework- to matrix-supported breccia with subangular to subrounded clasts of rhyolite (aphyric to feldspar phyric) and subrounded mafic scoriaceous clasts in a finer tuff-sized mafic matrix. Clasts range from 3 cm to 25 cm in diameter, which would place the rocks in the lapillistone to tuff breccia range. The stretching ratio of clasts is approximately 6:1. The breccia is both massive and well bedded in the lapilli tuff beds. Individual beds

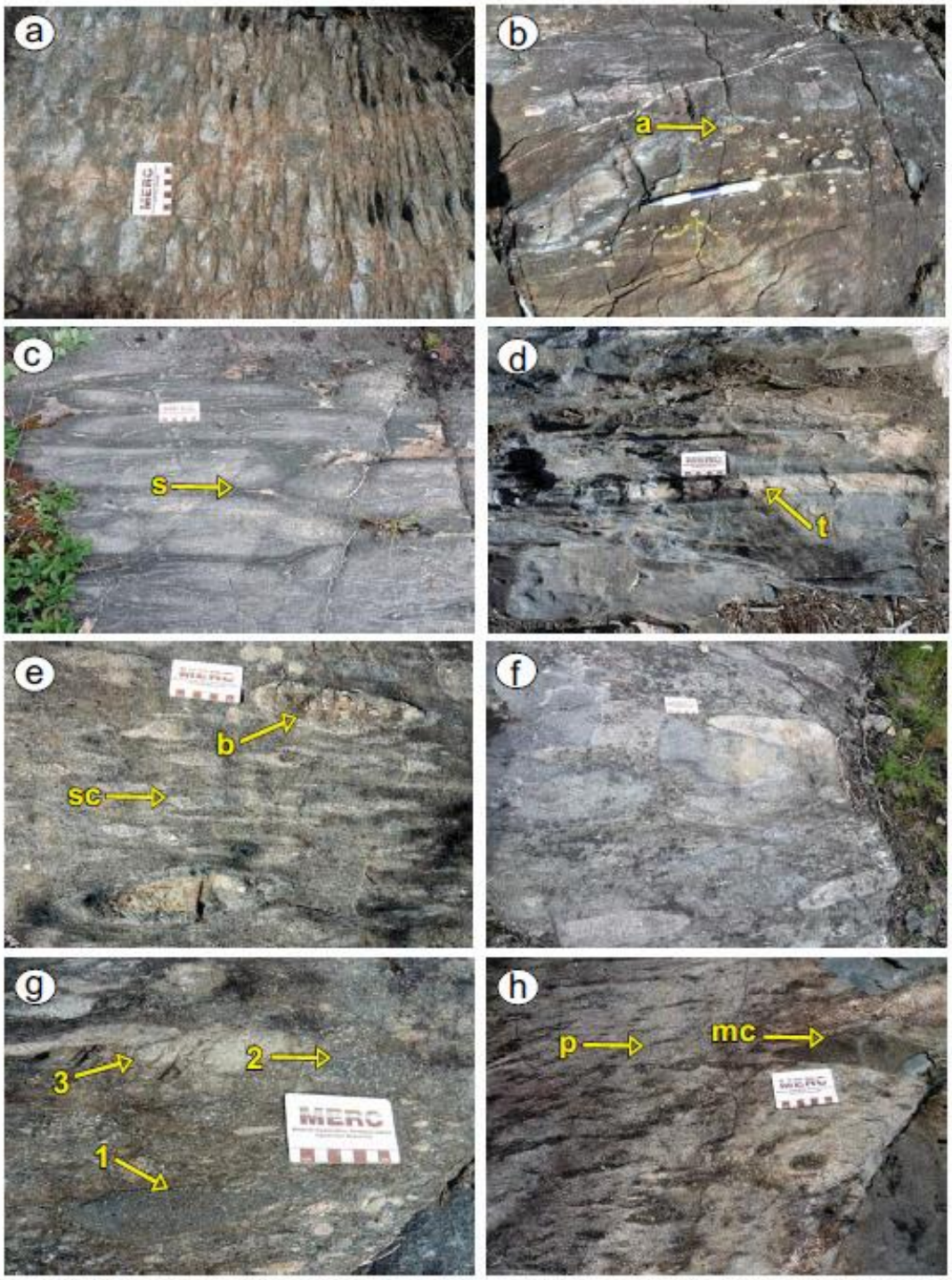

Figure GS-7-5: Volcanic rocks of the McLeod Road–Birch Lake thrust panel: a) unit 1, heterolithic tuff breccia of the well-bedded volcaniclastic lithofacies; b) unit 1, plagioclase-phyric pillow lithofacies showing quartz-filled amygdules (a); c) unit 1, plagioclase-phyric pillows with selvages (s); d) unit 1, crystal-rich, well-bedded volcaniclastic lithofacies with tuff beds (t); e) unit 1, scoriaceous clasts and bomb lithofacies (Abbreviations: b, bomb with intact chilled contact; sc, scoriaceous clast); f) unit 2, heterolithic felsic volcaniclastic rocks; g) unit 3, heterolithic mafic volcaniclastic breccia (1, plagioclase-phyric basalt; 2, scoria; 3, rhyolite); h) unit 4, dacitic volcaniclastic with wispy flattened pumice (p) and mafic clasts (mc) with intact chilled contact.

range in thickness from 8 to 50 cm. Bedding is defined by abrupt changes in clast size, which are typically observed within the lapillistone to lapilli tuff beds. Normal grading is observed and is younging to the north. A sharp contact is observed with the overlying plagioclase-phyric pillow lithofacies.

3) Plagioclase-phyric pillows

The plagioclase-phyric pillow lithofacies is 3–55 m thick and is continuous across all three transects. This lithofacies consists of densely packed pillows, with narrow thin aphanitic selvages, pillow breccia and bombs (Figure GS-7-5b, c). The pillowed unit is plagioclase phyric (10%) and pyroxene phyric (10%). Amygdules are located in the centres to the tops of the pillows and they range in diameter from 0.3 to 1.5 cm and in abundance from <1% to 25%. A gradational contact is observed with the overlying aphyric pillow lithofacies.

4) Aphyric pillows

The aphyric pillow lithofacies, which may also be pyroxene phyric with rare amygdules, is less densely packed than the plagioclase-phyric lithofacies because its pillows are larger and were observed up to 2.5–3.0 m in length. The pillows are elongated, with an aspect ratio of approximately 5:1, with an average width of 0.5 m. This lithofacies is observed up to 4 m thick and is only observed on transect 1. The lower contact with the plagioclase-phyric pillow lithofacies is gradational and the upper contact with the overlying lithofacies is sharp.

5) Well-bedded, crystal-rich mafic volcaniclastic rocks

The crystal-rich mafic volcaniclastic rocks consist of well-bedded pyroxene-phyric tuff. The thickness of the lithofacies varies from 5 to 24 m and is continuous across all three transects. Normal grading is observed in beds ranging in thickness from 0.3 to 1.5 m. Moderately good indicators for a north-younging direction were interpreted based on moderately defined bed contacts. Beds vary in composition from dominantly quartz amygdaloidal to beds that are pyroxene rich. Fine felsic tuff beds separate individual mafic volcaniclastic beds (Figure GS-7-5d) and grading is observed within tuff layers. In addition, tuff beds are observed to scour into underlying beds, defining good younging indicators. The contact with the overlying lithofacies is sharp and defined by a tuff bed. The contact with the underlying lithofacies is also sharp.

6) Monolithic scoriaceous clasts and bombs

The framework- to matrix-supported monolithic scoria breccia lithofacies was identified on two easternmost transects. Where present, the thickness of this lithofacies varies from 4 to 10 m. The lithofacies is monolithic and comprises subrounded mafic scoriaceous clasts and bombs (5% abundance) with a crystal-rich matrix (Figure GS-7-5e). The scoriaceous clasts contain quartz and feldspar amygdules, which are evenly distributed throughout the clasts. The clasts and bombs have chilled margins, which remain intact (Figure GS-7-5e). The beds are locally reverse graded, which was determined by the concentration of bombs. Narrow, 15 cm thick tuffaceous beds with sharp contacts are intermittent through this lithofacies. The contact with the plagioclase-phyric pillows above is sharp.

Unit 2: Felsic volcaniclastic rocks

Unit 2 comprises a single lithofacies. The dominantly felsic volcaniclastic unit is 6–10 m in thickness; it is framework to matrix supported and contains subangular to subrounded heterolithic clasts of plagioclase-phyric rhyolite, mafic scoriaceous and rare basaltic clasts in a crystal-rich, pyroxene-phyric matrix. Rhyolite clasts dominate and some subangular clasts exhibit jigsaw fit fractures (Figure GS-7-5f), possibly due to autoclastic fragmentation. Clasts range from 2 to 40 cm in diameter (i.e., lapilli tuff, lapillistone to tuff breccia). The composition of this unit is primarily rhyolite clasts, including 5% quartz-filled amygdules, 10% plagioclase; mafic clasts (aphyric basalt and mafic scoria) comprise 3–5% of the clast population. The clasts have a strong lineation and L>>S. Epidotized rounded alteration patches up to 5 cm in diameter are observed locally throughout this unit. Bombs are 5% in abundance with intact chilled margins and are up to 30 cm in length. The unit was determined to be moderately graded with beds defined by variations in clast size; bed thickness varies from 0.5 to 2 m and overall the beds showed normal grading. The contact is sharp with the underlying plagioclase-phyric pillows of unit 1, but it is gradational with the overlying mafic volcaniclastic rocks (unit 3), as the percentage of felsic rhyolite clasts decreases and the percentage of mafic clasts increases.

Unit 3: Mafic volcaniclastic rocks

This unit comprises a single lithofacies. Heterolithic, dominantly mafic clasts, which are framework to matrix supported and subrounded, are surrounded by a pyroxene-phyric matrix. This unit was identified on all three transects and its thickness varies from 8 to 25 m. The clast population composition includes basaltic fine-grained clasts, both plagioclase-phyric and aphyric, mafic scoriaceous clasts and aphyric to plagioclase-phyric rhyolite clasts, which are surrounded by a pyroxene-phyric matrix (Figure GS-7-5g). There is an average of 15% felsic clasts in the total clast population. The unit is graded with beds defined by variations in clast size; bed thickness varies from 1 to 2 m. The lower contact is gradational with the dominantly felsic volcaniclastic unit and the upper contact is intruded by an aphyric rhyolite sill, which is observed on the adjacent transect and is continuous over 1 km. The contact is otherwise gradational with the dacitic volcaniclastic rocks of unit 4.

Unit 4: Dacitic volcaniclastic rocks

The dacitic volcaniclastic unit comprises a single lithofacies. This unit is a distinct marker horizon, which can be traced continuously across 4 km in strike length; its thickness ranges from 130 to 165 m. The composition is consistent: 8–10% feldspar and quartz phyric with 1% matrix and rare blue quartz eyes were observed. It is moderately well bedded and clast size varies from lapillistone to lapilli tuff with locally observed mafic and wispy shard fragments, which are interpreted to be flattened pumice fragments (Figure GS-7-5h). These flattened pumice fragments have irregular margins and are up to 20 cm in length. Rare isoclinal folds were observed in this unit and overall the foliation is well developed and defined by biotite. Epidotized rounded alteration patches are observed locally throughout this unit. Reverse grading is observed due to the fine ash and pumice settling to the top of the beds. The unit varies laterally across its strike length with some beds containing distinct flattened shards and other beds containing none. The lower contact is gradational with the mafic heterolithic volcaniclastic rocks of unit 3, but the upper contact with the overlying rhyolite is not observed due to lack of outcrop.

Unit 5: Felsic volcaniclastic rocks and flows

This unit comprises two lithofacies, a plagioclase-phyric rhyolite flow and volcaniclastic rocks. The plagioclase-phyric rhyolite unit is not continuous along strike, but is observed on two transects and where present, it is up to 30 m thick. Its composition includes 5% plagioclase and 1–2% quartz in lapilli tuff to lapillistone beds. The grading of the beds was not determined conclusively, but it appears to be weakly defined to the north. Monolithic plagioclase-phyric rhyolite clasts are of similar composition to the matrix. A well-developed foliation is present and is defined by biotite alignment and a moderately well-developed stretching lineation, which is defined by elongation of the clasts. The lower contact is not observed because there is no outcrop and the upper contact, where observed, is gradational.

Unit 6: Quartz- and feldspar-phyric rhyolite

Unit 6 consists of a single lithofacies. It is a framework-supported, angular to subangular monolithic quartz- and feldspar-phyric rhyolitic breccia (Figure GS-7-6a). Unit 6 is observed on the two westernmost transects; where present, its thickness varies from 20 to 45 m. The composition of the clasts includes 10–15% quartz and 10–15% plagioclase feldspar and crystal size ranges from 2 to 10 mm in diameter, with an average of 5 mm. This quartz-feldspar–phyric volcaniclastic unit is well bedded with clasts up to 0.6 m in diameter (i.e., lapillistone to tuff breccia) and locally the clasts display in situ brecciation. The contact with the underlying unit is gradational, but the upper contact with the felsic volcaniclastic rocks and flows (unit 7) is sharp and the quartz-feldspar–phyric unit appears intermittently within unit 7.

Unit 7: Felsic volcaniclastic rocks and flows

This rhyolite unit comprises two lithofacies: aphyric to plagioclase-phyric flows and volcaniclastic rocks. It is observed on all three transects and the thickness of the unit varies from 80 to 110 m. It comprises plagioclase-phyric (3%) to aphyric rhyolite flows and volcaniclastic rocks. The rhyolite flows display flow banding (Figure GS-7-6d), and there is evidence for in situ brecciated hyaloclastite lapilli tuff at the contact with unit 6 (Figure GS-7-6b). There is a sharp lower contact with unit 6 marked by a tuffaceous finely laminated bed. Clast diameter varies from 2 to 5 cm (i.e., lapillistone to lapilli tuff; Figure GS-7-6c) and it is matrix supported. The clasts are quartz feldspar phyric and of the same composition as unit 6, but the matrix composition includes 10% feldspar with no quartz. The upper contact of unit 7 with the mafic volcaniclastic rocks of unit 8 is sharp and highly strained.

Unit 8: Mafic volcaniclastic rocks

Unit 8 comprises a single lithofacies of well bedded, matrix supported, heterolithic mafic volcaniclastic rocks with subrounded to rounded clasts and a crystal-rich pyroxene- and plagioclase-phyric matrix. This unit is continuous across all three transects and is part of the mine horizon package; the total thickness of the unit varies from 40 to 60 m. Heterolithic clasts comprise aphyric rhyolite, fine-grained basalt and mafic feldspar-filled amygdaloidal scoriaceous clasts (Figure GS-7-6e, f). Clasts range in size from 0.5 to 5 cm in diameter (i.e., lapilli tuff to lapillistone). The bedding was determined on sharp contacts and a decrease in crystal size in the mafic pyroxene-phyric beds. Beds range in thickness from 2 to 8 m. Younging was observed to the north, which was consistent with facing directions in the previous units. The mafic volcaniclastic rocks contain a well-developed foliation defined by biotite alignment and a stretching lineation defined by clast elongation. The lower contact with the felsic volcaniclastic rocks and flows (unit 7) and the upper contact with the rhyolite flows (unit 9) are both sharp and highly strained.

Unit 9: Felsic flows

Unit 9 comprises two lithofacies: an aphyric aphanitic rhyolite flow (Figure GS-7-6g) and minor felsic volcaniclastic rocks. It is a continuous unit that forms a thick rhyolite flow package stretching across the three transects and ranging in thickness from 110 to 155 m. The unit displays flow banding and quartz-filled amygdules, which range from 2 to 5 mm in diameter, are locally observed. The foliation is well developed as spaced disjunctive cleavage defined by biotite. Mineral stretching lineation, defined by quartz, feldspar and garnet, is well

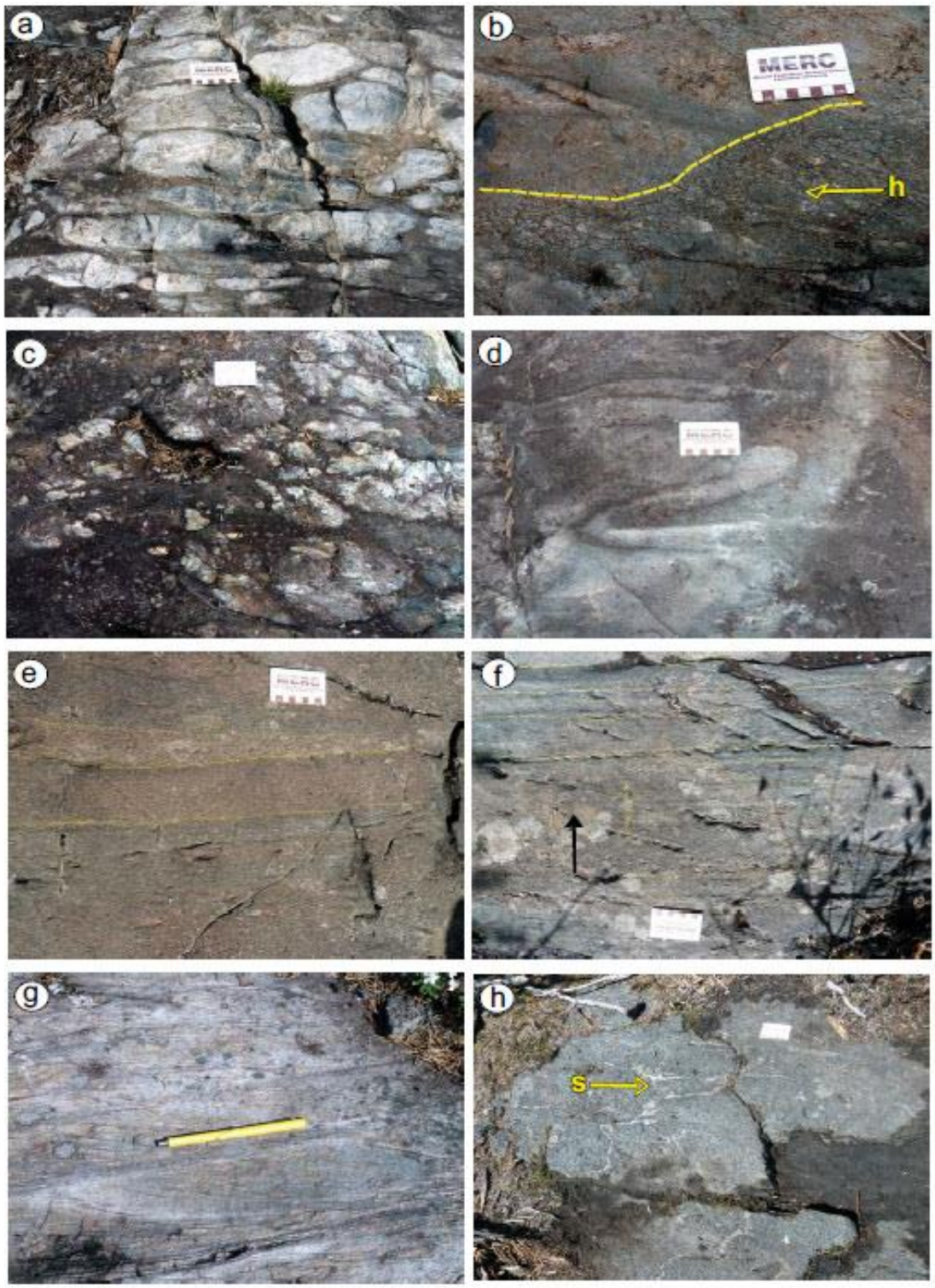

Figure GS-7-6: Volcanic rocks of the McLeod Road–Birch Lake thrust panel: a) unit 6, quartz-feldspar–phyric monolithic tuff breccia; b) unit 7, plagioclase-phyric rhyolite with hyaloclastite (h) in flow contact breccia, the dashed line marks the boundary between the two lithofacies; c) unit 7, plagioclase-phyric rhyolite flow breccia; d) unit 7, plagioclase-phyric rhyolite displaying a flow lobe; e) unit 8, well-bedded, heterolithic mafic volcaniclastic rocks; f) unit 8, graded beds in well-bedded heterolithic mafic volcaniclastic rocks, arrow shows younging direction to the north; g) unit 9, aphyric rhyolite; h) unit 10, pyroxene-plagioclase–phyric pillows with thin selvages (s).

developed. Rare felsic volcaniclastic rocks are observed within this otherwise dominantly massive rhyolite flow unit. The clasts are monolithic aphyric rhyolite fragments, subrounded and framework to matrix supported. The clasts range from 3 to 6 cm in diameter (i.e., lapillistone to lapilli tuff). No internal bedding is defined. The lower and upper contacts with the mafic volcaniclastic rocks of unit 8 and unit 10, respectively, are both sharp and highly strained.

Unit 10: Mafic volcaniclastic rocks and flows

This unit comprises two lithofacies: mafic volcaniclastic rocks and flows. It ranges in thickness from 45 to 90 m. The unit thins towards the west, but is present on all three transects as the uppermost horizon besides the Birch basalt. The mafic volcaniclastic rocks have a pyroxene-plagioclase–phyric crystal matrix, monolithic aphyric rhyolite clasts and a mafic flow lithofacies, comprising massive and pillowed pyroxene-phyric pillows defined by thin selvedges (Figure GS-7-6h). The pyroxene crystals range from 0.5 to 1 cm in diameter and clasts are up to 3 cm in diameter (i.e., lapillistone to lapilli tuff). Graded beds were not determined within this lithofacies. The mafic pyroxene-plagioclase–phyric volcaniclastic lithofacies occurs stratigraphically below the pyroxene-plagioclase–phyric mafic flows.The lower contact is sharp and highly strained with the underlying rhyolite flows (unit 9).

Discussion

The objective of the 2011 field season was to test for repetition of lithostratigraphic units once a stratigraphy was defined. The stratigraphic section defined a consistent stratigraphy for the upper 1000 m of the McLeod Road–Birch Lake thrust panel across a strike distance of more than 3 km (Figure GS-7-2). Stratigraphic mapping determined that no apparent repetition of stratigraphic units exists within the project area to the east of Snow Lake and that the rocks form a moderately to steeply north-dipping homoclinal sequence, as previously discussed by Bailes and Schledewitz (1998).

The absence of stratigraphic repetition and polarity reversal within the studied sequence invalidates the earlier hypothesis that a large-scale F_1 fold is present within this sequence. The stratigraphy documented during the 2011 fieldwork will be used to delineate the main structural features of the mine horizon during subsequent field seasons. The newly acquired stratigraphic information will aid in testing for any potential repetition south of Bud Lake.

Economic considerations

Gold mineralization is spatially associated at lithological contacts; however, the controls and timing of gold mineralization at the New Britannia mine are not well understood. Therefore, to focus exploration efforts within the mine and target new potential horizons within the thrust panel, the main objective of this study is to improve the understanding of the controls on gold mineralization. To achieve this, a multiyear project was established and the initial objective during the 2011 field season was to complete lithostratigraphic mapping across the thrust panel, to refine the stratigraphy within the McLeod Road–Birch Lake thrust panel, and to test for early structures through the repetition of lithological units. Stratigraphy of the upper portion of the McLeod Road–Birch Lake thrust panel was established during the 2011 field season and no repetition of lithostratigraphic units was identified. In the subsequent field seasons, the lower portion of the McLeod Road–Birch Lake thrust panel will be tested, which lies from the McLeod Road Thrust to the swamp south of Bud Lake. There is, therefore, still the potential for repetition in this lower panel and this could prove a useful exploration target if repetition of the mine horizon units is observed.

Acknowledgments

Funding for this field season was generously provided by Alexis Minerals Corporation, the Manitoba Geological Survey and Laurentian University. The author thanks H. Gibson, B. LaFrance, A. Bailes, S. Gagné, the field assistant E.Tetlock and the staff at Alexis Minerals for their support and invaluable discussions during the 2011 field season.

References

Bailes, A.H. and Galley, A.G. 1996: Setting of Paleoproterozoic volcanic-hosted massive base metal sulphide deposits, Snow Lake, Manitoba; *in* EXTECH I: A Multidisciplinary Approach to Massive Sulphide Research in the Rusty Lake–Snow Lake Greenstone Belts, Manitoba, G.F. Bonham-Carter, A.G. Galley and G.E.M. Hall (ed.), Geological Survey of Canada, Bulletin 426, p. 105–138.

Bailes, A.H. and Galley, A.G. 1999: Evolution of the Paleoproterozoic Snow Lake arc assemblage and geodynamic setting for associated volcanic-hosted massive sulphide deposits, Flin Flon Belt, Manitoba, Canada; Canadian Journal of Earth Sciences, v. 36, p. 1789–1805.

Bailes, A.H. and Galley, A.G. 2007: Geology of the Chisel–Anderson lakes area, Snow Lake, Manitoba (NTS areas 63K16SW and west half of 63K13SE); Manitoba Science, Technology, Energy and Mines, Manitoba Geological Survey, Geoscientific Map MAP2007-1, scale 1:20 000, 1 map plus notes.

Bailes, A.H. and Schledewitz, D.C.P. 1998: Geology and geochemistry of the Paleoproterozoic volcanic rocks between the McLeod Road and Birch Lake faults, Snow Lake area, Flin Flon belt (parts of NTS 63K/16 and 63J/13); *in* Report of Activities 1998, Manitoba Energy and Mines, Geological Services, p. 4–13.

Beaumont-Smith, C.J. and Lavigne, J. 2008: Structural geology and gold metallogenesis of the New Britannia Mine area, Snow Lake, Manitoba (NTS 63K16); *in* Report of Activities 2008, Manitoba Science, Technology, Energy and Mines, Manitoba Geological Survey, p. 7–17.

Connors, K.A., Ansdell, K.M. and Lucas, S.B. 1996: Coeval sedimentation, magmatism, and fold-thrust development in the Trans-Hudson Orogen: propagation of deformation into an active continental arc setting, Wekusko Lake area, Manitoba; Canadian Journal of Earth Sciences, v. 36, p. 275–291.

Fieldhouse, I. 1999: Geological setting of gold mineralization in the vicinity of the New Britannia mine, Snow Lake, Manitoba; M.Sc. thesis, University of Manitoba, Winnipeg, Manitoba, 136 p.

Froese, E. and Moore, J.M. 1980: Metamorphism in the Snow Lake area, Manitoba; Geological Survey of Canada, Paper 78-27, 16 p.

Fulton, P.J. 1999: Distribution of gold mineralization at the New Britannia mine in Snow Lake, Manitoba: implications for exploration and processing; M.Sc. thesis, University of Manitoba, Winnipeg, Manitoba, 207 p.

Gagné, S. 2009: Geological investigation of the McLeod Road-Birch Lake allochthon east of Snow Lake, Manitoba (part of NTS 63J13); *in* Report of Activities 2009, Manitoba Innovation, Energy and Mines, Manitoba Geological Survey, p. 58–68.

Gale, G.H. 1997: Geological settings and genesis of gold mineralization in the Snow Lake area (NTS 63K/16); *in* Report of Activities 1997, Manitoba Energy and Mines, Geological Services, p. 73–78.

Gale, G.H. 2002: Geology of the New Britannia Mine, Snow Lake (NTS 63K16), Manitoba; *in* Report of Activities 2002, Manitoba Industry, Trade and Mines, Manitoba Geological Survey, p. 83–86.

Galley, A.G., Bailes, A.H., Syme, E.C., Bleeker, W., Macek, J.J. and Gordon, T.M. 1991: Geology and mineral deposits of the Flin Flon and Thompson belts, Manitoba (Field Trip 10); Geological Survey of Canada, Open File 2165, 8th IAGOD Symposium Field Trip Guidebook, 137 p.

Galley, A.G., Franklin, J.M. and Ames, D.E. 1988: Geological setting of gold mineralization, Snow Lake, Manitoba; Geological Survey of Canada, Open File 1700, scale 1:50 000.

Galley, A.G., Ziehlke, D.V., Franklin, J.M., Ames, D.E. and Gordon, T.M. 1986: Gold mineralization in the Snow Lake–Wekusko Lake region, Manitoba; *in* Gold in the Western Shield, A.L. Clark (ed.), Canadian Institute of Mining and Metallurgy, Special Volume 38, p. 379–398.

Harrison, J.M. 1949: Geology and Mineral Deposits of File-Tramping Lakes area, Manitoba; Geological Survey of Canada Memoir 250, 92 p.

Hogg, N. 1957: Nor-Acme mine; *in* Structural Geology of Canadian Ore Deposits, Volume II; Canadian Institute of Mining and Metallurgy, 6th Commonwealth Mining and Metallurgical Congress, p. 262–275.

Kraus, J. 1998: Structural and metamorphic studies in the Snow Lake area, Trans-Hudson Orogen, Manitoba, central Canada; Ph.D. thesis, University of New Brunswick, Fredericton, New Brunswick, 229 p.

Kraus, J. and Williams, P.F. 1999: Structural development of the Snow Lake allochthon and its role in the evolution of the southeastern Trans-Hudson Orogen in Manitoba, central Canada; Canadian Journal of Earth Sciences, v. 36, p. 1881–1899.

Lucas, S.B., Stern, R.A., Syme, E.C., Reilly, B.A. and Thomas, D.J. 1996: Intraoceanic tectonics and the development of continental crust: 1.92–1.84 Ga evolution of the Flin Flon Belt, Canada; Geological Society of America Bulletin, v. 108, p. 602–629.

Schledewitz, D.C.P. 1997: Squall Lake Project: geology and gold mineralization north of Snow Lake (NTS 63K/16NE); *in* Report of Activities 1997, Manitoba Energy and Mines, Geological Services, p. 79–83.

Schledewitz, D.C.P. 1998: Squall Lake Project: geology and mineralization in the area of Snow Lake and Squall Lake (NTS 63K/16NE); *in* Report of Activities 1998, Manitoba Energy and Mines, Geological Services, p. 14–18.

Syme, E.C, Bailes, A.H. and Lucas, S.B. 1995: Geology of the Reed Lake area (parts of NTS 63K/9 and 10); *in* Report of Activities 1997, Manitoba Energy and Mines, Geological Services, Report of Field Activities, p. 42–60.

Syme, E.C., Bailes, A.H. and Lucas, S.B. 1996: Tectonic assembly of the Paleoproterozoic Flin Flon belt and setting of VMS deposits; Geological Association of Canada–Mineralogical Association of Canada, Joint Annual Meeting, Winnipeg, Manitoba, May 27–29, 1996, Field Trip Guidebook B1, 131 p.

Zwanzig, H.V. 1999: Structure and stratigraphy of the south flank of the Kisseynew Domain in the Trans-Hudson Orogen, Manitoba: implications for 1.845–1.77 Ga collision tectonics; *in* NATMAP Shield Margin Project, Volume 2, Canadian Journal of Earth Sciences, v. 36, p. 1859–1880.

Appendix B

Appendix B. Rubingh, K.E., Lafrance, B. and Gibson, H.L. 2012: Lithostratigraphy and structural geology of the McLeod Road– Birch Lake thrust panel, Snow Lake, west-central Manitoba (parts of NTS 63K16, 63J13); in Report of Activities 2012, Manitoba Innovation, Energy and Mines, Manitoba Geological Survey, p. 104–114.

GS-9

Lithostratigraphy and structural geology of the McLeod Road–Birch Lake thrust panel, Snow Lake, west-central Manitoba (parts of NTS 63K16, 63J13)

by K.E. Rubingh[1], B. Lafrance[1] and H.L. Gibson[1]

Rubingh, K.E., Lafrance, B. and Gibson, H.L. 2012: Lithostratigraphy and structural geology of the McLeod Road–Birch Lake thrust panel, Snow Lake, west-central Manitoba (parts of NTS 63K16, 63J13); *in* Report of Activities 2012, Manitoba Innovation, Energy and Mines, Manitoba Geological Survey, p. 104–114.

Summary

The New Britannia mine is a structurally controlled gold deposit hosted in mafic and felsic volcanic and volcaniclastic rocks. Mineralization is spatially associated with the hangingwall of the McLeod Road Thrust (MRT), and the gold deposits are located at stratigraphic contacts between units of contrasting competency at the intersection of a fault and a secondary structure, typically a fold hinge.

Completion of the 2012 lithostratigraphic mapping of the McLeod Road–Birch Lake thrust panel (MB panel) has identified additional thrust faults, which repeat stratigraphic units of the panel. These structures appear to be truncated by the MRT and have been interpreted as early D_1 structures. The main foliation in the MB panel (S_1) is defined by the flattening of the clasts and is interpreted as a fabric formed during D_1 folding and thrust imbrication of the MB panel. The S_1 foliation is axial planar to the Nor-Acme anticline (F_1 fold) and is consistently parallel to the MRT (late D_1 thrust) contact. These D_1 structures are overprinted by a spaced cleavage (S_2), which overprints the Howe Sound Fault, the MRT and the Nor-Acme anticline. This fabric is correlative with the regional S_2 fabric in the Burntwood Group, and it is inferred that the S_2 fabric in the MB panel may be related to sinistral reactivation of the MRT. A spaced, steeply dipping, S_3 fracture cleavage related to the Threehouse synform (F_3 fold) consistently overprints all fabric elements. Gold mineralization is associated with D_1 structures and there is evidence to suggest that emplacement was late D_1 with later remobilization during D_2.

Introduction

The New Britannia mine has been renamed 'Snow Lake mine' by QMX Minerals Corporation in 2012; however, for consistency with earlier publications, this report will continue to use 'New Britannia mine'. The McLeod Road–Birch Lake thrust panel (MB panel) is a fault-bounded package of mafic and felsic volcanic and volcaniclastic rocks, which hosts four gold deposits: the Birch zone; the No. 3 zone; and the Boundary zone, including the Nor-Acme deposit of the New Britannia mine that produced 1,404,950 oz. (43 699 kg) gold. The Nor-Acme deposit is associated with the Howe Sound Fault, which cuts the MRT (Beaumont-Smith and Gagné, 2008; Galley et al., 1991). However Fieldhouse (1999) interpreted the Howe Sound Fault to precede the MRT. In this study, the Howe Sound Fault is interpreted to be a late D_1 structure. Numerous authors have either studied the geological controls on the gold mineralization (Hogg, 1957; Galley et al., 1988; Bailes and Schledewitz, 1998; Fieldhouse, 1999; Fulton, 1999; Gale, 2002; Beaumont-Smith and Lavigne, 2008) and/or mapped the regional geology of the thrust panel; however, the structural history and structural controls on gold mineralization are as yet undefined.

The MB panel can be internally subdivided into two fault-bounded panels. The upper MB panel comprises the package of rocks between an unnamed stratigraphy-parallel fault that passes through an unnamed lake to the south, and the Birch Lake Fault to the north. The lower MB panel comprises the package of rocks that extends south of the unnamed stratigraphy-parallel fault to the MRT. The lithostratigraphy of the upper MB panel was presented and described in Rubingh (2011).

Fieldwork in 2012 focused on three main objectives: 1) completion of stratigraphic mapping and sample collection for geochemistry of the lower MB panel; 2) correlation of the stratigraphic units as defined by lithostratigraphy and chemostratigraphy in 2011, through mapping the town of Snow Lake and the New Britannia mine property at 1:1000 scale; and 3) property-scale mapping (1:50 scale) of the Howe Sound Fault and the No. 3 zone deposit to determine the structural controls on gold mineralization. The stratigraphic and structural relationships of the rocks in the study area are presented on (Rubingh et al., 2012). An improved lithostratigraphic understanding will aid in determining the internal geometry of the MB panel and will provide an improved framework to help define the structural controls on gold mineralization.

Regional geology

The Flin Flon–Snow Lake greenstone belt (Figure GS-9-1) is located in the internides of the Trans-Hudson Orogen. It is bounded to the east by the Superior Boundary Zone, to the west by the Wollaston Fold Belt, to the north by metaturbidite and sandstone of the

[1] Department of Earth Sciences and Mineral Exploration Research Centre, Laurentian University, 935 Ramsey Lake Road, Sudbury, Ontario P3E 2C6

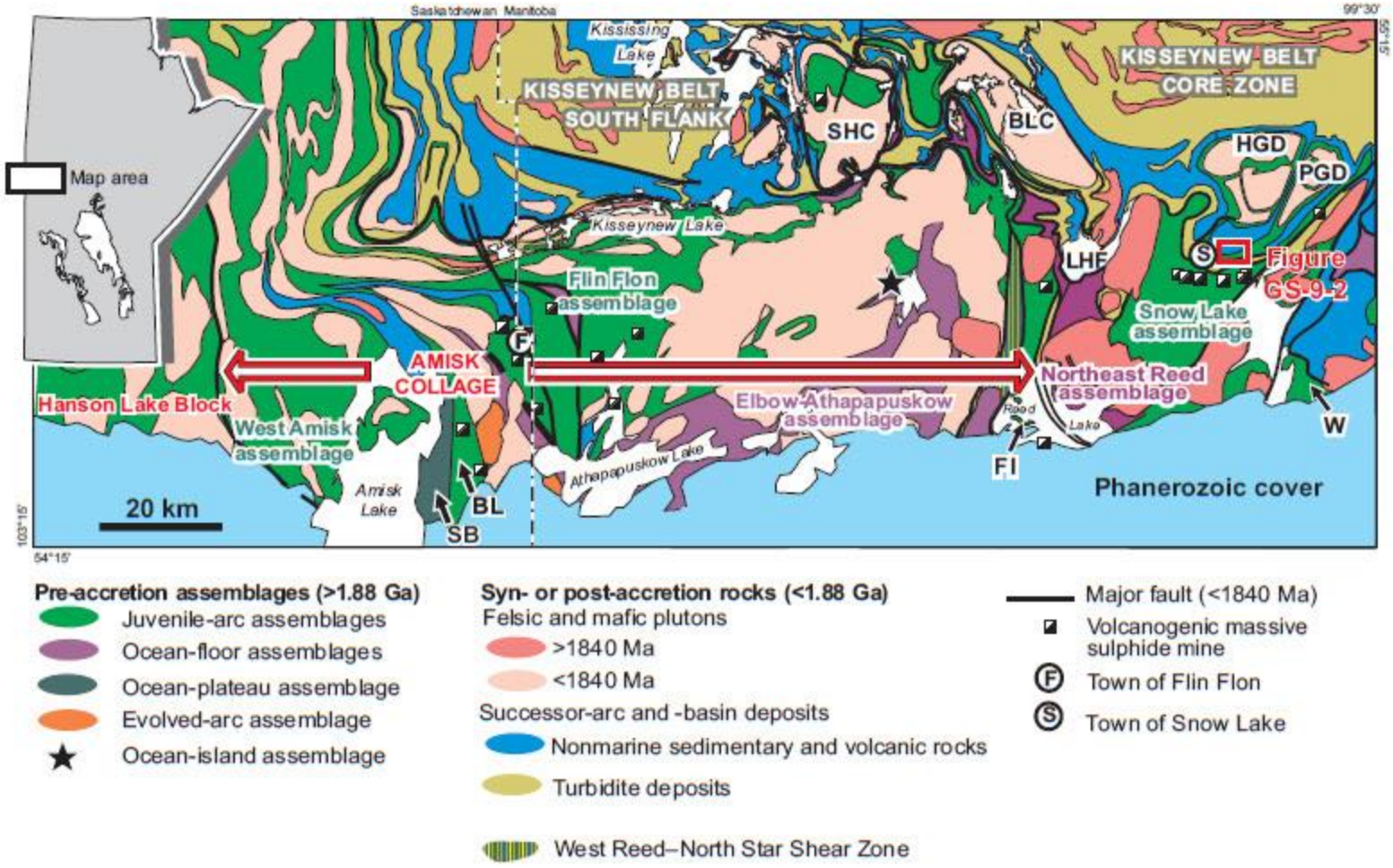

Figure GS-9-1: *Regional geology of the Flin Flon–Snow Lake greenstone belt (modified after Bailes and Schledewitz, 1998), west-central Manitoba. Abbreviations: BL, Birch Lake; BLC, Batty Lake complex; FI, Fourmile Island; HGD, Herblet gneiss dome; LHF, Loonhead Lake Fault; PGD, Pulver gneiss dome; SB, Sandy Bay; SHC, Sheridon–Hutchinson Lake complex; W, Schist-Wekusko assemblage.*

Kisseynew basin and, to the south, it is buried beneath a Paleozoic basin. The belt is an amalgamation of different tectonostratigraphic assemblages that are distinct in terms of geochemistry, metamorphic grade and structural history (Lucas et al., 1996; Syme et al., 1996). The main panel of volcanic rocks, located south of Snow Lake, forms a 6 km thick succession referred to as the Snow Lake arc assemblage (SLA). The SLA consists of three separate sequences that reflect its evolution from a primitive arc (Anderson sequence: mafic and felsic flows) to a mature arc (Chisel sequence: mafic volcaniclastic rocks with minor felsic volcanic and volcaniclastic rocks) to an evolved-arc rift (Snow Creek sequence: mafic flows and pillows; Bailes and Galley, 1996, 1999, 2007). The SLA developed as a result of a fold-and-thrust style of tectonics (Connors et al., 1996; Lucas et al., 1996; Kraus, 1998; Kraus and Williams, 1999; Zwanzig, 1999), in which the north-dipping SLA is overthrust from north to south by panels of Burntwood Group turbidites (ca. 1.86–1.84 Ga), the MB volcanic sequence (interpreted at ca. 1.89 Ga) and Missi Group conglomeratic rocks (ca. 1.86–1.84 Ga; Kraus and Williams, 1999).

The MB panel, as defined by Bailes and Schledewitz (1998), is a north-dipping homoclinal sequence of mafic and felsic volcanic and volcaniclastic rocks that is bounded to the south by the MRT and to the north by the Birch Lake Fault. Imbrication of the panels occurred during southwest-directed transport, historically attributed to D_2 regional deformation, and resulted in the formation of a strong, regional, northeast-plunging stretching lineation; a regional foliation; and the Nor-Acme anticline within the MB panel. These structures and panels were subsequently folded around the northeast-trending D_3 Threehouse syncline (Kraus and Williams, 1999; Beaumont-Smith and Lavigne, 2008; Gagné, 2009).

Metamorphic conditions in the Snow Lake area range from lower to middle amphibolite facies, with a northward increase in metamorphic grade reflecting temperatures in the range 500–700°C and a pressure increase from 4 to 6 kbar (Kraus and Menard, 1997). Mineral assemblages show the progression from the chlorite zone, south of the New Britannia mine, through the staurolite zone at the mine to the sillimanite zone in the Squall Lake area.

Stratigraphy of the MB panel

Structural and lithostratigraphic mapping conducted this field season has a potentially significant implication for understanding the stratigraphic relationships of the mine horizon. The 2012 structural and lithostratigraphic mapping indicates that the thrust panel is more deformed than previously interpreted, as a potential repetition of lithostratigraphic units has been identified within the MB panel (Figure GS-9-2; Rubingh et al., 2012). The following section provides a brief description, from oldest to youngest, of each stratigraphic unit in the MB panel (units 1–7), from the MRT to the Birch Lake basalt (Figure GS-9-2). The description of units 1–7 incorporates 1) the completion of stratigraphic mapping conducted in 2012, and 2) a reinterpretation of stratigraphic mapping from 2011. In the descriptions that follow, all primary pyroxene phenocrysts have been pseudomorphed by hornblende due to peak amphibolite-facies metamorphism; therefore, the pyroxene phenocrysts described refer only to relict pyroxene.

Description of stratigraphic units

Unit 1: Mafic volcaniclastic rocks

Unit 1 is interpreted as a repeated unit within the lower panel (Figure GS-9-2; Rubingh et al., 2012). This unit comprises a single lithofacies of moderately well bedded heterolithic felsic and mafic clasts, which vary from lapillistone to tuff breccia. The volcaniclastic rocks are typically matrix to clast supported, with subangular to subrounded, strongly flattened clasts and a crystal-rich, pyroxene- and plagioclase-phyric matrix. They comprise pyroxene-phyric mafic clasts of similar composition to the matrix, plagioclase-phyric mafic clasts, aphyric to plagioclase-phyric mafic clasts and plagioclase-phyric to aphyric felsic clasts.

Unit 2: Felsic volcaniclastic rocks

Unit 2 is interpreted as a thrust-repeated unit within the lower MB panel (Figure GS-9-2). It comprises two lithofacies: quartz- and plagioclase-phyric felsic volcaniclastic rocks and aphyric to plagioclase-phyric flows/sills. Plagioclase-phyric (5–8%) and quartz-phyric (3–5%) volcaniclastic rocks form a crudely bedded sequence (lapillistone to tuff breccia). Clasts are typically monolithic and of the same composition as the matrix; some are aphyric felsic. The massive, coherent, aphyric to 1–2% plagioclase-phyric rhyolite has a sharp contact with the felsic volcaniclastic rocks and is interpreted as a possible sill.

Unit 3: Heterolithic felsic volcaniclastic rocks

Unit 3 was previously subdivided into stratigraphic units 4, 5 and 6: dacitic volcaniclastic rocks, felsic volcanic and volcaniclastic rocks, and quartz-feldspar–phyric volcaniclastic rocks, respectively (Rubingh, 2011). During 2012 mapping and as a result of preliminary geochemistry from 2011, characteristics of these units have been identified in the lower MB panel; therefore, these units are grouped within a single unit 3. This unit now comprises three lithofacies: dacitic volcaniclastic rocks, with distinctive wispy mafic shards that are interpreted as flattened pumice fragments (Rubingh, 2011); amygdaloidal plagioclase-phyric felsic volcanic flows/sills; and heterolithic felsic volcaniclastic rocks (dominantly quartz-feldspar–phyric clasts, with minor plagioclase-phyric and aphyric to plagioclase-phyric mafic clasts).

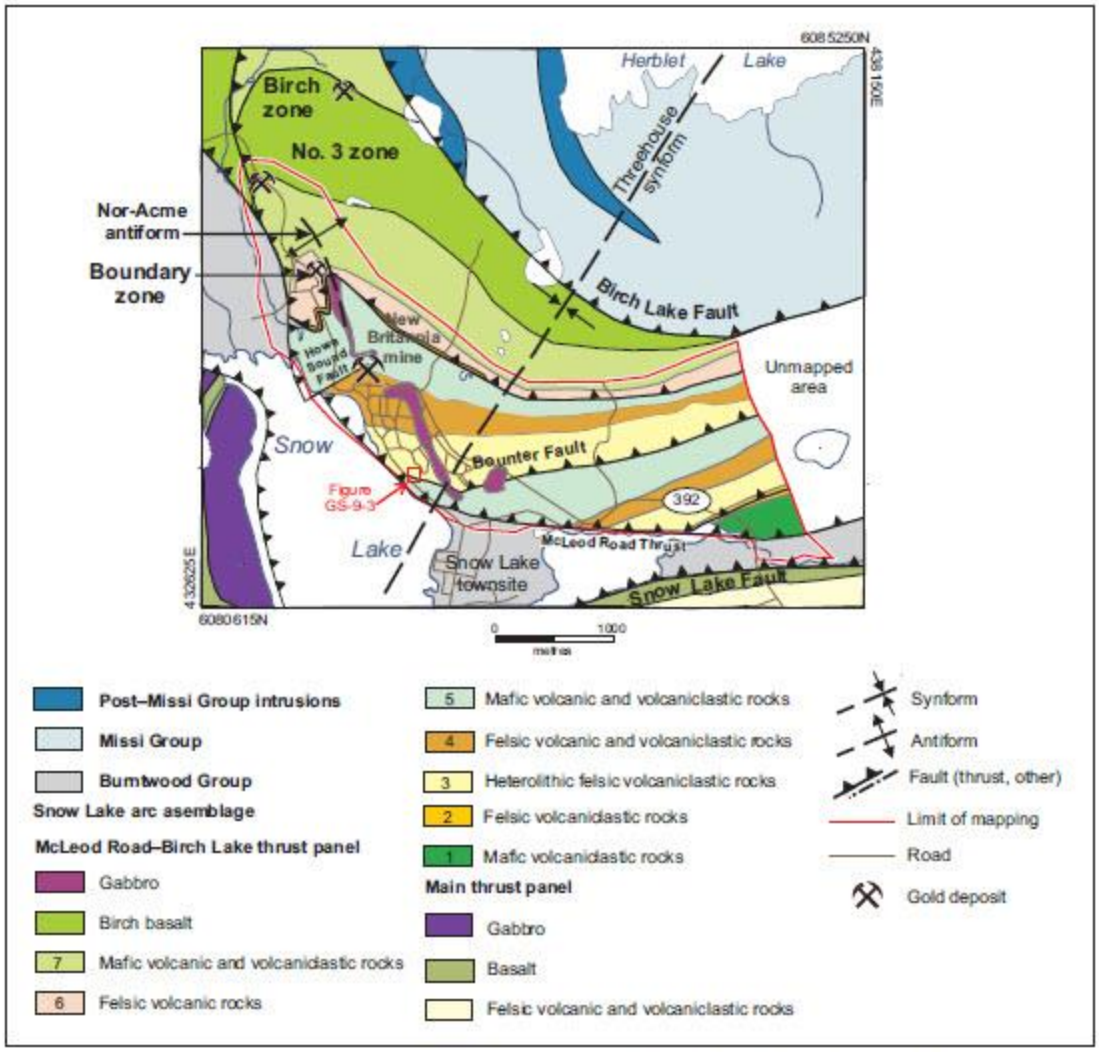

Figure GS-9-2: Simplified lithostratigraphy and structural geology of the McLeod Road–Birch Lake thrust panel, Snow Lake area, west-central Manitoba (modified after Rubingh et al., 2012).

Unit 4: Felsic volcanic and volcaniclastic rocks

Unit 4 was described in Rubingh (2011) as unit 7. This unit was also observed during 2012 mapping, characterized by its plagioclase-phyric composition. It comprises two lithofacies: dominantly plagioclase-phyric (1–5%) rhyolite flows and lesser felsic volcaniclastic rocks. The unit displays flow banding, well-preserved flow lobes, flow-top breccias and local quartz-filled amygdules.

Unit 5: Mafic volcanic and volcaniclastic rocks

Unit 5 was described in Rubingh (2011) separately as units 1, 2, 3 and 8. It comprises dominantly well-bedded, heterolithic, mafic volcaniclastic rocks and minor plagioclase-phyric pillowed flows. Clast composition includes aphyric to plagioclase-phyric mafic, aphyric to plagioclase-phyric felsic, scoriaceous and plagioclase- and pyroxene-phyric mafic. The matrix is crystal rich and comprises pyroxene and plagioclase crystals. Individual lithofacies within unit 5 can be monolithic, but heterolithic clasts are typically observed. Clast size varies from lapilli tuff to lapillistone to tuff breccia.

Unit 6: Felsic volcanic rocks

This unit was previously described in Rubingh (2011) as unit 9. It comprises a single lithofacies: a massive, aphyric, aphanitic rhyolite flow with flow banding and rare quartz-filled amygdules.

Unit 7: Mafic volcanic and volcaniclastic rocks

Unit 7 was described in Rubingh (2011) as unit 10, and it was further mapped in 2012 at the No. 3 zone. It comprises two lithofacies: mafic volcaniclastic rocks and pillowed flows. A distinguishing characteristic of this unit is the coarse pyroxene crystals, which range from 0.5 to 1 cm in diameter. The mafic volcaniclastic rocks vary from lapillistone to tuff breccia, and they are distinct from mafic volcaniclastic rocks of unit 5 because they comprise a pyroxene-plagioclase–phyric crystal matrix with monolithic clasts of a similar composition. The pillowed and massive flows comprise a similar, distinct, coarse-pyroxene-crystal–rich matrix with thin selvages.

Reinterpretation of the MB panel stratigraphy

The lower panel, mapped in 2012, has led to a reinterpretation of the entire panel. There are two distinct sequences of rocks in the MB panel—units 1 and 2 and units 3, 4 and 5—which are interpreted as thrust-repeated packages. Units 6 and 7 do not appear to be repeated within the MB panel. The lower-panel thrust is a different part of the MB panel, with a thrust along the upper contact of unit 2. The upper panel repeats units 3, 4 and 5 along the upper contact of unit 5 (Figure GS-9-2; Rubingh et al., 2012).

In the town of Snow Lake, a structural repetition of the Burntwood Group turbidites has been identified at the base of unit 3 (Figures GS-9-2, -3). This is interpreted as the repeated contact of the MRT. The contact is continuous along strike and was previously interpreted as the Bounter Fault (Galley et al., 1991; Fieldhouse, 1999), a series of anastomosing shears associated with the Bounter occurrences that were considered either as a splay of the MRT or to be truncated by the MRT. There is also

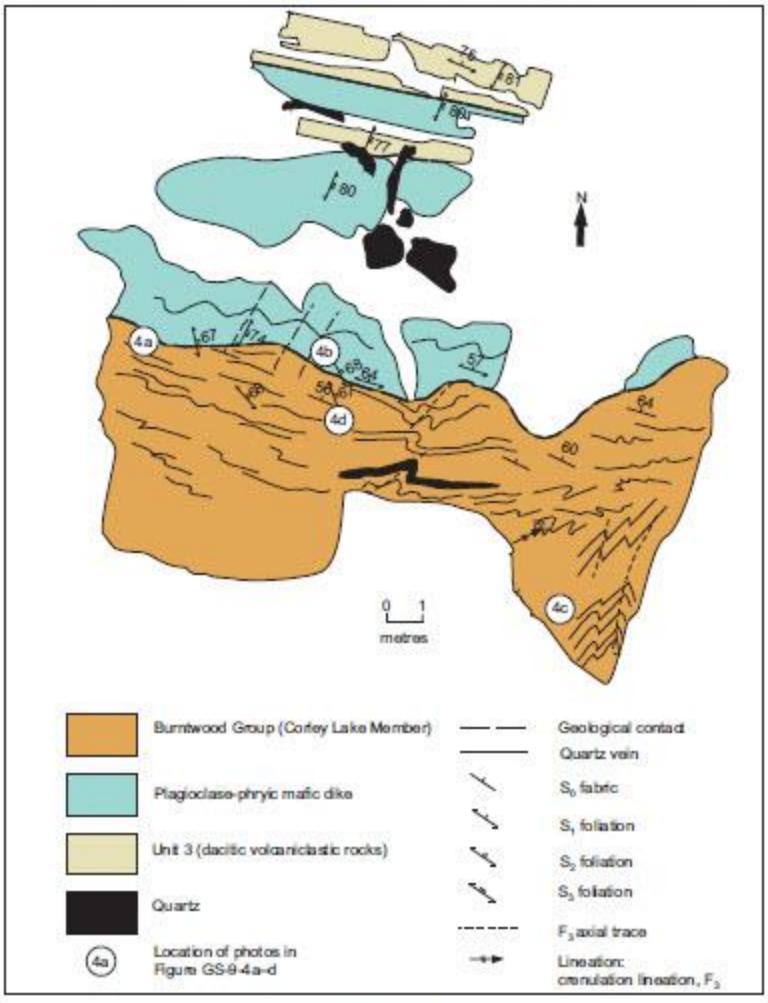

Figure GS-9-3: Sketch map of the contact of the McLeod Road Thrust and the unit 3 dacitic volcaniclastic rocks intruded by an early mafic dike, Snow Lake area, west-central Manitoba.

evidence to suggest that unit 4 is repeated above unit 5, in the mine horizon, as a result of a potential thrust repeating unit 4 at the base of unit 6 (Figure GS-9-2).

Structural geology

Previous authors have described four main deformational events in the Snow Lake area (Kraus, 1998; Kraus and Williams, 1999). Three deformational events (D_1–D_3) are recognized in this study, and their relationship to the previous interpretations by Kraus and Williams (1999) and Beaumont-Smith and Lavigne (2008) is presented in Table GS-9-1. The deformational events described by Kraus and Williams (1999) have been simplified into D_1–D_3 events for correlation between authors. Previously, the main fabric identified in the MB panel was interpreted as an S_2 fabric, whereas this study presents this main foliation as S_1, which is not correlative with a macroscopic S_2 foliation in the Burntwood. The main fabric in the Burntwood (S_2) is related to an S_2 cleavage that is a pervasive fabric observed in the MB panel. The S_1 fabric elements identified in this study correlate with those of Kraus and Williams (1999), Beaumont-Smith and Lavigne (2008) and Gagné (2009).

D_1 deformation

This deformation is attributed to south- to southwest-directed thrusting of the MRT, causing early thrust imbrication and formation of the Nor-Acme fold, a drag fold related to thrusting. In the MB panel, the oldest planar fabric attributed to D_1 deformation is the S_1 foliation, defined by flattening of the clasts. The clasts also have a strong stretching lineation (L_1) that plunges moderately to the northeast. The S_1 fabric is related to thrusting along the MRT; the early thrust repetitions, which appear to be truncated by the MRT and may represent an earlier thrusting event, are included as a D_1 deformational event in this report for simplification. A change in orientation of S_1 is documented through the town of Snow Lake, and it is observed that the S_1 fabric rotates and becomes parallel to the MRT. The S_1 fabric is axial planar to the Nor-Acme fold, and displays a counter-clockwise relationship to bedding on the west limb and a clockwise relationship to bedding on the east limb. The Nor-Acme fold is a macroscopic F_1 fold defined by the folding of units 7, 8 and 9. The S-asymmetric drag folds observed along the bedding-parallel contact of the Howe Sound Fault are due to rotation of the S_1 fabric into parallelism with the fault. However, the Howe Sound Fault is interpreted to be a late D_1 structure due to the overprinting relationship of the S_2 fabric.

D_2 deformation

The second deformation event (D_2) has been interpreted in this study to represent sinistral reactivation of the MRT. The S_2 fabric in the MB panel is correlated with the S_2 fabric in the Burntwood Group (Table GS-9-1). In the volcanic rocks, S_2 is a moderately defined northwest- to north-northeast-trending, moderately northeast- to east-dipping, penetrative spaced cleavage, defined by the alignment of hornblende in mafic rocks and biotite in felsic rocks. No macroscopic folds in the MB panel

Table GS-9-1: Comparison of the interpretation by several authors of deformation events in the McLeod Road–Birch Lake thrust panel, Snow Lake area, west-central Manitoba. Bold face indicates principal known structures in each deformational event.

Kraus and Williams (1999)	Beaumont-Smith and Lavigne (2008)	This study (2012)
D_3: macroscopic north-northeast-trending **Threehouse synform** (F_3 fold); chevron folds; S_3 spaced fracture cleavage	D_3: macroscopic northeast-trending **Threehouse synform** (F_3 fold); S_3 fabric is a weak to penetrative axial-planar foliation and spaced fracture cleavage	D_3: macroscopic northeast-trending **Threehouse synform** (F_3 fold); S_3 fabric is a northeast- to east-northeast-trending, steeply dipping, axial-planar, weakly spaced fracture cleavage
D_2: F_2 isoclinal south-verging folds (**Nor Acme**); S_2 is a weakly spaced, differentiated foliation and alignment of staurolite porphyroblasts; **McLeod Road Thrust Fault** is a north- to northeast-trending, moderately dipping, F_2 thrust fault with a down-dip stretching lineation and sinistral, transcurrent shear-sense indicators that indicate oblique slip	D_2: shallow to moderately inclined, open to close, northeast-trending F_2 folds (**Nor-Acme**); axial-planar S_2 foliation; S_2 is a north-dipping, penetrative, slaty to spaced cleavage; **McLeod Road Thrust Fault** is north- to northeast-trending and moderately dipping with a down-dip stretching lineation and sinistral, transcurrent shear-sense indicators that indicate oblique slip	D_2: S_2 in volcanic rocks is defined by hornblende mineral alignment as a northwest- to north-northeast-trending spaced cleavage, clockwise of S_1/S_0; it is associated with south-trending, asymmetric, northeast-plunging, shallowly inclined F_2 folds; S_2 fabric in the Burntwood Group is a spaced cleavage defined by biotite and aligned staurolite
D_1: **F_1 isoclinal south-verging folds**; S_1 is a mesoscopic pervasive fabric; microlithons in staurolite porphyroblasts	D_1: **isoclinal folds**; S_1 is a rarely preserved, layer-parallel fabric adjacent to stratigraphic contacts	D_1: **McLeod Road Thrust Fault**; Howe Sound Fault; F_1 **Nor-Acme fold**; axial-planar S_1 foliation defined by flattening of the clasts; early thrust repetition pre–McLeod Road Thrust Fault

have been identified as being related to D_2 deformation. The mineral lineation (L_2) is rarely observed and it trends north-northeast to east, which is similar to the orientation observed due to the stretching lineation (L_1) of the clasts. The S_2 fabric of the MB panel displays a clockwise relationship to S_1; it overprints the Howe Sound Fault, the MRT and the Nor-Acme anticline. Figures GS-9-3 and -4a both show the contact of the Burntwood Group with a mafic dike, which intruded the inferred MRT contact. The S_2 fabric in the Burntwood Group is post D_1 (Figure GS-9-4d), it clearly overprints the MRT (D_1 thrust) contact (Figure GS-9-3).

Previously identified sinistral transcurrent shear-sense indicators (Table GS-9-1) are interpreted to be related to thrust imbrication of the panel during D_2. In this study, the S_2 fabric in the Burntwood Group undergoes a counter-clockwise rotation as it approaches the MRT; however, it is observed to transect the MRT at an angle of >30° and is therefore not related to initial thrust imbrication of the panel. This S_2 fabric is characterized by S-asymmetric F_2 folds with axial planes parallel to the regional S_2 fabric in the Burntwood Group. Therefore, the S_2 fabric in the MB panel may be related to sinistral reactivation of the MRT.

D_3 deformation

It is rare to observe S_1, S_2 and S_3 together, as the S_3 fabric is weakly developed; however, it is recognized in the hinge of the Threehouse syncline at the contact between unit 4 dacitic volcaniclastic rocks and the MRT (Figures GS-9-3, -4b). The S_3 fabric is a moderate, northeast- to east-northeast-trending, steeply southeast-dipping, spaced fracture cleavage. It is parallel to the axial planes of Z-asymmetric folds, which fold the S_0/S_1 fabric (Figure GS-9-4c); these folds lack a true axial-planar S_3 cleavage. However, a moderate to strong, S_3 penetrative fracture cleavage is observed in dacitic volcaniclastic rocks (unit 4) and in the mafic dike (Figure GS-9-4b).

Gold mineralization

The characteristic features of gold mineralization at the New Britannia mine are consistent across all the deposits. Mineralization is localized at the hinge of the Nor-Acme F_1 fold between two different lithological units, and gold is associated with quartz–albite–iron carbonate veins and fine-grained acicular arsenopyrite (Fieldhouse, 1999; this study). The association with quartz veins is most significant at the No. 3 zone (Figure GS-9-5), where mineralization is associated with a main shear vein and numerous ladder veins at the folded contact between coarse pyroxene mafic volcaniclastic rocks (Figure GS-9-4f) of unit 10 and plagioclase-phyric pillowed flows of the Birch Lake basalt. The No. 3 zone has two surface exposures that show the changing orientation of the main shear structure: in the portal area and at the main quartz-vein showing. The portal area displays a main west-northwest- to northwest-trending shear, whereas the main quartz-vein area shows the shear vein striking due west.

The crosscutting relationships of different structures and fabric elements in the area of the No. 3 zone portal are shown in Figure GS-9-5. Bedding is defined by the normal grading of clasts, which defines bed sets 1–2 m thick (Figure GS-9-4e). The facing direction is weakly defined as north, based on weak normal grading. Beds are folded with an S_1 axial-planar fabric, defined by the flattening of the clasts, but there is no associated penetrative foliation (Figure GS-9-4g). The S_1 fabric is also axial planar to folded, gold-bearing, quartz–albite–iron carbonate veins, indicating mineralization associated with D_1. Counter-clockwise rotation of the clasts into the main west-northwest- to northwest-trending shear fracture indicates sinistral movement. The overprinting relationship between S_2 and the rotation of S_1 into the main shear fracture constrains the timing of the shear fracture to either late D_1 or early D_2 (Figure GS-9-4h).

The S_3 fabric is a steep north-northeast-trending fracture cleavage, which is observed to cut the shear zone and overprint all fabric elements. North-trending shears are associated with the S_3 fabric. East-trending tension gashes, and small-amplitude folds (some of which display Z-asymmetry) with their axial planes parallel to the north-trending shears, are also associated with D_3. The D_3 fabric elements may therefore reorient structures associated with the mineralization. The main vein area of the No. 3 zone exhibits several generations of veins and, on an outcrop scale, the S_1 and S_2 fabrics are both rotated into parallelism with the main shear fracture, indicating a D_2 timing for mineralization.

Discussion

Stratigraphic and structural analysis has redefined the structural history of the MB panel, and early thrust imbrications have been identified in both upper and lower panels. The correlation of these repeated units will be tested using geochemistry to validate this argument. Thrust imbrication of the panel appears to be coincident with thrusting during D_1 deformation and a pervasive S_1 fabric, which is parallel to the MRT and axial planar to the Nor-Acme fold. Movement along the MRT appears to have been reactivated during D_2 southwest-directed thrusting. During D_3, there was an apparent dextral component, as observed by brittle offset of quartz veins at the No. 3 zone and dextral folds at the No. 3 zone portal. Mapping of the No. 3 zone has implications for the timing of gold mineralization, appearing to constrain gold emplacement to late D_1 or syn-D_2 deformation events.

Economic considerations

Gold mineralization at the Snow Lake mine is structurally controlled its spatial occurrence with the hangingwall

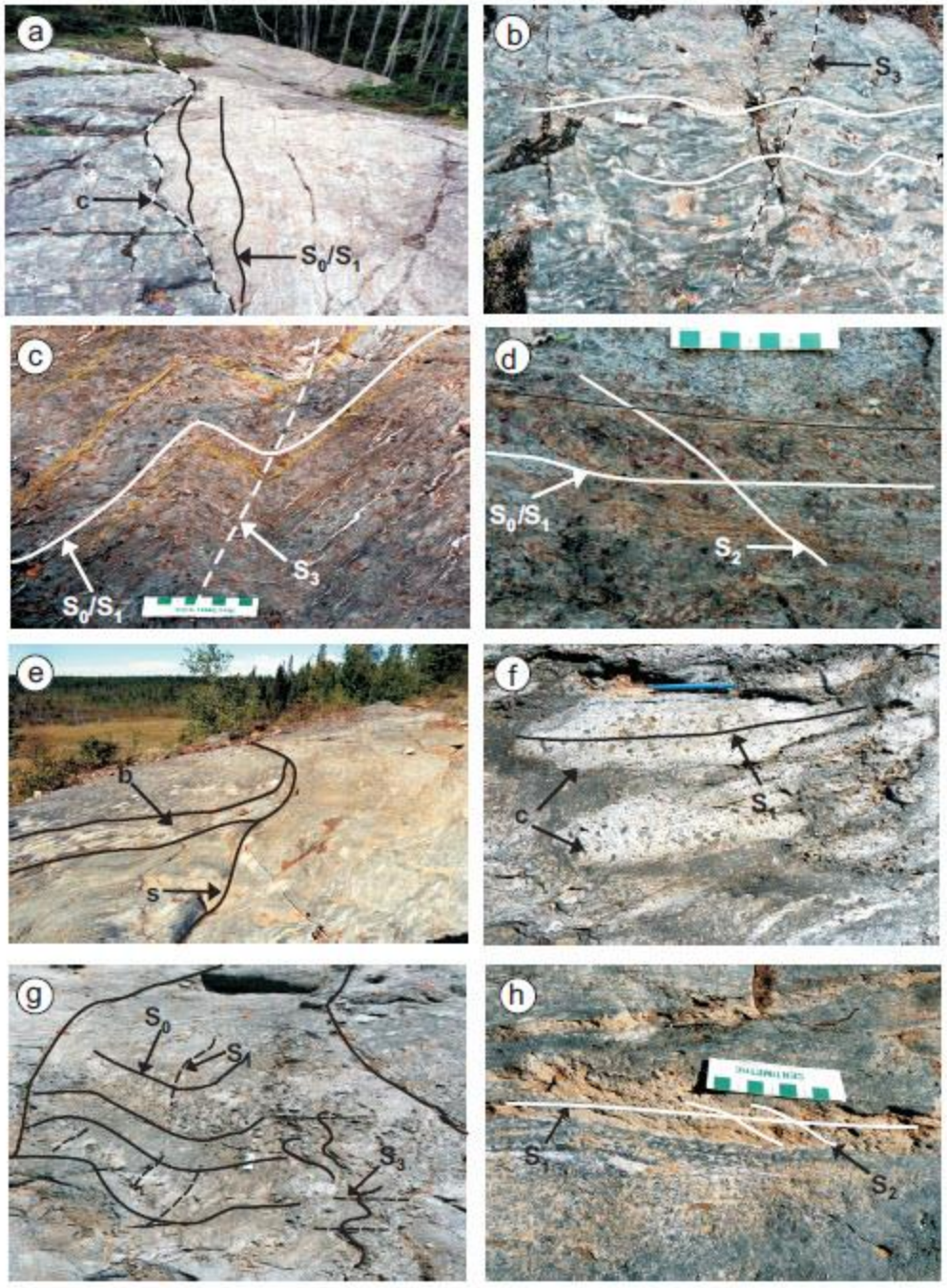

Figure GS-9-4: Structural features and fabrics on the contact between the McLeod Road Thrust (MRT) and the dacitic volcaniclastic rocks (a–d) and at the No. 3 zone portal (e–h), Snow Lake area, west-central Manitoba: a) bedding and S_1 (microscopic fabric preserved in microlithons) are truncated along the MRT contact (c) by an early mafic dike; b) F_3 open folds fold the mafic dike, as indicated by the axial plane of the S_3 fabric; c) S_0/S_1 fabric is folded during D_3, producing Z-asymmetric F_3 folds; d) S_2 fabric overprinting S_0/S_1 fabrics, close to the MRT contact, e) main shear fracture(s), which offsets bedding (b); orange flags are at 1 m intervals), f) flattening of pyroxene-phyric Threehouse volcaniclastic clasts (c) defines S_1 foliation; g) S_0 defines bedding being folded with S_1 axial plane; S_3 axial planes indicate small tight F_3 folds; h) S_2 cleavage overprints S_1 fabric parallel to margins of an iron-carbonate vein.

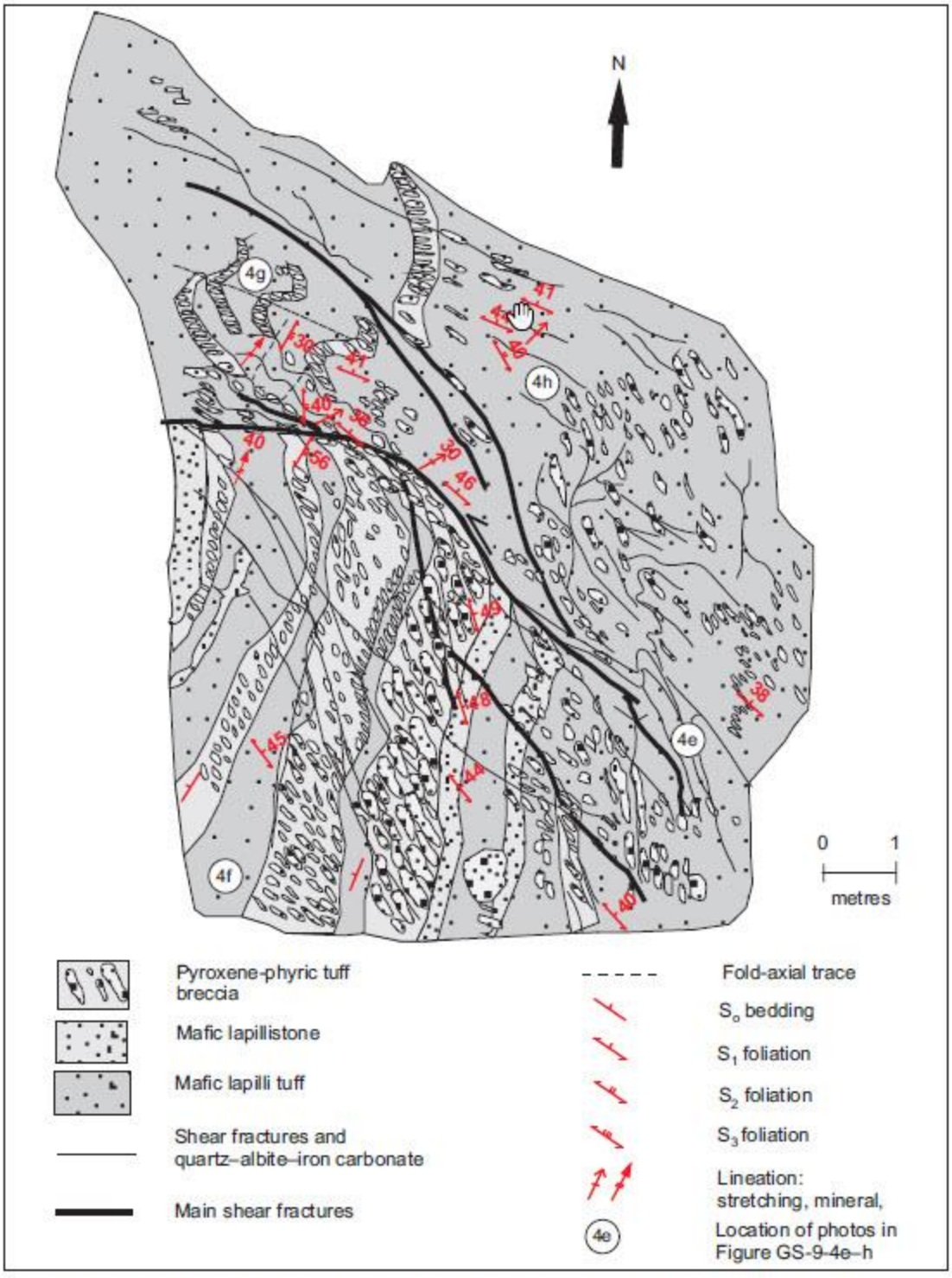

Figure GS-9-5: Sketch map of the No. 3 zone portal, Snow Lake area, west-central Manitoba.

of the MRT, and its consistent relationship with lithological contacts and secondary fault structures at fold hinges, is well defined. Improved understanding of the volcanic stratigraphy and structural history of the MB panel has identified early structural repetition within the panel, identified new thrust faults and highlights the importance of another fault, the Bounter Fault, which appears to offset the MRT. This structure is related to known mineralization at the Bounter occurrence along strike. Mineralization appears to be related in time to early D_1 thrust movement and was possibly reactivated during D_2. Further understanding of the internal geometry of the MB panel and identification of major structural breaks will help in developing new guidelines for gold exploration at a property scale.

Acknowledgments

Funding for this field season was generously provided by QMX Gold Corporation, the Manitoba Geological Survey and Laurentian University. The first author thanks B. Lafrance, H. Gibson, S. Gagné, A. Bailes, field assistant E. Reimer and the staff at QMX Gold Corporation for their support and invaluable discussions during the 2012 field season.

References

Bailes, A.H. and Galley, A.G. 1996: Setting of Paleoproterozoic volcanic-hosted massive base metal sulphide deposits, Snow Lake, Manitoba; *in* EXTECH I: A Multidisciplinary Approach to Massive Sulphide Research in the Rusty Lake–Snow Lake Greenstone Belts, Manitoba, G.F. Bonham-Carter, A.G. Galley and G.E.M. Hall (ed.), Geological Survey of Canada, Bulletin 426, p. 105–138.

Bailes, A.H. and Galley, A.G. 1999: Evolution of the Paleoproterozoic Snow Lake arc assemblage and geodynamic setting for associated volcanic-hosted massive sulphide deposits, Flin Flon Belt, Manitoba, Canada; Canadian Journal of Earth Sciences, v. 36, p. 1789–1805.

Bailes, A.H. and Galley, A.G. 2007: Geology of the Chisel–Anderson lakes area, Snow Lake, Manitoba (NTS areas 63K16SW and west half of 63K13SE); Manitoba Science, Technology, Energy and Mines, Manitoba Geological Survey, Geoscientific Map MAP2007-1, scale 1:20 000.

Bailes, A.H. and Schledewitz, D.C.P. 1998: Geology and geochemistry of the Paleoproterozoic volcanic rocks between the McLeod Road and Birch Lake faults, Snow Lake area, Flin Flon belt (parts of NTS 63K/16 and 63J/13); *in* Report of Activities 1998, Manitoba Energy and Mines, Geological Services, p. 4–13.

Beaumont-Smith, C.J., Gagné, S. 2008: Structural geology of the Snow Lake–Squall Lake area, Manitoba (parts of NTS 63K16, 63J13); Manitoba Science, Technology, Energy and Mines, Manitoba Geological Survey, Preliminary Map PMAP2008-1, scale 1:20 000.

Beaumont-Smith, C.J. and Lavigne, J. 2008: Structural geology and gold metallogenesis of the New Britannia mine area, Snow Lake, Manitoba (NTS 63K16); *in* Report of Activities 2008, Manitoba Science, Technology, Energy and Mines, Manitoba Geological Survey, p. 7–17.

Connors, K.A., Ansdell, K.M. and Lucas, S.B. 1996: Coeval sedimentation, magmatism, and fold-thrust development in the Trans-Hudson Orogen: propagation of deformation into an active continental arc setting, Wekusko Lake area, Manitoba; Canadian Journal of Earth Sciences, v. 36, p. 275–291.

Fieldhouse, I. 1999: Geological setting of gold mineralization in the vicinity of the New Britannia mine, Snow Lake, Manitoba; M.Sc. thesis, University of Manitoba, Winnipeg, Manitoba, 136 p.

Fulton, P.J. 1999: Distribution of gold mineralization at the New Britannia mine in Snow Lake, Manitoba: implications for exploration and processing; M.Sc. thesis, University of Manitoba, Winnipeg, Manitoba, 207 p.

Gagné, S. 2009: Geological investigation of the McLeod Road–Birch Lake allochthon east of Snow Lake, Manitoba (part of NTS 63J13); *in* Report of Activities 2009, Manitoba Energy and Mines, Geological Services, p. 58–68.

Gale, G.H. 2002: Geology of the New Britannia mine, Snow Lake (NTS 63K16), Manitoba; *in* Report of Activities 2002, Manitoba Industry, Economic Development and Mines, Manitoba Geological Survey, p. 83–86.

Galley, A.G., Bailes, A.H., Syme, E.C., Bleeker, W., Macek, J.J. and Gordon, T.M. 1991: Geology and mineral deposits of the Flin Flon and Thompson belts, Manitoba (Field Trip 10); Geological Survey of Canada, Open File 2165.

Galley, A.G., Franklin, J.M. and Ames, D.E. 1988: Geological setting of gold mineralization, Snow Lake, Manitoba; Geological Survey of Canada, Open File 1700, scale 1:50 000.

Hogg, N. 1957: Nor-Acme mine; *in* Structural Geology of Canadian Ore Deposits, Volume II; Canadian Institute of Mining and Metallurgy, 6th Commonwealth Mining and Metallurgical Congress, p. 262–275.

Kraus, J. 1998: Structural and metamorphic studies in the Snow Lake area, Trans-Hudson Orogen, Manitoba, central Canada; Ph.D. thesis, University of New Brunswick, Fredericton, New Brunswick, 229 p.

Kraus, J. and Menard, T. 1997: A thermal gradient at constant pressure: implications for low- to medium-pressure metamorphism in a compressional tectonic setting, Flin Flon and Kisseynew Domain, Trans-Hudson Orogen, central Canada; The Canadian Mineralogist, v. 35, p. 1117–1136.

Kraus, J. and Williams, P. F. 1999: Structural development of the Snow Lake allochthon and its role in the evolution of the southeastern Trans-Hudson Orogen in Manitoba, central Canada; Canadian Journal of Earth Sciences, v. 36, p. 1881–1899.

Lucas, S.B., Stern, R.A., Syme, E.C., Reilly, B.A. and Thomas, D.J. 1996: Intraoceanic tectonics and the development of continental crust: 1.92–1.84 Ga evolution of the Flin Flon Belt, Canada; Geological Society of America Bulletin, v. 108, p. 602–629.

Rubingh, K.E 2011: Stratigraphy of the McLeod Road–Birch Lake thrust panel, Snow Lake, west-central Manitoba (parts of NTS 63K16 and 63J13); *in* Report of Activities 2011, Manitoba Innovation, Energy and Mines, Manitoba Geological Survey, p. 68–78.

Rubingh, K.E., Lafrance, B., Gibson, H.L. and Gagné, S. 2012: Preliminary lithostratigraphic map of the McLeod Road–Birch Lake thrust panel, Snow Lake, west-central Manitoba (parts of NTS 63K16, 63J13); Manitoba Innovation, Energy and Mines, Manitoba Geological Survey, Preliminary Map PMAP2012-7, 1:5000 scale.

Syme, E.C., Bailes, A.H. and Lucas, S.B. 1996: Tectonic assembly of the Paleoproterozoic Flin Flon belt and setting of VMS deposits; Geological Association of Canada–Mineralogical Association of Canada, Joint Annual Meeting, Winnipeg, Manitoba, May 27–29, 1996, Field Trip Guidebook B1, 131 p.

Zwanzig, H.V. 1999: Structure and stratigraphy of the south flank of the Kisseynew Domain in the Trans-Hudson Orogen, Manitoba: implications for 1.845–1.77 Ga collision tectonics; *in* NATMAP Shield Margin Project, Volume 2, Canadian Journal of Earth Sciences, v. 36, p. 1859–1880.

Appendix C

Appendix C. Rubingh, K.E., Lafrance, B., Gibson, H.L., and Gagné, S. 2012: Preliminary lithostratigraphic map of the McLeod Road-Birch Lake thrust panel, Snow Lake, west-central Manitoba (parts of NTS 63K16, 63J13); Manitoba Innovation, Energy and Mines, Manitoba Geological Survey, Preliminary Map PMAP2012-7, scale 1:5000.

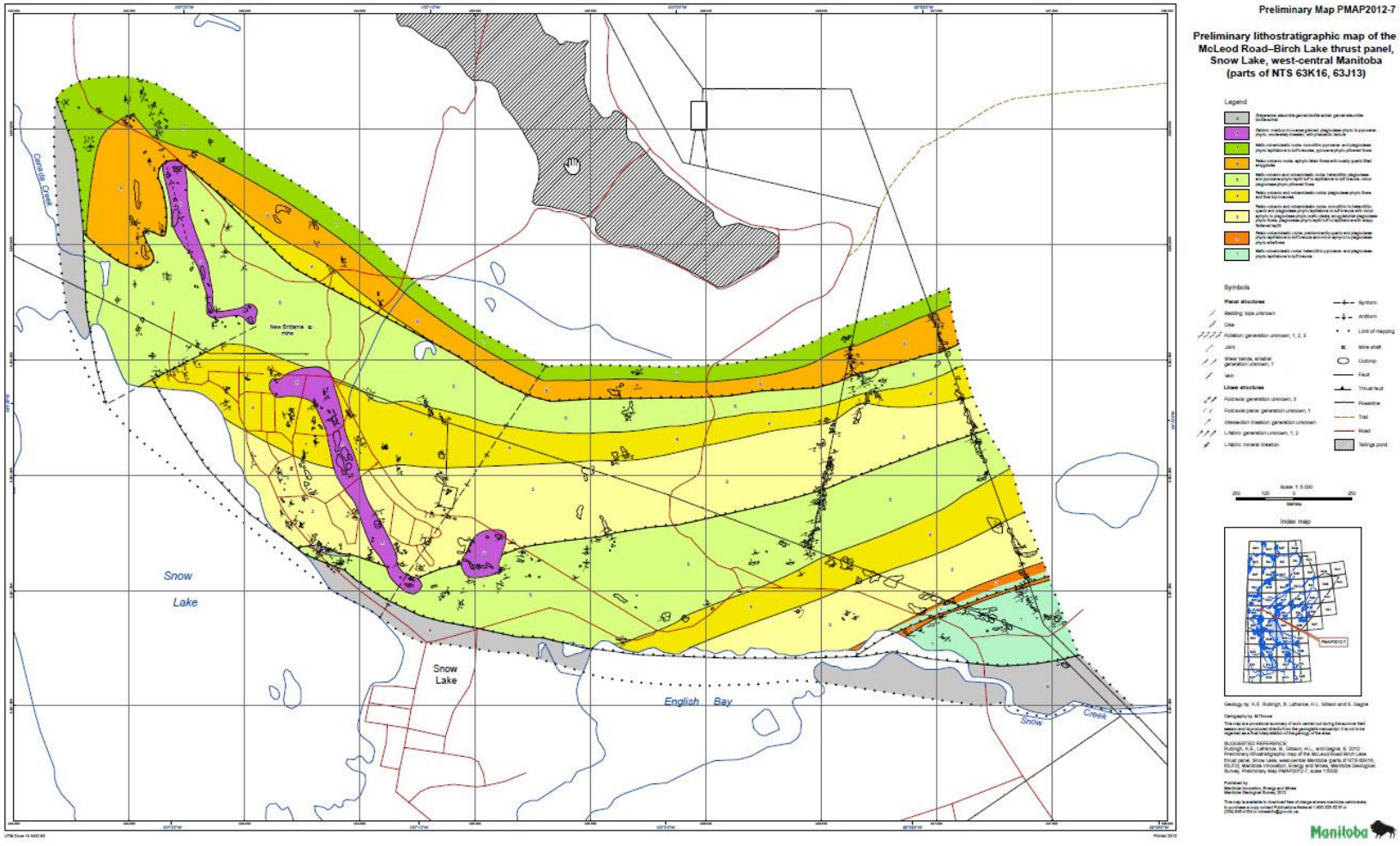
Preliminary Map PMAP2012-7
Preliminary lithostratigraphic map of the McLeod Road–Birch Lake thrust panel, Snow Lake, west-central Manitoba (parts of NTS 63K16, 63J13)
Legend
Symbols
Index map
Snow Lake
Snow Lake
English Bay
Snow Creek
Cantrip Creek
New Britannia mine
Manitoba

Appendix D

Appendix D. Stratigraphy, structural geology and gold mineralization of the McLeod Road-Birch Lake Thrust panel. A field trip prepared for Hudbay Minerals Inc. 2016. by Kate Rubingh

STRATIGRAPHY, STRUCTURAL GEOLOGY AND GOLD MINERALISATION OF THE MCLEOD ROAD-BIRCH LAKE THRUST PANEL

A FIELD TRIP PREPARED FOR HUDBAY MINERALS INC. (GUIDEBOOK IS NOT FOR PUBLIC DISSEMINATION)

KATE RUBINGH
LAURENTIAN UNIVERSITY
935 Ramsey Lake Road, Sudbury, ON

Table of Contents

List of Figures

Regional Geology

Introduction

The Snow Lake area occurs within the eastern portion of the Flin Flon belt, (Figure 1), which is within the internides of the Paleoproterozoic Trans Hudson Orogen. The belt consists of an amalgamation of several tectonic domains that are distinct in terms of geochemistry, metamorphism and structural history (Lucas et al., 1996, Syme et al., 1996). In the Snow Lake area, the deformation was determined to be that of a fold and thrust belt (Connors et al., 1996; Kraus, 1998; Zwanzig, 1999), producing a tectonically imbricated package of volcanic (ca. 1.89Ga) and metasedimentary rocks (ca. 1.84 – 1.86 Ga; Syme et al., 1995; Kraus and Williams, 1999). The Flin Flon belt is renowned for its base metal endowment and contains 29 volcanogenic massive sulphide (VMS) deposits in total (Bailes et al., 2013). The VMS deposits at Snow Lake occur in volcanic and volcaniclastic rocks of the Snow Lake arc assemblage (SLA), which is host to 8 past -producing and 2 producing base metal mines (Figure 2). (Stern et al. 1995; Lucas et al. 1996; Bailes and Galley., 1999). The SLA assemblage is divisible into three sequences, which are interpreted to define an evolution from a primitive arc (Anderson sequence) to a mature arc (Chisel sequence) to an evolved arc-rift environment (Snow Creek sequence; Bailes and Galley, 1996; Bailes, 1997; Bailes and Schledewitz, 1998).

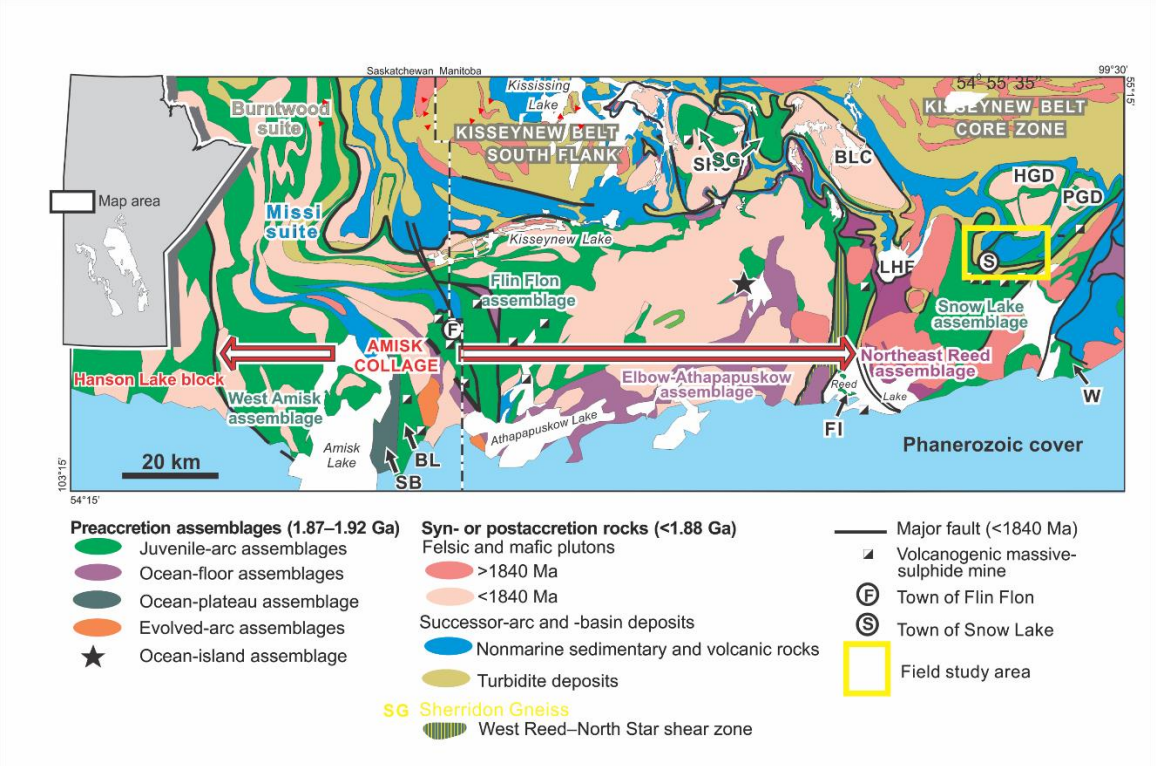

Figure 1: Regional geology of the Flin Flon – Snow Lake belt, of Manitoba (modified after Syme et al., 1995). Abbreviations: BL, Birch Lake; BLC, Batty Lake complex; FI, Fourmile Island; HGD, Herblet Lake gneiss dome; LHF, Loonhead Lake fault; PGD, Pulver gneiss dome; SB, Sandy Bay; SHC, Sherridon- Hutchinson Lake complex; W, Schist-Wekusko assemblage. Inset of Manitoba with location of the map area. Field study area is highlighted by the yellow box.

The mafic and felsic volcanic and volcaniclastic rocks, which lie in a north dipping thrust bounded panel, to the north of the SLA is herein named the McLeod Road – Birch Lake (MB) sequence (Figure 2). Previously the MB sequence was interpreted as a homoclinal, north-facing sequence of mafic and felsic volcanic and volcaniclastic rocks, with no identified internal stratigraphy (Bailes and Schledewitz, 1998;

Bailes and Galley, 1999), bound to the south by the McLeod Road Thrust (MRT), and to the north by the Birch Lake fault (BLF) (Figure 3). The MB sequence is imbricated with the Burntwood group (1.86 – 1.84 Ga) turbidites, and Missi group (1.845 Ga) arkosic sandstones (David et al. 1996).

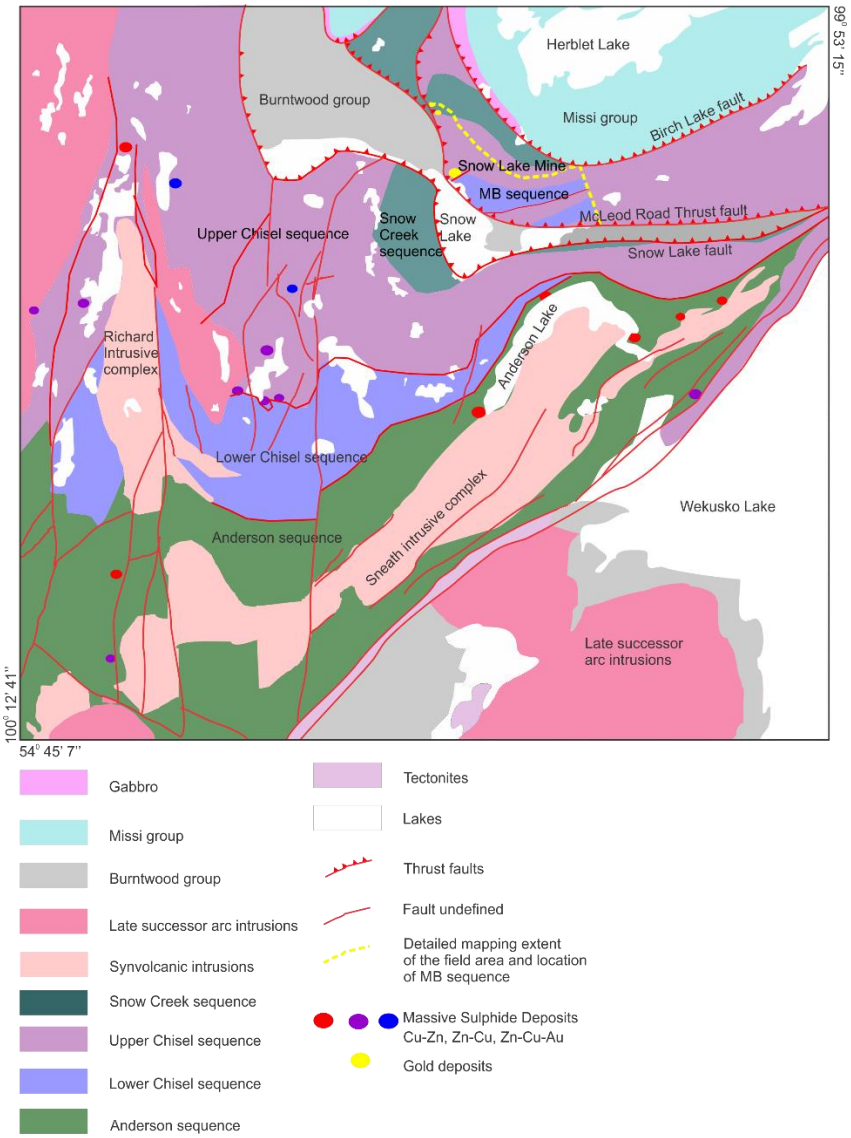

Figure 2: Geology of the Snow Lake arc assemblage and the McLeod Road-Birch Lake sequence, showing the location of the Snow Lake gold mine (New Britannia mine) and volcanogenic massive sulphide (VMS) deposits. Modified after Bailes and Galley (2007).

The MB sequence has no known VMS deposits, but is host to four structurally controlled gold deposits located along stratigraphic contacts at the intersection of a fault and fold hinge in the hanging wall of the MRT (Figure 3). The largest gold deposit, the Nor-Acme, (renamed the Snow Lake Mine by QMX Gold Corporation in 2012), produced 1,404,950 oz. gold (43,699 kg) between 1949–1958 and 1995–2005 (Beaumont Smith and Lavigne, 2008).

This field trip guide reviews the stratigraphy, structure and gold mineralization for the McLeod Road Birch Lake Thrust panel (MB panel). The new stratigraphy for the MB sequence established from 2011 – 2014 field work (Rubingh, K. 2011; Rubingh, et al., 2012; Rubingh, et al., 2013) which was part of a

collaborative research project with NSERC, Laurentian University, the Manitoba Geological Survey, and QMX Gold Corporation.

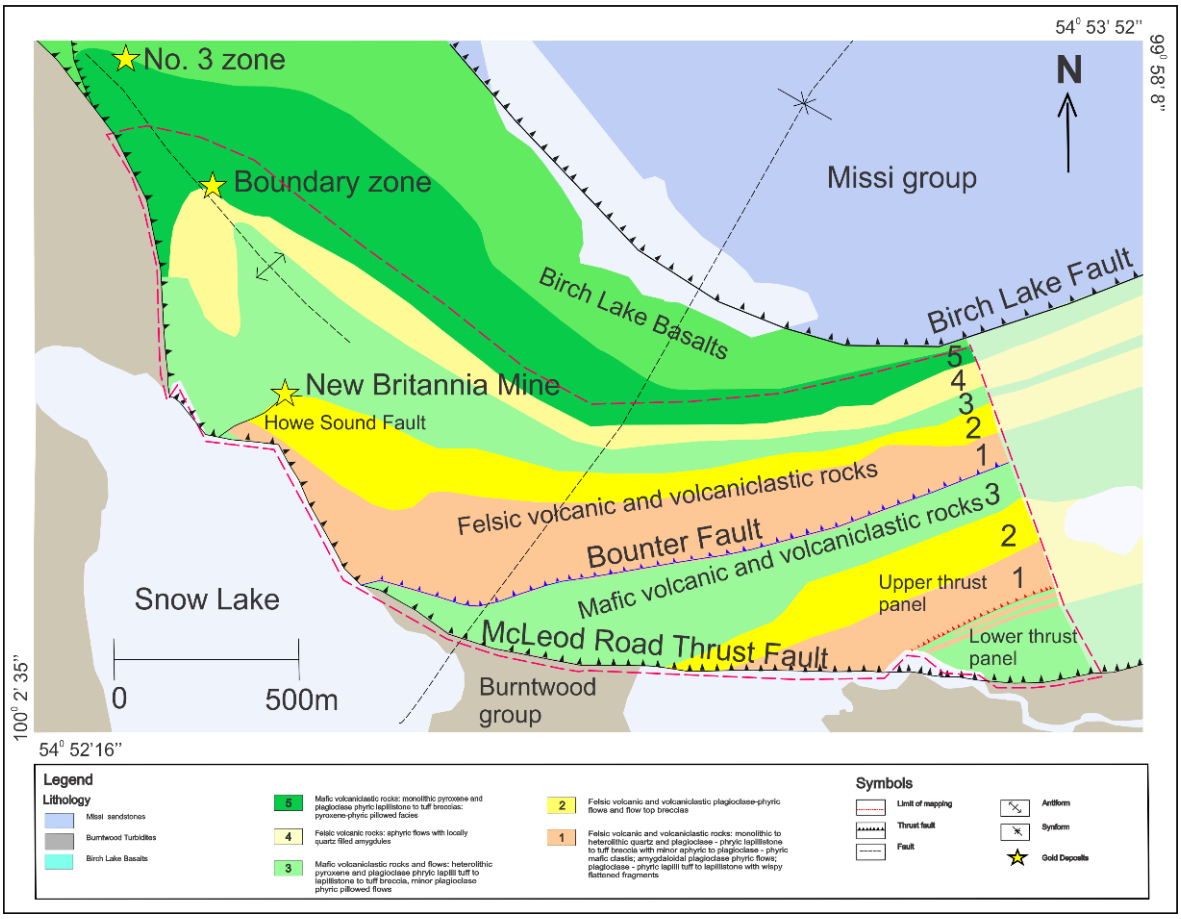

Figure 3: Geology of the McLeod Road-Birch Lake thrust panel, showing the locations of gold deposits (1:7000 scale; modified after Rubingh et al. 2012)

Stratigraphy of the McLeod Road Birch Lake sequence

The newly defined stratigraphy of the MB sequence (Figure 4) has provided a correlation with strata of the Lower and Upper Chisel and Snow Creek sequences of the Snow Lake Arc assemblage. This research has recognized voluminous submarine pyroclastic eruptions and subsidence events, which were previously unrecognized, and which correlate with the thrust-bounded Chisel and MB sequences. In addition, early structures previously unrecognized within the panel have been identified. In combination with detailed structural studies, we have identified early brittle thrust faults which repeat sequences of stratigraphic units and provide evidence for an earlier deformational event for the MB panel that was previously unrecognized.

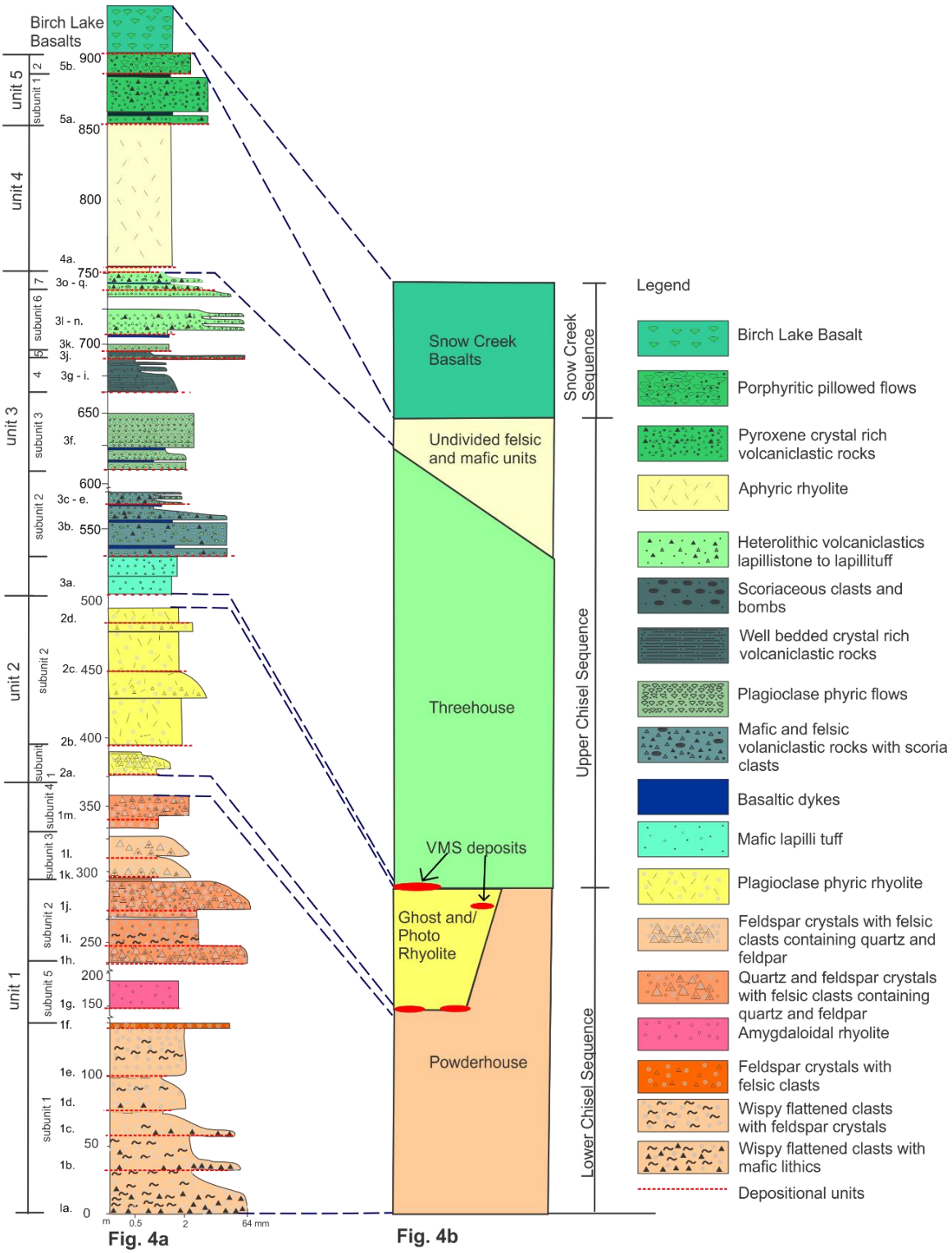

Figure 4 : Stratigraphic column illustrating lithostratigraphic units of the McLeod Road - Birch Lake sequence. The five lithostratigraphic units are denoted with their subunits, and depositional units are outlined by red dashed lines. Black dashed lines indicate interpreted correlation with equivalent stratigraphic unit of the Chisel sequence. (b) Chisel sequence stratigraphy with location of VMS deposits in red, (modified after Bailes and Galley, 2007). The vertical scale is in meters.

The MB sequence contains 5 distinct lithostratigraphic units (Figure 3; Rubingh, 2011, Rubingh et al.

2012a, b). Three of the units are repeated by two bedding-parallel thrust faults, (Figure 3) which subdivides the MB sequence into 3 separate structural panels (Rubingh et al. 2012a, b). The location of the lower thrust fault is inferred by the juxtaposition of unit 1 above younger unit 3. The upper thrust fault, called the Bounter Fault (Hogg, 1957), hosts gold mineralization. It repeats units 1, 2 and 3, which are identical in the two panels separated by the fault, and locally this fault contact is marked by an aphyric sill. A full description of stratigraphic units is provided together with the Traverse that we will complete starting at field trip stop location 5.

Geochemistry of the McLeod Road Birch Lake sequence and a comparison with the Snow Lake Arc Assemblage

The recognition of distinct volcanic units of the MB sequence which compare to those of the Snow Lake arc assemblage based on field observations and geochemistry provides an important correlation of the MB sequence stratigraphy to the SLA. Unit 1 of the MB sequence and the Powderhouse Dacite of the SLA, share consistent physical characteristics. Comparative photos on Figure 8, represent the physical similarity between these two units, such as the ash-rich nature, crystal type and content, and occurrence of the distinctive dark wispy "pumice" fragments (Figure 8, e, f) and mafic lithic clasts, (Figure 8, g, h). On chondrite normalized plots the REE profile (Figure 7a) of the Powderhouse Dacite is similar to that of Unit 1, as both have negative Nb and Ti anomalies and a distinct slightly steeper LREE trend (Figure 7a), compared to the other felsic units 2 and 4, (Figure 7b, c).

Unit 2 and 4 rhyolitic flows are flow banded and have lobes and associated flow breccias, which are similar to those described for the Photo Lake / Ghost / Chisel and un-subdivided rhyolite of the SLA (Bailes, 1996; Bailes and Schledewitz, 1998). Their primitive mantle and chondrite normalized REE profiles are also similar (Figs. 6b, 7b) with both having negative Nb, Ti (Figure 6b) and weak negative Eu anomalies and similar LREE enrichment (Figure 7b) (Bailes and Galley, 1996; Bailes, 1997; Bailes and Galley, 1999). However, rhyolites of the MB sequence do not have a negative Zr anomaly (Figure 6b) and have a higher REE abundance. There is no comparable unit in the Chisel sequence to unit 4, however they may be correlative with the undivided felsic flows of the Chisel sequence, which lie at the same stratigraphic position (Figure 4b).

Mafic volcaniclastic rocks of unit 3 and the Threehouse unit of the Chisel sequence (Figure 4b) are plagioclase and pyroxene crystal-rich (Figure 8a, b), well bedded, and contain scoriaceous and amoeboid fragments and associated bomb sags (Figure 8c, d). Their REE profiles on primitive mantle and chondrite normalized plots (Figure 6d, 7d) are similar and both display negative Nb and Ti anomalies, although unit 3 has a minimal Zr anomaly and has a higher REE abundance. Unit 5 porphyritic basalts are similar to Threehouse basalts, in that they both display negative Nb, Zr, and Ti, anomalies, on primitive mantle normalized plots (Figure 6e; Bailes and Schledewitz, 1998), implying an arc influence in its geochemical profile, and therefore unit 5 is considered to be analogous to the Chisel sequence.

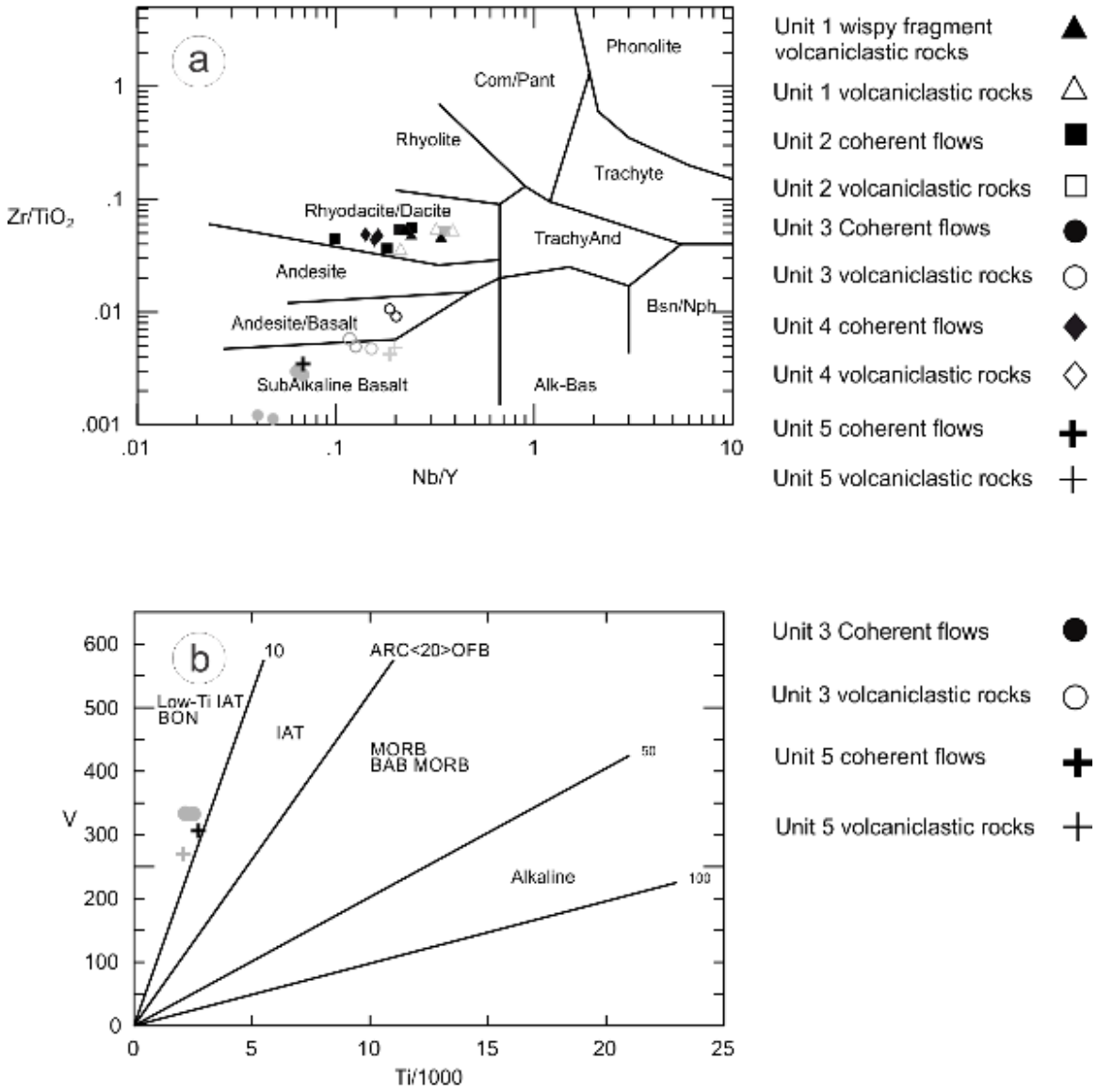

Figure 5: (a) Discrimination diagram to classify the felsic units 1, 2 and 4 and mafic units, 3 and 5 (from Winchester and Floyd, 1974). (b) V vs Ti tectonomagmatic discrimination diagram for mafic units 3 and 5 (from Shervais, 1982). Altered samples, where shown, are denoted in pale grey on all diagrams.

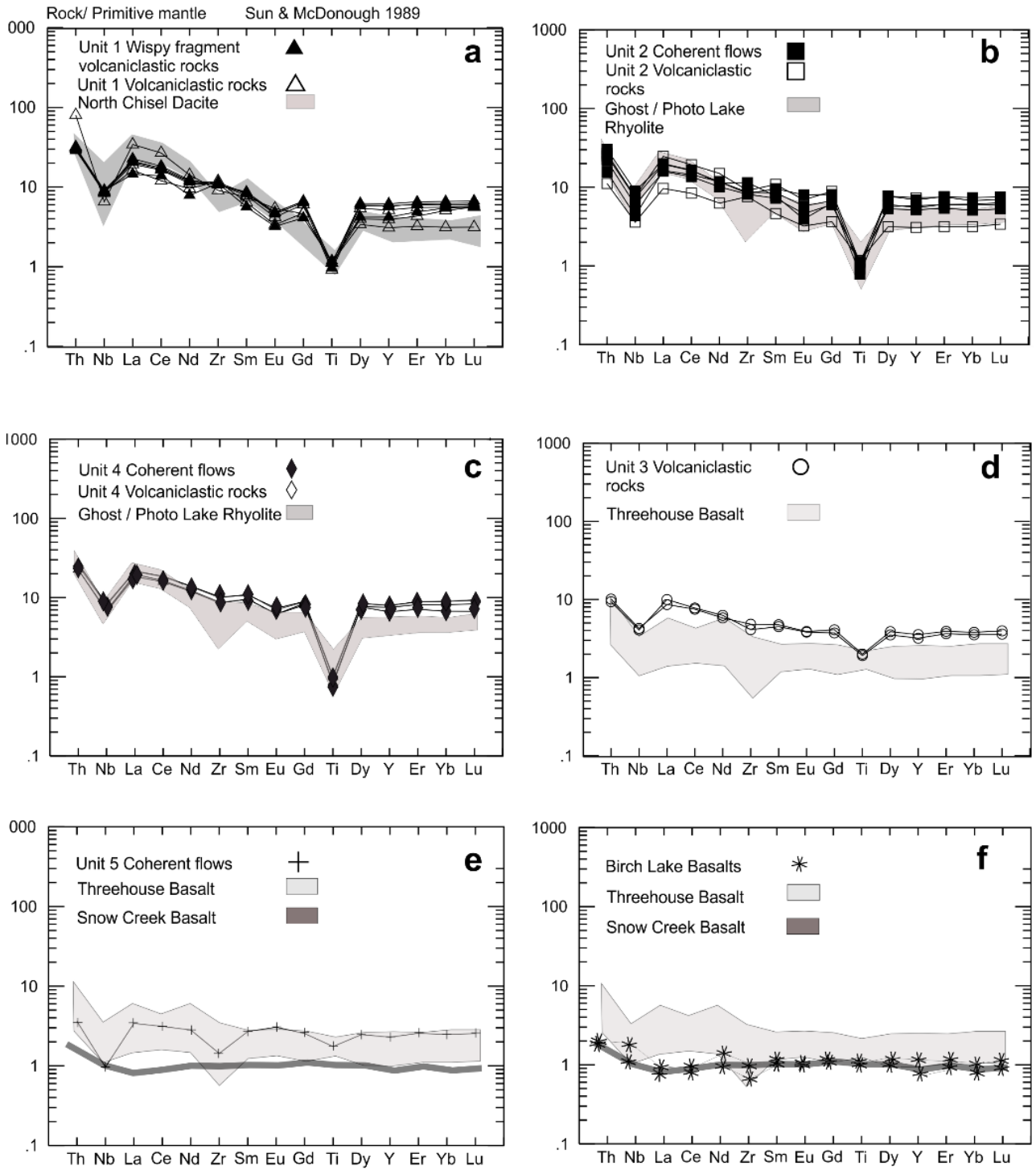

Figure 6: Caption for figure on previous page. Primitive mantle-normalized trace element plots (normalized to values from Sun and McDonough 1989) for all units of the MB sequence. (a) Unit 1 is subdivided to show wispy fragment volcaniclastic rocks and volcaniclastic rocks. (b) Unit 2 coherent lithofacies. (c) Unit 4 coherent and volcaniclastic lithofacies. (d) Unit 3 volcaniclastic lithofacies. (e) Unit 5 coherent lithofacies. (f) Birch Lake Basalts. Units 2,3,4,5 have been subdivided to show samples of coherent flows versus volcaniclastic rocks. Data for mafic and felsic units of the Snow Lake arc assemblage, including the North Chisel Dacite and the Powderhouse unit at Lalor, are from Bailes and Schledewitz (1998) and Bailes (written comm, 2015) and are included for comparison where applicable.

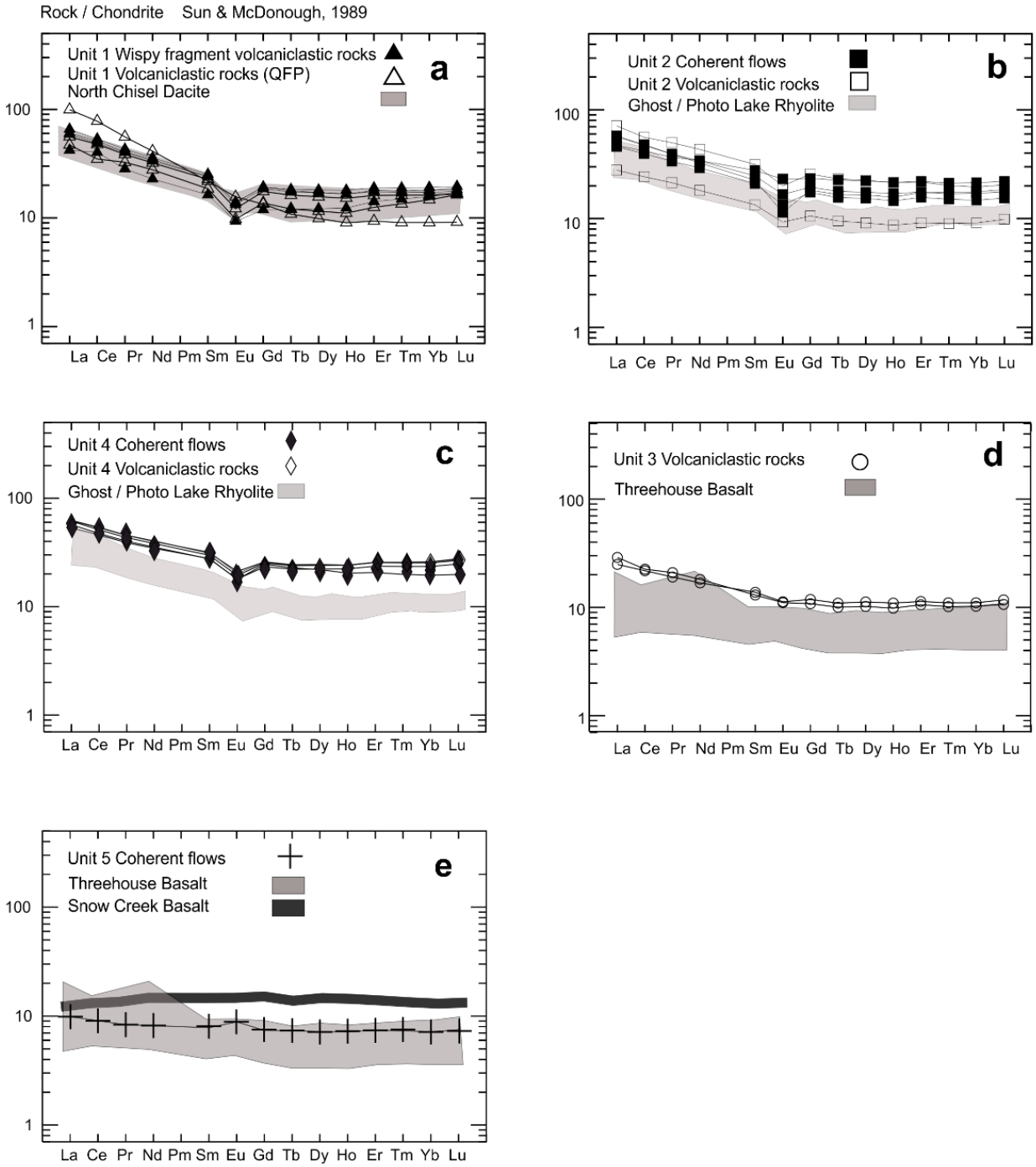

Figure 7: Chondrite normalized trace element plots (normalized to chondrite values from Sun and McDonough 1989) for the MB sequence. (a) Unit 1 is subdivided to differentiate wispy fragment volcaniclastic rocks and volcaniclastic rocks. (b) Unit 2 coherent and volcaniclastic lithofacies. (c) Unit 4 coherent and volcaniclastic lithofacies. (d) Unit 3 volcaniclastic lithofacies. (e) Unit 5 coherent basalt. Data for mafic and felsic units of the Snow Lake arc assemblage, including the North Chisel Dacite and the Powderhouse unit at the Lalor, are from Bailes and Schledewitz (1998) and Bailes (Written comm, 2015) and are included for comparison where applicable.

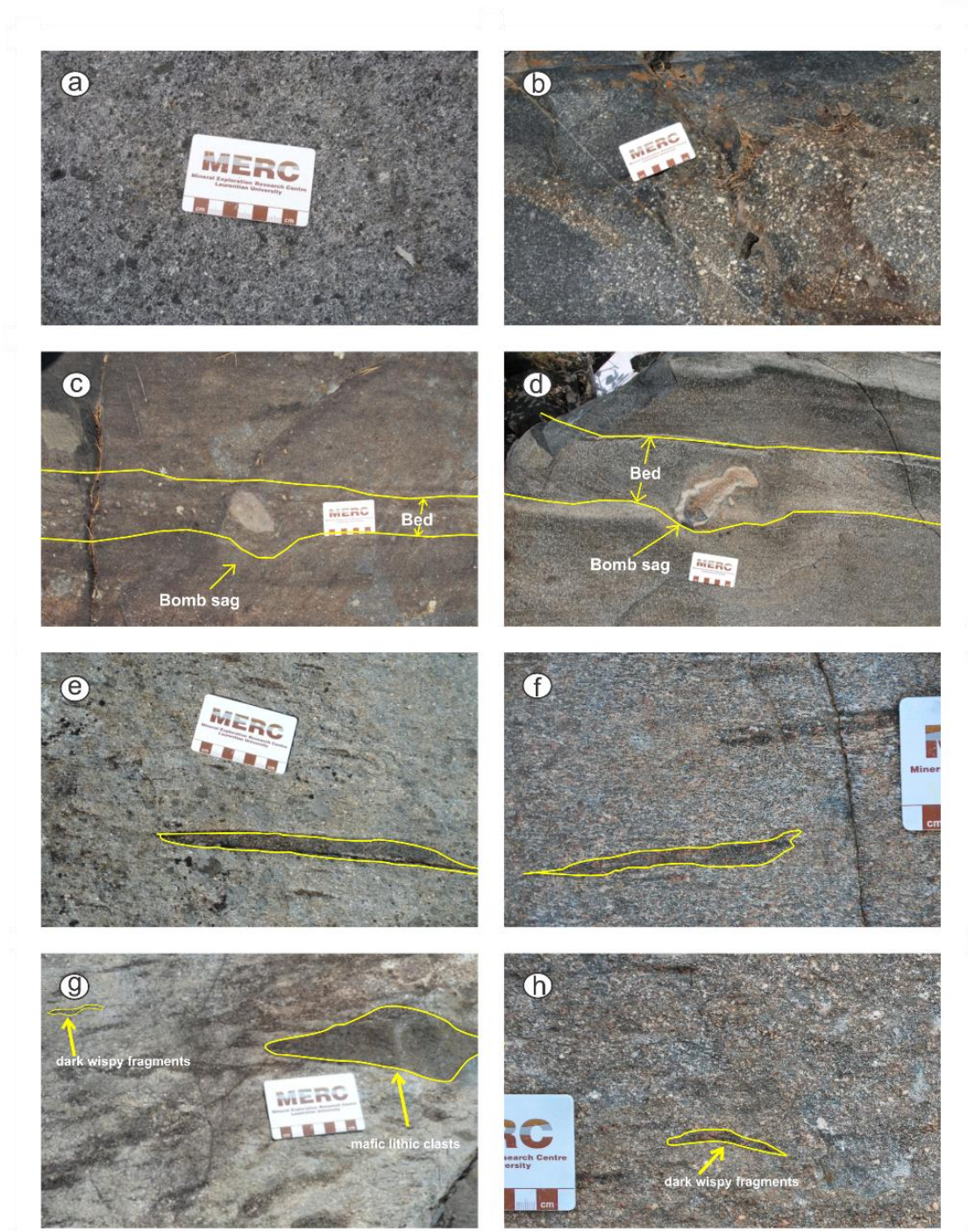

Figure 8: Comparison of features for units in the Chisel sequence and McLeod Road - Birch Lake (MB) sequences. (a) Unit 3: Crystal rich mafic volcaniclastic rocks of the MB sequence. (b) Threehouse mafic volcaniclastic rocks of the Chisel sequence. (c) Unit 3: Well bedded volcaniclastic rocks with bomb sags and draping over the top of the bomb of the MB sequence. (d) Threehouse mafic volcaniclastic rocks of the Chisel sequence with bomb sags. (e) Unit 1 pyroclastic flows of the MB sequence with dark wispy fragments highlighted in yellow. (f) Powderhouse Dacite (Lalor shaft location) showing flattened dark wispy fragments highlighted in yellow. (g) Unit 1 pyroclastic flows, MB sequence, with mafic lithic clasts and dark wispy fragments both highlighted in yellow. (h) Powderhouse Dacite (Lalor shaft location) showing a higher percentage of flattened dark wispy fragments of the Chisel sequence, with one clast highlighted in yellow. (a-h) Scale is denoted by a white 8.5cm scale card.

Structural geology of the McLeod Road Birch Lake sequence

The sequence of deformational events for the MB panel is compared with previous authors' interpretation for the MB panel (Table 1). The main difference in our interpretation is the recognition of early brittle D1 thrust faults, and other early faults which form prior to the MRT (Cleaver Lake and Birch Lake Faults). The S2 cleavage, which was previously interpreted as the main fabric attributed to the MRT fault, has been identified as an overprinting cleavage which results in later reactivation of the MRT. This evidence is supported by observations at the Cleaver Lake fault. At this structure we also observe the effect of shortening during D2 and formation of the S2 overprinting cleavage.

Kraus and Williams (1999)	**Beaumont-Smith and Lavigne (2008)**	**Rubingh, et al., (2016)**
D3 F3 Fold (Macroscopic NNE - trending Threehouse synform) chevron folds., S3 spaced fracture cleavage	**D3** F3 fold (Macroscopic NNE trending Threehouse synform) S3 foliation is weak to penetrative and axial planar foliation and spaced fracture cleavage.	**D3** F4 fold (Macroscopic NNE trending Threehouse synform) S3 foliation is NNE to ENE, steeply dippping, axial planar to z folds, weakly spaced fracture cleavage.
D2 F2 folds (Nor Acme) isoclinal south verging S2 is a weakly spaced differentiated foliation and is assoicated with preferential alignment of staurolite porphyroblast; F2 thrust fault (McLeod Road Thrust Fault, MRT) N to NNE trending, moderately dipping a down dip stretching lineation and sinistral transcurrent shear sense indicators indicate oblique slip. Howe Sound Fault (sinistral offset of the MRT.	**D2** F2 folds (Nor-Acme) shallow to moderately inclined, open to close, NNE trending. Axial planar S2 foliation which is a north dipping, penetrative, slaty to spaced cleavage. F2 thrust fault (MRT), N to NNE trending, moderately dipping, a down dip stretching lineation and sinistral transcurrent shear sense indicators indicate oblique slip) Howe Sound fault (sinistral offset of the MRT).	**D2** **G4** S2 overprinting cleavage, sinistral reactivation of MRT and dextral reactivation of the Cleaver Lake fault. **G3** MRT fault, N to NNE trending fault. F3 folds - Herblet Lake gneiss domes, whitefish bay synform, Herblet Lake fold. **G2** Cleaver Lake Fault, Birch Lake Fault, F2 Mc Leod Lake fold **G1** **F**1 Nor Acme Fold **S1 flattening of the clasts**, L1 stretching lineation, Howe Sound fault forms as an accommodation structure during folding.
D1 F1 isoclinal south verging folds. S1 is preserved as a mesoscopic pervasive fabric as microlithons in staurolite porphyroblasts.	**D1** F1 isoclinal folds S1 is only preserved as a layer parallel fabric at stratigraphic contacts.	**D1** Brittle Faulting / thrusting. Bounter Fault and unnamed fault of the MB panel.

Table 1: Comparison table of deformational events by various authors in the McLeod Road Birch Lake thrust panel.

A new regional structural interpretation for the Snow Lake area

We propose a new hypothesis for the regional interpretation of the Snow Lake area, which may explain

why the stretching lineation and all folds are coaxial with this lineation. Our new interpretation (Table 1), proposes a two prong style collisional event, similar to the interpretation by (Connors, et al., 2002). However, the difference is that we suggest north directing thrusting, as opposed to south west directed thrusting which has been considered for the Snow Lake area by previous authors. (Kraus and Williams, 1999; Connors, 1999; Connors et al., 2002). The south west directed thrusting evidence in the Snow Lake area was based on the movement on the MRT and sinistral transucrrent shear sense indicators, which were previously interpreted to indicate south west thrusting. However, based on our structural analysis these shear sense indicators are attributed to a later reactivation along the MRT. Evidence for early north directed has been indicated at Flin Flon and in the File Lake area (Zwanzig, 1999; Zwanzig, 2010). The north directed thrusting we consider to be a long lived progressive deformational event during D1 and D2 (Table 1) that began with thrusting of the Snow Lake volcanic rocks to the north above the Kisseynew basin, at the same time as the Superior craton was colliding with the Sask craton. During north-directed thrusting, the Snow Lake Belt would be moving in a dextral sense with respect to the Superior. Therefore, later during the same deformation the McLeod Road Thrust and the Cleaver Lake fault are overprinted by (S2). Due to their different orientations, the McLeod Road Thrust shows sinistral reactivation and the Cleaver Lake Fault is reactivated as a normal fault, with a dextral strike slip offset. This provides one hypothesis to explain why S2 contains the stretching lineation and the folds are coaxial to the stretching lineation. They are possibly all part of the same deformation event but during a two prong collision.

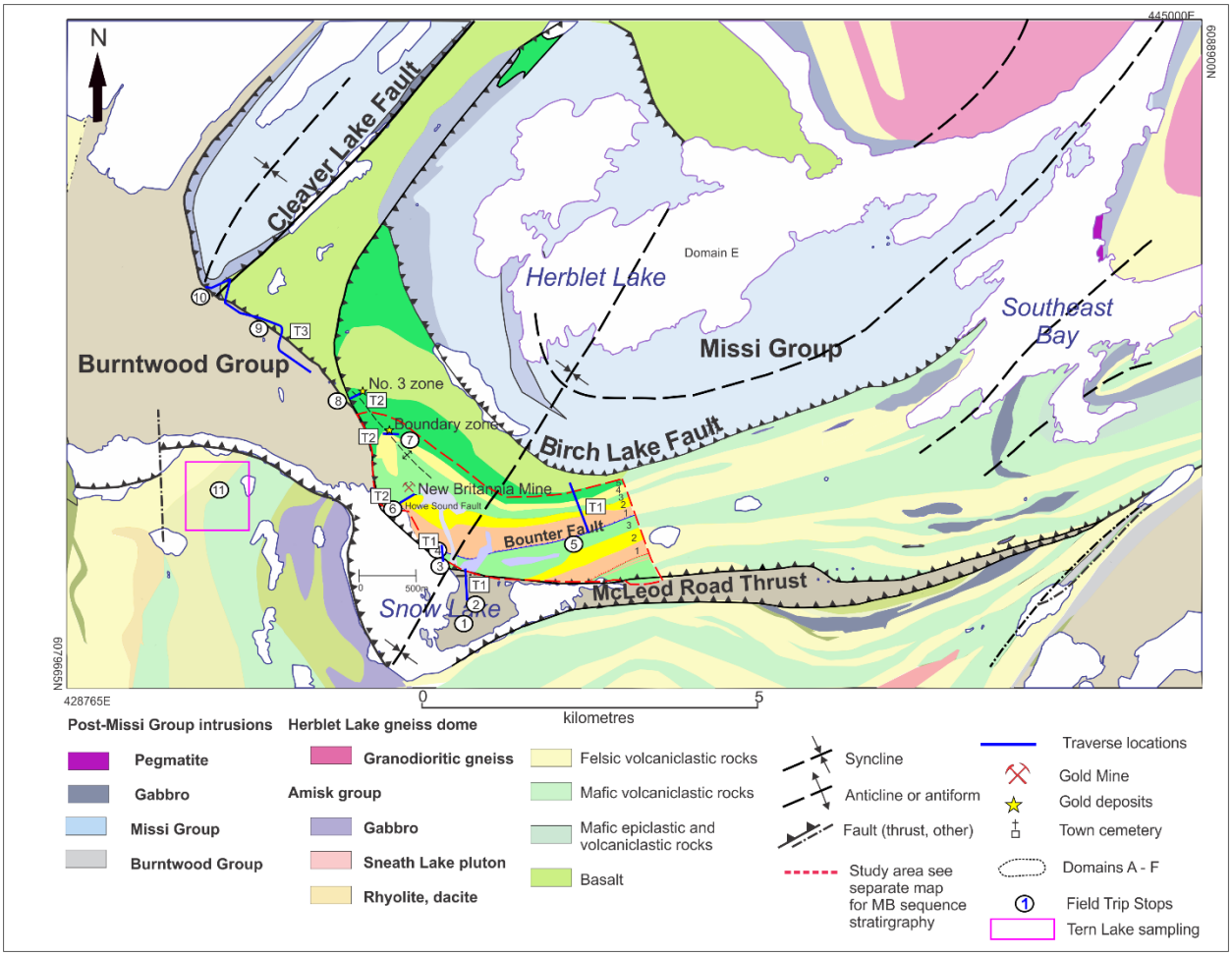

Figure 9: Map to show traverse locations for stops 1- 9 of the McLeod Road Birch Lake Thrust panel and Stop 11 which is part of a separate attachment for the Tern Lake sampling on Day 3.

Field trip stops June 15 – June 17 2016

The purpose of this field trip guide is to present the recent work on the structures and stratigraphy of the MB panel and provide a framework for understanding the gold mineralisation at the New Britannia Mine and on other properties within the MB sequence, and potentially further exploration within the MB panel.

Day 1

The Burntwood group (*ca*. 1.85-1.83 Ga) represented here in the Town of Snow Lake are well bedded greywacke-siltstone-mudstone meta-turbidites, characterised by the metamorphic mineral assemblage, garnet, biotite and staurolite. These meta-turbidites they post-date the 1.88-1.87 Ga intra-oceanic accretion of the Snow Lake Arc assemblage to the Amisk Collage and are imbricated within the Snow Lake arc assemblage volcanic rocks, along thrust faults. They provide a useful framework to present the structural and stratigraphic interpretation for the MB panel, as they record the primary sedimentary characteristics and preserve structural and metamorphic features, which have been well studied and documented by the work of Jurgen Kraus, (Kraus, 1998). The purpose of visiting these stops in the Burntwood group is to review the characteristics, structure and alteration of the Burntwood group. These outcrops will establish a framework for understanding the sequence of deformational events we observe in the volcanic rocks of the MB panel and in particular at the Bounter Fault. We will visit three outcrops in the Burntwood sediments.

Stop descriptions 1 to 3 (Post Accretion Sedimentary Rocks)

Stop 1: F1 fold with axial planar cleavage 6080953N 434781E

This outcrop shows the well bedded Burntwood Group metaturbidites (biotite – staurolite – garnet). Beds are east trending and steeply north dipping, sizes range from 10 cm up to 40 cm in width, and facing directions are defined based on metamorphic grading, which is to the north. The important feature at this outcrop is the early isoclinal F1 fold (Figure 10) with a well preserved S1 cleavage. This S 1 cleavage is defined by biotite, and is only evident in the hinge of the isoclinal fold where it is at a high angle to the contact whereas on the limbs of the fold the S1 becomes parallel. The S1 cleavage is overprinted by an S2 crenulation cleavage and F2 folds, which are identified in the hinge of the F1 Fold. The overprinting of the F1 fold by a refracted S2 cleavage is also apparent from the staurolite growth and strain shadows parallel to S2. Weakly developed S3 spaced cleavage can be seen in places. Typically, F1 folds observed in the Burntwood Group lack an axial-planar foliation, as S1 is usually transposed parallel to bedding. Kraus (1998) and Kraus and Williams (1999) identified preservation of S1 as internal foliations in the microlithons of crenulation cleavage in staurolite porphyroblasts, which suggests pervasive S1 development in the Burntwood Group.

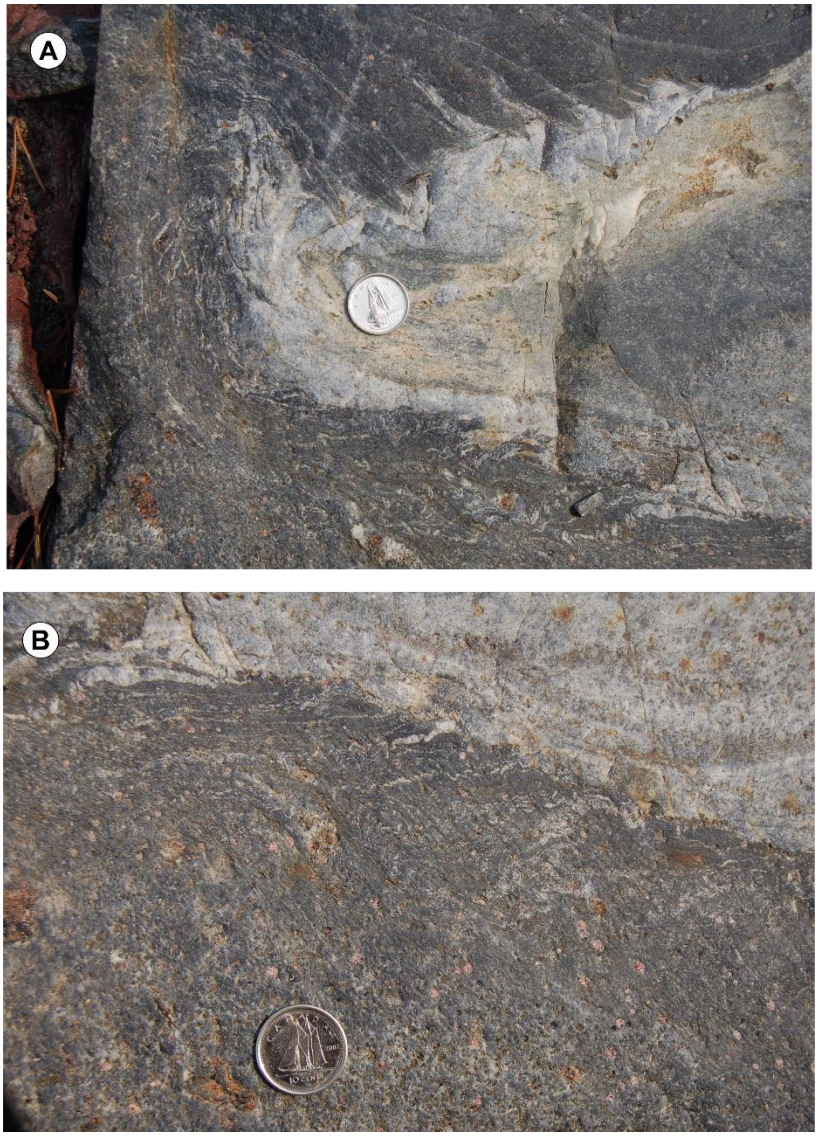

Figure 10: Photos of the isoclinal F1 fold in the Burntwood group at stop 1. (a) HInge of the F1 fold with S1 axial plane cleavage, (b) close up view of photo (a) to show the lower limb of the isoclinal fold with well-developed S2 crenulation cleavage and F2 folds which overprint the F1 fold.

Stop 2: Crystal Park 6081255N 434924E

At this location we observe well bedded greywacke-siltstone-mudstone meta-turbidites, illustrating the reverse (metamorphic) size grading where sandstone-siltstone bases grade rapidly upward into dark grey mudstone tops, which are overgrown by coarse 2-10cm staurolite porphyroblasts and biotite. Bedding on the south side of the outcrop strikes 295-305^0 and dips 70-75^0 to the north and faces south. Bedding on the north side of the outcrop strikes 275-285^0 and dips 85-90^0 to the north and faces north (Bailes et al., 2013). These are considered minor reversals in facing directions as typically the Burntwood meta-turbidites young to the north in the outcrops studied in the Town of Snow Lake. This location shows that S1 has also been overprinted by a strong S2 crenulation cleavage. S1 is not observed at this outcrop, it is considered to be preserved in microlithons between the S2 cleavage planes and within porphyroblasts,

(Kraus and Williams, 1999).

Staurolite and biotite porphyroblasts overgrow S1 and S2, however they are weakly aligned with the S2 cleavage. Staurolite porphyroblasts are boudinaged with quartz occupying pull-aparts formed in the staurolite. The strong refraction of the S2 cleavage between competent sandstone and less competent mudstone-siltstone layers is clearly shown at this locality. We also observe s asymmetrical folding of the S2 In the mudstone layers, which correlates with F3 (Kraus and Williams, 1999) and in the more sandstone rich component of the beds, we observe tension veins which are parallel to the S2 cleavage.

Stop 3: Corley Lake member of the Burntwood suite (UTM - 434389E, 6072050N)

The Corley Lake member, as defined by Bailes (1980) is a distinctive marker unit of coarsely garnet-porphyroblastic metasedimentary rocks, which lies in the footwall of the McLeod Road Thrust Fault, on surface. This units' extent along strike can be traced for over 60 km (from its type locality at File Lake area to Squall Lake, north of Snow Lake), (Bailes, et al., 2013). Southwest of Cleaver Lake the Corley Lake member has been observed at the upper contact of the Burntwood suite metaturbidites interpreted as an indication of the location of the McLeod Road Thrust Fault (Bailes and Schledewitz,1998). This is consistent with the recent interpretation on the location of this thrust fault and the work by (Beaumont – Smith and Gagné, 2008) thus we do not consider that this structure projects through Cleaver Lake to Angus Bay on Herblet Lake as previously suggested by Russell (1957) and Froese and Moore (1980), and Kraus and Williams, (1999). At this outcrop we can observe the narrow beds within these garnet poprhyroblastic metasedimentary rocks. The bedding and S1 are transposed forming a composite S0/S1 fabric and we can observe the sinistral rotation of the S2 cleavage as observed by strain shadows on garnets which imply sinistral rotation.

Stop 4 (UTM: 6081670 N; 0434365 E): The Bounter Fault

Introduction

At this stop (Figure 9) we observe the field relationships and discuss the significance of the Bounter fault. This fault was described by Galley et al. (1991) and Fieldhouse (1999) as a series of anastomosing shears that are associated with the Bounter gold occurrences. The Bounter fault has a strike length of 3km and it lies at the contact between the felsic and mafic volcanic rocks, which now appears to be the site of the early thrust faults. Gold mineralisation occurs intermittently along the structure; the most important occurrence is the Bounter showing, with gold values > 2000ppb (Galley et al., 1991).

Description

The contact between the Burntwood Group and pillowed mafic rocks of the Snow Lake arc assemblage is exposed on this outcrop (Figure 11). This is the only known exposed contact between the Burntwood Group and older metavolcanic rocks in the belt. The Burntwood on this outcrop is garnet-rich thus it correlates with the Corley Lake member which occurs all along the trace of the McLeod Road thrust.

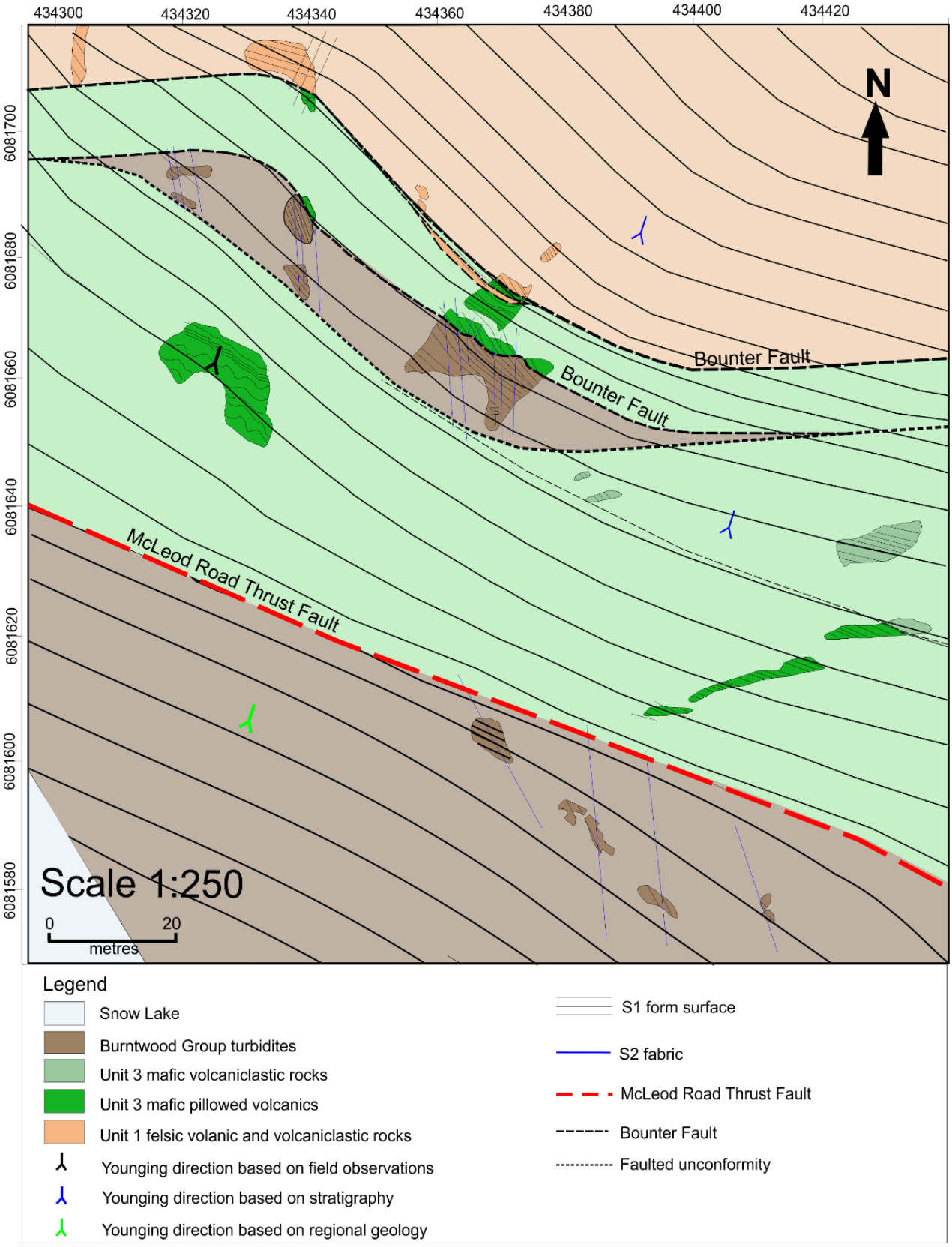

Figure 11: S1 Form surface map of the Bounter Fault, with the trace of the S2 fabric and the McLeod Road Thrust.

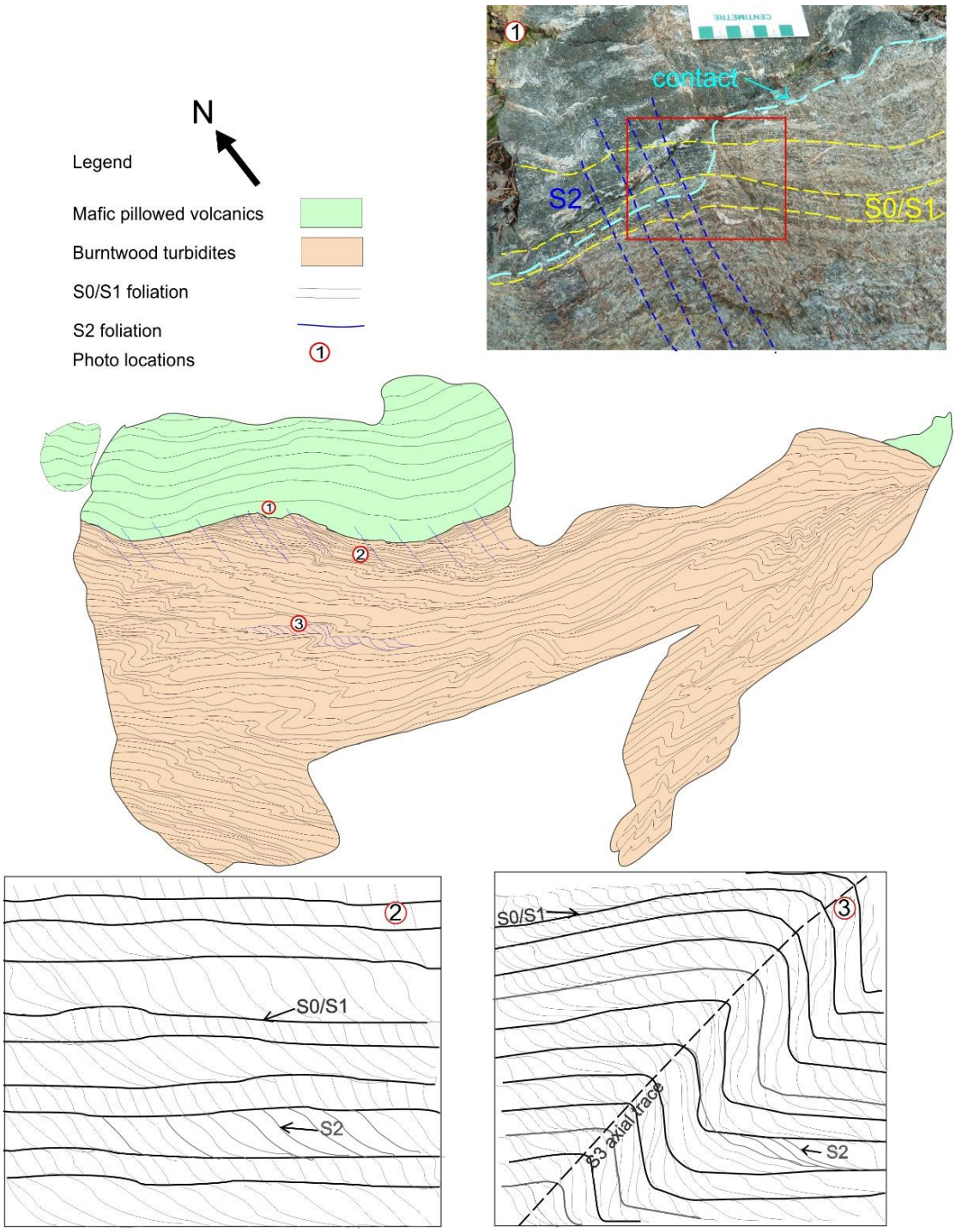

Figure 12: Detailed map of the Bounter Fault, (1) Photo illustrating the overprinting of the fault contact by S0/S1, (2) Sketch to show detail at location 2 on the map. This sketch shows the sinistral rotation of S2 along narrow meta-sedimentary beds, due to the competency contrast, (3) Z folds which fold S0/S1/S2, denoting the S3 axial trace. Note there is no axial plane cleavage.

Prominent structural features include (1) a contact-parallel compositional layering, (2) a bedding-parallel foliation (S1) defined by biotite, (3) an S2 foliation defined by biotite and strain shadows around garnet and staurolite porphyroblasts, and (4) Asymmetrical Z-shaped folds overprinting S1 and S2, (Figure 11).

The contact-parallel foliation is a differentiated layering defined by green amphibole. It is present along the contact only and does not extend beyond 10 cm across strike in the Corley Lake member and mafic metavolcanic rocks. In the Corley Lake member, S1 is defined by biotite and a compositional banding representing modified bedding. So, S1 is a composite S0-S1 foliation. It overprints and is oriented clockwise to the contact and the contact-parallel compositional layering (Figure 12). In the metavolcanic rocks, S1 is defined by amphibole at the contact and by the flattening of the pillows immediately north of the contact and flattening of clasts in a felsic lapilli tuff to the north of the pillowed mafic metavolcanic rocks. A strong stretching lineation (L1) defined by the elongation of the clasts lies along S1.
S2 is also oriented clockwise to the contact but at higher angle than S1 (Figure 12). In the Corley lake member, it refracts in anticlockwise manner as it passes from more competent to less competent S0-S1 layers, suggesting sinistral shear. S2 is axial planar to open to tight folds overprinting the contact. Although S2 is a pronounced foliation in the Corley Lake member and it overprints the contact between the Corley Lake member and mafic volcanic member, it does not extend beyond 1 m of the contact in the mafic metavolcanic rocks. The youngest structures on outcrop, the Z-shaped folds, have no weak axial planar cleavage. Their significance is discussed below.

Interpretation

Because S1 overprint the contact between the Corley Lake member and the metavolcanic rocks of the Snow Lake assemblage, this contact could represent either an unconformity or an early, now metamorphosed, brittle fault. Several lines of evidence suggest that the contacts is an early brittle fault, as follows:
1. The contact-parallel foliation is an early fabric that was later metamorphosed. One possibility is that it originated as weathering features prior to the deposition of the Corley Lake member. However, as the mafic pillowed volcanic rocks observed at this outcrop and the entire McLeod Road Thrust (MB) sequence stratigraphy has been determined to be below wave base conditions, weathering could not have produced a regolith and a compositional zoning prior to the deposition of the Corley Lake member. Furthermore, the foliation is observed within both the mafic volcanic rocks and turbidites suggesting that it postdates the deposition of the turbidites. Thus this contact parallel foliation could not have resulted from weathering processes. This contact parallel fabric is interpreted to be as a result of alteration during early brittle thrusting, forming a chlorite alteration, which has later been metamorphosed during peak metamorphism to the coarse grained amphiboles we can observe at the contact.
2. If this contact was an erosional contact, there should be evidence for erosion. However, there are no volcanic clasts produced through erosion observed at the base, and therefore no evidence of erosion. There is also no observed change in composition of the Corley Lake member at this location, and the younging in the sediments throughout the Snow Lake area is consistently to the north.
3. Although younging indicators are lacking on this outcrop, regional mapping indicates that the metavolcanic rocks and turbidites consistently young to the north across the map area. As the volcanic rocks in contact with the turbidites are north of the turbidites, this contact cannot be an unconformity and must be interpreted as an early brittle fault. 4. The Corley lake member is observed only along the trace of the McLeod Road Thrust and the Bounter Fault. There is therefore a spatial relationship between faults and this member. The Corley Lake member

differs in composition from the rest of the Burntwood as it is a garnet- rich fault. It is suggested here that these change in composition are due to alteration along an early fault within its damage zone, and this produces garnet during metamorphism. The logical extension of this interpretation is that the McLeod Road Thrust also originated as an early brittle fault.

Comparison with faults at the Lalor deposit and significance of the Bounter Fault

At the Lalor deposit faults exist based on stratigraphic changes, however no evidence has been found for these faults in drill core. The Bounter Fault is not exposed in drill core and has not been observed, despite reviewing the relevant intervals. Previous work, has also determined there to be a known fault at this location, which is associated with the Bounter mineralisation. At this outcrop we can observe good bedding and a well exposed contact, which provide key relationships and evidence for this fault. The Bounter Fault is considered an example of an early brittle thrust fault, which has imbricated stratigraphic units of the MB sequence stratigraphy and the Corley Lake member of the Burntwood group.

Stop 5 Stratigraphy of the Mcleod Road Birch Lake sequence

The following is a description of the stratigraphic units which we will observe along the traverse across the MB sequence, (Figure 13). (Located at Stop 5 on the Regional map, Figure 9).

Unit 3: Mafic volcanic and volcaniclastic lithofacies

This unit is repeated in 2 structural panels within the MB sequence, (Figure 3) and it is continuous along strike for up to 3.5 km, and it changes in thickness from 40 to 250 m. The dominant lithofacies include; well-bedded, heterolithic, lapilli tuff, lapillistone to tuff breccia and lesser plagioclase-phyric pillowed flows. Clasts are lapilli and block size, and clast types include aphyric to plagioclase-phyric mafic, aphyric to plagioclase-phyric felsic, scoriaceous, and plagioclase- and pyroxene-phyric mafic clasts. The groundmass contains 50 –55% hornblende, 15 – 20% biotite, 10 – 15% quartz, 10 –15% feldspar, 5 – 8% muscovite, and 5 – 8 % chlorite. The unit is subdivided into seven sub units, which are, in turn divisible into 18 depositional units defined by changes in lithofacies (Figure 4a).

Unit 1: Heterolithic felsic volcaniclastic lithofacies

Unit 1 is repeated in all structural panels (Figure 3). It consists of heterolithic plagioclase-phyric and lesser quartz-phyric felsic volcaniclastic rocks with distinctive, dark wispy fragments (Figure 8g). The 4 volcaniclastic subunits are grouped within a single unit, because they share distinctive dark wispy clasts (Figure 8e). The unit is divided into four subunits based on bedforms and components (i.e. clasts, ash, crystals), as described below. As shown in Figure (4a), the 4 subunits can be divided into 13 depositional units (1a -1m). Depositional units are defined by normal grading of mafic lithic and dark wispy fragments, and by an increase in fine tuff (ash sized component), which occurs towards the top of some beds (1c and 1d, Figure 4a). The components, in variable amounts, comprising each of the depositional units are; i) tuff, less than 2mm, ii) plagioclase crystals (whole and broken which range in size from 1 to 2 mm), iii) dark wispy fragments, iv) mafic lithic fragments, and v) plagioclase phyric felsic clasts.

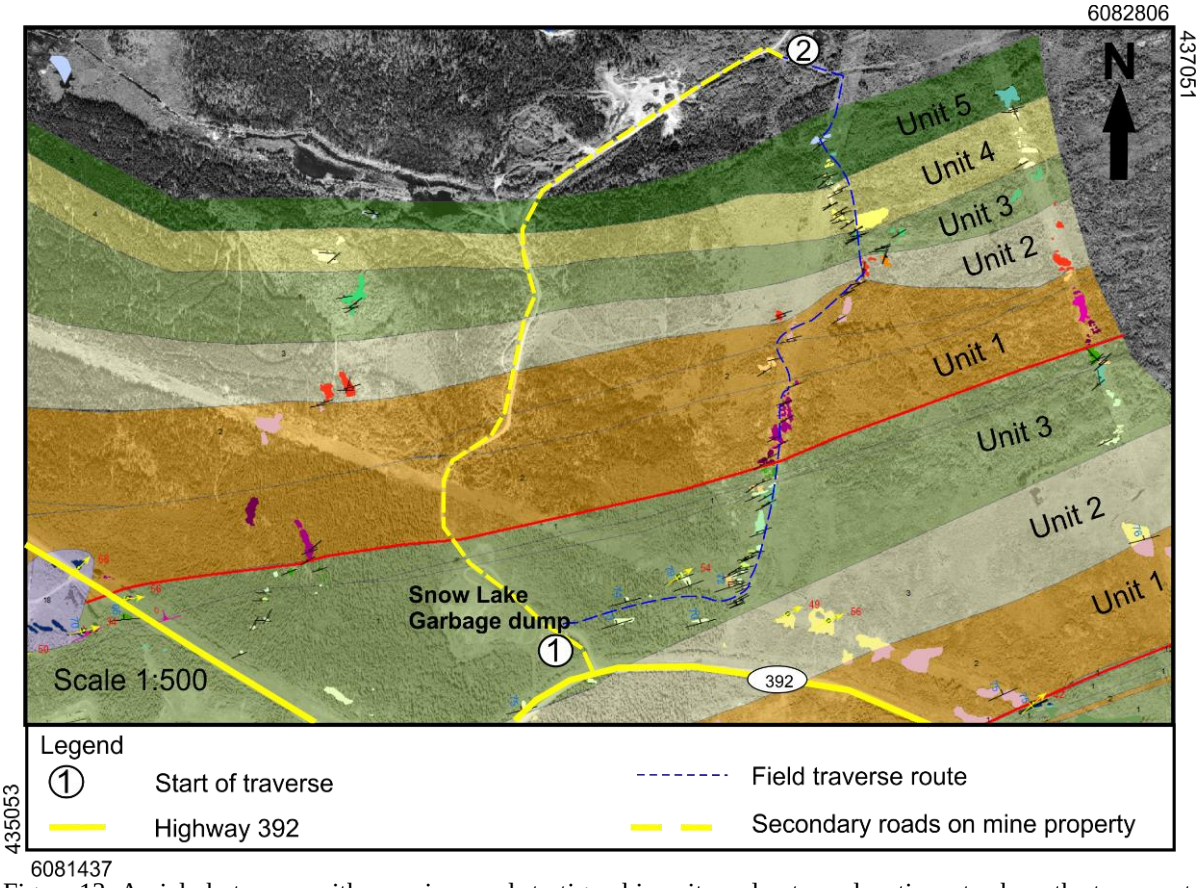

Figure 13: Aerial photo map with superimposed stratigraphic units and outcrop locations, to show the traverse to examine the stratigraphy of the McLeod Road Birch Lake Thrust panel. The traverse will start at location 1 and finish at location 2.

Unit 2: Felsic coherent and volcaniclastic lithofacies

This unit is repeated in 2 structural panels within the MB sequence. It comprises 2 sub units; a plagioclase-phyric (1–5%) coherent felsic lithofacies and a lesser felsic volcaniclastic lithofacies, which can be divided into 4 depositional units (2a – 2d) (Figure 4a). The felsic groundmass contains 50-60 % quartz, 15 % feldspar, 3-5 % garnet, 5-8% biotite, 5% muscovite, and 1-3% sericite.

Unit 3: Mafic volcanic and volcaniclastic lithofacies

At this location we observe a narrow part of the main succession of unit 3 which we observed previously. Here we observe one of the main sub units of this lithofacies, which is the well-bedded heterolithic lapilli tuff, lapillistone to tuff breccia. We can also observe the highly strained contact with the unit 4 rhyolite stratigraphically overlying this unit. However, this contact is not considered to be a thrust fault, S1 is parallel to the contact strain intensity increases at the contact due to the competency contrast between the two units.

Unit 4: Coherent Felsic lithofacies

This unit is not repeated within the MB panel. Unit 4 is a massive, aphyric, aphanitic coherent rhyolite (Figure, 4a) which is not subdivided into individual subunits or depositional units. The rhyolite varies in thickness from 110 to 155 m over a strike length of 4km (Figure 3). It weathers

a dark grey to orange, and is salmon pink to light grey/white on fresh surfaces. The groundmass contains 60-70 % quartz, 5-10% feldspar, 10 % garnet, 5-8% biotite, 3-8% muscovite.
A characteristic feature of the rhyolite is well-developed lobes that have a banded appearance along their margins reflecting different biotite content. The lobes are mantled by breccia containing clasts that are identical to coherent rhyolite. The rhyolite displays columnar jointing and contains rare quartz-filled amygdules, (2 to 5 mm in size). This unit displays a well-developed, spaced disjunctive cleavage defined by biotite, and a mineral stretching lineation defined by quartz, feldspar and garnet. The lower contact of the coherent rhyolite unit with mafic volcaniclastic rocks of subunit 7 is sharp and highly strained.

Unit 5: Mafic volcaniclastic and flow lithofacies
The mafic volcaniclastic and flows lithofacies, which is divided into 2 subunits and 2 depositional units (5a-b) of Figure 4a) varies in thickness from 45 to 90 m over 4km in strike length. They represent the uppermost unit of the MB sequence (Figure 3) and this unit is not repeated within the structural panels. The groundmass comprises 45-50% hornblende, 15% biotite, 5% quartz, 15% feldspar, 2-5% muscovite, 5% chlorite, and 1-5% sericite.

Day 2

Stop 6 (UTM: 6082438N; 0433614E): Howe Sound Fault

Introduction

The New Britannia mine (Figure 14) has produced 1,404,950 oz. (43 699 kg) gold, since production commenced in 1949. The Mine property contains several gold deposits; Nor Acme, Birch, Boundary, and the No. 3 Zone, (Figure 3) including several other gold occurrences; e.g. Bounter, Thorne. The Nor-Acme deposit is the largest gold deposit on the mine property, and it is the largest gold deposit, of the Manitoba – Saskatchewan portion of the Trans Hudson Orogen. The Nor-Acme deposit consists of four zones—Toots, Dick, Ruttan and Hogg (Figure 15), which are located at the contact with the Howe Sound Fault and the Nor Acme fold hinge (F_1 fold). The ore zones plunge northeast to north-northeast at 40–80° dip and are 3–30 m wide (Galley et al., 1991).
The Howe Sound Fault transects the hinge of the Nor-Acme anticline, (Figure 16), it is subparallel to the contact between the mafic volcaniclastic rocks (unit 3) and the felsic volcanic and volcaniclastic rocks (units 1 and 2), and is itself slightly folded (Figure 16).

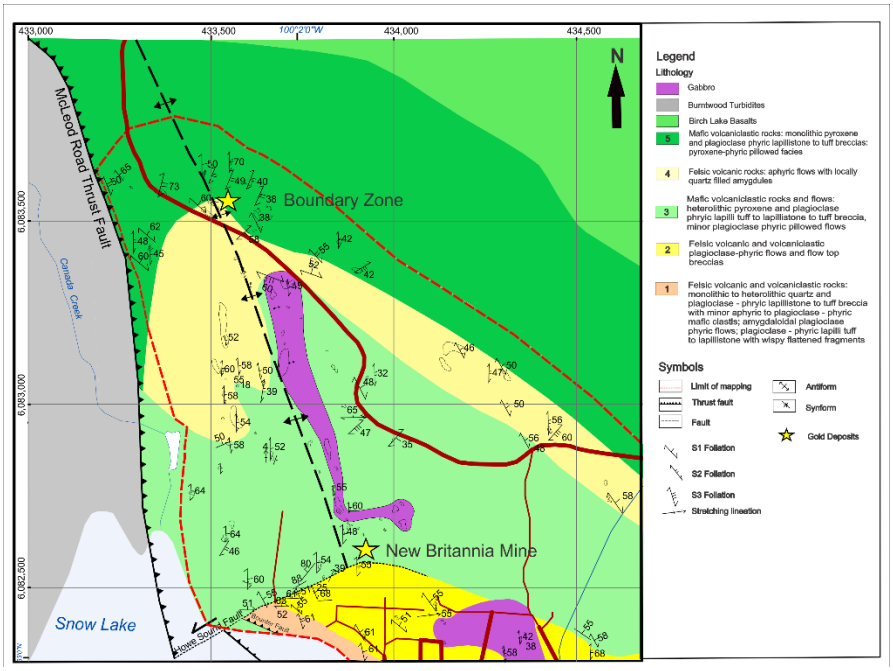

Figure 14: Lithostratigraphic map to illustrate the Howe Sound Fault located in the Hinge of the Nor Acme Fold (Rubingh et al., 2012)

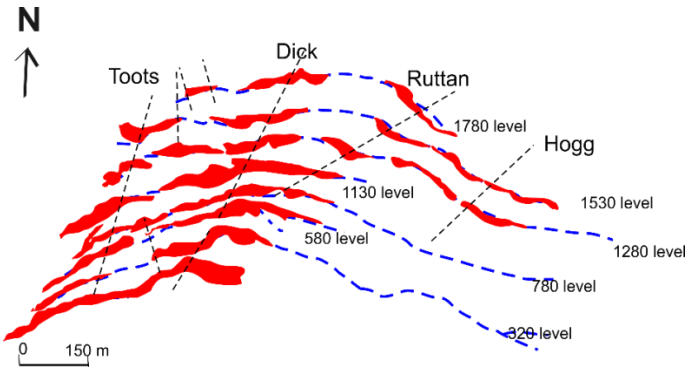

Figure 15: Down plunge projection of the ore zones at the Howe Sound, to illustrate the folded mineralisation in red and the Howe sound fault (blue), (modified after Hogg, 1957)

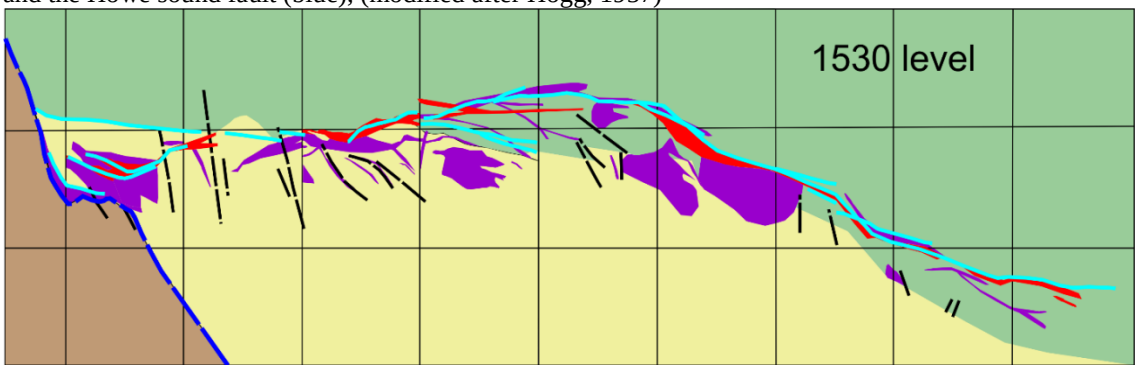

Figure 16: 1530 Mine Level facing north, modified from composite mapping of level plans from (Tom Flemming, 2012). Ore zones are in red, and gabbro is in purple along the trace of the Howe Sound fault in pale blue. Note that the fault does not follow the contact between mafic and felsic units and is cut by the McLeod Road Thrust fault in dark blue.

At this stop we will first visit a series of outcrops (a- d) (Figure 17) along the interpreted contact

of the Howe Sound Fault, and then at the vent raise adjacent to the Howe Sound Fault, we will review outcrops (e-i). Mineralization at the main mine is hosted by the east trending fault breccias, the massive to brecciated quartz carbonate vein system in the wall rock at the Howe Sound, (Galley et al., 1991), none of which are observed in situ at this outcrop. However large remnant blocks of the brecciated quartz carbonate veins and wall rock can be observed, which are considered to be representative of this rock type.

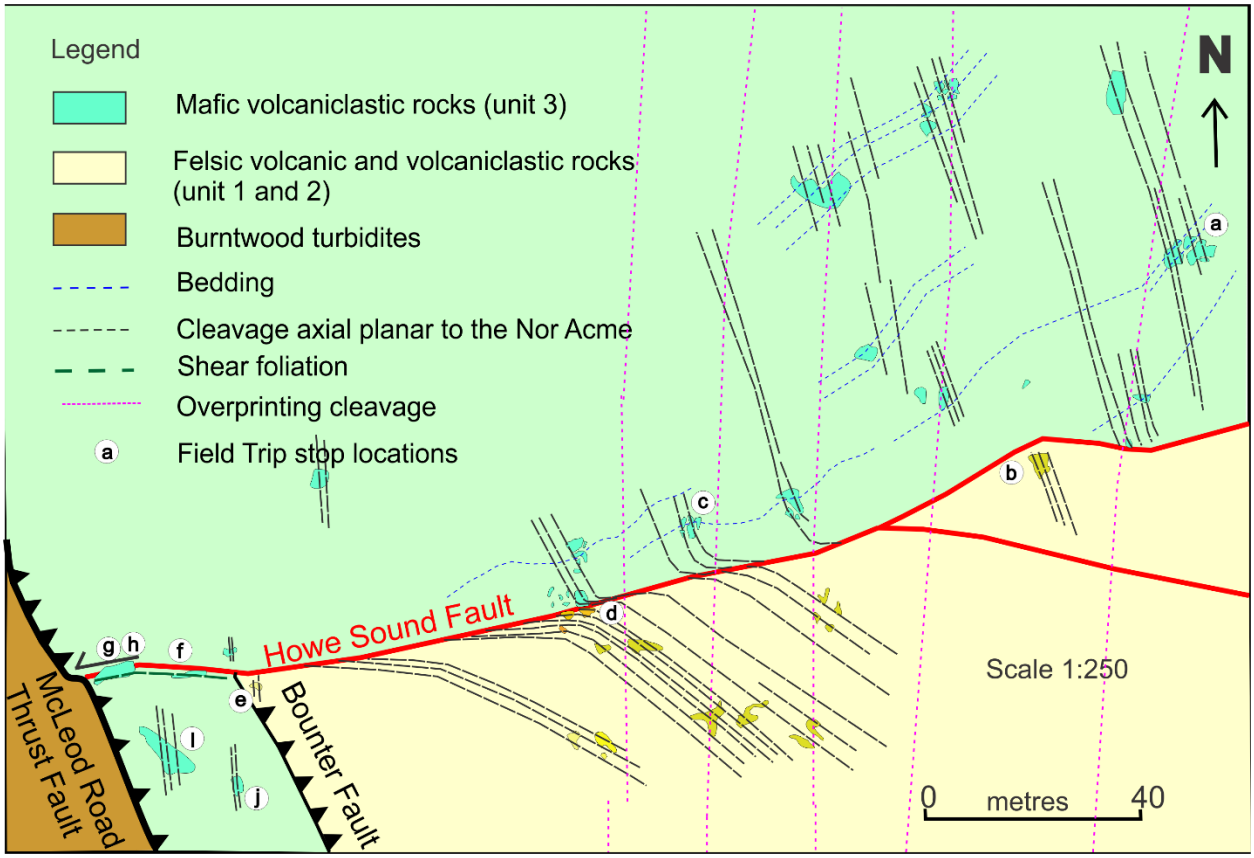

Figure 17: Map of the outcrops along the Howe Sound (Rubingh, 2014). Note the location of the interpreted Bounter fault extension.

Description

A traverse along the Howe Sound Fault will examine outcrop locations (a – d) (Figure 4). This traverse will illustrate the lithological contacts between stratigraphic units along the Howe Sound Fault and the relationship of bedding, the well-defined S1 flattening foliation of the clasts, strong stretching lineation of the clasts, and the weak S2 cleavage.

At location (**a**) we will observe bedding in the mafic volcaniclastic rocks (unit 3) and a strong NE (35 – 073) stretching lineation of the clasts, which is parallel to the hinge of the Nor Acme Anticline. This location shows an L-tectonite, the foliation S1 is weak although it is at a high angle to bedding. At location (**b**) the mafic volcaniclcastic rocks of unit 3, are well bedded, defining a younging to the north, and we can observe the relationship between bedding and the S1 foliation which is perpendicular to bedding. Outcrop location (**c**) in the felsic volcanic rocks of unit 2 illustrates the bedding and S1 foliation which does not appear to have rotated and towards the contact, therefore the Howe Sound fault possibly lies south of this outcrop (Figure 17). We also observe a quartz tourmaline vein parallel to the S1 foliation which is weakly folded. Location (**d**) shows the contact relationships between the felsic volcaniclastic rocks of unit 1 and

the mafic volcaniclastic unit 3. Here we can observe the strong anticlockwise refraction of the S1 cleavage at the Howe Sound fault contact. Outcrops south of this location also shows an anticlockwise deflection of the S1 foliation towards this contact (Figure 17).

Outcrop locations (e- j) (Figure 18) represent the surface expression of the Toots zone, which is illustrated in detail on Figure 19. The Toots zone is located at the intersection between the Howe Sound Fault and the MRT, and extends for 900 m down plunge.

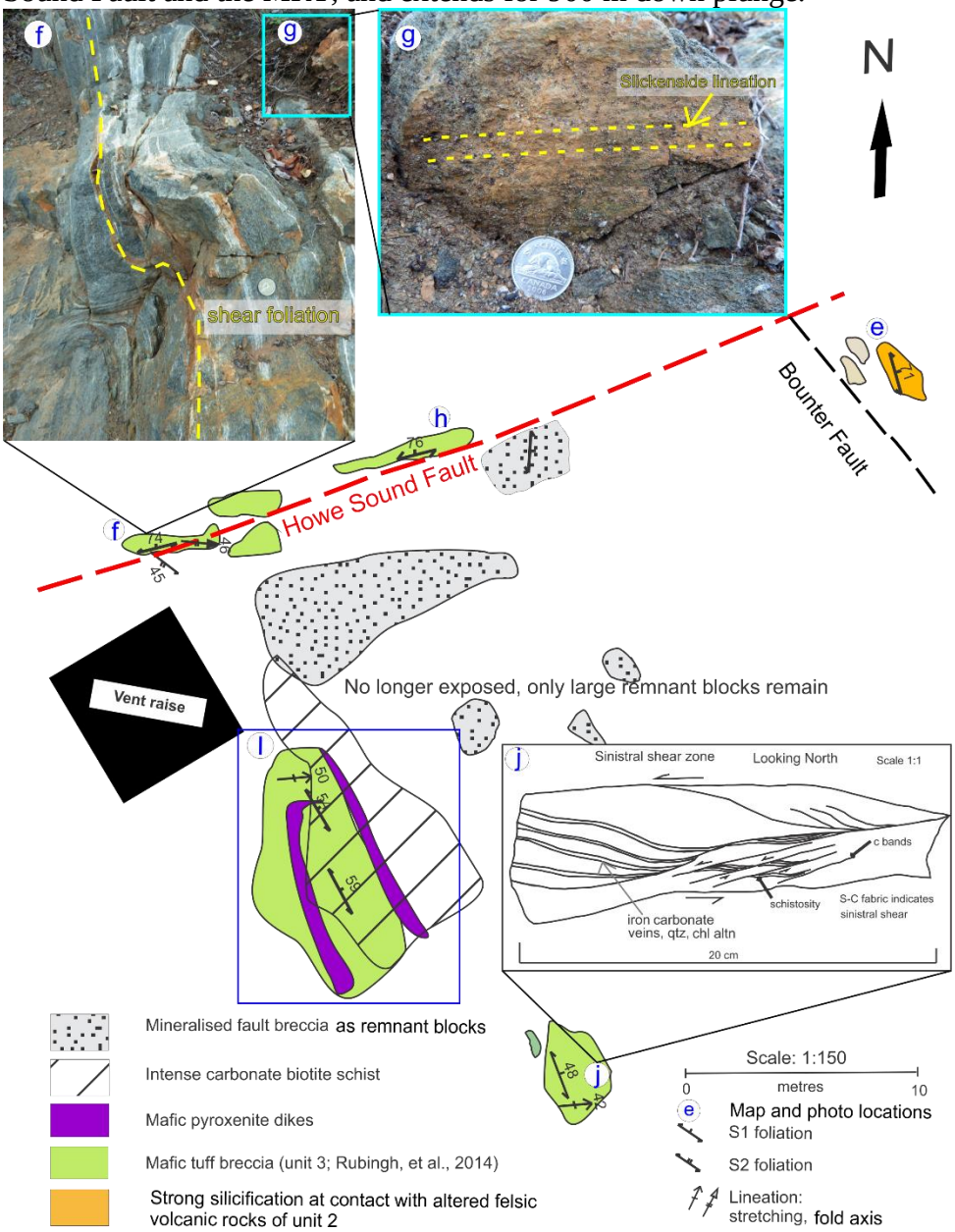

Figure 18: Detailed surface map of the Toots zone, (e) interpreted Bounter Fault location, (f) photo to show drag folds along the Howe Sound, (g) photo to show horizontal slickenlines, (h) location of open F2 folds which overprint the Howe Sound Fault, (i) Location of Figure 19; a detailed map to illustrate the structure, alteration and mineralization at the Howe Sound, (j) sinistral shear sense indicators illustrated by the corresponding sketch of location (j)

At outcrop location (**e**) we observe a strong silicification at the contact with the felsic volcanic

rocks at the inferred contact with the mafic volcaniclastic rocks of unit 3. Using the known stratigraphy of the McLeod Road Birch Lake panel (Figure 3) we have moved down stratigraphy from felsic volcaniclastic rocks of unit 2 to unit 1 and to the underlying younger structural panel separated by the Bounter Fault.
Location (**f**) is within the mafic volcaniclastic rocks of unit 3 (Figure 18). An open fold is present overprinting the shear foliation of the Howe Sound Fault. It has a weak axial planar cleavage which is parallel to the S2 foliation. Three metres farther west along the Howe Sound Fault at location (**g**) we observe S shaped drag folds which fold the shear foliation (Figure 18) and a subhorizontal mineral slickenlines can be seen at location (**h**).

The relationship between structure, alteration and mineralization can be seen at locality (**i**) (Figure 18). The mafic volcaniclastic rocks of unit 3, are cross cut by pyroxene phyric dykes (which have now been metamorphosed to amphibole after pyroxene). There are two main styles of alteration: -
Iron carbonate veins and pyroxene phyric dykes are folded and the S1 foliation in the mafic volcaniclastic rocks of unit 3, is axial planar to the hinge of the fold. Biotite, iron carbonate and chlorite alteration are associated with sinistral ductile shearing along a folded shear fracture.
Strong silicification, hematite alteration and sulphides are offset by shear fractures labelled (2) and (3). These shear fractures also cut the early biotite alteration and offset the mafic volcaniclastic rocks and pyroxene phyric dyke. Iron carbonate veins cut these zones of intense silicification and sulphide mineralisation.

Location (**j**) which is close to the inferred location of the McLeod Road Thrust shows the S1 foliation in the mafic volcaniclastic rocks of unit 3, which is approximately parallel to the contact with the McLeod Road Thrust Fault. There are at least two sets of iron carbonate veins which display a sinistral offset and are also folded with their axial planes parallel to the main S_1 foliation. An S-C fabric is observed in the mafic volcaniclastic rocks suggesting sinistral movement (Figure 18).

Interpretation
The abrupt truncation of the thrust repeated units 1 and 2 against the Howe Sound suggest that the fault acted as an accommodation structure during the formation of the Nor Acme. The hinge of which lies immediately north of the Howe Sound. The Howe Sound is thus interpreted as a syn-folding structure.

The deflection of S1 and S shaped drag folds along the Howe Sound fault suggest sinistral shear along the structure. Along the Howe Sound Fault a shear foliation is parallel to this contact, and drag folds within the iron carbonate alteration along this fault are expressed, which have formed during sinistral rotation of the S1 foliation. Later during formation of the overprinting cleavage the Howe Sound is folded by F2 folds.

The alteration map (Figure 19) provides evidence for a long lived hydrothermal system during D2. Early iron carbonate veins are folded during F1 folding, the rock undergoes silicification, and it is then cut by later iron carbonate veins.

Further map scale evidence suggests that the mineralisation is syn folding. The mineralisation

lies along the Howe Sound, which formed as an accommodation structure during folding, it is itself gently folded and continues along the north limb of the fold at Mine East as a shear zone consistent with flexural slip during folding.

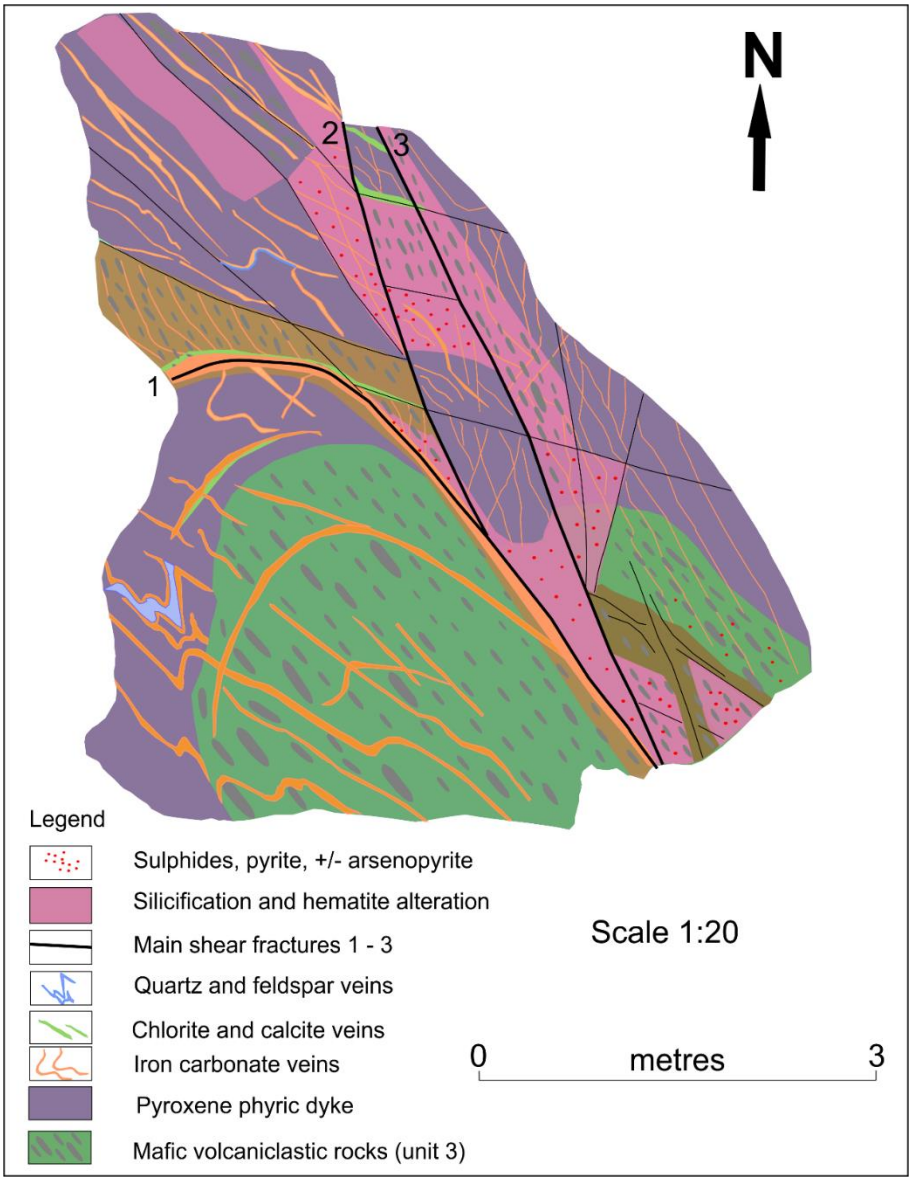

Figure 19: Location (i) on Figure 18, this map illustrates the alteration, structure and mineralization at the Howe Sound Fault, (mapped by Rubingh, 2014)

STOP 7 (UTM: 6083561N; 433511E): Boundary zone

Introduction

The Boundary zone is associated with shearing along a limb of a parasitic fold of the Nor Acme Anticline; located at the folded contact between the felsic volcanic and volcaniclastic rocks of unit 4 and the mafic volcanic and volcaniclastic rocks of unit 5. The geological map (Figure 20) illustrates the distribution of lithological units and gold assay values, associated with quartz and

quartz carbonate veins which are folded with an S1 axial planar cleavage. Previous authors have associated these quartz and quartz carbonate veins with gold mineralisation (Beaumont-Smith and Lavigne, 2008), and described the Boundary zone, as a vein breccia system that formed parallel to the regional foliation within the felsic volcanic rocks (Galley et al. 1991).

Outcrop description

The rhyolite and felsic volcanic breccias illustrate a south to north progression from a massive aphyric coherent rhyolite flow, to in situ breccias and flank breccias, all of which are monotlithic and derived from autobrecciation and mass wasting of the coherent rhyolite dome. Bedding strikes east-northeast and dips steeply, and the clasts display a strong flattening foliation, consistent with $S_{1,}$ which has a north-northwest orientation and a strong lineation, and dips moderate to shallow to the northeast. At the contact with the mafic volcaniclastic rocks of unit 5, a strong sinistral refraction of the clasts and foliation is evident, within the well bedded felsic volcaniclastic unit, as shown in the photo see Fig. 21 for location.

The relationship between bedding and the main S1 flattening foliation of the clasts, is perpendicular in the hinge of the Nor Acme fold and at this outcrop we observe the rotation of the clasts in an anticlockwise sense into the shear zone, together with the mafic dikes, all of which indicate a sinistral sense of shear Figure 21 (photo 2 and inset photo 3). Other sinistral shear indicators observed are; boudinaged and rotated quartz veins, and en echelon tension gashes, which all show an anticlockwise rotation along the main shear fracture.

The main quartz vein folded in this photo Figure 21, (photo 4), illustrates the perpendicular relationship of the axial planar cleavage S1, to the hinge of the quartz vein. These quartz veins are also located in the hinge of the Nor Acme fold, where the strain would be higher. These observations are consistent with the highest gold assay values from samples collected in 2013, which indicate mineralisation is localised in the hinge of the fold, shown on the map (Figure 20), and in the wall rock at the margins of veins. Gold mineralisation is also associated with the limbs of the fold. Later tension veins that cut across the S1 cleavage but are also gently folded, are shown in Figure 21, (photo 5).

Interpretation

The younging direction at this outcrop is confirmed to the north, based on the south to north progression of felsic volcanic rocks, from mass wasting of the coherent rhyolite dome. Previous work by Beaumont-Smith and Lavigne (2008) had interpreted that this portion of the stratigraphy was overturned, but based on our facing directions at this outcrop, this is no longer a valid interpretation. The north facing at this outcrop is compatible with the consistent north facing of almost all the rocks in the thrust panel. S1 is parallel to the axial plane of the Nor Acme and to the parasitic S shaped fold defined by the folded units on the outcrop. S1 underwent sinistral shear along less competent beds, as strain was accommodated by flexural slip during the formation of the Nor Acme Anticline. The quartz veins and mineralisation were emplaced as tension gashes late during folding and were subsequently folded during the same event.

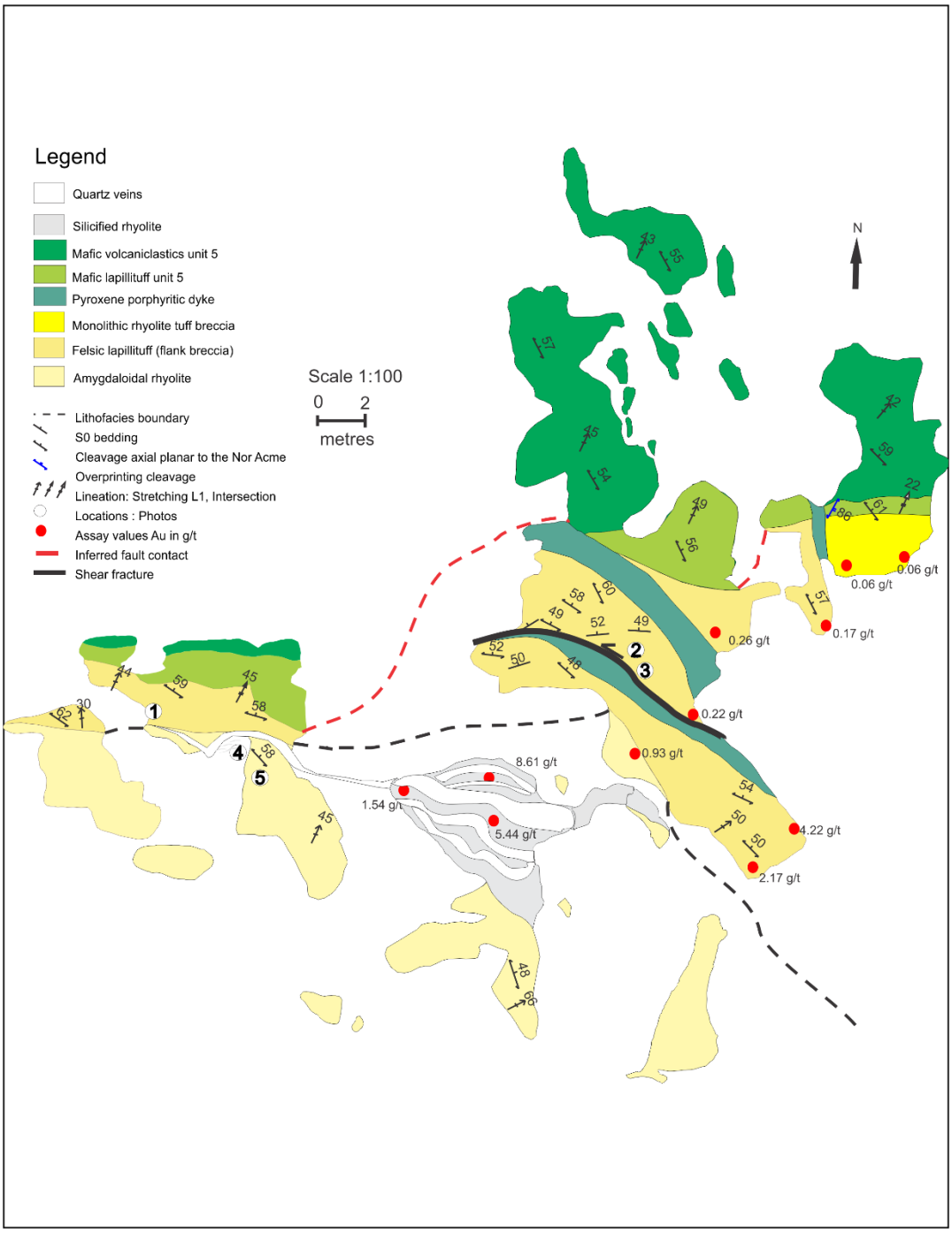

Figure 20: Map of the Boundary Zone Mineralisation, showing recent assay grades from surface sampling of the outcrop (mapped by Rubingh, 2013). Photo locations 1 – 5 are shown on the map.

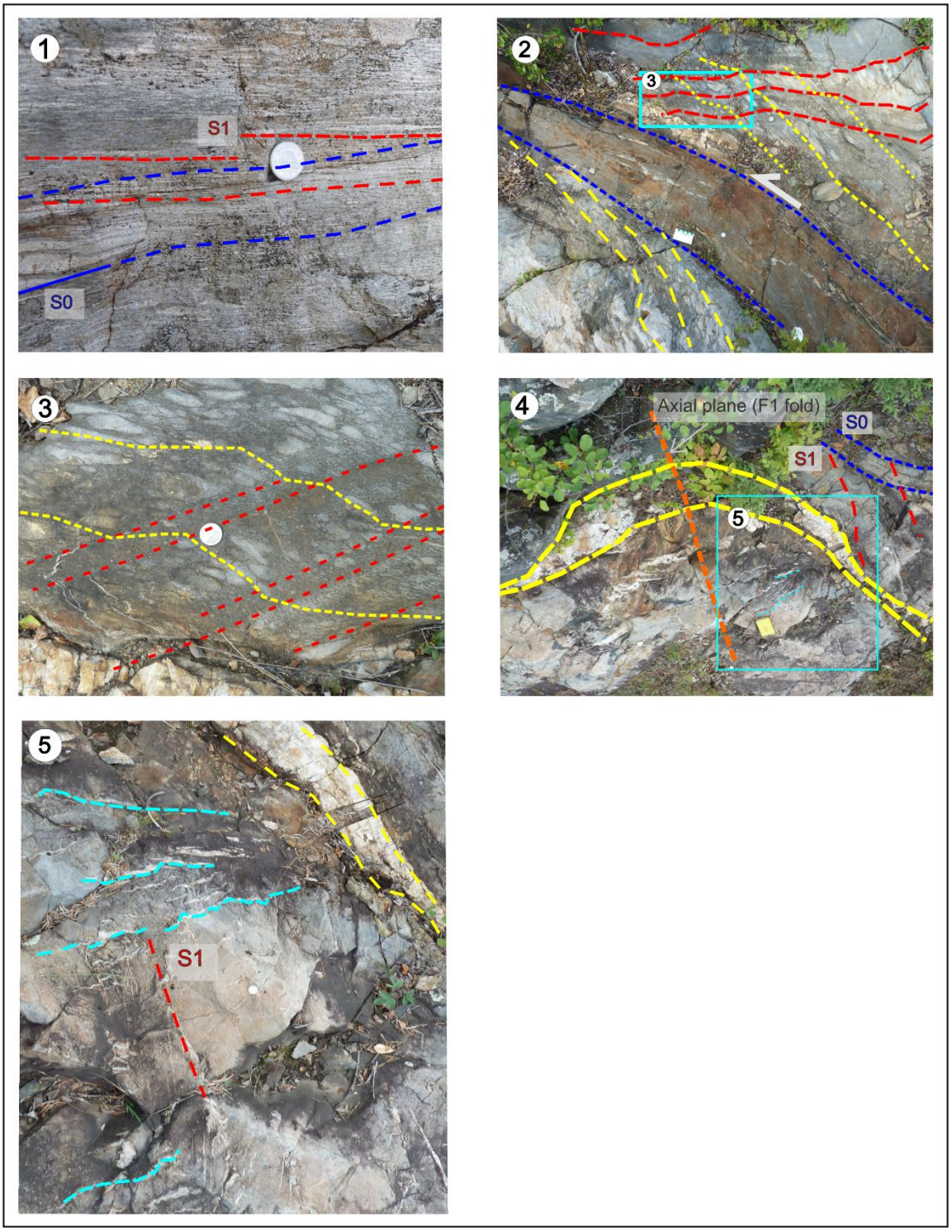

Figure 21: Photos to illustrate key locations as illustrated on Figure 20. (1) Sinistral refraction of the S1 foliation. Bedding is defined in blue and S1 is in red. (2) Sinistral rotation of the S1 fabric along the shear into parallelism with the mafic dyke highlighted in blue. (3) Blue box highlights the location in photo 2, the clasts are refracted due to the changing competency of the beds. (4) Bedding which highlighted in blue and the S1 in red. The thick white quartz veins are highlighted in yellow with an axial planar S1 foliation. (5) Blue box highlights the location in photo 4, this image shows the folded tension veins highlighted in blue which are forming perpendicular to S1 and thus forming slightly later during Nor Acme folding.

Stop 8 (UTM: 6084071N; 433238E): The No. 3 zone

Introduction

The second largest deposit on the New Britannia Mine property is the No.3 zone (Figure 3). The No. 3 Zone is located at the tightly folded contact between coarse pyroxene mafic volcaniclastic rocks (unit 5), and the mafic pillowed volcanic rocks of the Birch Lake basalt, which lie in close proximity to the hinge of the Nor Acme Anticline, and McLeod Road Thrust fault, (Figure 3). The No. 3 zone has two surface exposures, the portal area (Location A) and the main mineralized quartz-vein showing (Location B).

LOCATION A

Description

The No. 3 Zone portal (Location A) (Figure 22) located in the hinge of the tight to isoclinal Nor Acme Anticline, which is in close proximity to the McLeod Road Thrust Fault, at this location. We observe the well bedded coarse pyroxene mafic volcaniclastic rocks (unit 5, as defined by Rubingh, 2014) which are highlighted in yellow (Figure 22), and we can demonstrate the relationship between bedding, the S1 foliation defined by the flattening of clasts, (highlighted in blue, Figure 22) and the S3 foliation highlighted in green, Figure 22).

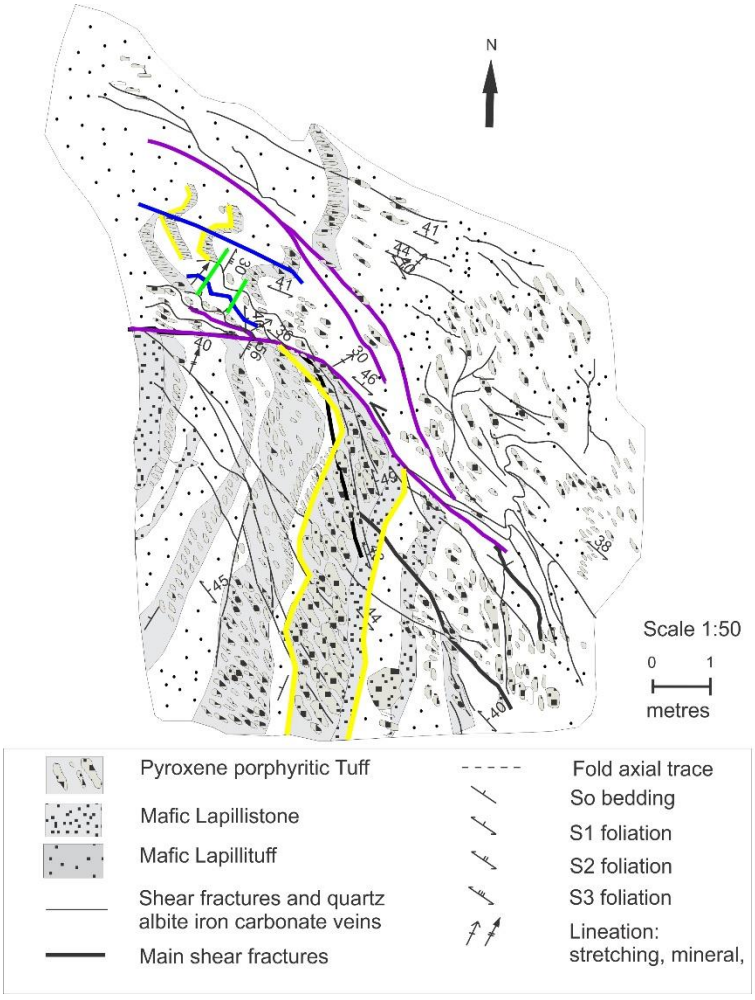

Figure 22: Location A: No 3 Zone portal. (Rubingh et al., 2012)

The beds are 1–2 m thick and the clasts which are 3–80 cm in size are all similar in composition and texture. They are characterised by 15% pyroxene (3–25 mm) and 5–7% plagioclase (2–4 mm) phenocrysts in a light-coloured ground mass. Facing directions are weakly defined to the north, based on normal grading. The orientation of bedding is at a high angle to the S1 foliation, and smaller scale beds are also folded with an S_1 axial-planar foliation, defined by the flattening of the clasts, but there is no associated penetrative foliation with the matrix. The S_1 foliation is also axial planar to folded, quartz–albite–iron carbonate veins, similar to observations at the Main Mine mineralisation along the Howe Sound Fault.

A west-northwest- to northwest-trending shear fracture, of unknown displacement, truncates bedding and indicates sinistral movement, as determined from the anticlockwise rotation of the clasts into the shear fracture. Quartz–albite–iron carbonate veins display a foliation, which overprints the veins and forms late during this sinistral shear. There are also small-amplitude folds which fold the shear fabric (some of which display Z-asymmetry) and display an S_3 axial planar foliation).

Interpretation
Due to the proximity of the McLeod Road Thrust Fault, the effects of late D2 reactivation of the McLeod Road Thrust Fault are observed here forming this foliation which overprints the quartz–albite–iron carbonate veins. The Z folds which fold the shear fabric are associated with a weak S3 cleavage and are forming during the D3 deformation.

LOCATION B

Description

Location B, which is the main mineralized zone at the No. 3 zone (Figure 23) illustrates the same relationships, which can be observed with respect to the mineralized veins as Location A. However, this location is located on the north east limb of the Nor Acme Anticline, close to the hinge. There are three main types of quartz veins at the No. 3 Zone: - 1) Early brecciated pale pink veins which contain enclaves of the mafic volcaniclastic rocks of unit 5, which are cut by later 2) milky white quartz veins locally with tourmaline, and 3) these veins are cut by later iron carbonate veins. In 2016 assay samples from the No. 3 Zone channel sampling are shown on Figure 23. The highest grades of gold mineralization range from 11.25 – 29.3 g/t, and are observed in the pale pink and white brecciated veins, which contain abundant wall rock fragments within them, and contain abundant fine grained arsenopyrite in the wall rock along the margin of the veins, and in the wall rock fragments within the veins. The milky white quartz veins with tourmaline have less wall rock inclusions and have lower grades (1.4 g/t). Quartz-tourmaline veins with no wall rock inclusions, are weakly mineralized (0.023 g/t), and the host mafic volcaniclastic rocks with quartz carbonate veins also have only minor gold mineralization (0.138 g/t).

The S1 foliation defined by the flattening of the clasts, is parallel to the axial plane of the main quartz vein, (S shaped large thick laminated vein) (Figure 23), and the S1 foliation becomes rotated in an anticlockwise rotation towards the main laminated vein. The S1 foliation is also preserved within pieces of mafic volcaniclastic rock, which are incorporated within the

brecciated quartz veins (Figure 24, photo 1 and 2). These veins are also folded with their fold axis parallel to the stretching lineation. The stretching lineation in the veins is observed as a corrugation (Figure 24, photo 3), which is itself parallel to the stretching lineation, defined by the elongation of the clasts, in the mafic volcaniclastic rocks.

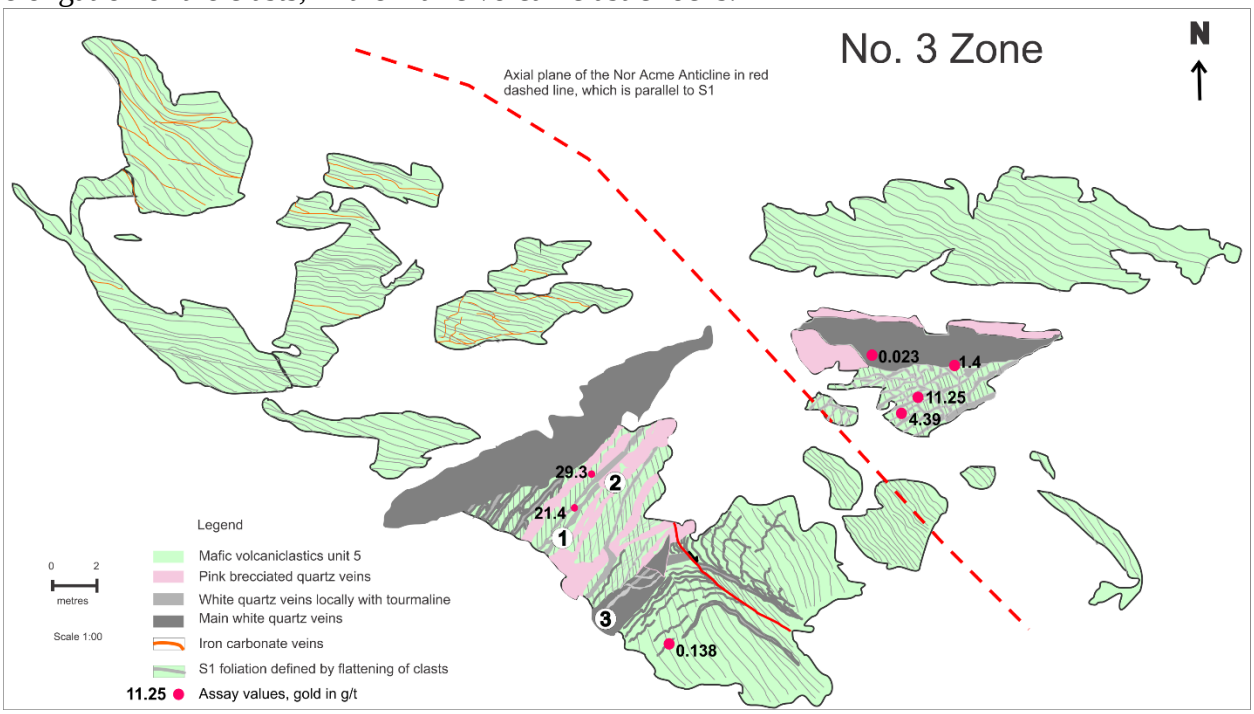

Figure 23: Map of the No. 3 Zone showing. (Mapped by Rubingh, 2014)

Interpretation

Mineralization is located in the hinge of the Nor Acme Fold. At this location the S1 foliation, which is parallel to the axial plane of the main quartz vein, becomes rotated as the main quartz vein acts as an anisotropy during Nor Acme folding. Thus the vein must be pre folding. However, the preservation of the S1 foliation in clasts within the vein suggests that the Nor Acme axial planar foliation formed before folding. These mutually exclusive overprinting relationships suggest that the veins are syn- folding.

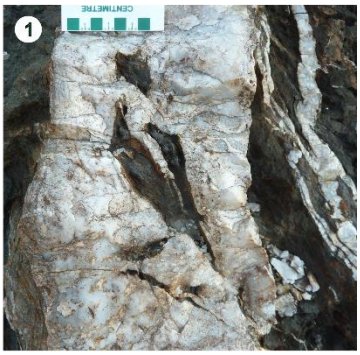

Figure 24: Photo locations shown on the No. 3 zone map figure 23; (1), Brecciated vein with mafic wall rock fragments(2) Mafic wall rock within a brecciated vein displaying the S1 foliation, (3) Strong corrugation of veins parallel to the stretching lineation.

Day 3

Stop 9 (UTM: 6084810N; 432097E) MRT Powerline

Introduction

The McLeod Road Thrust stop along the Powerline is an important location where we can observe the McLeod Road Thrust, which is well exposed at the base of the hill where it lies at the strongly deformed and altered contact between the pillowed mafic volcanic rocks of the Birch Lake Basalts and the Burntwood group turbidites. The structural significance of this stop is the overprinting relationship of the S2 cleavage and shear foliation along the McLeod Road Thrust contact. At this stop we will first examine the outcrops in the Burntwood group prior to examining the thrust contact.

Description

The map (Figure 25) illustrates the bedded meta turbidites of the Burntwood Group, which are folded with axial planar S2 cleavage, overprinting earlier folds in the bedding, as seen in the Town of Snow Lake at field trip stops 1 - 3. Although not observed on this outcrop the S2 cleavage overprints an older F1 fold in the Town of Snow Lake at field trip stop 2. The S2 foliation is moderately northwest- to north-northeast-trending, moderately northeast- to east-dipping, and is defined by biotite and strain shadows around garnet and staurolite porphyroblasts within the Burntwood Group. Figure 25(a) shows the relationship of the S2 cleavage, which undergoes a slight sinistral rotation between beds within the Burntwood group, due to the difference in competency between individual beds, as observed previously at stop 2.

The overprinting relationship of S2 at the MRT is shown on Figure 25 and on the stereonet (Figure 26). The MRT is expressed as a deformation zone with strongly folded iron carbonate veins. Note how this strong iron carbonate alteration is different from the alteration style

observed at the Bounter Fault. The regional orientation of the MRT at this location is 295 degrees based on the orientation of the outcrop expression of the thrust, on the regional map (Beaumont Smith and Gagné, 2008). At the base of the MRT we observe S asymmetrical folds (Figure 25 b) which fold the shear foliation and have an axial planar cleavage, which is parallel to the S2 cleavage in the Burntwood Group. The asymmetry of the fold and sinistral shear bands C – C' indicates sinistral movement along the MRT, (Figure 25c). The mineral lineation is rarely observed and it trends north-northeast to east, which is similar to the orientation observed due to the regional stretching lineation of the clasts. The stereonet shows the orientation of the shear foliation and the stretching lineation. The intersection lineation of the shear bands is not perpendicular to the stretching lineation, which would be expected if the movement was related to the stretching lineation.

Interpretation

The sinistral movement observed along the MRT is determined to be related to the effect of the overprinting cleavage (S2) forming late during D2, Table 1. Previously (Kraus, et a., 1999; Beaumont-Smith and Lavigne, 2008) interpreted this S2 cleavage as related to initial SW directed thrusting of the MRT over the Burntwood sediments. However, based on field evidence, we interpret the initial movement direction on the MRT to be undetermined. We present a new model that may support evidence for initial movement on the MRT to be related to north directed thrusting of the volcanic rocks of the Snow Lake Arc Assemblage over the Kisseynew basin to the north.

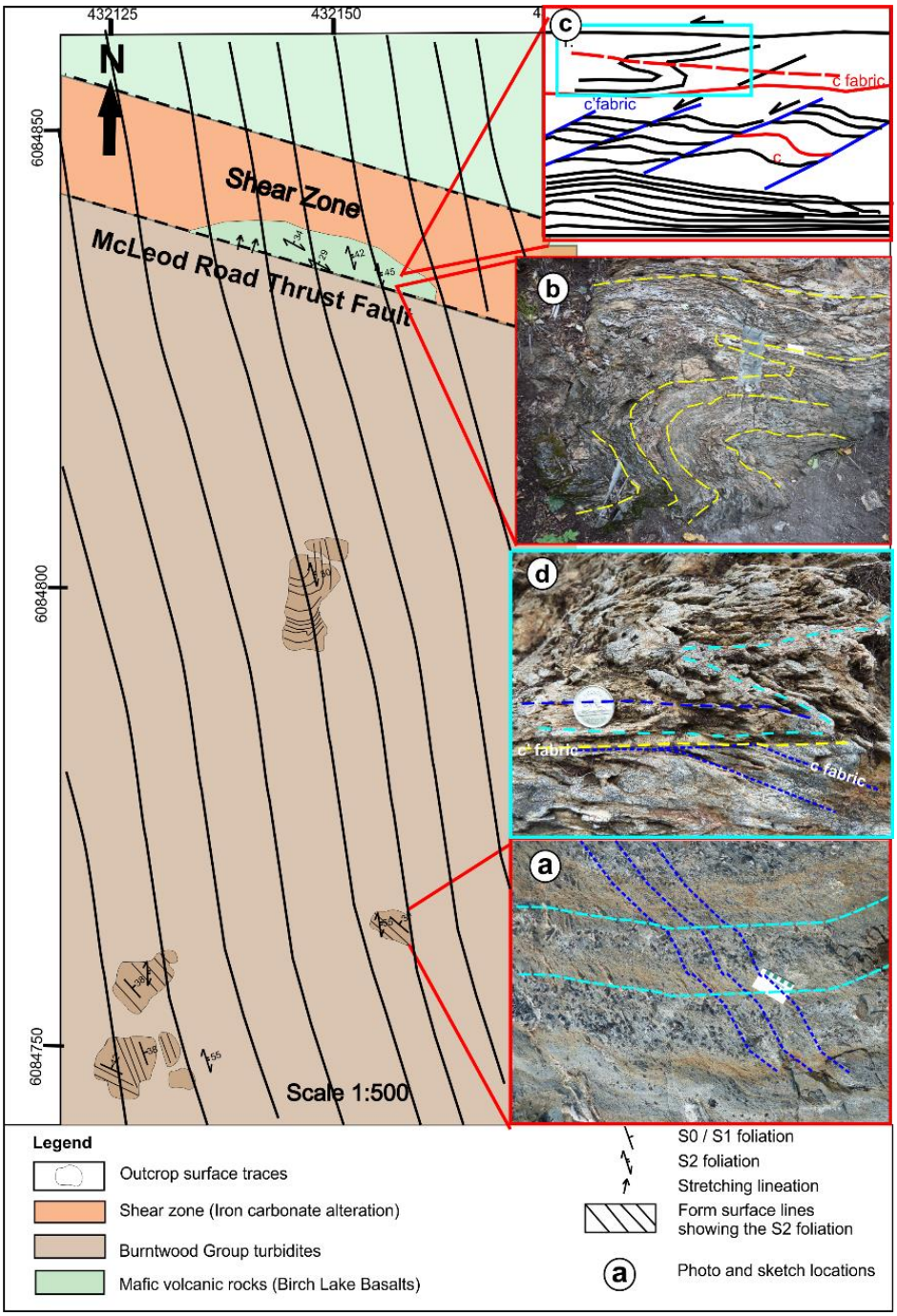

Figure 25: Map of the McLeod Road Thrust powerline location, photo locations and sketches a- d. (a)Sinistral refraction of S2 across beds within meta turbidites of the Burntwood Group highlighted in pale blue, (b) s asymmetry of folds which fold the shear foliation, and have an S2 axial planar cleavage. (c) c-c' shear bands, indicate sinistral movement, (d) the box highlighted on blue in sketch c is illustrated here to show the s asymmetry of folds.

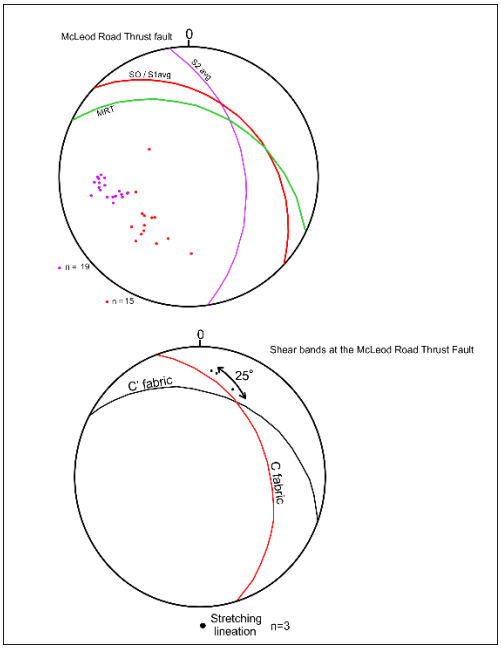

Figure 26: Equal area projections, (lower hemisphere, Schmidt net), to illustrate the S2, relationship at the MRT and the shear bands at the MRT.

Stop 10 (UTM: 6085750N; 431124E) Cleaver Lake Fault

Introduction

This outcrop of the Cleaver Lake Fault (Figure 9) was discovered during the 2014 field season. The Cleaver Lake Fault is a 045 NE trending fault, which runs parallel to the shore of Cleaver Lake, parallel to the southern limb of the McLeod Lake synform, along the contact between the mafic volcanic rocks of the Birch Lake Basalt and the gabbro associated with the Missi Group sediments. This fault is also represented well on the Golder IVD Geophysics (Figure 27) as a distinct lineament which appears to displace the MRT in a small dextral manner. This fault was previously interpreted the same as the extension of the MRT (Kraus and Williams, 1999). However, the contact between the two faults is perpendicular and therefore it is unlikely that the MRT would show such a drastic change in orientation. We follow the interpretation by (Gagné et al, 2009), that considers the trace of the MRT to follow the contact with the Burntwood group sediments to the North and the northern limb of the McLeod Lake synform. The north eastern extension of the Cleaver Lake Fault based on previous geological mapping by (Froese 1980) is interpreted as folded around the Herblet Lake Basin. We interpret this folding of the Herblet Lake Basin to be during D2, but prior to the late overprinting cleavage and reactivation of the MRT.

Outcrop Description

The character and style of alteration at the Cleaver Lake fault (Figure 28) we observe here is remarkably similar to the alteration previously observed at the MRT, with the same intense iron carbonate alteration, and strong deformation. Gabbro similar to the one within the Missi Group is strongly boudinaged and folded parallel to the shear foliation. Early folds deform the iron carbonate alteration and mafic volcanic rocks. The S-C fabrics, (Figure 29a) and back rotated gabbroic boudins (Figure 29b) indicate a normal movement. The stereonet (Figure 30) of the Cleaver Lake fault shows that the orientation similarity of the

intersection lineation between shear bands and foliations is similar to that along the MRT. The S-C fabrics are subsequently folded by a later generation of folds. These late folds appear as open folds and S-shaped. The fold axes in the strongly folded iron carbonate veins appear to be all coaxial to the stretching lineation we observe here.

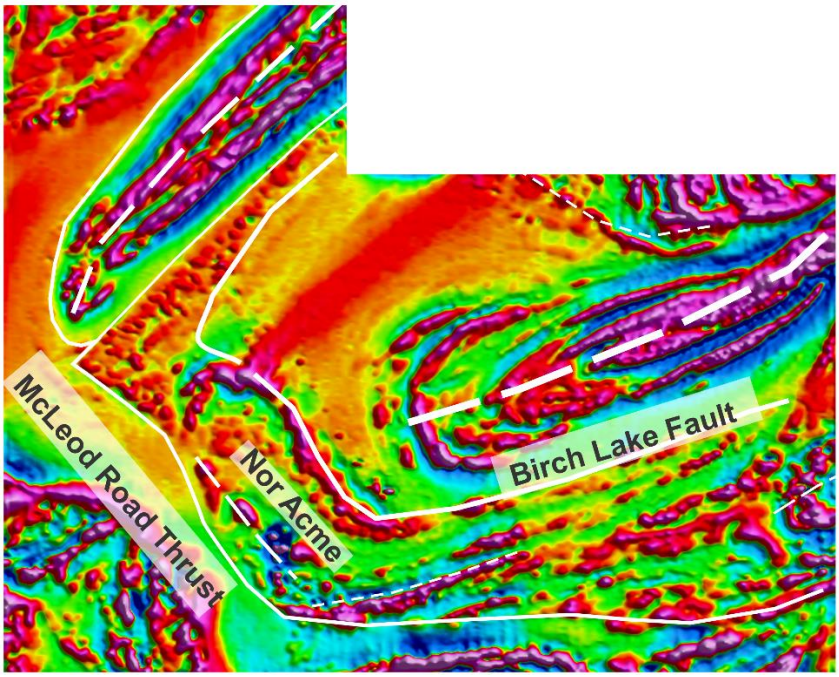

Figure 27: Golder IVD Geophysics (2008)

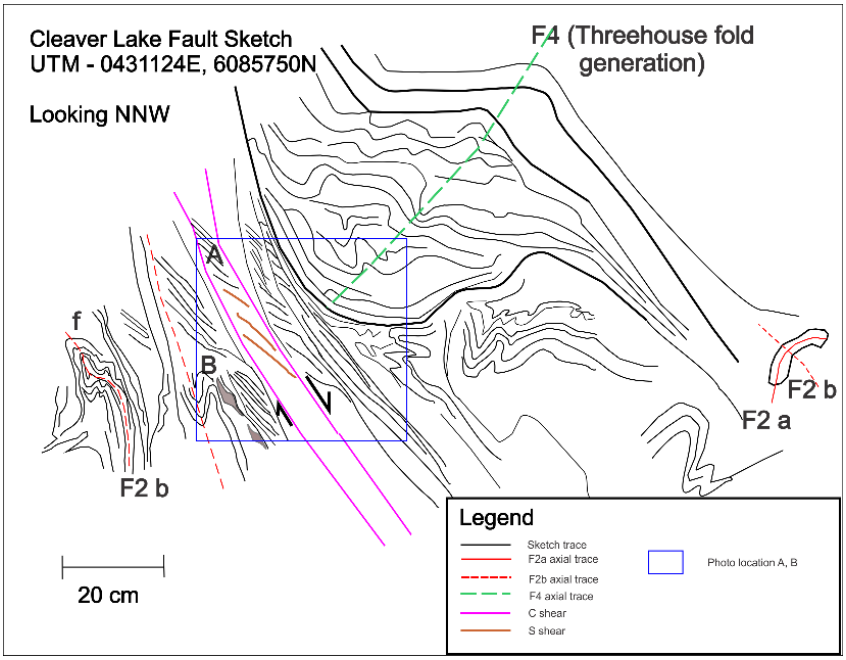

Figure 28: Sketch to illustrate key relationships at the Cleaver Lake Fault (mapped by Rubingh, 2014).

Interpretation

The Cleaver Lake Fault is interpreted as representing a normal fault movement attributed to shortening

during the formation of the S2 overprinting cleavage, (Table 1). This shortening direction would also result in a dextral offset of the Cleaver Lake fault, which is observed at this location based on the Geophysics. Thus the movement represents a reactivation during the formation of the S2 cleavage of the Cleaver Lake Fault, which originated as a thrust similar to the MRT. The open S folds which fold the shear foliation are interpreted as forming during D3 Threehouse folding.

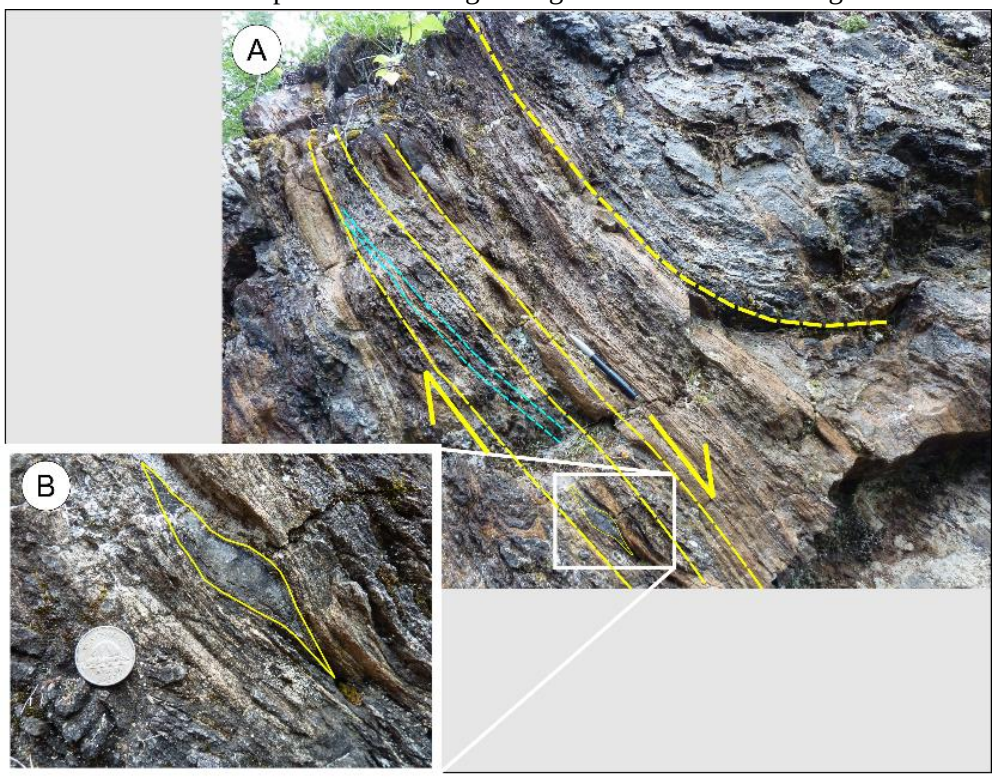

Figure 29: Photo locations A and B from Figure 28. (a) S-C shear bands indicate normal fault movement, (b) back rotated mafic boudins also indicate normal movment on this fault.

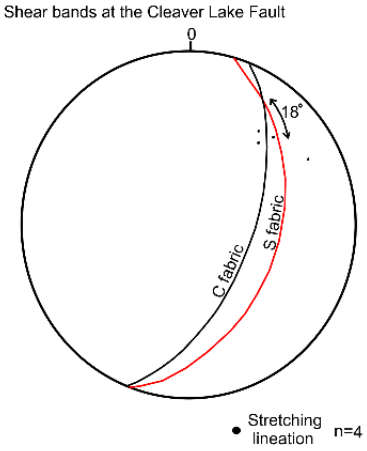

Figure 30: Equal area projection (lower hemisphere, Schmidt net) of shear bands at the Cleaver Lake fault

Tern Lake Sampling
Stops 11 - 16

These stops are suggested field stop locations to sample the anomaly highlighted on the

TMI_RTP_1VD magnetics, from a survey flown by Goldak Airborne Surveys in 2007, provided by Matt Holden.
Geological maps and data provided by Simon Gagne, from geological mapping of the area in (Gagné, 2011) and a compilation map (Bailes et al., 2011) which combines data from geological mapping by Al Bailes (Bailes and Schledewitz, 1999a). Discussions from Matt and Simon have assisted in the field sampling plan for this area.

The Geophysics highlights a structure which trends to the NE, which transects the contact between unit 8a (gabbro) and unit 6a. Structural data along this geophysical anomaly indicates rotation of the main foliation and infers the presence of shear along this structure. The proposed traverse of the Tern Lake area will follow the powerline to the north starting from the road (highway 395). Location 11, 12, 13 and 14 on Figure 31 b will intersect this anomaly and are closest to the powerline for access. Sampling site 15 was chosen to investigate the contact between the gabbro and the unit 6a, which would be the northern extent of the Edwards lake fault, highlighted in red. This sampling site would compare the alteration and structure between the potential fault highlighted by the anomaly and the known Edwards Lake fault. Location 16 is an optional sampling location. The photo lake rhyolite appears to have been transected by the fault which passes through Tern Lake. If this is an early fold in the rhyolite, and intersected by a fault it could be a prospective site for mineralisation. However not enough is known about this structure. Considering the model for the MB thrust panel, that the New Britannia mine is a metamorphosed orogenic gold deposit one would expect to target gold mineralisation in early folds that are transected by early faults during initial thrusting and imbrication of the volcanic sequence.

Stop 11a: 430451 /6082035 (Al Bailes 1998 sample location 1042)
Stop 11b: 430377 /6082035 (Al Bailes 1998 sample location 1043)
Stop 12: 430874/6082149: Gagne 2011 station 11110039
Stop 13: 430927/6082402: Gagne 2011 station 11110041
Stop 14 (431253/6082952): Gagne 2011 station 11110042
Stop 15: (430621/6082486): Gagne 2011 station 11110040
Stop 16 1046 Bailes ref. (optional stop)

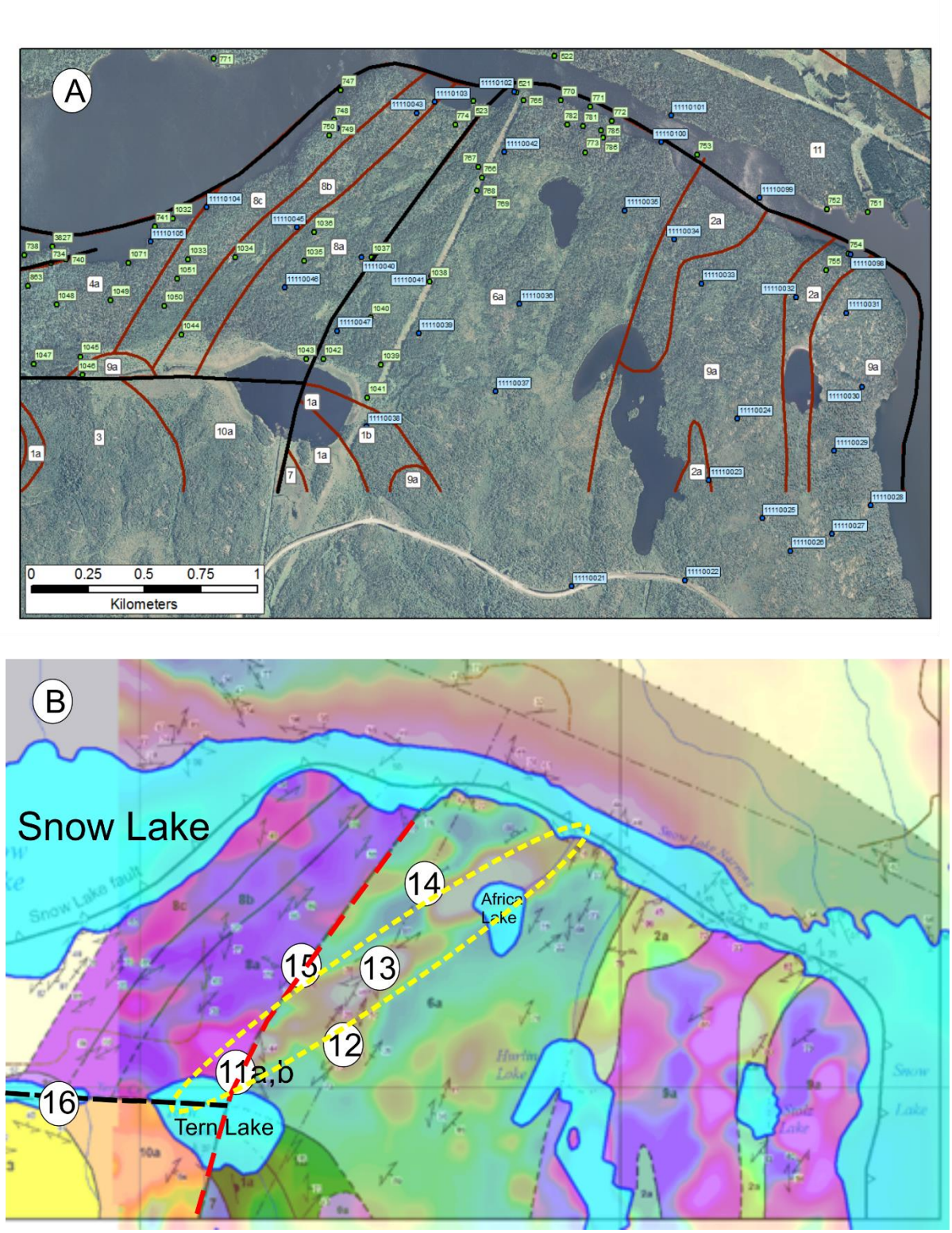

Figure 31: Tern Lake area sampling. (a) Air photo map provided by Simon Gagne displaying field locations visited by Bailes in green and Gagne in blue. This might highlights the boundaries between mapping units and illustrates the road to access the site. (b) Sampling site locations chosen 11-16 and overlain geophysics over geological mapping by Gagne 2011. The fault highlighted in red is the Edwards lake fault. The fault highlighted through Tern Lake is the Tern Lake fault. The anomaly to investigate is shown by dashed yellow lines.

References

Ansdell, K.M. and Norman, A.R. 1995: U-Pb geochronology and tectonic development of the southern flank of the Kisseynew Domain, Trans-Hudson Orogen, Canada; Precambrian Research, **72**, 147-167.

Bailes, A.H. 1980. Origin of Early Proterozoic volcaniclastic turbidites, south margin of the Kisseynew sedimentary gneiss belt. Precambrian Research, **12**: 197–225.

Bailes, A. H., and Galley, A. G. 1996. Setting of Paleoproterozoic volcanic-hosted massive base metal sulphide deposits, Snow Lake, Manitoba; in EXTECH I: a multidisciplinary approach to massive sulphide research in the Rusty Lake– Snow Lake greenstone belts, Manitoba, G. F. Bonham- Carter, A. G. Galley and G. E. M. Hall, (ed.), Geological Survey of Canada, Bulletin 426, p. 105–138.

Bailes, A. H. 1997. Geochemistry of Paleoproterozoic volcanic rocks in the Photo Lake area, Flin Flon Belt (parts of NTS 63 K/16). Manitoba Energy and Mines, Mineral Resources Division, Report of Activities, 61-62.

Bailes, A.H., and Galley, A.G. 1999. Evolution of the Paleoproterozoic Snow Lake arc assemblage and geodynamic setting for associated volcanic-hosted massive sulphide deposits, Flin Flon Belt, Manitoba, Canada; Canadian Journal of Earth Sciences, v. 36, p. 1789–1805.

Bailes, A.H. Galley, A.G. 2007: Geology of the Chisel–Anderson lakes area, Snow Lake, Manitoba (NTS areas 63K16SW and west half of 63J13SE); Manitoba Science, Technology, Energy and Mines, Manitoba Geological Survey, MAP Geoscientific map 2007-1, 1 colour map with accompanying notes, scale 1:20 000.

Bailes, A.H., and Schledewitz, D.C.P. 1998. Geology and geochemistry of the Paleoproterozoic volcanic rocks between the McLeod Road and Birch Lake faults, Snow Lake area, Flin Flon belt (parts of NTS 63K/16 and 63J/13); in Report of Activities 1998, Manitoba Energy and Mines, Geological Services, p. 4–13. 78 Manitoba Geological Survey.

Bailes, A.H., Schledewitz, D.C.P., Gagné, S. 2011: Updated geology of the Squall–Varnson lakes area, west-central Manitoba (part of NTS 63K16), Manitoba Innovation, Energy and Mines, Manitoba Geological Survey, Preliminary Map 2011-2, 1 colour map. scale 1:20_000.

Bailes, A., Gagné, S., Rubingh, K., & Taylor, C. 2013. Volcanological and structural setting of Paleoproterozoic VMS and gold deposits at Snow Lake, Manitoba. Geoscience Canada, 39(4).

Beaumont-Smith, C.J. Gagné, S. 2008: Structural geology of the Snow Lake–Squall Lake area, Manitoba (parts of NTS 63K16, 63J13); Manitoba Science, Technology, Energy and Mines, Manitoba Geological Survey, PMAP Preliminary Map 2008-1, 1 colour map. scale 1:20_000.

Beaumont-Smith, C.J. Lavigne, J. 2008: Structural geology and gold metallogenesis of the New Britannia mine area, Snow Lake, Manitoba (NTS 63K16); in Report of Activities 2008, Manitoba Science, Technology, Energy and Mines, Manitoba Geological Survey, p. 7–17

Connors, K.A. 1996: Unraveling the boundary between turbidites of the Kisseynew Domain and volcano-plutonic rocks of the Flin Flon domain in the eastern Trans-Hudson Orogen, Canada; Canadian Journal of Earth Sciences, **33**, 811-829.

David, J., Bailes, A.H. and Machado, N. 1996: Evolution of the Snow Lake portion of the Paleoproterozoic Flin Flon and Kisseynew belts, Trans-Hudson Orogen, Manitoba, Canada; Precambrian Research, **80**, 107-124.

Froese, E. and Moore, J.M. 1980. Metamorphism in the Snow Lake area, Manitoba; Geological Survey of Canada, Paper 78-27, 16 p.

Gagné, S. 2009. Geological investigation of the McLeod Road- Birch Lake allochthon east of Snow Lake, Manitoba (part of NTS 63J13); in Report of Activities 2009, Manitoba Innovation, Energy and Mines, Manitoba Geological Survey, p. 58–68.

Gagné, S. 2011: Geochemistry and updated geology of the Squall Lake–Varnson lakes area, west-central Manitoba (part of NTS 63K16), in Report of Activities 2011, Manitoba Innovation, Energy and Mines, Manitoba Geological Survey, p. 55–67.

Galley, A.G., Bailes, A.H., Syme, E.C., Bleeker, W., Macek, J.J. and Gordon, T.M. 1991. Geology and mineral deposits of the Flin Flon and Thompson belts, Manitoba (Field Trip 10); Geological Survey of Canada, Open File 2165, 8th IAGOD Symposium Field Trip Guidebook, 137 p.

Kraus, J. 1998. Structural and metamorphic studies in the Snow Lake area, Trans-Hudson Orogen, Manitoba, central Canada; Ph.D. thesis, University of New Brunswick, Fredericton, New Brunswick, 229 p.

Kraus, J. and Williams, P.F. 1999: Structural development of the Snow Lake allochthon and its role in the evolution of the southeastern Trans-Hudson Orogen in Manitoba, central Canada; Canadian Journal of Earth Sciences, v. 36. no. 11, p. 1881–1899.

Lucas, S.B., Stern, R.A. and Syme, E.C. 1996: Flin Flon greenstone belt: intraoceanic tectonics and the development of continental crust (1.92-1.84 Ga); Geological Society of America Bulletin, **108**, 602-629.

Rubingh, K.E 2011. Stratigraphy of the McLeod Road–Birch Lake thrust panel, Snow Lake, west-central Manitoba (parts of NTS 63K16 and 63J13); *in* Report of Activities 2011, Manitoba Innovation, Energy and Mines, Manitoba Geological Survey, p. 68–78.

Rubingh, K.E., Lafrance, B., Gibson, H.L. and Gagné, S. 2012. Preliminary lithostratigraphic map of the McLeod Road– Birch Lake thrust panel, Snow Lake, west-central Manitoba (parts of NTS 63K16, 63J13); Manitoba Innovation, Energy and Mines, Manitoba Geological Survey, Preliminary Map PMAP2012-7, 1:5000 scale.

Rubingh, K.E., Lafrance, B. and Gibson, H.L. 2012. Lithostratigraphy and structural geology of the McLeod Road–Birch Lake thrust panel, Snow Lake, west-central Manitoba (parts of NTS 63K16, 63J13); *in* Report of Activities 2012, Manitoba Innovation, Energy and Mines, Manitoba Geological Survey, p. 104–114.

Rubingh, K.E., Lafrance, B. and Gibson, H.L. 2013. Structural analysis of the McLeod Road- Birch Lake thrust panel, Snow Lake, west-central Manitoba (parts of NTS 63K16, 63J13); *in* Report of Activities 2013, Manitoba Innovation, Energy and Mines, Manitoba Geological Survey, p. 106–113.

Russell, G.A. 1957. Structural studies of the Snow Lake–Herb Lake area; Manitoba Mines and Natural Resources, Mines Branch, Publication 55-3, 33 p.

Syme, E.C., Bailes, A.H. and Lucas, S.B. 1995: Geology of the Reed Lake area (parts of NTS 3K/9 and 10); in Report of Activities 1995, Manitoba Energy and Mines, Geological Services, p. 42-60.

Zwanzig, H.V. 1990: Kisseynew gneiss belt in Manitoba: stratigraphy, structure, and tectonic evolution*; in* Lewry, J.F. and Stauffer, M.R., eds.: The Early Proterozoic Trans-Hudson Orogen of North America: Geological Association of Canada, Special Paper **37**, 95-120.